THÈSE DE DOCTORAT DE L'UNIVERSITÉ DE LA REUNION

Spécialité : Physique de l'atmosphère

École doctorale : « Sciences, Technologies et Santé (STS) ED542 »

Présentée et soutenue le 26 février par

Gabriela Cacilda Godinho dos Reis

En vue de l'obtention du grade de

DOCTEUR DE L'UNIVERSITÉ DE LA RÉUNION

Sujet de la thèse :

Temporal Variability of Solar Ultraviolet Radiation in Low and Mid-Latitude South American Sites

---

Jury

Mme	Damaris kirsch Pinheiro	UFSM, Santa Maria, BR	Examinatrice
Mme.	Lucieta Guerreiro Martorano	UFOPA, Santarém, BR	Rapporteuse
Mme.	Fanny Minvielle	LOA, Lille, FR	Examinatrice
M.	Hassan Bencherif	LACy, Saint-Denis, FR	Examinateur
M.	Marcelo de Paula Corrêa	UNIFEI, Itajubá, BR	Rapporteur
M.	Rodrigo da Silva	UFOPA, Santarém, BR	Co-Directeur de thèse
M.	Thierry Portafaix	IRD, Madagascar	Directeur de thèse

Temporal Variability of Solar Ultraviolet Radiation in Low and Mid-Latitude South American Sites

by

Gabriela Cacilda Godinho dos Reis

Submitted in fulfillment of the requirements for the degree
Doctor in Environmental Sciences in the Graduate Program in Society, Nature, and Development,
Federal University of Western Pará

Supervisor: Dr. Rodrigo DA SILVA
Co-Supervisor: Lucas VAZ PERES

and

Docteur és Sciences (Physique de l'atmosphere)
Sciences Technologies Santé (ED542), Physique de l'Atmosphère,
Laboratoire de l'Atmosphère et des Cyclones – LACy UMR 8105
Université de La Réunion

Supervisor : Thierry PORTAFAIX

26 Février 2025

FEDERAL UNIVERSITY OF WESTERN PARÁ
DEAN'S OFFICE FOR RESEARCH, POSTGRADUATE AND TECHNOLOGICAL INNOVATION
POSTGRADUATE PROGRAM IN SOCIETY, NATURE, AND DEVELOPMENT

GABRIELA CACILDA GODINHO DOS REIS

Temporal Variability of Solar Ultraviolet Radiation in Low and Mid-Latitude South American Sites

SANTARÉM, PA
2025

GABRIELA CACILDA GODINHO DOS REIS

Temporal Variability of Solar Ultraviolet Radiation in Low and Mid-Latitude South American Sites

Thesis presented to the *Stricto Sensu* Postgraduate Program in Society, Nature and Development, as part of the requirements for obtaining the title of Doctor in Environmental Sciences from the Federal University of Western Pará (UFOPA). Area of concentration: Environmental and Social Impacts of Land Use Change in the Amazon.
Supervisor: Dr. Rodrigo da Silva
Co-supervisor: Dr. Lucas Vaz Peres

SANTARÉM, PA
2025

Dados Internacionais de Catalogação-na-Publicação (CIP)
Sistema Integrado de Bibliotecas – SIBI/UFOPA

R375t Reis, Gabriela Cacilda Godinho dos

Temporal variability of solar ultraviolet radiation in low and mid-latitude South American sites. / Gabriela Cacilda Godinho dos Reis. - Santarém, 2025.

180 p. : il. Color.

Supervisor: Rodrigo da Silva.

Co-supervisor: Lucas Vaz Peres.

Thesis (Doctor) – Federal University of Western Para, Dean's Office for Research, Posgraduate and Technological Innovation, Postgraduate Program in Society, Nature and Development.

1. Solar ultraviolet radiation. 2. Satellite and ground-based comparisons. 3. Environmental monitoring. 4. Cloud cover variability. 5. South America. I. Silva, Rodrigo da, *super*. II. Peres, Lucas Vaz, *co-super*. III. Título.

CDD: 23 ed. 551.5271

Bibliotecária - Documentalista: Cátia Alvarez – CRB/2 843

GABRIELA CACILDA GODINHO DOS REIS

Temporal Variability of Solar Ultraviolet Radiation in Low and Mid-Latitude South American Sites

Thesis presented to the *Stricto Sensu* Postgraduate Program in Society, Nature and Development, as part of the requirements for obtaining the title of Doctor in Environmental Sciences from the Federal University of Western Para (UFOPA). Area of concentration: Environmental and Social Impacts of Land Use Change in the Amazon.

Approved on 26 February 2025

oocumento assinado digitalmente
gov.br RODRIGO 111\SRVII
Data: 09/03/202519:57:28-0300
verifique em https://validar.iti.gov.br

Dr. Rodrigo da Silva - Supervisor
Federal University of Western Para (UFOPA)

Documento assinado digitalmente
gov.br MARCELO DE PAULA CORREA
Data: 19/03/2025 18:11:03-0300
Verifique em https://validar.iti.gov.br

Dr. Marcelo de Paula Corrêa
Federal University ofItajuba (UNIFEI)

Documento assinado digitalmente
gov.br LUCIETA GUERREIRO MARTORANO
Data: 14/03/2025 12:57:52-0300
Verifique em https://validar.iti.gov.br

Dr. Lucieta Guerreiro Martorano
Federal University of Western Para (UFOPA)

Dr. Thieny Portafaix - Co-supervisor
Institute ofResearch for Development (IRD)

Thierry PORTAFAIX

Documento assinado digitalmente
gov.br DAMARIS KIRSCH PINHEIRO
Data: 19/03/2025 09:39:07-0300
Verifique em https://validar.iti.gov.br

Dr. Damaris Kirsch Pinh
Federal University of Santa Maria (UFSM)

Dr. Hassan Bencherif
Lacy- University ofReunion Island

Dr. Fanny Minvielle
LOA, University of Lille

FACULTÉ DES SCIENCES
ET TECHNOLOGIES
Secrétariat Pédagogique
Cité scientifique
F-59655Villeneuve d'Ascq Cedex

ACKNOWLEDGMENTS

I gratefully acknowledge the support and funding provided by CNPQ, FAPESPA, CAPES, COFECUB, Campus France, and the French government throughout my journey as a young scientist. From my first scientific initiation scholarship, which inspired me to pursue a career in academia, to this doctoral stage, their support has been invaluable. A special thanks to the Federal University of Western Pará (UFOPA) for its foundational role, and I extend gratitude to LACy (UMR 8105 CNRS, Météo-France) and the University of Réunion for their collaboration and support.

My sincere thanks to Professor Rodrigo, who has been mentoring me since my master's degree, and to Professor Lucas, who also mentors me and facilitated all the connections necessary for me to obtain a sandwich PhD scholarship. I am also grateful to Professor Damaris, Professor Hassan, and Professor Thierry for their dedication to science and their efforts to secure funding for projects that transform the lives of young researchers like myself and many others.

A special thanks to my father, who has always believed in me and supported me in my decisions. I am also deeply thankful to Chloë, my brother, friends, and lab colleagues for all their emotional support and help during crucial moments, which enabled me to continue this journey and reach the defense of my doctoral thesis.

ABSTRACT

Solar Ultraviolet Radiation (UV), consisting of electromagnetic waves from 100–400 nm, accounts for about 5% of the sun's emitted energy. UV exposure has both risks and benefits, impacting human health, ecosystems, materials, and biogeochemical cycles. Climate change, influenced by land use changes and other factors, alters UV intensity based on location, seasons, and atmospheric composition. The UV Index, a dimensionless indicator, helps people assess UV levels and adopt protective measures. However, in middle-income countries like Brazil and Argentina, UV monitoring networks are sparse and underfunded, limiting reliable UV data. Satellite data become crucial, although they are also subject to instrument errors and algorithmic uncertainties. This research investigates the diurnal and seasonal variability of UV levels at five sites across low and mid-latitude South America, under both all-sky and clear-sky conditions, utilizing ground-based and satellite-derived data. The study spans from 2005 to 2022, varying according to each dataset. The sites are: Santarém in the Brazilian Amazon (2.25°S; 54.44°W, 18 m, Apogee SU-100-ss UV sensor), Natal in Northeast Brazil (05.78°S; 35.21°W, 30 m, Davis 6490 UV sensor), Itajubá in Southeast Brazil (22.41°S, 45.44°W, 885 m, Davis 6490 UV sensor), Santa Maria in the south of Brazil (29.4°S, 53.8°W, 476 m, Brewer Spectrophotometer MKIII #167), and Buenos Aires in Argentina (34.58°S, 58.48°W, 25 m, Solar Light UV Biometer – Radiometer model 501). Additionally, the study compares ground-based and satellite-derived UV Index levels from OMI at noon and overpass times, and GOME-2 at noontime during clear sky conditions, which are assessed using LER (Lambertian Equivalent Reflectivity) and METAR cloud cover data. Santarém and Natal, tropical low-latitude cities, displayed a semi-annual cycle with two maxima and consistently higher year-round UV index levels. In contrast, Itajubá, Santa Maria, and Buenos Aires exhibited an annual cycle, with UV index peaking during austral summer. Cloud cover played a dual role in UV variability. In Santarém, UV levels under all-sky conditions exceeded clear-sky levels during certain rainy months, while in Natal, noontime all-sky UV index were 6.8% higher during periods of prevalent broken clouds. Extreme UV index were observed from 10 AM to 2 PM in Natal and Santa Maria and from 11 AM to 2 PM in Buenos Aires. Satellite data comparisons showed that UV index derived from OMI had a lower bias than those from GOME-2, though both datasets exhibited low overall errors. At Natal, the LER method identified significantly more clear-sky days than METAR, with the combined dataset (LER & METAR) providing the most reliable results for overpass time. Data from Itajubá exhibited the largest discrepancies and highest errors, while Santa

Maria and Buenos Aires showed better agreement, with Buenos Aires presenting the most accurate results.This thesis makes an important contribution to understanding the variability of UV radiation in South America. The methodologies applied here also hold potential for expanding UV and cloud cover research to other underrepresented areas. This work confirms the reliability of instruments and datasets, providing a foundation for environmental and health studies in the complex field of UV radiation, its interactions, and its effects, addressing a critical knowledge gap in atmospheric and environmental sciences.

Keywords: Solar ultraviolet radiation. Satellite and ground-based comparisons. Environmental monitoring. Cloud cover variability. South America.

RESUMO

A Radiação Solar Ultravioleta (UV), composta por ondas eletromagnéticas entre 100–400 nm, representa cerca de 5% da energia solar. Sua exposição traz riscos e benefícios, afetando a saúde humana, ecossistemas, materiais e ciclos biogeoquímicos. Mudanças climáticas, influenciadas por alterações no uso da terra e outros fatores, modificam a intensidade da UV, dependendo da localização, das estações do ano e da composição atmosférica. O Índice UV (IUV) facilita a avaliação dos níveis de exposição e a adoção de medidas de proteção. Contudo, em países de renda média como Brasil e Argentina, as redes de monitoramento UV são escassas e subfinanciadas, limitando a obtenção de dados confiáveis. Dados de satélite tornam-se, portanto, essenciais, embora também sujeitos a erros instrumentais e incertezas algorítmicas. Esta pesquisa examina a variabilidade diurna e sazonal dos níveis de UV em cinco localidades na América do Sul, abrangendo latitudes baixas e médias, sob condições de céu limpo e nublado, utilizando dados terrestres e satelitais de 2005 a 2022. Os locais estudados incluem: Santarém, na Amazônia Brasileira (2,25°S; 54,44°W, 18 m, sensor Apogee SU-100-SS), Natal, no Nordeste Brasileiro (05,78°S; 35,21°W, 30 m, sensor Davis 6490), Itajubá, no Sudeste brasileiro (22,41°S; 45,44°W, 885 m, sensor Davis 6490), Santa Maria, no Sul do Brasil (29,4°S; 53,8°W, 476 m, Espectrofotômetro Brewer MKIII #167) e Buenos Aires, na Argentina (34,58°S; 58,48°W, 25 m, Biômetro UV Solar Light – Radiômetro 501). Adicionalmente, os níveis de Índice UV derivados de satélite (OMI em horários de sobrevoo e meio-dia, e GOME-2 ao meio-dia) foram comparados com dados terrestres sob condições de céu limpo, selecionados por meio da Refletividade Equivalente Lambertiana (LER) e dos dados de cobertura de nuvens do METAR. Santarém e Natal apresentaram um ciclo semi-anual, com dois máximos e níveis de IUV consistentemente mais elevados ao longo do ano. Em contraste, Itajubá, Santa Maria e Buenos Aires mostraram um ciclo anual, com picos durante o verão austral. Em Santarém, os níveis de radiação UV sob céu nublado superaram os de céu limpo durante alguns meses chuvosos. Em Natal, o IUV ao meio-dia foi 6,8% maior em condições de céu parcialmente nublado (5–7 octas). Níveis extremos de IUV foram observados das 10h às 14h em Natal e Santa Maria, e das 11h às 14h em Buenos Aires. As comparações indicaram que os dados derivados do OMI apresentaram um viés menor do que os do GOME-2, com ambos exibindo baixos erros gerais. O método LER identificou significativamente mais dias de céu limpo do que o METAR, e o conjunto de dados combinado (LER & METAR) apresentou os melhores resultados para o horário de sobrevoo do satélite. Os dados de Itajubá

apresentaram os maiores erros, enquanto Santa Maria e Buenos Aires mostraram melhor concordância, sendo Buenos Aires o local com os resultados mais precisos. Esta tese contribui para a compreensão da variabilidade do UV na América do Sul. As metodologias aplicadas têm potencial para expandir a pesquisa sobre UV e cobertura de nuvens em outras áreas sub-representadas. Este trabalho confirma a confiabilidade de instrumentos e conjuntos de dados, fornecendo uma base para estudos ambientais e de saúde no campo do UV, suas interações e seus efeitos, abordando uma lacuna no conhecimento em ciências atmosféricas e ambientais.

Palavras-Chaves: Radiação solar ultravioleta. Comparações entre dados satélite e terrestres. Monitoramento ambiental. Variabilidade da cobertura de nuvens. América do Sul.

RÉSUMÉ

La radiation solaire ultraviolette (UV), composée d'ondes électromagnétiques de 100 à 400 nm, constitue environ 5 % de l'énergie émise par le soleil. Elle présente des risques et des bénéfices, affectant la santé humaine, les écosystèmes, les matériaux et les cycles biogéochimiques. Le changement climatique, influencé par les modifications d'utilisation des terres et d'autres facteurs, modifie l'intensité des UV selon la localisation, les saisons et la composition atmosphérique. L'indice UV, un indicateur sans dimension, aide à évaluer les niveaux d'exposition et à adopter des mesures de protection. Cependant, dans des pays comme le Brésil et l'Argentine, les réseaux de surveillance UV sont rares et insuffisamment financés, ce qui limite les données fiables. Les satellites deviennent essentiels malgré les erreurs instrumentales et les incertitudes algorithmiques. Cette recherche analyse la variabilité diurne et saisonnière des niveaux d'UV sur cinq sites en Amérique du Sud, de 2005 à 2022. Les localités étudiées sont : Santarém (2,25°S, capteur UV Apogee SU-100-SS), Natal (05,78°S, capteur Davis 6490), Itajubá (22,41°S, capteur Davis 6490), Santa Maria (29,4°S, spectrophotomètre Brewer MKIII #167), et Buenos Aires (34,58°S, Biomètre UV Solar Light modèle 501). Les données terrestres et satellitaires (OMI et GOME-2) ont été comparées sous ciel dégagé, à l'aide de la réflectivité équivalente lambertienne (LER) et des données METAR. Santarém et Natal, localités tropicales de basse latitude, ont présenté un cycle semi-annuel avec deux maxima et des niveaux d'UV élevés toute l'année. Itajubá, Santa Maria et Buenos Aires, situées plus au sud, ont montré un cycle annuel avec des pics en été austral. La couverture nuageuse joue un rôle double dans la variabilité UV : à Santarém, les niveaux d'UV sous ciel nuageux surpassent ceux sous ciel dégagé pendant certain mois pluvieux. À Natal, l'indice UV à midi était 6,8 % plus élevé sous un ciel partiellement nuageux (5-7 octas). Des niveaux extrêmes d'UV ont été observés entre 10 h et 14 h à Natal et Santa Maria, et entre 11 h et 14 h à Buenos Aires. Les comparaisons entre satellites montrent qu'OMI présente un biais moindre que GOME-2, bien que les deux affichent des erreurs globales faibles. À Natal, la méthode LER a identifié plus de jours de ciel dégagé que METAR. Les résultats les plus précis ont été obtenus avec le jeu de données combiné (LER et METAR). Parmi les sites étudiés, Itajubá présente les plus grandes divergences et erreurs, tandis que Santa Maria et Buenos Aires montrent une meilleure concordance, Buenos Aires offrant les résultats les plus fiables. Cette thèse apporte une contribution majeure à la compréhension de la variabilité de la radiation UV en Amérique du Sud, où ces études sont encore limitées. Les méthodologies appliquées peuvent être étendues à d'autres

zones sous-représentées. Ce travail valide la fiabilité des instruments et des données, fournissant une base solide pour des études environnementales et sanitaires sur les effets de la radiation UV et ses interactions dans les sciences atmosphériques et environnementales.

Mots-clés: Rayonnement solaire ultraviolet. Comparaisons entre données satellitaires et mesures au sol. Surveillance environnementale. Variabilité de la couverture nuageuse. Amérique du Sud.

LIST OF FIGURES

LIST OF TABLES

LIST OF ABBREVIATIONS

A.S.L. - Above Sea Level

AERONET - Aerosol Robotic Network

BDC - Brewer Dobson Circulation

BKN - Broken sky coverage

CAVOK - Clear Sky

COD - Cloud optical depth

DEr - Daily Erythemal doses

ED - Erythemal Ultraviolet Dosage

EER - Erythemally-effective radiation

EUMESAT - European Organisation for the Exploitation of Meteorological Satellites

EUV - Erythemal Irradiance

FTD - Development of photodermatoses

GAW - Global Atmospheric Watch

GDP - Gross Domestic Product

GOME–2 - Second Global Ozone Experiment

INCA - Brazilian National Cancer Institute

INMET - National Institute of Meteorology

LER - Lambertian Equivalent Reflectivity

MBE - Mean Bias Error

MEDs - Minimum erythemal doses

METAR - Meteorological Aerodrome Reports

MOCAGE - Modelisation de la Chimie Atmospheric Grande Echelle

NEB - Northeast Brazil

NSF - National Science Foundation

OMI - Ozone Monitoring Instrument

OVC - Overcast sky coverage

PAR - Photosynthetically Active Radiation

QBO - Quasi-Biennial Oscillation

REDEMET - Air Force Command Meteorology Network

RMSE - Root Mean Square Deviation

S5P - Sentinel 5 Precursor

SCIAMACHY - Scanning Imaging Absorption SpectroMeter for Atmospheric CHartography

SCT - Scattered sky coverage

SEDs - Standard erythemal doses

SMN - Argentine National Weather Service

SPMR - São Paulo Metropolitan Region

SZA - Solar Zenith Angle

TOC - Total Ozone Column

TOMS - Total Ozone Mapping Spectrometer

TROPOMI - TROPOspheric Monitoring Instrument

TURV - Total Ultraviolet Radiation

TUV - Tropospheric Ultraviolet and Visible radiative transfer model

UFOPA - Federal University of Western Pará

UR - University of Reunion

UTC - Coordinated Universal Time

UV - Solar Ultraviolet Radiation

UVER - Ultraviolet erythemal radiation

UVGAME - Ultraviolet Global Atmospheric Model

UVI - Ultraviolet Radiation Index

UVSIMN - Ultraviolet Spectral Irradiance Monitoring Network

UV–A - Ultraviolet radiation with wavelengths between 315-400 nm

UV–B - Ultraviolet radiation with wavelengths between 280-315 nm

UV–C - Ultraviolet radiation with wavelengths between 100-280 nm

WMO - World Meteorological Organization

WOUDC - World Ozone and Ultraviolet Radiation Data Center

TABLE OF CONTENTS

1 INTRODUCTION

Solar ultraviolet radiation (UV) consists of electromagnetic waves with wavelengths ranging from 100 to 400 nm, constituting about 5% of the solar energy that reaches the Earth's surface (CADET et al., 2020). The beneficial and detrimental effects of UV on life on Earth have been recognized for many years (DIFFEY, 1991; UNEP, 2023) and include impacts on human health, materials, terrestrial and aquatic ecosystems, and biogeochemical cycles (LUCAS et al., 2019; ANDRADY et al., 2023; BORNMAN et al., 2014; SULZBERGER et al., 2019). The UV impact is influenced by both the duration of exposure and several additional factors. Key elements that affect its variability include the sun elevation, the amount of total ozone present, cloud cover, aerosols, surface albedo, and altitude (PORFÍRIO et al., 2012; BROGNIEZ et al., 2016). Other factors that play a lesser role in controlling UV levels consist of the ozone profile, the presence of trace gases, seasonal variations in the Earth-Sun distance, fluctuations in solar activity, and volcanic events (UNEP, 2023; BERNHARD et al., 2023).

UV radiation is categorized into three distinct regions, each corresponding to its biological effects based on different wavelengths: UV–A (315–400 nm), UV–B (280–315 nm), and UV–C (100–280 nm) (WHO, 2006; CORRÊA, 2015; SUÁREZ et al., 2017). When sunlight traverses the atmosphere, all UV–C and nearly 90% of UV–B radiation is absorbed by ozone, water vapor, oxygen, and carbon dioxide, while UV–A experiences minimal absorption by atmospheric constituents (SUÁREZ et al., 2017). Consequently, the UV radiation that reaches the Earth's surface is predominantly UV–A, making up approximately 94% of the total. UV–B constitutes a smaller fraction at around 6% (WHO, 2002; BILBAO & DE MIGUE, 2020).

On human health the effects of UV can be beneficial or harmful (LAMY et al., 2021; GHOLAMNIA et al., 2021). Higher exposure to UV is associated with a higher incidence of skin cancers as well as other UV-related health issues, such as cataracts and photosensitivity disorders (UNEP, 2018). Additionally, exposure to this spectrum of solar radiation stimulates the production of vitamin D, serving as the primary source of this vitamin for most of the global population (BAIS et al., 2018).

Brazil is a country of continental dimensions, characterized by significant climate diversity and a highly mixed population. Nearly the entire national territory is situated between the equator and the Tropic of Capricorn, with the Earth's axial tilt towards the south contributing to making Brazil

one of the countries in the world with the largest land area in proximity to the Sun (SCHALKA et al., 2014). Due to its geographic characteristics and cultural behaviors, Brazilians are among those with the highest annual sun exposure (SCHALKA et al., 2014).

For the triennium of 2020–2022, the Brazilian National Cancer Institute (INCA, 2019) estimated approximately 177,000 new cases of non-melanoma skin cancer. This number is projected to rise for the 2023–2025 triennium, with an estimated 220,490 new cases of non-melanoma skin cancer each year throughout this period (INCA, 2023). Non-melanoma skin cancer represents the most prevalent type of cancer among men in the southern, central western, and southeastern regions of Brazil (INCA, 2019, 2023). In the northern and northeastern regions, it ranks second (INCA, 2019, 2023). For women, non-melanoma skin cancer is the most frequently diagnosed cancer across all regions of Brazil (INCA, 2019). Furthermore, cataracts remain the primary cause of blindness and vision impairment in the country (CBO, 2019). The economic impact, reflected as a loss of GDP (Gross Domestic Product) exceeding USD 9 million, has been estimated for Latin America and the Caribbean due to the effects of blindness and vision impairment. This loss could potentially be reduced to just over USD 3 million if effective education and prevention programs targeting risk factors, such as prolonged and unprotected UV exposure, were implemented (CBO, 2019).

Diseases associated with prolonged exposure to UV radiation, including skin cancer and cataracts, can largely be prevented through adequate sun protection measures (WHO, 2002). Addressing the need for relevant information, the World Health Organization (WHO) developed the ultraviolet index (UVI), a dimensionless indicator that quantifies the amount of UV radiation reaching the Earth's surface. The UVI values range on a scale from 0 to 11 or higher (WHO, 2002). This scale is categorized into five levels, from low to extreme, with specific sun protection recommendations provided for each level (WHO, 2002). The UV index serves as a crucial tool for raising public awareness about the dangers of excessive sun exposure (LOPO et al., 2014). Therefore, due to the significant impacts of UV radiation, it is essential to understand the factors that affect UV index levels and how they vary over time and at specific locations.

Natural factors, such as solar activity (the 11-year solar cycle), dynamic atmospheric processes (including the quasi-biennial oscillation, QBO), and ocean dynamics, induce variations in atmospheric conditions across different regions of the world (FOUNTOULAKIS et al., 2019). Climate change, driven by land-use changes like deforestation, agricultural transformations, and urban and industrial development, also impacts the atmosphere, notably by altering cloud cover

(FOUNTOULAKIS et al., 2019; UNEP, 2018), a significant regulator of the radiative balance within the Earth-atmosphere system (CADET et al., 2017). Furthermore, each year, gases and emissions from tropical biomass burning contribute significantly to air quality in South America, particularly from fires in the north-central regions of Brazil and Bolivia (MOREIRA et al., 2017; CHAND et al., 2006). Biomass burning aerosols diminish direct solar radiation reaching the surface while simultaneously increasing the diffuse fraction of solar radiation (MOREIRA et al., 2017).

An additional critical factor to consider is the ozone layer depletion. The stratospheric ozone shields life on Earth by absorbing harmful UV radiation (NEALE et al., 2021). Preserving this layer has been an international priority since the recognition of ozone depletion (NEALE et al., 2021). Cordero et al. (2022) states that the Montreal Protocol has been effective in the reduction of the levels of human-made substances that deplete ozone, leading to the recovery of the stratospheric ozone layer above Antarctica. Nevertheless, the Antarctic ozone hole continues to occur every year, with significant ozone loss. These losses contribute to increased levels of UV radiation at the surface in Antarctica, and can also reach mid-latitude regions, a phenomenon referred to as the "secondary effect of the ozone hole" (BRESCIANI et al., 2018; CORDERO et al., 2022).

In middle-income countries like Brazil, UV monitoring networks and instruments are typically limited and face challenges related to funding, as well as the maintenance and calibration required for these instruments, making it difficult to obtain reliable UV data. The northern and central-western regions of Brazil lack stations that provide long-term UV data. Among the limited studies addressing UV variability in Brazilian cities, the majority have been concentrated in the southeastern region, and second, the northeast. The absence of UV data is even more pronounced in the northern region (REIS et al., 2022). Currently, only two papers have reported ground-based UV measurements in this area: one study focuses on the city of Humaitá in Amazonas state (ALVES et al., 2022), while the other, which originate from this thesis project, focus on Santarém in Pará. Both articles were published in 2022 and utilize data exclusively from the years 2019 and 2020.

Despite the critical relevance of UV radiation to public health, significant knowledge gaps persist regarding local UV levels (TERAMOTO, ESCOBEDO & MARTINS, 2014). Furthermore, there are even fewer locations that provide data on cloud cover from ground-based imagers, increasing the challenges in understanding UV exposure. The influence of clouds is difficult to accurately account for because they attenuate and enhance UV (UNEP, 2018; FOUNTOULAKIS

et al., 2019). Traditionally, human observers have been responsible for monitoring cloud cover from the ground (FONTANA et al., 2013; SILVA & SOUZA-ECHER, 2013) such as through METAR, which is the standard aerodrome weather report. However, advancements in technology have enhanced cloud observation capabilities by employing automatic ground-based and satellite imaging systems (SILVA & SOUZA-ECHER, 2013). Satellites offer a mean for systematic and continuous monitoring of cloud cover across extensive spatial areas (DAMIANI et al., 2014). They also enable other methods for cloud characterization, including the use of LER (Lambertian Equivalent Reflectivity). LER can be useful for identifying clear-sky days, as shown in the work of CADET et al. (2017), which analyzed and compared ground-based and satellite-derived UV index levels at different sites in South Africa.

The limited number of stations providing long-term UV measurements across various countries significantly restricts the ability to extrapolate this data to all populated areas (GONZÁLEZ-RODRÍGUEZ et al., 2022). A way for continuous UV monitoring is also through satellites (MARINHO & SILVA, 2013; KOSMOPOULOS et al., 2021). Satellite measurements, like ground-based observations, are affected not only by instrument errors but by uncertainties in the algorithms used to calculate surface UV radiation (BERNHARD & SECKMEYER, 1999; ZHANG et al., 2019). Therefore, it is important to evaluate satellite-based estimates of surface UV against available ground measurements from various locations around the world to characterize errors and improve these surface UV estimates (ZHANG et al., 2019). This is particularly important in the southern hemisphere, where there has been relatively limited research comparing ground-based and satellite-derived UV measurements (DU PREEZ et al., 2021).

Given these complexities, this research investigates the diurnal and seasonal variability of UV levels at five sites across low and mid-latitude South America, under both all-sky and clear-sky conditions, utilizing ground-based and satellite-derived data. The study spans from 2005 to 2022, varying according to each dataset. The sites are: Santarém in the Brazilian Amazon (2.25°S; 54.44°W, 18 m, Apogee SU-100-ss UV sensor), Natal in Northeast Brazil (05.78°S; 35.21°W, 30 m, Davis 6490 UV sensor), Itajubá in Southeast Brazil (22.41°S, 45.44°W, 885 m, Davis 6490 UV sensor), Santa Maria in the south of Brazil (29.4°S, 53.8°W, 476 m, Brewer Spectrophotometer MKIII #167), and Buenos Aires in Argentina (34.58°S, 58.48°W, 25 m, Solar Light UV Biometer – Radiometer model 501). Additionally, it compares ground-based and satellite-derived UV Index

levels from OMI at noon and overpass times, and GOME-2 at noontime during clear sky conditions, which are assessed using LER and METAR cloud cover data.

A process of data verification is important to ensure that these data can be used for long-term trend analysis or for monitoring UV exposure risks and potential impacts on human health. Additionally, because cloudy conditions complicate the comparison between ground-based and satellite-derived UV (KERR & FIOLETOV, 2008), clear-sky conditions creates a more consistent and controlled environment. This reduces the variable attenuation effects of clouds on UV radiation, allowing any differences observed between the two measurement sets to be attributed more accurately to the sensors themselves rather than other atmospheric variables. Comparisons between satellite-derived data and ground-based measurements for different places is also vital for confirming the reliability of satellite and ground-based observations.

Using different data sources and techniques, this research promotes a greater understanding of the UV variability at multiple sites, while also addressing the limitations of the instruments and methods used. Moreover, it is important to highlight that this study contributes to the scientific understanding of UV radiation levels in South America's region, particularly in Brazil, where until now, there has been relatively limited research focusing on this field of study.

Given the challenges and complexities discussed, this thesis seeks to answer the following scientific guiding questions, framed with consideration of the data limitations for each site:

Santarém:

- What is the UV temporal variability at Santarém, Brazil, under all and clear sky conditions?
- What is the monthly and seasonal variability of the UV index in Santarém, Pará, according to OMI and GOME-2?

Natal:

- What is the UV index temporal variability at Natal, Brazil, under all and clear sky conditions?
- How is the correlation between ground-based and satellite-derived UV index data for Natal, Brazil?
- Which source of satellite-derived UV index data (OMI, GOME-2) is most reliable for conducting studies of UV at Natal?

Itajubá, Santa Maria and Buenos Aires:

- What is the temporal variability of the UV index at Itajubá and Santa Maria in Brazil, and Buenos Aires, Argentina?
- How accurate and reliable are the instruments used in measuring the UV index at these locations?

1.1 OBJECTIVES

1.1.1 General objective

The main objective of this doctoral research is to analyze and characterize the temporal variability of UV at low- and mid-latitude South American sites, focusing on Santarém, Natal, Itajubá, and Santa Maria in Brazil, and Buenos Aires in Argentina, to contribute to a better understanding of UV patterns in these regions.

1.1.2 Specific objectives

1. To characterize and analyze the temporal variability of the surface UV at Santarém, Natal, Itajubá, Santa Maria, and Buenos Aires using ground-based UV data.
2. To characterize and analyze the temporal variability of surface UV in Santarém and Natal with and without the influence of cloud cover.
3. To determine the accuracy and reliability of the ground-based and satellite instruments used in measuring the UV index at Natal, Itajubá, Santa Maria, and Buenos Aires in this research.

1.2 THESIS OUTLINE

In Chapter 1, an introduction to the study is provided, including the rationale, aim, and objectives of the research.

Chapter 2 presents a theoretical review of UV radiation and the factors influencing its variability. It also includes a literature review summarizing existing research related to UV, focusing in South America, Antarctica and Brazil.

Chapter 3 brings the articles that focuses on the results of UV temporal variability in Santarém. Initially, only ground-based UV data are considered, followed by an analysis using satellite-derived UV Index data.

In Chapter 4, the article containing the time variability of the ground-based UV Index levels in Natal under both all-sky and clear-sky conditions is assessed. This chapter also compares ground-based and satellite-derived UV Index levels in Natal under clear-sky conditions.

Chapter 5 compares ground-based and satellite-derived UV Index levels from the Ozone Monitoring Instrument (OMI) during overpass times under clear-sky conditions for two Brazilian cities, Itajubá and Santa Maria, as well as Buenos Aires in Argentina. Additionally, this chapter reports the diurnal and seasonal variability of ground-based UV Index levels for these locations.

Chapter 6 summarizes the results presented for each site, discusses the strengths and limitations of the study, and offers recommendations for future research.

Chapter 7 provides the overall conclusion of the study.

2 THEORETICAL REVIEW

2.1 Solar radiation

Radiation is defined as the emission or propagation of energy in the form of electromagnetic waves (Figure 1) (YAMASOE & CORRÊA, 2016). Every body with a temperature above absolute zero (0K = 273.2ºC) emits radiation (YAMASOE, 2006). The energy emitted by the Sun (solar radiation) represents the main natural factor in the earth's radiation balance (OLIVEIRA et al., 2018).

Figure 1 – Schematic representation of an electromagnetic wave. The electric (E) and magnetic (B) field vectors, as well as the wavelength (λ). K indicates the direction in which the wave progresses.

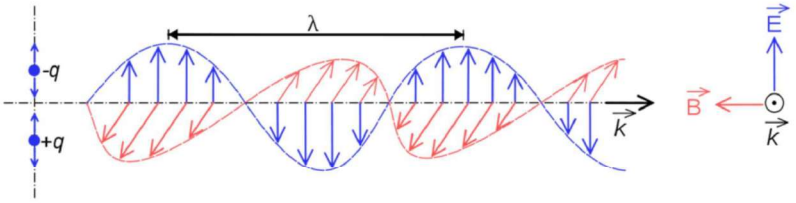

Source: Retrieved from Coariti (2017).

Solar radiation basically corresponds to a black body emission spectrum at a temperature of approximately 5250°C (Figure 2), which can be separated into groups, according to the wavelength: Visible radiation, UV, Infrared radiation, Microwaves, Radio waves, X-rays, and Gamma rays, but mostly distributed among the spectral ranges of infrared (approximately 49% of the total), visible (approximately 43% of the total) and UV (less than 10%) (GRIMM, 2006; COARITI, 2017).

Figure 2 – Solar radiation spectrum for direct light at the top of the Earth's atmosphere (yellow area) and at sea level (red area) compared with the blackbody radiation spectrum from a 5250◦C source.

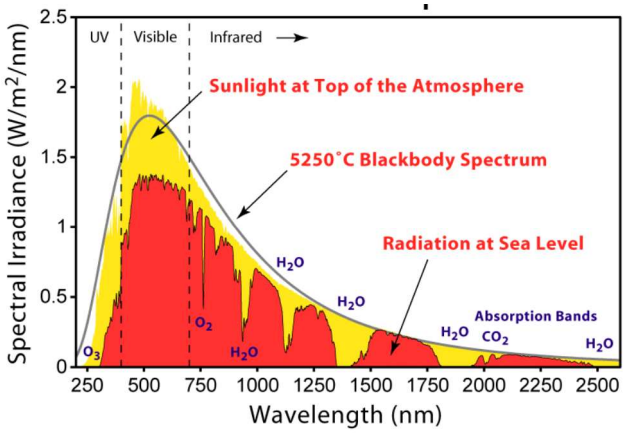

Source: Retrieved from Mazzi (2017).

The Earth continuously receives at the top of its atmosphere a flux of solar energy whose value, on average, is approximately 1.365 Wm^{-2} (OLIVEIRA et al., 2018). According to Oliveira et al. (2018) the sun also exhibits oscillations in emissions on a periodic basis, known as the solar cycle or Schwabe cycle, which last approximately 11 years. Each cycle is characterized by a variation in the appearance and disappearance of sunspots: periods of high solar activity are known as solar maximum (largest number of sunspots), and periods of reduced activity are called solar minimum (smallest number of sunspots) (Figure 3) (OLIVEIRA et al., 2018).

Figure 3 – Schwabe cycles: alternation between periods of solar maximum and minimum, as shown in the variations (since 1978) of: (A) solar radiation ($\boldsymbol{Wm^{-2}}$); (B) sunspot number.

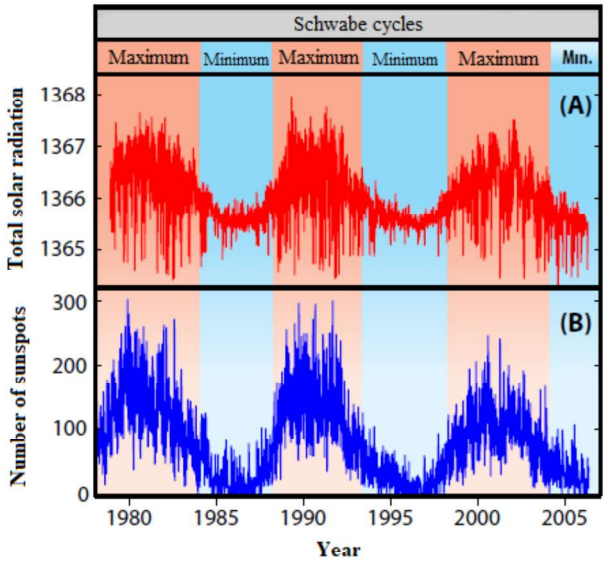

Source: Retrieved and adapted from Oliveira et al. (2018).

Although solar fluctuations influence UV levels, their role in determining UV radiation at the Earth's surface is relatively limited compared to other factors, which will be discussed in subsequent sections. As noted by Arsenovic et al. (2018) and Bernhard et al. (2023), while reduced solar emissions may slightly decrease UV-B radiation at the top of the atmosphere, weaker solar activity also reduces stratospheric ozone production. This, in turn, results in an overall increase in UV-B radiation reaching the Earth's surface. Therefore, even though solar irradiance entering the atmosphere decreases during periods of low solar activity, the associated reduction in stratospheric ozone leads to higher UV-B radiation levels at the surface (BERNHARD et al., 2023).

Only around 25% of solar radiation directly penetrates the Earth's surface without any interference (GRIMM, 2006). The rest interacts with components of the atmosphere through absorption, scattering, or reflection (Figure 4), depending directly on the wavelength of the incident radiation as well as the size and nature of the intervening material (COARITI, 2017).

Absorption results in the removal of radiative energy from the incident beam by transforming it into other forms of energy (WALD, 2018). Scattering happens when the energy incident in one direction is deflected to other directions, with the production of diffuse radiation (YAMASOE, 2006). The reflection occurs when the energy changes direction in relation to that in which it was emitted (LIOU, 2002).

Figure 4 – Processes of interaction between solar radiation and matter: transmission, reflection, scattering and absorption.

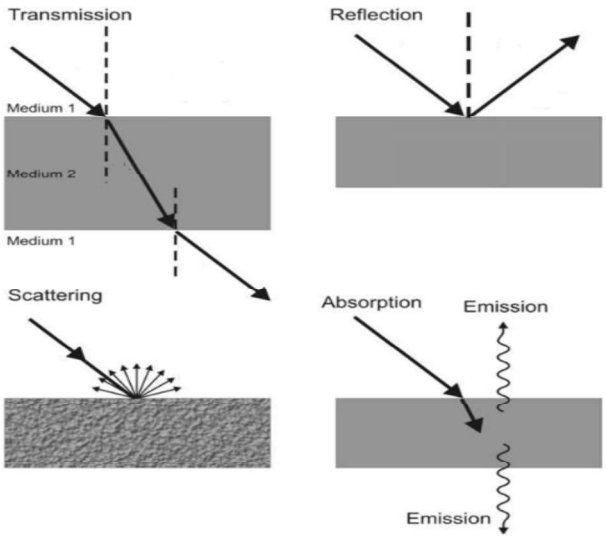

Source: Retrieved and adapted from Sofiu et al. (2011).

2.2 Solar Ultraviolet Radiation

UV is the electromagnetic spectrum band between wavelengths of 100 and 400 nm (1 nm = 1 nanometer = 10^{-9}m) (Figure 5), corresponding to less than 10% of the total solar radiation incident on the top of atmosphere (CORRÊA, 2015). For a better understanding and research, UV is divided in three regions: UV–A (315–400 nm), UV–B (280–315 nm) and UV–C (100–280 nm) (SUÁREZ et al., 2017).

Figure 5 – The electromagnetic spectrum and ultraviolet radiation subdivisions.

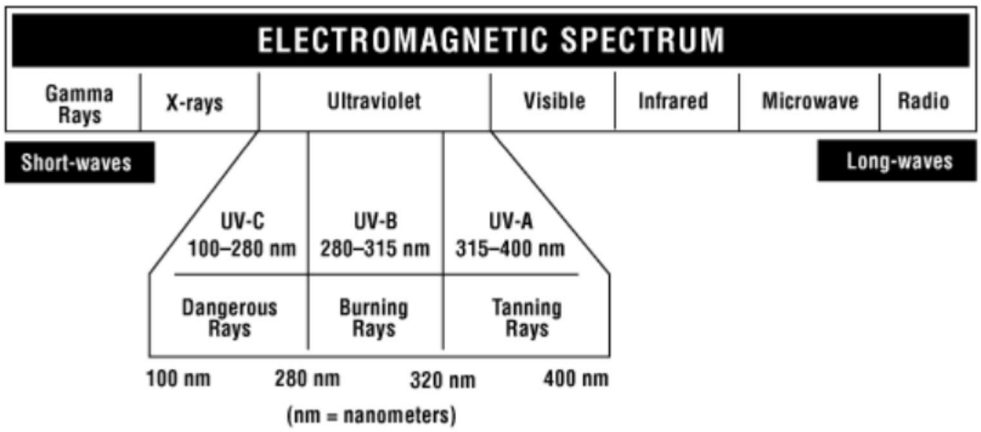

Source: Retrieved from Canadian center for Occupational Health and Safety (2022).

As sunlight passes through atmosphere, all UV–C (the most harmful UV) and approximately 90% of UV–B, considered the most biologically important because it is the only part of the UV spectrum that initiates vitamin D synthesis in the skin (LUCAS et al., 2015) are absorbed by ozone, while UV–A is the least affected by the atmosphere (LUCAS et al., 2015; SUÁREZ et al., 2017). Consequently, the UV radiation reaching the Earth's surface has a small UV–B component (6%) and is predominantly composed of UV–A (94%) (WHO, 2002; BILBAO & DE MIGUE, 2020).

The biological impact of UV intensifies at shorter wavelengths, meaning that even minor increases in UV–B radiation can lead to significant biological consequences (DIFFEY, 1991; BILBAO & DE MIGUE, 2020). The erythemal action spectrum demonstrates how different wavelengths contribute to causing erythema (sunburn) (DIFFEY, 1991). UV that is adjusted according to this spectrum is called ultraviolet erythemal radiation (UVER) (BILBAO et al., 2015). UVER is calculated by weighting the spectral curve of the incident UV at the surface with the spectral action curve proposed by the International Commission on Illumination (MCKINLAY & DIFFEY, 1987).

UVER can serve as a basis for estimating several commonly used variables, including the UV index (Figure 6), standard erythemal doses (SEDs), minimum erythemal doses (MEDs), and sun exposure time (t_{ery}) (GONZÁLEZ-RODRIGUEZ et al., 2021). The UV index is a dimensionless indicator that is usually divided into five levels of risk: UVI ≤ 2 (low); 3 ≤ UVI ≤ 5 (moderate); 6 ≤ UVI ≤ 7 (high); 8 ≤ UVI ≤ 10 (very high); and UVI ≥ 11 (extreme). This index is defined by Equation (1) (WHO, 2002).

$$UVI = K_{er} \int_{250nm}^{400nm} E_{\lambda} S_{er} d\lambda \quad (1)$$

where K_{er} is a scaing fator originally equal to $40m^2W^{-1}$, E_{λ} is the erythemal action spectrum, and S_{er} is the spectral solar irradiance at the surface Wm^2nm^{-1} (WHO, 2002; PARRA et al., 2019).

Figure 6 – The Ultraviolet Index (UVI) values ranging from lowest to highest.

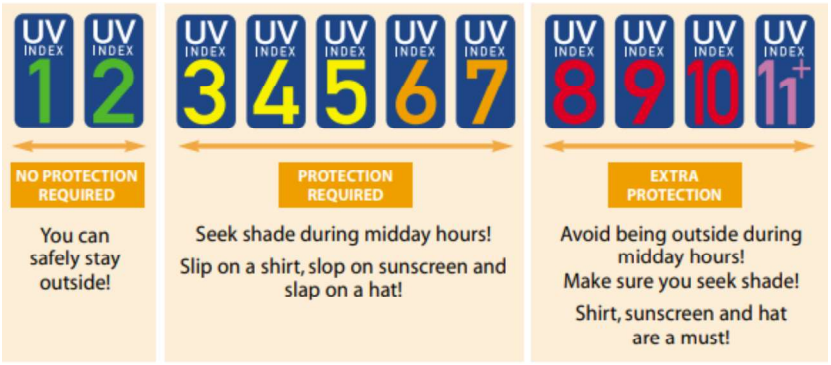

Source: Retrieved from WHO (2002).

2.3 Factors affecting surface UV

When UV penetrates the atmosphere, its intensity along the atmosphere and on the ground depend on geographic factors (altitude, latitude and type of surface), temporal (time of day and time of year), atmospheric (concentration of ozone, aerosols and clouds) and astronomical (solar zenith angle, distance from the sun) (COARITI, 2017, LAMY et al., 2021). In the following subsections, several factors affecting solar UV at the surface are presented.

2.3.1 Solar Zenith Angle (SZA)

The Solar Zenith Angle (SZA) is defined as the angle measured from the surface between the Sun and a point directly overhead the observer (DU PREZZ, 2021) (Figure 7). Smaller SZAs result in a higher solar flux reaching the Earth's surface, which is more common around noon and during the summer months (WALD, 2018; DU PREZZ, 2021).

Figure 7 – Solar zenith angle position relative to the observer.

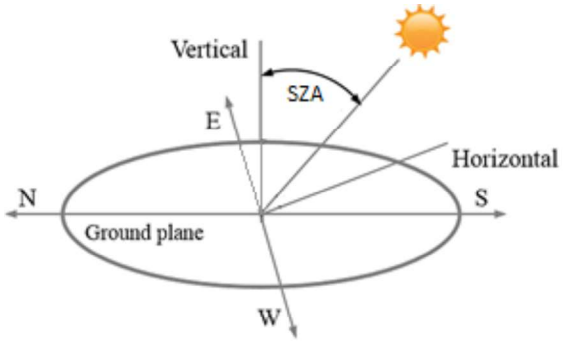

Source: Retrieved and adapted from Liu (2016).

At larger SZAs (during dawn and dusk), UV levels are reduced due to the longer path through the atmosphere, leading to greater attenuation of UV radiation from scattering and absorption by atmospheric particles and gases (WALD, 2018; COARITI, 2017; DU PREZZ, 2021).

2.3.2 Latitude and altitude

Geographic location constitutes an important factor in the analysis of UV (LAMY et al., 2021; DU PREEZ, 2021). Generally, latitudes close to the equator receive greater amounts of radiation and this UV flux decreases with increasing distance from the equator (COARITI, 2011). In the tropical zone, between the two tropics, the sun passes through the zenith twice a year (SZA=0) and, in general, the SZA are lower than at intermediate latitudes (Figure 8) (ZARATTI, 2003). Therefore, the intensity of UV depends on the latitude. Also, at a fixed latitude, the intensity of UV levels varies with the season: typically, the sun's position is higher during summer than in winter, leading to stronger UV intensity in summer compared to winter (ZARATTI, 2003).

Figure 8 – The noontime solar zenith angle varying throughout the year for four of the locations studied. Natal, located closer to the equator, generally has lower SZA values, resulting in stronger UV radiation through the year. In contrast, Itajubá, Santa Maria, and Buenos Aires, which are farther from the equator, experience higher SZA values. These higher latitude locations see stronger UV radiation in the summer when SZA values are smaller, and lower UV levels in winter when SZA values are bigger.

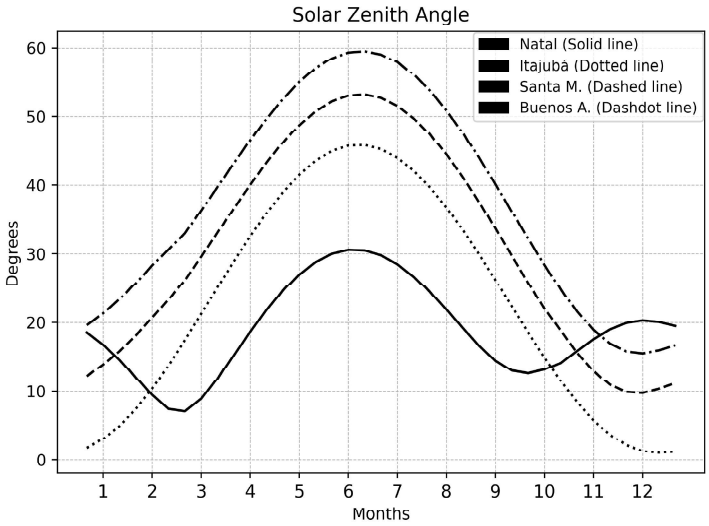

Source: Author (2023).

The dependence of surface UV with altitude is due to the reduction of the atmosphere (less scattering and absorption effects on the radiation and reduction of ozone content (ZARATTI, 2003). Also, in high altitude regions, when the surface is covered by snow, the surface albedo (percentage of energy reflected by the earth's surface) is high (KYLLIN et al., 2000). Changes in Earth's surface reflectivity, whether on land or over the ocean, can influence downwelling UV radiation (KYLLIN et al., 2000).

2.3.3 Atmospheric ozone

The concentrations of certain gases, such as ozone (O_3), in the atmosphere plays an essential role (ZARATTI, 2003; LAMY et al., 2021; PREEZ, 2021). O_3 is generated in the tropical regions due to intense solar radiation and is subsequently transported toward the poles via the Brewer-Dobson circulation (BDC). This circulation pattern involves air masses moving from the troposphere into the stratosphere in the tropics, ascending and then flowing poleward, before descending in the mid and high latitude regions (BUTCHART, 2014; LAMY et al., 2021; DU PREEZ, 2021). About 90% of atmospheric ozone resides in the stratosphere, within the so-called ozone layer (Figure 9), located between 16 and 50 km in altitude (BEKKI et al., 2009).

Figure 9 – Ozone profile with stratospheric and tropospheric ozone ranges.

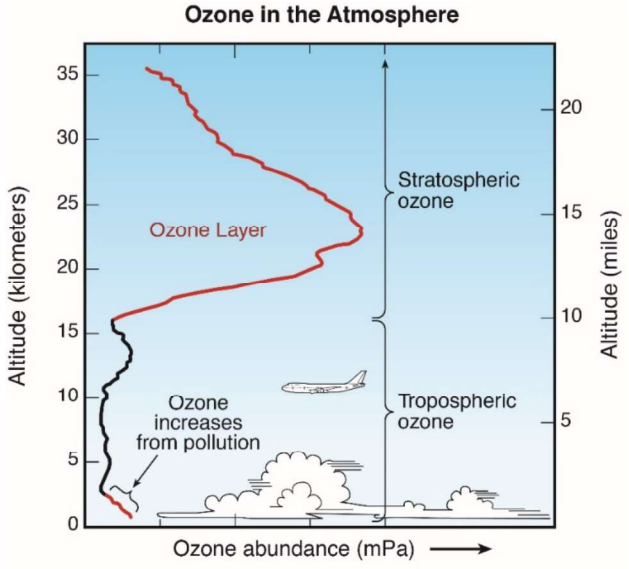

Source: Retrieved from Langematz (2019).

The amount of O_3 in the stratosphere strongly absorbs UV–C and UV–B and causes surface UV sharply decreases with decreasing wavelength (DU PREEZ, 2021). According to Lamy et al. (2018) and Bais et al. (2018), the increase in CO_2 due to human activities and climate change is expected to speed up the BDC. This faster circulation would transport ozone from the tropics to the poles more quickly, leading to an increase in the total ozone column (TOC) in mid-latitudes and a decrease in the tropics. Consequently, surface UV radiation is likely to increase in the tropics and decrease in mid-latitudes.

The need to protect the stratospheric ozone layer has been a global priority since ozone depletion was first identified (CORDERO et al., 2022). The Montreal Protocol, an international agreement signed in 1987, aimed to limit the use of ozone-depleting substances to protect ecosystems from harmful UV levels (WMO, 2018; LAKKALA, 2020). Latest studies suggests that the Antarctic ozone hole has started to recover, attributable to the Montreal Protocol, even though it continues to occur each year (LAKKALA, 2020). Significant ozone depletion results in notable increases in UV radiation levels at the surface in Antarctica, but also can reach mid-latitudes (BRESCIANI et al., 2018).

Projections of erythemal UV irradiance (expressed in terms of the UV Index) for the late 21st century (average of 2085–2095) compared to the decade of 2010–2020 suggest that ozone recovery could result in a reduction in the UV Index by about 30% over Antarctica and up to 6% over mid-latitudes (BERNHARD et al., 2023). These predictions carry some uncertainty, as future

stratospheric ozone concentrations will not only be influenced by the reduction of ozone-depleting substances (ODSs) as regulated by the Montreal Protocol, but also by the levels of other greenhouse gases like carbon dioxide and methane, which will be heavily influenced by policy decisions made in the coming decades (BERNHARD et al., 2023).

Besides O_3, other naturally occurring UV absorbers include sulfur dioxide (SO_2), which primarily absorbs UV-B, and nitrogen dioxide (NO_2), the dominant absorber in the UV-A range (Bais et al., 1993). Generally, the UV absorption by these gases is small; however, when emitted in large quantities by major volcanic eruptions, they can cause significant absorption, reducing UV levels by up to 50% (Fioletov et al., 2010).

2.3.4 Atmospheric aerosols

Aerosols are solid and liquid particles suspended in the atmosphere (UNEP, 2018) (Figure 10). It is a consensus that aerosols have an important effect on the Earth's radiation budget due to directly effects, which are from the ability of aerosols to reflect or absorb radiation, both processes leading to a dimming radiation at the Earth's surface, and indirectly effects, by altering the formation and precipitation efficiency of clouds (BEVAN et al., 2009; COSTA et al., 2016). The regional-scale aerosol layer limits solar energy reaching the surface, cools the air near the ground, and raises the portion of diffuse radiation (MOREIRA et al., 2017).

Figure 10 – These scanning electron microscope images (not scaled equally) illustrate the diverse shapes of aerosols. The samples, shown from left to right, include volcanic ash, pollen, sea salt, and soot.

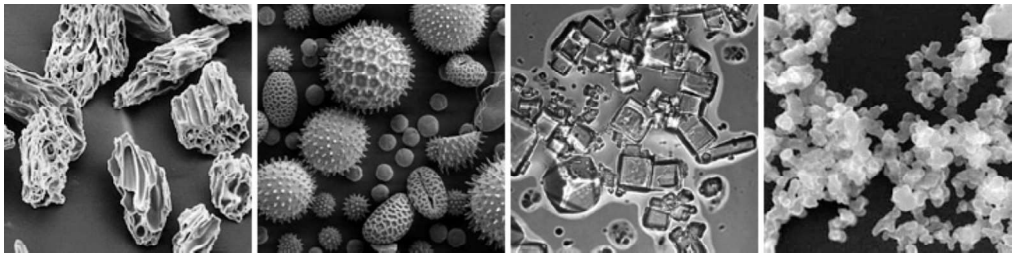

Source: Retrieved from Nasa Earth Observatory (2016).

Aerosols have different natural origins, such as the erosive action of winds on the ground and ocean surface (CARSLAW et al., 2010). It also has an anthropogenic origin, as well as the emission of particulates from fossil fuel combustion, generally abundant in regions of large urban centers, where there is a lot of industrial activity and vehicle emissions, and in rural areas aerosols are produced by suspended dust, agricultural activities or by fires (TOMASI & LUPI, 2017). In these

regions the concentrations have a lot of variability throughout the year due to the periodicity of these activities (SILVA, 2008).

The tropics and subtropics are major sources of anthropogenic aerosols, and these regions are very susceptible to the effects of enhanced atmospheric aerosol (RAMANATHAN et al., 2001). In the Amazon region, biomass burning is the primary factor influencing changes in atmospheric composition, leading to a substantial rise in the concentration of gases and particles during the dry season (ARTAXO et al., 2002; ARTAXO et al., 2009).

The radiative impact of aerosols extends beyond their origin, influencing aerosol levels and solar UV radiation in regions downwind (DU PREEZ, 2021). This effect occurs because aerosols can travel long distances, influenced by dynamic processes in both the stratosphere and troposphere (DU PREEZ, 2021). Aerosol levels have also been linked to reductions in UV levels in cities with significant air pollution. For example, in Mexico City, historical air pollution caused a decrease in the UV index under cloud-free conditions, with values about 40% lower in 2000 and about 25% lower in 2019, compared to what would be expected in a clean atmosphere (IPIÑA et al., 2021). Furthermore, the effects of increased aerosol levels and tropospheric ozone on surface UV radiation were examined during the biomass burning season in Pretoria, South Africa. The study showed that aerosols reduced the noontime UVI by 13% on cloudless days during the peak of the biomass burning period in September (DU PREEZ et al., 2021).

Volcanic aerosols, which can spread widely and stay in the atmosphere for long periods, also affect UV radiation (BERNHARD et al., 2023). These particles can either lower UV–B levels at the Earth's surface by scattering sunlight back into space or increase UV–B when they contribute to ozone layer thinning, allowing more UV through. This shows the complex relationship between aerosols, ozone and UV levels.

2.3.5 Cloud Cover

Under cloudy conditions the interaction of UV with the Earth's atmosphere is more complex. While clouds can decrease direct radiation, they can produce an increase in the amount of diffuse radiation reaching the Earth's surface (RAMAN et al., 1996, CAZORLA et al., 2008). For example, in the UV this enhancement can reach 30% (RAMAN et al., 1996). Thus, in atmospheric radiative processes not only is the total cloud cover an important parameter, but also the cloud configuration, cloud type (Figure 11), and cloud–sun apparent distance (CAZORLA et al., 2008).

Figure 11 – Different types of cloud.

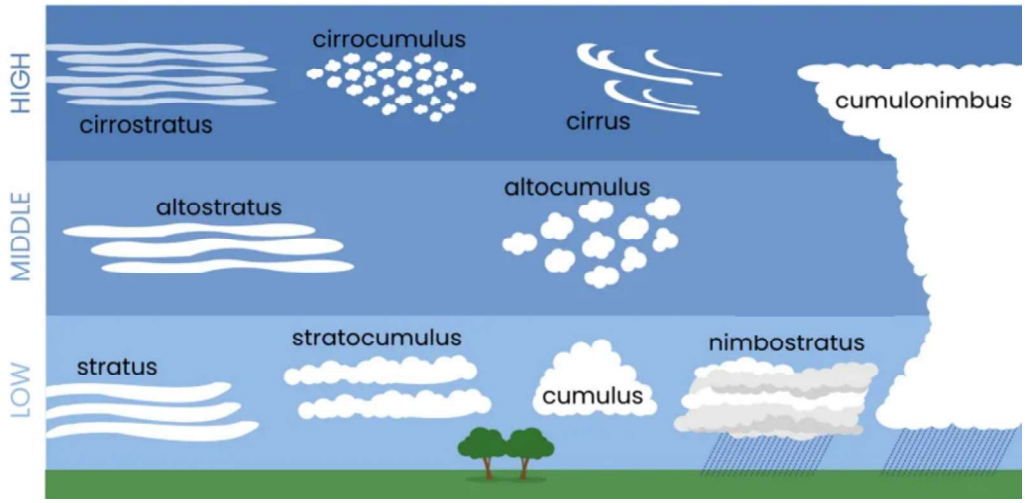

Source: Retrieved from Center for Science Education (2024).

The attenuation of UV radiation by clouds is frequently larger than any other atmospheric parameter (LOPEZ et al., 2012). Nevertheless, factors such as cloud location, percent cover, cloud optical thickness, liquid water content, and particle distribution make it difficult to develop a quantitative relationship relating cloud properties to the attenuation of UV radiation (RAMAN et al., 1996). Cloud microphysical structures and their microphysical properties (liquid/ice, water content, particle effective sizes, and distribution of water/ice particles) determine their optical characteristics, which affect absorption and scattering of solar radiation (LOPEZ et al., 2012). The most challenging problem in cloud studies is that their macro and micro physical properties are highly variable in space-time and these variations are responsible for the great variability observed in UV under cloudy skies (LOPEZ et al., 2012).

Since the 1990s, researchers have been showing the effects of cloud cover on UV radiation (RAMAN et al., 1996; CEDE et al., 2002; ANTÓN et al., 2012). However, the extent of these effects, especially UV enhancements, varies and is not fully understood (ANTÓN et al., 2012). Some studies suggest that UV levels can increase by up to 30% above clear-sky values, especially when large cloud cover does not obstruct the solar disk (CEDE et al., 2002). These effects are most prominent for clouds with 5 to 7 oktas of coverage, and are less pronounced in the UV band compared to the visible and infrared bands (PFISTER et al., 2003; PORFÍRIO et al., 2012).

Looking ahead, changes in cloudiness are projected to cause small (up to 4%) localized increases in UVI over the mid latitudes and tropics (BERNHARD et al., 2023). Therefore, even

with the presence of clouds, the population will continue to experience high levels of UV radiation, highlighting the need for adequate protection (PORFÍRIO et al., 2012).

2.4 Solar UV exposure and public health

The human skin acts as the body's outermost layer, serving as the primary barrier against various environmental factors such as microbes, particulates, irritants, allergens, and UV radiation (LEE & KIM, 2022). The skin is composed of two main layers (Figure 12): the outer layer, or epidermis, which is about 50–100 micrometers thick and the dermis, which ranges from 300 to 3000 micrometers in thickness (WANG et al., 2022). UV–A can penetrate the dermis, while UV–B affects the surface layer of the epidermis (D'ORAZIO et al., 2013). While small amounts of solar UV are beneficial for health by promoting vitamin D production (REICHRATH et al., 2017), excessive exposure can cause harmful effects. These include various skin diseases, with skin cancer being the most severe (SOLANO, 2020; TANG et al., 2024).

Figure 12 – The sun's UV rays: the UV–A (320–400 nm), can pass through the epidermis to reach the dermis; UV–B (280–320 nm), most of which is absorbed by the ozone layer, with a small portion remaining in the epidermis; and UV–C (100–280 nm), which is absorbed by the ozone layer in its entirety and can't reach the earth's surface.

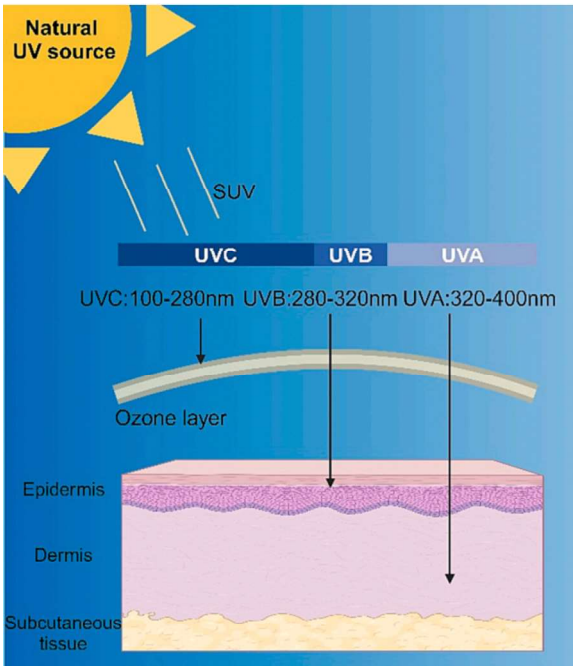

Source: Retrieved from Tang et al. (2024).

Chronic UV exposure can result in degenerative changes to the skin's cells, fibrous tissues, and blood vessels, contributing to skin aging and the development of conditions like freckles, nevi, and lentigines, pigmented areas on the skin, and diffuse brown pigmentation (KIM et al., 2022).

Individuals with fairer skin (Figure 13) are more susceptible to sunburn and skin damage compared to those with darker skin (GUPTA & SHARMA, 2019). The ability to develop a tan is also skin-type dependent (GUPTA & SHARMA, 2019).

Beyond skin-related effects, UV exposure is increasingly linked to other health conditions. For instance, low sun exposure has been associated with a higher risk of cardiovascular diseases (LINDQVIST et al., 2021). Moreover, a growing body of research suggests a connection between UV radiation and neurodegenerative conditions like Alzheimer's disease (DRAGANOVA-FILIPOVA et al., 2022). UV radiation impacts the immune system, contributes to photoaging and increasing the risk of cataracts and macular degeneration in the eyes (LEITER et al., 2020; RAIMONDI et al., 2020). Additionally, moderate UV exposure has demonstrated benefits for mental health, with studies suggesting that moderate sunlight exposure can reduce the risk of depression and improve overall well-being (BURNS et al., 2023).

Figure 13 – A numerical classification system for skin color based on how different skin types respond to UV radiation.

	Phenotype	UV sensitivity		Skin cancer risk
Type I 	Very fair, pale white, light coloured or red hair, often freckled	++++	Skin burns very easily, and never, or hardly ever, develops a tan	Greatest risk of skin cancer
Type II 	Fair, white skin, light hair, and blue or brown eyes. Some may have dark hair	+++	Skin burns easily, and tans slowly	High risk of skin cancer
Type III 	Light brown, light olive skin with dark hair and brown or green eyes	++	Skin does not burn easily, and develops a tan	High risk of skin cancer
Type IV 	Moderate brown, brown eyes and dark hair	+	Skin hardly ever burns, and develops a tan easily (Mediterranean skin type)	At risk of skin cancer
Type V 	Dark brown, brown eyes and dark hair	+/_	Skin never burns, naturally darker skin (Asian skin types)	Skin cancers are relatively rare, but those that occur are often detected at later, more dangerous stage.
Type VI 	Deeply pigmented dark brown to black, dark brown eyes and black hair	–	Skin never burns, naturally dark-coloured skin (Negroid skin types)	Skin cancers are relatively rare, but those that occur are often detected at later, more dangerous stage.

Source: Retrieved from Greinert et al. (2015).

The limited scientific understanding of UV radiation in Brazil and South America has often led to the adoption of protective measures derived from studies in Europe and the United States, (CORRÊA, 2015). However, these regions experience different UV levels at the surface, and their

populations have distinct sun-exposure habits compared to Brazil (CORRÊA, 2015). For the North hemisphere recent findings show that, under realistic conditions (summer at noontime and wearing informal clothing such as T-shirts and shorts), it takes between 27 and 38 minutes of UV exposure, depending on latitude (30–60° N), to generate sufficient vitamin D (GREINERT et al., 2015). These exposure times can already lead to erythema in individuals with sensitive skin types (I/II). For those not exposed around noon or during other seasons, longer exposure times are needed to produce adequate vitamin D (GREINERT et al., 2015).

To address these differences, the Brazilian Society of Dermatology published the Brazilian Consensus on Photoprotection (SCHALKA et al., 2014). However, further studies are needed to evaluate the impacts of UV across different regions and population habits in Brazil.

2.5 Satellite-based instruments for UV monitoring

A variety of satellite instruments have been deployed over the years to monitor atmospheric ozone and UV radiation, contributing significantly to the understanding of these critical components of the Earth's atmosphere. The TOMS – Total Ozone Monitoring Spectrometers (KROTKOV et al., 1998; KROTKOV et al., 2001), Global Ozone Monitoring Experiments (GOME and GOME–2) (BURROWS et al., 1999; KUJANPÄÄ & KALAKOSK, 2015), and the Ozone Monitoring Instrument (OMI) (LEVELT et al., 2018) aboard the Aura satellite. In more recent years, other satellite instruments have been launched to continue monitoring ozone and UV radiation from space. For instance, the TROPOspheric Monitoring Instrument (TROPOMI), positioned on the Sentinel-5 Precursor satellite launched in 2017 (LINDFORS et al., 2018), continues atmospheric gases, aerosols and UV monitoring for the European Space Agency (CORTESI et al., 2018; BERNHARD et al., 2023).

Satellite-based UV measurements are derived using radiative transfer models, which incorporate inputs such as ozone and aerosol levels, surface albedo, and cloud coverage (BROGNIEZ et al., 2016). Some of these parameters, like ozone and cloud cover, are measured directly by the satellite instrument, while others, including aerosol content and albedo, are sourced from climatological datasets (BROGNIEZ et al., 2016). The characteristics of the two satellite instruments used in this study, OMI (Ozone Monitoring Instrument) (Figure 14) and GOME-2 (second Global Ozone Monitoring Experiment) are described below.

Figure 14 – Model of the Aura spacecraft showing the location of the four instruments, HIRDLS, MLS, OMI, and TES.

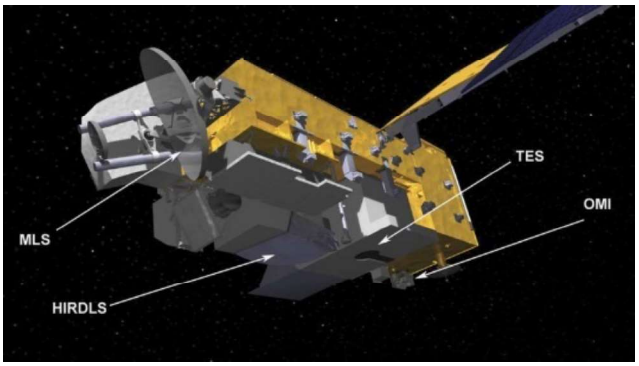

Source: Retrieved from Schoeberl et al. (2006).

The OMI instrument, onboard NASA's Aura satellite, which was launched in July 2004, operates in a sun-synchronous quasi-polar orbit (BROGNIEZ et al., 2016). It is a nadir-viewing UV/visible spectrometer designed to monitor atmospheric ozone, trace gases, aerosols, cloud cover, and surface UV levels (BROGNIEZ et al., 2016). The backscattered solar radiation by the atmosphere is measured for OMI with a spectral resolution of ~0.45 nm in the UV spectrum and with a spatial resolution at nadir of 13 km (along track) by 24 km (across track) (LEVELT et al., 2006; BROGNIEZ et al., 2016). The Aura satellite orbits at a 98.2° inclination in a sun-synchronous path at 705 km altitude, crossing the equator in the afternoon around 13:45 ± 15 minutes and completing 14 orbits daily (LEVELT et al., 2006; TAIPE et al., 2021).

The OMI surface UV algorithm builds upon the NASA Goddard Space Flight Center's UV algorithm initially created for the Total Ozone Mapping Spectrometer (TOMS) (TANSKANEN et al., 2007). The 1.2 version of the OMI algorithm first calculates clear-sky surface UV irradiance by using a radiative transfer model that incorporates total ozone column data, obtained through a separate algorithm specific to OMI, along with surface albedo from climatological data, a high-resolution extraterrestrial solar spectrum, and standard profiles of ozone and temperature (TANSKANEN, 2007; BROGNIEZ et al., 2016). Additionally, adjustments are made for the presence of nonabsorbing aerosols and cloud cover through a correction factor to estimate actual surface UV levels. The cloud cover parameter, represented by cloud optical depth (COD), is derived from OMI data. For products estimated around noon, any changes in cloud cover between the OMI overpass and noontime are not considered (JÉGOU et al., 2011). Finally, the UV Index is calculated from spectral irradiance values (BROGNIEZ et al., 2016).

According with Antón et al. (2012) and Brogniez et al. (2016), a large part of the high positive bias between OMI UVI and ground-based UVI is due to absorbing aerosols. Also, according Brogniez et al. (2016) and Kinne et al. (2013) the new algorithm version (v1.3) accounts for absorbing aerosols via an aerosol climatology, which is used in a correction factor (CF) applied to v1.2 UV estimates.

Uncertainties in OMI derived UVI arise from factors affecting clear-sky irradiance modeling, such as ozone levels and surface albedo, and from the cloud-aerosol correction factor (ANTÓN et al., 2010; BROGNIEZ et al., 2016). When the satellite's overpass time differs significantly from local noon, an additional uncertainty arises because UVI values are given for noontime while the correction factor is based on the overpass time (JÉGOU et al., 2011; BROGNIEZ et al., 2016). As a result, the overall uncertainty is estimated to be around 5%–10% in clear-sky conditions and 7%–14% in cloudy conditions (BROGNIEZ et al., 2016).

The GOME–2 is a nadir-viewing UV/VIS spectrometer that scans and measures back-scattered and reflected radiation from the Earth-atmosphere system across a spectral range of 240 to 790 nm (MUNRO et al., 2016; KUJANPÄÄ & KALAKOSK, 2015). The first GOME–2 instrument was launched in October 2006 aboard the EUMETSAT Metop–A satellite (Figure 15), followed by a second on Metop–B in September 2012. The dataset's continuity was further extended with the deployment of a third GOME–2 instrument on the Metop–C platform in November 2018 (LIU et al., 2021).

Figure 15 – Series of Metop satellites. From left to right Metop-A, Metop-B and Metop-C.

Source: Retrieved and adapted from EUMESAT – Metop series (2023).

Flying in sun-synchronous orbits, the Metop satellites equator crossing times is at approximately 09:30 LT (local time) and present repeat cycle of 29 days (412 orbits) (CHAN et al., 2022). The summary of the GOME–2 instrument characteristics is on Table 1. Consider GOME–2A the instrument onboard MetOp–A, GOME–2B the instrument onboard MetOp–B and GOME–2C the instrument onboard MetOp–C.

Table 1 – Summary of the GOME-2 instrument characteristics.

Sensor	GOME-2A	GOME-2B	GOME-2C
Operational Period	Jan 2007 - Nov 2021	Dec 2012 - Present	Jan 2019 - Present
Spectral Range	240 - 790 nm	240 - 790 nm	240 - 790 nm
Ground Pixel Resolution	80 km × 40 km / 40 km × 40 km	80 km × 40 km	80 km × 40 km
Swath Width	1920 km / 960 km	1920 km	1920 km
Equator Crossing Time	9:30 (local time)	9:30 (local time)	9:30 (local time)
Global Coverage	1.5 days	1.5 days	1.5 days

Source: Retrieved and adapted from Chan et al. (2022).

The UV processing algorithm for GOME–2 involves gridding total ozone data, calculating cloud optical depth from reflectance, and using a radiative transfer model to derive surface UV quantities (KUJANPÄÄ & KALAKOSK, 2015). GOME–2 UV products include the daily and maximum dose rates of integrated UV–B and UV–A radiation, with results adjusted by different biological weighting functions and the solar noon UV index (IALONGO et al., 2011).

Uncertainty in GOME-2-derived UV index stems from factors affecting irradiance modeling, such as variations in ozone, surface albedo, cloud cover, and aerosols. In clear-sky conditions, this uncertainty ranges from 8% to 16%, increasing to approximately 10%–20% (and up to 20%–40%) under cloudy conditions (BROGNIEZ et al., 2016).

2.6 Ground-based instruments for UV monitoring

Several types of ground-based instruments have been developed for measuring and monitoring surface UV radiation. These instruments have an extensive range of complexity, capabilities, and cost. The most complex instruments are spectroradiometers; these measure radiation wavelength by wavelength (LESZCZYNSKI, 1995; CADET, 2020). Other type of instrument are radiometers, that provides signals that correspond to irradiance integrated over a number of discrete wavelength bands (SECKMEYER et al., 2005).

Broadband radiometers are instruments that use one filter that transmits radiation over a large wavelength range (KERR & FIOLETOV 2008). In other words, unlike spectroradiometers, which measures irradiance by wavelength, radiometers measure the intensity of radiation integrated over a frequency band (CADET, 2020). Figure 16 shows an example of a spectroradiometer and a broadband radiometer.

Figure 16 – Ground-based instruments to monitor UV. From left to right, radiometer Kipp & Zonen UVS-E and BENTHAM DM 300 spectrometer.

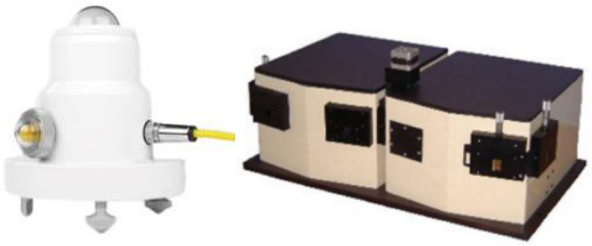

Source: Retrieved and adapted from Lamy (2018).

More information about the specific ground-based instruments used in this project can be found in Chapters 3, 4, and 5. Appendix A provides a table of some locations where ground-based UV monitoring has been performed around the world, as well as the instruments used, study period and other information.

2.7 State of the art of UV

The scientific study of light and its properties began with Isaac Newton in 1666, when he demonstrated that white light could be dispersed into a spectrum of colors (DIFFEY, 2002). According to Thomas (1991) Newton allowed sunlight to enter through a small hole in the shutter of a window and pass through a glass prism. He observed that the white light from the sun was separated into a regular series of colors, a spectrum, which he projected onto a screen (THOMAS, 1991). By passing the individual colors through a prism in the reverse position, he observed the restoration of white light. From these experiments, Newton concluded that light was composed of colors and that each was bent differently as it passed through the prism (DIFFEY, 2002). This experiment marked the beginning of spectroscopy, which enabled the future discovery of UV (DIFFEY, 2002).

Although the discovery of the visible spectrum of solar radiation was before 1700, only in 1800 William Herschel discovered infrared radiation and in 1801 Johan Ritter discovered the region of the solar spectrum known as ultraviolet radiation (DIFFEY, 2002). According to Thomas (1991) Ritter was studying the effect of the visible spectrum on silver chloride compound, a sensitive compound, which turned dark when exposed to light. He passed white light through a prism to produce the various colors and irradiated a sample of silver chloride with each specific color. He observed that violet light caused the salt to darken the most. When Ritter placed silver chloride in unlit space just beyond the violet region, the compound was darkened further. Ritter therefore

extended the electromagnetic spectrum beyond the visible region, and this new invisible part of the solar spectrum was called the ultraviolet, in other words "beyond violet" (THOMAS, 1991).

Technology has evolved and today it is possible to find a variety of research aiming at the study of UV, different methodologies, and places of application with the monitoring of UV performed with a wide range of equipment, through ground-based stations, satellites, and even with the use of portable and wearables sensors. In the next topics are some examples of UV related researcher conducted in the South America, Antarctica and specifically in Brazil.

2.7.1 Study of UV in South America

South America, with its unique and diverse environments, like the Amazon rainforest, Andes mountains, Pantanal wetlands, Cerrado, among others, has fewer published studies on UV radiation compared to other parts of the world. Additionally, the impact of the Antarctic ozone hole on southern parts of the continent adds further complexity.

Excluding Brazil, among the other South American countries, Argentina and Chile are the ones that have conducted the most studies related to UV between the 1980s and 2022. A nearly continuous data set of solar ultraviolet spectral irradiance from Ushuaia, Argentina, over the period from mid-September 1990 to mid-March 1991 was investigated by Frederick et al. (1993). This period included a season of prolonged depletion in column ozone over Antarctica, 10° or more in latitude poleward of Ushuaia. The equipment used to monitor the solar spectral irradiance at Ushuaia was a scanning spectroradiometer assembled by Biospherical Instruments. Their results indicated that during December the average noontime irradiance at 306.5 nm, was 45% larger than the mean climatological prediction. The largest noontime radiation levels observed at Ushuaia were equivalent to moving 20° in latitude closer to the equator at the summer solstice (FREDERICK et al., 1993).

Ultraviolet erythemal and total (300–3000 nm) irradiance measurements of the Argentine National Meteorologic Service Network were related to ground-based cloud observations on the work of Cede et al. (2002). No geographical dependence was observed in the effects of each cloud-type on the irradiance, from tropical to Antarctic regions. The stations of the Argentine UV net were distributed from the northernmost to the southernmost location on the continental area of Argentina and in the Antarctic continent. All the sites were equipped with UV biometers, whose measurements are given in terms of the erythemal action spectrum defined by the International Commission on Illumination (CIE). Irradiance enhancement by broken cloud fields was more

pronounced from 5 to 7 octas cloud coverage and could last even hours, with peak instantaneous values of 113% for erythemal and 133% for total irradiance, with respect to the very clean clear sky situation. In each case, the total irradiance was usually more attenuated and more enhanced by clouds than the erythemal irradiance (CEDE et al., 2002).

UV–B and total radiation values recorded at solar noon between November 1998 and December 2002 in Cordoba city, Argentina, measured using a pyranometer YES UVB–1 (UV–B) and a pyranometer YES TSP-700 (total), were analyzed by Palancar & Toselli (2004). They found out that the clear sky values for UV–B radiation calculated by using a radiative model and assuming ozone absorption were in good agreement with the experimental ones. This agreement was better than 10% for SZA <70° (PALANCAR & TOSELLI, 2004).

The relationship between UV and global radiation was also the subject of study by Argentine researchers. An analysis of broadband solar irradiation, I_T, and the erythemal UV, I_{UVER}, was conducted using measurements from 2013 to 2015 at three sites located at altitudes above 1000 m a.s.l. in Northwestern Argentina (Salta, El Rosal, and Tolar Grande) by Utrillas et al. (2018). The primary objective of this study was to develop a relationship between I_T, and I_{UVER}, that would allow the estimation of I_{UVER} in locations with limited data, particularly in areas where appropriate photoprotection measures were crucial due to dense populations and high altitudes. The daily values of I_{UVER} and I_T showing good correlation in the three measurement sites ($R^2 > 0.77$). Furthermore, the I_{UVER}/I_T increased by 0.32 ± 0.03 units per km of altitude, highlighting the more significant influence of altitude on I_{UVER} than on I_T (UTRILLAS et al., 2018).

Of the numerous studies conducted in Chile, here are some examples: Daily and annual cycles of solar ultraviolet radiation were characterized at Valdivia, Chile (39.83°S), using data collected with a multichannel radiometer (GUV-511) between January 1995 and March 1999 (LOVENGREEN, FUENZALIDA & VILLANUEVA, 2000). Also, for the city of Valdívia, Huovinen, Gómez & Lovengreen (2006) reported a study spanning five years (1998–2003) of continuous solar-irradiation measurements from a scanning spectroradiometer (SUV-100), accompanied by an evaluation of the impact of UV on marine macroalgae at this site. UV conditions showed a strong seasonal variation (HUOVINEN, GÓMEZ & LOVENGREEN, 2006).

Ground-based UV continuously measured between January 1995 and December 2011, using a multi-channel filter radiometer (PUV–510) were compared with satellite-derived data retrieved from the TOMS, the OMI, and the SCIAMACHY in the study of Cabrera et al. (2012). They found

that satellite derived UVI products largely overestimate surface UVI. The ground-based UVI measurements were significantly lower than TOMS–derived UVI data and OMI–derived UVI data.

An example of a more recently published study on the variability of UV in Chile is the work of González-Rodriguez et al. (2021). The analysis performed in their work took into consideration the effect of climate features, mainly sky conditions, on the seasonal variation of UVER in an urban area of Santiago. It was concluded that the population is exposed to a high risk of developing sunburn and/or other sun-related skin damage in 46% of days with UVI ≤ 5, even under cloudy conditions and before 11:00 local time during spring, summer, and fall, (GONZÁLES-RODRIGUEZ et al., 2021).

Regarding research focused on investigating UV in other South American countries, Coariti et al. (2017) carried out a study in which the main objective was to evaluate the behavior of the UVI levels and number of new cases of FTD (development of photodermatoses) for the period 1998-2012, in La Paz, capital of Bolivia, with 3.600 m of altitude. Information on FTD cases was collected from the “Caja Nacional de Salud” Hospital. The UV information was obtained using a Brewer spectrophotometer MKIV. A descriptive evaluation of the incidence rates of FTD, UVI and Minimum Erythematosus Dose (MED) was performed. It was observed that, regardless of the time of the year, at around midday, 94.6% of the UVI records corresponded to the "Very High and Extreme" scales, the MED for phototype IV ($450 Jm^{-2}$) was soon reached in the first two hours of the day (COARITI et al., 2017).

Yamamoto et al. (2018) conducted research in Peru, examining UV measurements across six locations, Ica, Tacna, Moquegua, Arequipa, Cajamarca, and Marcapomacocha, at altitudes ranging from sea level to 4,479 meters. This study aimed to validate and analyze the UV index along with daily erythemal doses (DEr). For accuracy, clear-sky data were filtered and compared to numerical simulations from the TUV radiation model, enabling the development of numerical regression equations. Regarding the UVI, at times close to local noon, high values were observed (6 < UVI < 7) at all locations and in all seasons of the year. The town of Marcapomacocha showed UVI measurements values higher than 20 in summer, autumn and spring (YAMAMOTO et a., 2018). During the past years, there were also UV studies in Quito Ecuador: (HUACA et al., 2018) and (PARRA et al., 2019).

2.7.2 Study of UV in Antarctica

In 1985, scientists Joseph Farman, Brian Gardiner, and Jon Shanklin reported a 30% decrease in ozone levels over Antarctica during October (FARMAN et al., 1985). This marked reduction was unprecedented in terms of its magnitude, timing, location, and seasonal pattern. The ozone depletion occurred annually each spring, concentrated in the lower stratosphere, an area previously thought to be unaffected by increased chlorine levels (DOUGLAS et al., 2014). Satellite data subsequently showed that the depleted ozone region, later called the ozone hole, expanded rapidly throughout the 1980s and reached a size comparable to North America by 1992 (DOUGLAS et al., 2014).

Most of the studies related to UV that have occurred in Antarctica have focused on investigating the increase in intensity of incident UV in response to ozone depletion. As an example, the US National Science Foundation's (NSF) Ultraviolet Spectral Irradiance Monitoring Network (UVSIMN) was established in 1987 for measuring UV at high latitudes, and included seven sites, three of which in Antarctica (BERNHARD et al., 2008). The network primarily employed SUV-100 spectroradiometers (BERNHARD et al., 2008).

The UV data from Antarctic sites has been used in the validation of satellite-derived UV radiation (KALLISKOTA et al., 2000; TANSKANEN et al., 2007). Validation of radiative transfer model calculations (KANCLER et al., 2005; BERNHARD et al., 2008); and the establishment of UV climatologies and trends (BERNHARD et al., 2008). Data have further been used by biologists analyzing the effects of UV irradiance on aquatic (SMITH et al., 1992) and terrestrial (DAY et al., 1999) ecosystems.

In 2020, the study by Bernhard and Stierle provided additional evidence that UV index levels in Antarctica were beginning to decrease during the summer months. However, no statistically significant reductions in UVI were observed during October and November, a period characterized by high UVI variability due to the presence of the ozone hole, even when data from the spring of 2019, when an unusually small ozone hole was observed, were included (BERNHARD & STIERLE, 2020).

Cordero et al. (2022) found that, despite progress in ozone recovery, the Antarctic ozone hole still forms each year, causing significant ozone loss. In late November and early December 2020, they recorded some of the highest UV levels in Antarctica in the last two decades, especially around the northern Antarctic Peninsula. On December 2nd, the UV index reached 14.3 at noon on King

George Island, close to the continent's record high. On the next day, December 3rd, the erythemal daily dose at the same site was among the highest globally, comparable to those found at high-altitude sites in the Atacama Desert, near the Tropic of Capricorn (CORDERO et al., 2022).

Furthermore, the proximity of South America to Antarctica is a relevant factor as the ozone hole is present in the southern region of the planet from the end of winter to the beginning of summer in some years This translates to higher potential health risks for the South American population and is a feature that leads researchers to investigate the variability and impacts of UV in this region.

2.7.3 Study of UV in Brazil

The monitoring of UV radiation in Brazil began in the early 1990s (KIRCHHOFF et al., 1993). To complement the existing Brazilian ozone network of Dobson spectrophotometers, three Brewer spectrophotometers were installed: one in Cuiabá (14.6°S, 56.1°W, Brewer number 056), with O_3, SO_2, and UV observations starting in October 1990; one in Santa Maria (29.4°S, 53.5°W, Brewer number 081), with measures starting in 1992; and another in Rio Branco (9.5°S, 67.5°W, Brewer number 073), which began measuring O_3, SO_2, NO_2, and UV in 1991 (KIRCHHOFF et al., 1993). Due to technical issues, such as computer failures caused by the highly variable energy supply common in the Amazon region at the time, a long-term data record was not established at Rio Branco. As a result, in 1994, the Brewer spectrophotometer was relocated to Natal. In 1997, UV measurements began in Cachoeira Paulista (23°S, 45°W) with a Brewer spectrophotometer (number 124) (ECHER et al., 1999). Although UV monitoring in Brazil started during this period, publications on UV radiation in the country do not comprehensively cover all these sites or the entire monitoring period. The following paragraphs provide examples of research conducted since the 1990s.

Time series of biologically active UV–B radiation observed at sites in Brazil, La Paz, Bolivia, and Punta Arenas, Chile, were presented by Kirchhoff et al. (2000). Regarding Brazil's data, they used measurements acquired since 1991 by the National Institute for Space Research (INPE) network of radiometers to measure UV–B at ground level. Results showed that the regions of La Paz, Campo Grande, and Natal had the highest UV–B intensities. The UV–B radiation exhibited a dependency on geographical latitude and altitude. The UV Index for summer was close to 15 in La Paz and above 12 for Campo Grande and Natal (KIRCHHOFF et al., 2000).

For the city of Botucatu in the state of São Paulo, southeast Brazil, Escobedo et al. (2006) presented equations for estimating hourly and daily UV, photosynthetic (PAR), and infrared (IR) radiation as a function of global radiation, measured between 2001 and 2005. Global irradiance was monitored using an Eppley PSP pyranometer, and UVI was measured with a CUV-3 radiometer (ESCOBEDO et al., 2006).

In the same year, Corrêa and Fattori (2006) published a study that evaluated UVI variations over São Paulo, specifically in the metropolitan region (SPMR). This study was based on observations of ozone and aerosol optical properties. For ozone content, they used satellite data from TOMS observations between 1996 and 2002, and for aerosol properties, they used surface data from a Cimel 318A photometer of the AERONET, collected between 2001 and 2002. The researchers also used a multiple scattering radiative transfer algorithm, UVGAME (Ultra-Violet Global Atmospheric Model), to calculate the UVI. The results showed high levels of UV during practically all seasons, even during high-pollution episodes commonly observed in SPMR (CORRÊA & FATTORI, 2006).

Ground–based UV observations were conducted in Tokyo, Japan; São Martinho da Serra, Brazil; and Punta Arenas, Chile by Nozawa et al. (2007). Their study used UV spectroradiometers and UV radiometers, manufactured by EKO Instrument Co., Ltd. Data from Punta Arenas revealed a sudden increase in UV–B radiation at the start of spring, suggesting that the arrival of the ozone hole could be detected from the ground (NOZAWA et al., 2007). Silva (2008) presented erythemal dose measurements obtained with a biometer solar light, for one of the densest Brazilian metropolitan area, Belo Horizonte (19.92°S, 43.94°W, 858 m a.s.l.), for the period 2005 to 2007.

In addition to research related to UV conducted in the southeast, the second region with the largest number of research investigating UV in Brazil is the northeast, especially in Natal, the capital of Rio Grande do Norte. Measurements of the UV index in Natal, taken between 2001 and 2007, using a GUV-511 C surface radiometer, were used to generate hourly mean value curves for all days during that period and monthly mean values for the same period as reported by Silva, Oliveira, and Marinho (2008). Their results indicated that besides the expected difference in values between the rainy and dry seasons, there was an increase of about 1 point between the peak hour indexes between 2001 and 2007, also, the peak of the index occurred before 12:00 (noon) in all years of the study (SILVA, OLIVEIRA & MARINHO, 2008). Other studies on UV in Natal:

(MARINHO & SILVA, 2013); (LOPO et al., 2013); (LOPO et al., 2014) and (CORRÊA et al., 2015).

The information regarding UV in Brazil is scarce with low spatial and temporal coverage (LEAL, TÍBA & PIACENTINI, 2011). This information scarcity, due to the small number of measuring stations, has directed some researchers towards the creation of computational parametric models or the generation of statistical models for the estimation of the UV radiation from the measurement of the global radiation. As example of this type of research, Leal, Tíba & Piacentini (2011) worked with measurements of daily global solar and UV radiation from 2 stations in Pernambuco, one in the city of Pesqueira and other in Araripina, for the period of 2008 to 2010. The measurement of the UV was carried out using a TURV pyranometer (Total UV Radiation) and for the measurement of the daily global solar radiation a black and White pyranometer was used. (LEAL, TÍBA & PIACENTINI, 2011).

To the capital of Pernambuco, Recife, Tíba & Leal (2012) presented a work that aimed at the elaboration of an hourly statistical model for determining the UVI from UV irradiation (A+B). Simultaneous measurements of erythemal and UV irradiance (A+B) were performed using a biometer (501B) and a total ultraviolet radiometer (TUVR). The model generated from the measurements showed a statistical performance (MBE) of 0.41% and an (RMSE) of 14.1% (TÍBA & LEAL 2012). They highlighted the need for a greater number of measurements to improve the statistical validation of the model, however, it demonstrated a good prediction accuracy for the UV Index.

Another important research from the northeast was the one conducted by Porfírio et al. (2012). In their study, they presented the first UV observations made at an agro-meteorological and radiometric station in the metropolitan region of Maceió (9.28°S, 35.49°W, 127 m). They analyzed UV variability over various timescales and investigated its fractional contribution relative to global solar radiation (G), expressed as, F_{UV} = UV/G under different sky conditions. The UV was measured using the Kipp & Zonen model CUV3 radiometer. Broadband global solar irradiance was measured with Kipp & Zonen model CM5 Pyranometer (PORFÍRIO et al., 2012). The study found that cloud cover has a greater impact on annual variations in daily UV totals than seasonal changes. Under partially cloudy conditions, multiple reflections increased UV levels by 11.1% and 18.8% compared to clear days (PORFÍRIO et al., 2012).

Papers that have analyzed UV in other cities in Brazil: São Paulo, Itajubá and Ilhéus - (CORRÊA & PIRES, 2013); Santa Maria (RS) – (SCHUCH et al., 2015), (BRESCIANI et al., 2018); Conceição das Pedras (MG) – (SILVA et al., 2016); Recife, Rio de Janeiro, São Paulo and Porto Alegre – (CORRÊA et al., 2021). In the northern region there is a very large deficit of research investigating UV. In 2022, Alves et al. (2022) described the seasonality of the UVI in the city of Humaitá, in the Amazonas state, northen Brazil. The UVI data were collected from October 2019 to September 2020 by an UVM-30A Ultraviolet Ray sensor (200 – 370 nm), connected to an Arduino Uno R3 platform. The results obtained showed that in the spring the maximum mean UVI vary from 4 to 8, in summer it is constant and equals to 4, in autumn it varies from 4 to 6 and in winter it oscillates from 8 to nearby 11. The highest values occurred during the winter, which coincides with the dry period of the region (ALVES et al., 2022).

UV can be provided as past record, nowcast or forecast. To achieve information on UV it is necessary measurements, models, and validation procedures. In Brazil and around the world researchers have sought ways to expand the UV monitoring network, to improve and develop more robust modeling techniques to investigate UV, as well as the inclusion of satellite-derived data to understand the spatial-temporal variability of UV across the globe, but especially, in as many populated areas as possible where there are no monitoring stations. This PhD thesis adds to the efforts of all the aforementioned scientists, with the goal of characterizing the temporal variability of the incident UV in low and mid-latitude South American sites.

Figure 17 shows a map indicating locations where researchers have conducted UV monitoring using ground-based instruments, based on some papers published between 1983 and 2022. It is worth noting that a systematic review was not conducted, therefore, there may be places that have conducted or are conducting UV monitoring that are not included on the map, especially in the Northen hemisphere.

Figure 17 – Some sites where UV was measured using ground-based instruments according to articles related to UV published between 1983-2022. A systematic review was not conducted, therefore, there may be places that have conducted or are conducting UV monitoring that are not included on the map.

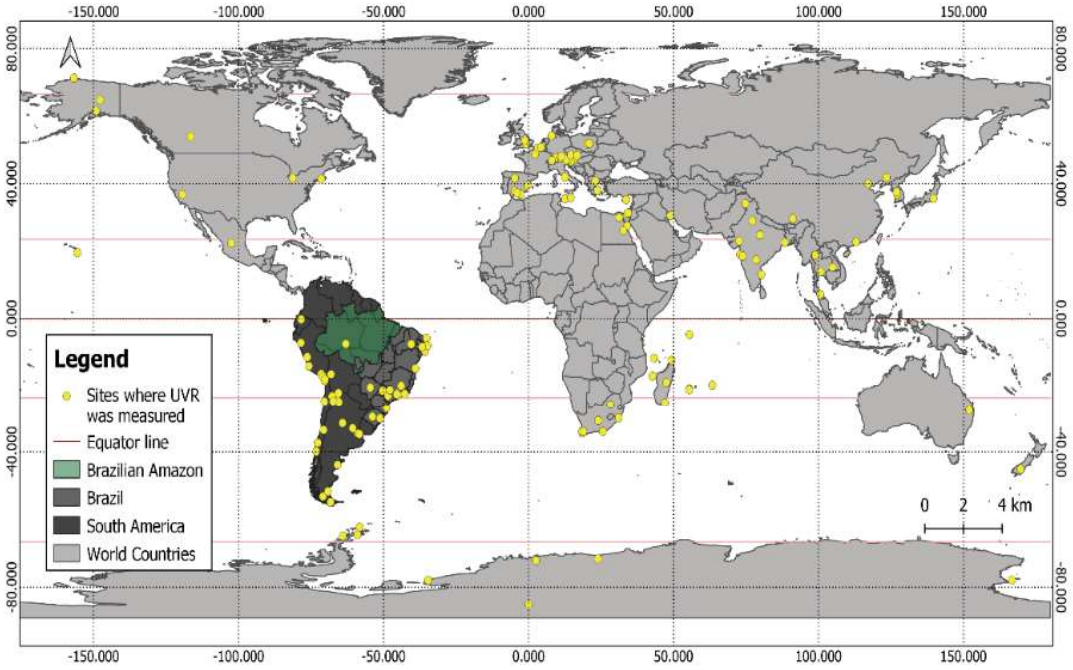

Source: Author (2023).

3 RESULTS: Temporal variability of UV radiation in Santarém using ground-based and satellite data

The results of this thesis are divided into three main sections (sections 3, 4 and 5):

Section 3: Subdivided into two subtopics, corresponding to two published articles. The first article, "Solar Ultraviolet Radiation Temporal Variability Analysis from 2-Year of Continuous Observation in an Amazonian City of Brazil" and the second, "UV Index Seasonal Variability in an Amazonian City of Brazil Based on Satellite Data."

Section 4: This section presents the findings for the city of Natal, as detailed in the paper "Comparative Analysis of Ground-Based and Satellite-Derived UV Index Levels in Natal, Brazil," which has been published.

Section 5: This section discusses the results from the study "Comparative Analysis of Ground-Based and Satellite-Derived UV Index: Variability and Reliability from Three South American Low- and Mid-Latitude Sites." While these findings have not yet been published, they were presented as a poster at EGU 2024 (European Geosciences Union General Assembly).

This division and the resulting publications emphasize the importance of understanding UV

radiation patterns at specific sites in different regions with distinct environmental characteristics and assessing the reliability of ground-based and satellite-derived data. By addressing these specific objectives, this thesis makes a significant contribution to environmental, atmospheric sciences, and public health, offering valuable data and insights that address the important and lacking research on UV radiation in regions of South America.

3.1 Article I overview and thesis contribution

UV is a highly energetic component of the solar spectrum that needs to be monitored because of the effects on human health and on the ecosystems. In Brazil, few cities monitor UV, especially in the Amazon region which is particularly poor in observation. This work was the first to address the short-term (2-year) temporal variability of UV in Santarém (2.25° S, 54.44° W, 51 m) using ground-based measurements. The irradiance in the wavelength range of 250–400 nm was investigated on different time scales. Furthermore, to understand how the UV varies without the influence of clouds, METAR was used to select the hours corresponding to the clear sky condition as well as the hours in all sky conditions.

The article "Solar Ultraviolet Radiation Temporal Variability Analysis from 2-Year of Continuous Observation in an Amazonian City of Brazil" contributes to the first and second specific objectives of this thesis, which aim to characterize the temporal variability of surface UV at Santarém and to analyze its variability with and without the influence of cloud cover. The study reveals smaller UV variation over the course of the year, as expected for a low latitude site close to the equator, even though the dry period presents higher UV values. It suggests the influence of cloud cover on UV variability, both in attenuation and enhancement, as observed when certain months in the rainy period showed more intense UV under all sky conditions compared to clear sky conditions. Due to missing data, it was not possible to confirm the expected semi-annual cycle. It will be necessary to extend the measurements over time to consolidate these results over several years and to obtain representative UV climatologies for this site, but this first study already provides a reference for other studies requiring knowledge of UV irradiance. Examples are health studies or the influence of UV on terrestrial and aquatic ecosystems. In the future, it will also be important to look at the influence of other factors on UV variability. Among these important factors are aerosol loading, atmospheric ozone amounts, and cloud cover. This study establishes a foundational reference for UV levels in Santarém, aiding in the broader understanding of UV variability across low and mid-latitude South American sites.

3.2 Publication status

REIS, Gabriela; SOUZA, Samuel; NETO, Helvécio; et al. Solar Ultraviolet Radiation Temporal Variability Analysis from 2-Year of Continuous Observation in an Amazonian City of Brazil. **Atmosphere**, v. 13, n. 7, p. 1054, 2022. Available in: https://www.mdpi.com/2073-4433/13/7/1054.

3.3 Article I

atmosphere

MDPI

Article

Solar Ultraviolet Radiation Temporal Variability Analysis from 2-Year of Continuous Observation in an Amazonian City of Brazil

Gabriela Reis [1,2,*], Samuel Souza [3], Helvécio Neto [4], Rardiles Branches [4], Rodrigo Silva [5], Lucas Peres [5], Damaris Pinheiro [6], Kevin Lamy [1], Hassan Bencherif [1] and Thierry Portafaix [1]

1 LACy, Laboratoire de l'Atmosphère et des Cyclones, UMR 8105 CNRS, Université de La Réunion, Météo-France, 97744 Saint-Denis de La Réunion, France; kevin.lamy@univ-reunion.fr (K.L.); hassan.bencherif@univ-reunion.fr (H.B.); thierry.portafaix@univ-reunion.fr (T.P.)
2 Postgraduate Program in Nature, Development and Society, Federal University of Western Pará, Santarém 68035110, Brazil
3 Postgraduate Program in Natural Resources of the Amazon, Federal University of Western Pará, Santarém 68035110, Brazil; sasouza32@gmail.com
4 National Institute Space Research, São José dos Campos 12227010, Brazil; helvecio.neto@inpe.br (H.N.); rardiles.ferreira@inpe.br (R.B.)
5 Institute of Engineering and Geosciences, Federal University of Western Pará, Santarém 68035110, Brazil; rodrigo.silva@ufopa.edu.br (R.S.); lucas.peres@ufopa.edu.br (L.P.)
6 Chemical Engineering Department, Federal University of Santa Maria, Santa Maria 97105900, Brazil; damaris@ufsm.br
* Correspondence: gabriela.godinho-dos-reis@univ-reunion.fr or gabriela.reis@discente.ufopa.edu.br; Tel.: +262-693-51-73-18

check for updates

Citation: Reis, G.; Souza, S.; Neto, H.; Branches, R.; Silva, R.; Peres, L.; Pinheiro, D.; Lamy, K.; Bencherif, H.; Portafaix, T. Solar Ultraviolet Radiation Temporal Variability Analysis from 2-Year of Continuous Observation in an Amazonian City of Brazil. *Atmosphere* **2022**, *13*, 1054. https://doi.org/10.3390/atmos13071054

Academic Editor: Antoaneta Ene

Received: 10 June 2022
Accepted: 30 June 2022
Published: 2 July 2022

Publisher's Note: MDPI stays neutral with regard to jurisdictional claims in published maps and institutional affiliations.

Abstract: Solar ultraviolet radiation (UVR) is a highly energetic component of the solar spectrum that needs to be monitored because of the effects on human health and on the ecosystems. In Brazil, few cities monitor UVR, especially in the Amazon region which is particularly poor in observation. This work is the first to address the short-term (2-year) time variability of UVR in Santarém (2°25′ S, 54°44′ W, 51 m) using ground-based measurements. The irradiance in the wavelength range of 250–400 nm was investigated on different time scales. Furthermore, to understand how the UVR varies without the influence of clouds, the hours corresponding to the clear sky condition were analyzed as well as the hours in all sky conditions. Regarding the averages, there is a slight variation over the year. In all sky and clear sky conditions, the dry season had a higher average than the rainy season, despite the slight difference. Also, both in all-sky and clear-sky conditions the maximums occurred around local solar noon, and reached a maximum of 87 W/m^2 in the dry season under the clear sky condition. Further understanding of the radiative effects of the clouds in UVR time variability is considered essential for future research. This study can serve as a reference for UVR levels in this region where no other ground-based UVR measurements are made.

Keywords: solar ultraviolet radiation; clear sky; atmospheric science; temporal variability; environmental monitoring; Amazon; Brazil

1. Introduction

Solar Ultraviolet Radiation (UVR) comprises a set of electromagnetic waves with wavelengths between 100 and 400 nm that represents a small fraction (5%) of the solar radiation that reaches the terrestrial surface [1–3]. This spectrum of solar radiation has a direct effect on human health, terrestrial and aquatic ecosystems, and the degradation of materials [4,5]. The amount of UVR reaching the Earth's surface depends on solar variations (such as Schwabe solar cycle), on the variations in the Earth's position relative to the Sun, on atmospheric, geographical, and temporal parameters which include the angle

of incoming UVR (affected by latitude, season and time of day), altitude, albedo, clouds, aerosols, and others atmospheric constituents [6–8].

For a better understanding and research, UVR is divided into three bands, depending on its transmission capability in the atmosphere and its biological effects: UVA (320–400 nm) that makes up most of the UVR received on the terrestrial surface; UVB (280–320 nm) which is partially absorbed into the atmosphere and UVC (100–280 nm) which is completely absorbed by stratospheric ozone [9].

In humans, exposure of the skin to solar radiation in the UV (ultraviolet) band results in the production of vitamin D, and it is the main source of this type of vitamin for most of the world's population [10]. Increasing evidence is identified for a range of other benefits; for example, for systemic autoimmune diseases (such as multiple sclerosis) [11], in the prevention of myopia [12] in addition, recent research suggests that adequate UVR exposure, may be substantial in reducing mortality [13].

A sharp increase in the incidence of skin cancer has been observed in populations worldwide since the early 1970s, strongly associated with personal behavior regarding sun exposure and its ultraviolet component [14]. The Brazilian National Cancer Institute (INCA) estimated for the 2020–2022 triennium about 177 thousand new cases of non-melanoma skin cancer in Brazil. In the northern region, it is the second most incident type of cancer among men [15]. Among women, it is the most incident cancer in all regions of the country [15].

Natural factors such as solar activity (11-year solar cycle), dynamical atmospheric processes (e.g., quasi-biennial oscillation (QBO)) and ocean dynamics induce changes in the atmosphere varying from each location in the world [16]. Climate change, influenced by land use change, such as deforestation, agricultural transformations, urban and industrial development also influences, for example, altering cloud cover [16,17], which is one important regulator of the radiance balance of the earth-atmosphere system [18]. Clouds can reflect and scatter solar radiation and increased cloud cover generally tends to reduce UVR on surface, but in some cases, there is an enhancement of local radiation depending on the type of clouds [19,20].

Under cloudy conditions, the interactions of UVR with the Earth's atmosphere are complex and for clear sky conditions, ozone is the main absorber and aerosols are the main contributors to UVR attenuation [21]. Every year the gas and particle emissions from tropical biomass burnings cover a large portion of South America originating from fires in the Amazon [22,23]. Aerosols reduce the direct solar radiation reaching the surface, while they increase the diffuse fraction of solar radiation [21]. Biomass-burning aerosols also act as cloud condensation nuclei affecting cloud microphysical properties and therefore change the radiation budget over disturbed areas [22–24].

In addition, it is increasingly apparent that the Amazon is under increasing threat from both climate change and human practices such as deforestation and biomass burning [24]. Amazonian cities such as Santarém, the study area of this research, may become a common pattern, thus representing a new challenge to understanding the atmosphere-biosphere interactions. For example, the presence of the urban region and the large rivers (such as the Tapajós and Amazon rivers, which pass through Santarém) alters the diurnal cycle of cloud formation and modifies the wind regime, which starts to lead to atmospheric pollution generated in cities, by burning fuels and industrial emissions, to distant regions, covered by forests or production areas [25].

Despite the importance of all these issues related to UVR for public health and sustainable development, there are knowledge deficits at local levels of UVR [19,25]. In Brazil, there are still few cities that monitor UVR and few are those that have been monitoring it continuously for more than 10 years [26]. The lack of UVR data is even greater when it comes to the Brazilian Amazon.

Therefore, given the importance of UVR, the lack of ground-based data, the uncertainty regarding the existence of trends, and both the increase or decrease in the incidence of surface UVR. The aim of this study is to characterize the temporal variability of surface UVR at different time scales (daily, monthly, seasonal) at Santarém-PA for the period of

2019–2020, a period for which we have ground-based measurement of UVR. Furthermore, in order to understand how the UVR varies without the influence of clouds, the hours corresponding to the clear sky condition were analyzed as well as the hours in all sky conditions. These findings are useful to improve the understanding of the UVR time variability at surface in an amazonian city in addition to serving as a first step for future study on the influence of cloud cover on surface UVR variability in the Amazon.

2. Materials and Methods

Santarém (2°25′ S, 54°44′ W) is situated in the western Pará, in the north of Brazil at approximately 51 m above sea level (Figure 1). The city fits into the climatic type Am, that is, the climate is humid equatorial with a well-defined dry and wet seasons [27]. The rainy season generally lasts from January to June and the dry season comprises the months between July and December [28]. It has little variability in relative humidity, air temperature, atmospheric pressure, and wind speed, due to being located in tropical latitudes close to the Equator [29].

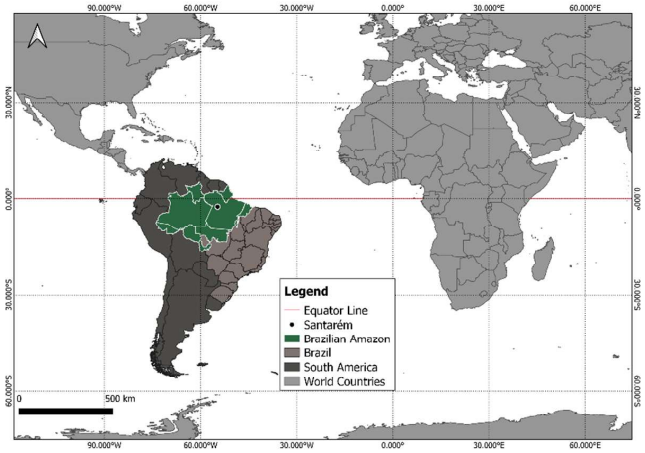

Figure 1. Map showing the location of Santarém in north Brasil.

Precipitations in the Amazon rain forest, where is Santarém, are dominated by convection with a summer rainy and a winter dry season [24]. During the nonpolluted periods in the rainy season, the atmosphere over this area has been described as a green ocean owing to very low aerosol concentrations and a maritime-like cloud regime [24,30]. In contrast, during the dry season, biomass-burning enhance aerosol concentrations [24,25].

2.1. Instruments and Data

2.1.1. Ground-Based UVR Instrument at Santarém

The UVR sensor was installed at a height of 18 m above ground level in a tower located on the UFOPA (Federal University of Western Pará) campus in Santarém (Figure 2). It was a used a UVR sensor, model SU-100-ss, manufactured by Apogee Instruments. The sensor is a photodiode designed for UVR detection in photon flow units (µmoles $s^{-1}m^{-2}$) and Wm^{-2} energy flow units. It has a spectrum range from 250 nm to 400 nm, that is, it comprises the entire UVA and UVB range. The calibration factors are 5 µmoles $s^{-1}m^{-2}$ per mV and 1.65 Wm^{-2} per mV. The sensitivity of the SU-100-ss is 0.20 mV per 1 µmoles $s^{-1}m^{-2}$, 0.61 mV per 1 Wm^{-2}, stability of ±3% change over the period of one year and an operating temperature of −40 °C to 70 °C [31]. The UVR sensor was brand new and calibrated by Apogee.

Figure 2. Tower where the UVR sensor was installed.

A two-year period of data (April 2019 to November 2020) was measured. The UVR data were collected continuously with a sampling frequency of 1 Hz, in watts per square-meter unit, and using the Campbell Scientific model CR10X data logger. The missing days are due to the period in which the sensor had not arrived and due to some technical problems.

2.1.2. Cloud Clover Data from Santarem's International Airport

Cloud cover data were obtained from METAR—data from the international airport of Santarém. Downloaded for free through the REDEMET (Air Force Command Meteorology Network) application [32] available in 1—h intervals. Metar data is the regular aerodrome weather report and contains elements such as wind, temperature, lightning, visibility, and others such as cloud height and cover [33].

Traditionally the cloud cover has been determined by human observers and The World Meteorological Organization (WMO) defines the rules for the register of cloud cover [34]. Observers estimate the cloud cover in oktas, dividing the sky into 8 regions and evaluating the regions covered by clouds (Table 1) [32,33]. Clear skies have 0 oktas, and overcast corresponds to 8 oktas [19,33,34].

Table 1. Metar sky coverage oktas and codes.

Octas	Sky Coverage Code
0	CAVOK
1	FEW
2	FEW
3	SCT (Scattered)
4	SCT (Scattered)
5	BKN (Broken)
6	BKN (Broken)
7	BKN (Broken)
8	OVC (Overcast)

2.2. Methods and Statistical Analysis

In order to understand how the UVR varies without the influence of clouds, the hours corresponding to the clear sky condition were analyzed as well as the hours in all sky conditions.

In this work, it is considered clear sky 0 oktas, denoted by the acronym CAVOK ("Ceiling in Visibility OK") and 1 to 2 oktas, denoted by the acronym FEW. [35] used a threshold of 20% of a cloud fraction measured by an all-sky camera, with up to about 70% of the clear sky condition in their survey of the Inter-Comparison Campaign of UVR Instruments under Clear Sky Conditions at Reunion Island (21° S, 55° E). Therefore, 0, 1 and 2 oktas can be used to represent clear skies, as they represent less than 30% sky coverage.

As the cloud cover data were in hourly frequency, the UVR series were grouped according to the hourly average in order to select the hours corresponding to the clear sky condition. For the 2 years of study, hours of clear sky represented 37% of the total, however, due to gaps in UVR data, this percentage was larger, 41% (Figure 3), since only the hours of sky coverage with corresponding UVR data were analyzed.

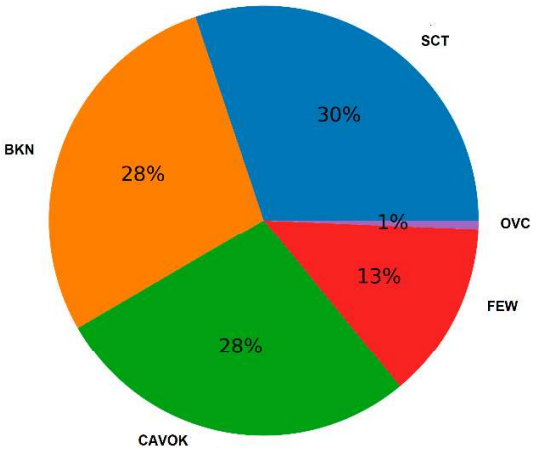

Figure 3. Cloud coverage at Santarém-PA for the 2019–2020 period.

In order to provide information about data variability, through the use of statistical measures, *boxplots* were prepared. The *boxplot* is a visual statistical method that composes a specific resource to detect trends and replace tables, besides contributing to better data interpretation, detection of outliers adend comparison of sample groups [36].

The monthly distribution of the data was also performed, as well as the seasonal distribution of the year: Rainy period (January, February, April, May, and June) and dry period (July, August, September, October, November, and December). The average over the study period for UVR in the two sky conditions was also calculated. Although the dataset does not cover a sufficient period to be climatologically significant, the monthly variability and the differences between clear sky and all-sky UVR present interesting results.

The climatology of the cloud cover using METAR data and precipitation using data obtained for free from the INMET (National Institute of Meteorology) website were also calculated (Figure 4) in order to illustrate the rainy and dry season divisions adopted in this work.

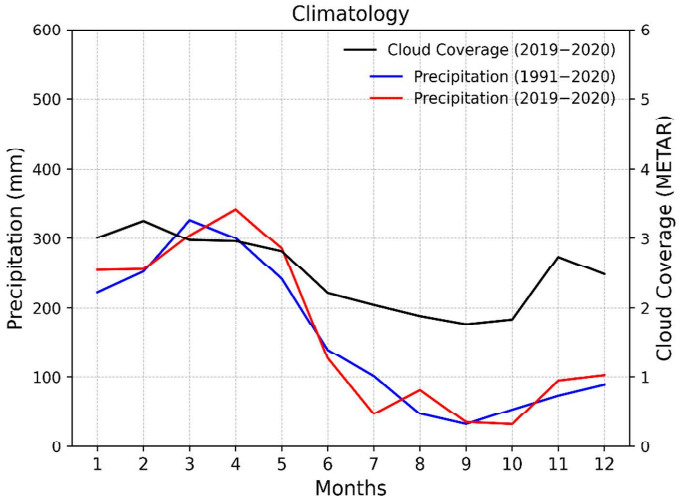

Figure 4. Cloud cover and precipitation monthly average at Santarém.

3. Results and Discussion

In this section, the UVR time variability in clear sky and all sky conditions patterns are presented to demonstrate how UVR varies without the influence of cloud cover, furthermore to understanding how seasonality influences the intensity of surface UVR in an Amazon city.

3.1. UVR Hour-Daily Series in Clear Sky and All Sky Conditions

Daily hourly averages of UVR from April 2019 to November 2020 are shown in Figure 5. Of the 731 days corresponding to the years 2019 and 2020, the UVR series obtained contains 443 days of data and thus 288 days without UVR data. Of all these days monitored, 333 had some hour of clear sky condition. A total of 3194 h of UVR data under all sky conditions and 1309 under a clear sky. In both all sky and clear sky conditions the maximums occurred around local solar noon (UTC−3) and reached a maximum of 87 W/m^2 at 11 am in November, in the dry period under clear sky condition. Although the maximum occurred at 11 am, the time of greatest intensity was at noon (Figure 6), with an average of 49.15 W/m^2 under all sky conditions and 52.24 W/m^2 under clear sky conditions. It can be observed that the hourly amplitude of UVR is greater under all sky conditions than under clear sky condition, mainly between 11 am and 3 pm. Also, intensity above 40 W/m^2 was recorded from 9 am to 3 pm, which indicates that even early in the morning (9 am) levels of UVR start being dangerous, requiring adequate sun protection. Between 6 pm and 7 pm when the sun sets, the average recorded was 2.33 W/m^2 and 2.91 W/m^2 under all sky conditions and clear sky conditions respectively.

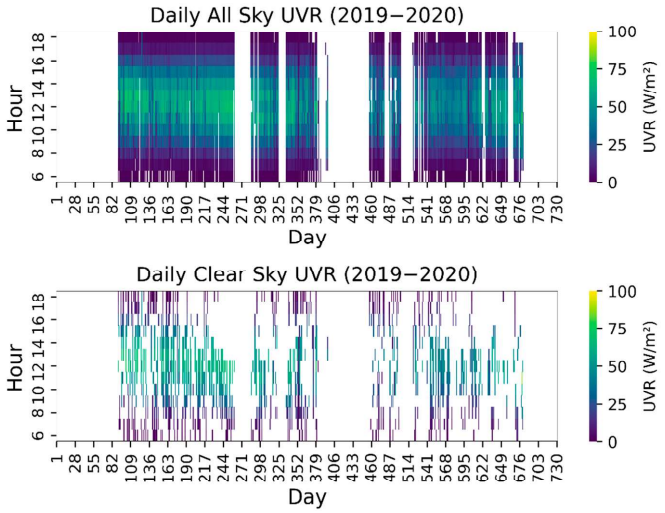

Figure 5. UVR hour-daily series in all sky and in clear sky conditions.

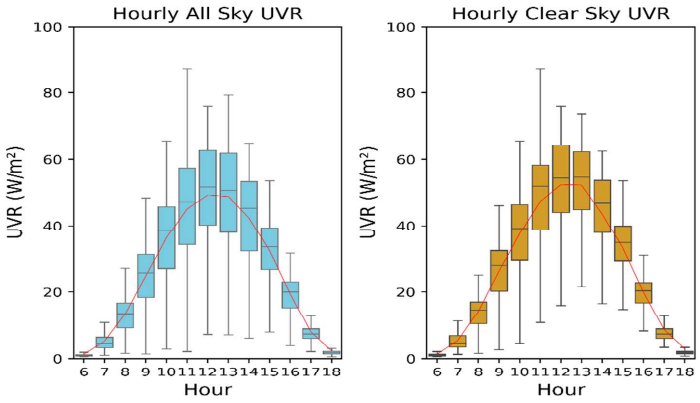

Figure 6. Hourly UVR variation under all sky and clear sky conditions, averaged over 2 years at Santarém.

Santarém is located in a tropical region, at a low latitude, close to the equator, therefore solar zenith angle (SZA) is lower throughout the year, which induces a higher UVR, smaller amplitude between the seasons, as well as a very low photoperiod variation. Predictably, the intensity of radiation on the ground is highest around solar noon when the SZA is minimum.

Global and UV irradiances had similar variation throughout the year and the maximum irradiances also occurred in the Spring/Summer months (dry period) at Maceió-Northeastern Brazil [37]. A maximum happening in months of transition to the dry period the rainy (December–January) was also reported by [4,38] in their studies of UVI variability at tropical latitudes. [4] found comparable characteristics by studying the variability of UVI at Indian Ocean stations located at different latitudes between the equator and 20° S. For example, they observed that Mahé, at 4.6° S, had a higher mean UVI than the cities more at the south and explained that the difference was due to latitude.

3.2. UVR Monthly Average in Clear Sky and All Sky Conditions

The monthly average for UVR in the two sky conditions (Figure 7) showed that, as can be seen from the boxplots, the UVR intensity is higher during the months that correspond to winter and spring in the south hemisphere, that is, between June and December, but especially between June and October. These months correspond to the dry period in this region and are characterised by less rainfall, higher temperature, and amount of aerosols in the atmosphere, due to the period of fires in the Amazon. Regarding the averages, the variation was smaller under all sky conditions. Ranging from 24.16 W/m^2 in January to 35.41 W/m^2 in September. Under clear sky condition the averages ranged from 23.49 W/m^2 in April to 37.35 W/m^2 in august. An interesting fact is that under clear sky conditions the averages were higher than at all sky conditions mostly in winter and early spring months (June to September) and presented greater amplitude in the transition between rainy and dry seasons. At a fixed latitude, the intensity of UVR depends on the season of the year: generally, in summer the sun is higher than in winter, resulting in more intense UVR in summer than in winter [39], even though, at Santarém's latitude the four seasons' characteristics are not predominantly, basic with just summer and winter divisions, indicating the dry (starting in winter in south hemisphere) and the rainy season (starting in summer). Also, the fact that under all sky condition the averages were higher than under clear conditon in some months, like in April, May, and December means that under all sky condition there is some factor that influences these higher averages, such as the presence of *cumulus* or deep *cirrus* clouds, which can produce multiple scatterings, increasing locally the UVR flux that reaches the surface [40].

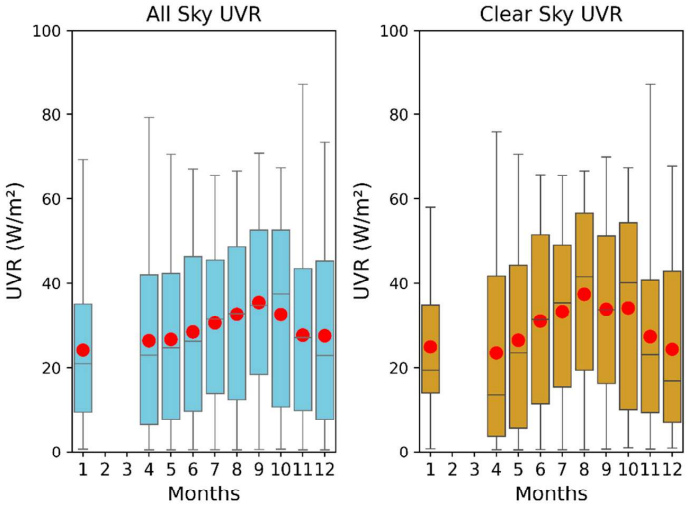

Figure 7. UVR monthly average in all sky and in clear sky condition.

Although the average, median, and third quartile are higher during the dry season months, with September being the month with more hours of higher UVR, the maximums occurred in November, followed by April, January, and December in all sky conditions. April and January are months of the rainy season, and December is a month of transition with cloud cover and pluviosity starting to increasing again, as can be seen in Figure 4. Therefore, cloud cover seems to play an important role in the variability of UV radiation, mostly by attenuation but sometimes by increasing the ground intensity. Besides, under clear sky condition, the maximums occurred in November, April, March, and September.

The fact that months of the rainy season have higher UVR intensity than months of the dry season under clear sky condition can be explained both by the fact that in rainy

season there are fewer aerosols in the air than in the dry season, when is the burning season in the Amazon and, like explained before, due to the presence of *cumulus* or deep *cirrus* clouds. In this latitude, aerosols and clouds can be expected to have a significant impact on the variability of surface UVR. [37] Observed that in the city Antananarivo, the capital of Madagascar (18.279° S, 47.564° E), aerosols also have an important impact on surface UVI variability.

In addition, the sun passes through the zenith of Santarém (equator) about twice a year at the equinoxes and this is when the highest UVR is expected [41]. In the September equinox there is a greater flow of solar radiation, a fact that added up the atmospheric characteristics of the month of September, such as longer weather with clear skies and less cloud cover, form an explanation for the higher intensity of incident UVR recorded in September. Unfortunately, due to the missing data, in this work, it is not possible to confirm the expected semi-annual cycle on the clear sky UVR during march equinox, when it's raining season and the heavy cloud cover is supposed to make the radiation levels on the ground drop.

3.3. *Average Level of UVR According to the Period in Clear Sky and All Sky Conditions*

Figure 7 reinforces the characteristics of the incident surface UVR variability discussed in the previous topics. Figure 8 shows that both in all and clear sky conditions, the dry season had a higher average than the rainy season. In clear sky condition the maximum reached 76 W/m^2 and 87 W/m^2 in rainy and dry seasons, respectively. Under all sky conditions the maximum in the rainy period was 79 W/m^2 and reaching 87 W/m^2 in the dry period, the same of the clear sky condition because all sky conditions englobe it. The area between the first and third quartiles also starts and ends at higher UVR levels in the dry season than in the rainy season, in both sky conditions, which means once again that the surface UVR intensity in the dry period is higher.

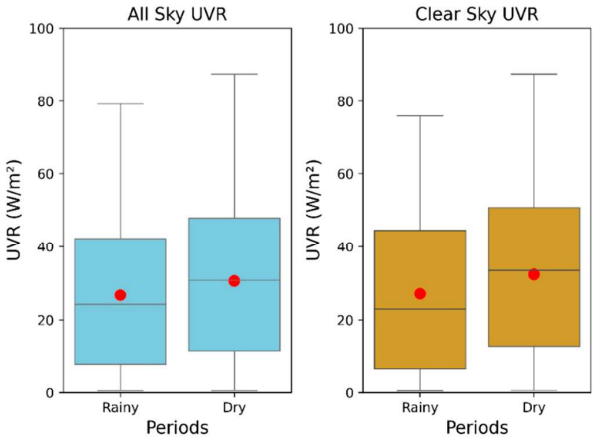

Figure 8. Variability of UVR according to the period considered (dry or wet).

In the rainy period under all sky conditions clouds can decrease direct radiation, and can also produce an increase in the amount of diffuse radiation reaching Earth's surface leading to an enhancement in surface UVR intensity, which can explain the small variation between the maximums and averages in the periods in all sky conditions, together with the latitude factor.

It is important to note that due to the missing months (February and March) the difference in UVR intensity between the dry and rainy periods may not correctly represent reality. Although it is a good indicator of what the temporal variation of UVR is like between these periods at this Amazonian site.

The characteristics of the temporal variability of the incident surface UVR under clear sky condition show that the UVR at this latitude, in the Amazon region, presents slight variation during the year, even so, the months corresponding to the dry period presents the highest intensities, demonstrating that the influence of seasonality does not happen as expected, with highest intense of UVR not happening in summer months, but in months corresponding to winter and spring in the southern hemisphere. Another factor that can influence and needs to be analyzed in the future is also the influence of aerosols, since, as already published by other authors, in the Amazon region, biomass burning is the main driver of changes in atmospheric composition, accounting for a significant increase in the particle numbers concentration in the dry season [25,42,43]. In the dry season, where biomass burning emissions are widespread, the reduction in the ground-based flux of photosynthetic active radiation (PAR) can reach values of the order of 70% [44–46]. Therefore, it is expected that this variation in the amount of aerosols also acts as an important factor influencing UVR variability and needs to be taken into account.

In summary, there is a large variation in the incident solar radiation at many locations throughout the year because of the changing angle of inclination of the Earth with respect to the Sun [47]. At the equator there is little difference, as was shown for Santarém's latitude here in this paper, with a slight UVR intensity difference between the periods. The results also indicate, as expected, that cloud cover has an influence on the variability of UVR in this region, both to dissipate and to intensify the incident UVR, for example, with the highest intensities recorded during summer months (less cloud cover) and the highest maximums in some rainy period months in all sky conditions, than in the same months in clear sky condition, indicating the presence of clouds with the characteristics to increase incident UVR. The same happens in relation to aerosols, which in months with more clear sky conditions, are the explanation for the decrease in incident UVR at the surface. The dynamics of aerosols, together with the behavior of cloud cover appears to be the main factors for the characteristics of the temporal variability of UVR at this site, under clear and under all sky conditions. In Amazonia, there are major gaps in understanding the complex relationship of biosphere-atmosphere interactions. Therefore, more long-term environmental measurements are necessary in order to substantiate the results of this first study.

4. Conclusions

Through this work, it was possible to start the monitoring of the surface UVR in Santarém and to characterize its temporal variability under clear and all sky conditions using ground-based UVR data and cloud cover METAR data.

In both all sky and clear sky conditions the maximums occurred around local solar noon. UVR showed slight variation throughout the year, even so, the months corresponding to the dry period presented the highest intensities. Of the entire study period, the maximum was reached under clear sky conditions in the dry period.

The results also indicate, as expected, that cloud cover has its influence on the variability of UVR in this region, both to dissipate and to intensify the incident UVR. These patterns are in agreement with what is reported in the literature for latitudes comparable to Santarém. Also, other factors that can influence and need to be analysed in the future are the influence of aerosols, and the influence of seasonality, which due to the missing data, in this work we could not confirm the semi-annual cycle of the clear sky.

This first study has made it possible to begin analysing the evolution of UVR on the ground at Santarém, in the Amazon region, over a period of 2 years. It will be necessary to extend the measurements over time to consolidate these results over several years and to obtain representative UVR climatologies for this site, but this first study already provides a reference for other studies requiring knowledge of UV irradiance. Examples are health studies or the influence of UVR on vegetation and forests. In the future, it will also be important to look at the influence of other factors on UVR variability. Among these important factors are aerosol loading, atmospheric ozone amounts or cloud cover.

Author Contributions: Conceptualization, R.S., G.R., L.P., T.P. and K.L.; methodology, G.R., L.P., T.P. and K.L.; software and hardware, R.S., H.N., S.S. and R.B.; formal analysis, G.R.; data curation, G.R., S.S. and H.N.; writing—Original draft preparation, G.R.; writing—Review & editing, G.R., T.P., H.B., K.L. and D.P.; funding acquisition, R.S., L.P., T.P., H.B. and D.P. All authors have read and agreed to the published version of the manuscript.

Funding: This research was funded by FAPESPA (Amazon Foundation for the Support of Studies and Research), CNPQ (National Council for Scientific and Technological Development) an entity linked to the Ministry of Science, Technology and Innovations to encourage research in Brazil, CAPES (Coordination for the Improvement of Higher Education Personnel) a foundation linked to the Brazilian Ministry of Education, CAPES project number 88887.130199/2017—01 and COFECUB (French Evaluation Committee of the University and Scientific Cooperation with Brazil).

Institutional Review Board Statement: Not applicable.

Informed Consent Statement: Not applicable.

Data Availability Statement: Data are available on request from G.R.

Acknowledgments: We acknowledge support and funding of this work by CNPQ (National Council for Scientific and Technological Development) during the main author's master's period in the post-graduate program in Natural Resources of the Amazon (PPGRNA) at the Federal University of Western Pará (UFOPA). Also, the FAPESPA for the PhD scholarship in the Post Graduate Program in Society Nature and Development. To CAPES (Coordination for the Improvement of Higher Education Personnel) and COFECUB (French Evaluation Committee of the University and Scientific Cooperation with Brazil) for the sandwich PhD scholarship awarded to the MESO project (Modeling and Prediction of the Secondary Effects of the Antarctic Ozone hole). To LACy (UMR 8105 CNRS, Météo-France) and the University of Réunion.

Conflicts of Interest: The authors declare not conflict of interest.

References

1. Corrêa, M.D.P.; Pires, L.C. Doses of erythemal ultraviolet radiation observed in Brazil. *Int. J. Dermatol.* **2013**, *52*, 966–973. [CrossRef]
2. Salas, L.F.S.; Rojas, J.L.F.; Filho, A.J.P.; Karam, H.A. Ultraviolet solar radiation in the tropical central Andes (12.0 °S). *Photochem. Photobiol. Sci.* **2017**, *16*, 954–971. [CrossRef] [PubMed]
3. Cadet, J.-M.; Bencherif, H.; Cadet, N.; Lamy, K.; Portafaix, T.; Belus, M.; Brogniez, C.; Auriol, F.; Metzger, J.-M.; Wright, C. Solar UV Radiation in the Tropics: Human Exposure at Reunion Island (21° S, 55° E) during Summer Outdoor Activities. *Int. J. Environ. Res. Public Health* **2020**, *17*, 8105. [CrossRef] [PubMed]
4. Lamy, K.; Portafaix, T.; Brogniez, C.; Lakkala, K.; Pitkänen, M.R.A.; Arola, A.; Forestier, J.-B.; Amelie, V.; Toihir, M.A.; Rakotoniaina, S. UV-Indien network: Ground-based measurements dedicated to the monitoring of UV radiation over the western Indian Ocean. *Earth Syst. Sci. Data* **2021**, *13*, 4275–4301. [CrossRef]
5. Bernhard, G.H.; Neale, R.E.; Barnes, P.W.; Neale, P.J.; Zepp, R.G.; Wilson, S.R.; Andrady, A.L.; Bais, A.F.; McKenzie, R.L.; Aucamp, P.J.; et al. Environmental effects of stratospheric ozone depletion, UV radiation and interactions with climate change: UNEP Environmental Effects Assessment Panel, update 2019. *Photochem. Photobiol. Sci.* **2020**, *19*, 542–584. [CrossRef]
6. De Oliveira, M.J.; Baptista, G.M.D.M.; Carneiro, C.D.R.; Vecchia, F.A.D.S. Ciclos climáticos e causas naturais das mudanças do clima. *Terrae Didat.* **2018**, *13*, 149–184. [CrossRef]
7. Gholamnia, R.; Abtahi, M.; Dobaradaran, S.; Koolivand, A.; Jorfi, S.; Khaloo, S.S.; Bagheri, A.; Vaziri, M.H.; Atabaki, Y.; Alhouei, F.; et al. Spatiotemporal analysis of solar ultraviolet radiation based on Ozone Monitoring Instrument dataset in Iran, 2005–2019. *Environ. Pollut.* **2021**, *287*, 117643. [CrossRef]
8. du Preez, D.; Bencherif, H.; Portafaix, T.; Lamy, K.; Wright, C. Solar Ultraviolet Radiation in Pretoria and Its Relations to Aerosols and Tropospheric Ozone during the Biomass Burning Season. *Atmosphere* **2021**, *12*, 132. [CrossRef]
9. Foyo-Moreno, I.; Vida, J.; Alados-Arboledas, L. Ground based ultraviolet (290–385 nm) and broadband solar radiation measurements in south-eastern Spain. *Int. J. Clim.* **1998**, *18*, 1389–1400. [CrossRef]
10. Bais, A.F.; Lucas, R.M.; Bornman, J.F.; Williamson, C.E.; Sulzberger, B.; Austin, A.; Wilson, S.R.; Andrady, A.L.; Bernhard, G.; McKenzie, R.L.; et al. Environmental effects of ozone depletion, UV radiation and interactions with climate change: UNEP Environmental Effects Assessment Panel, update 2017. *Photochem. Photobiol. Sci.* **2018**, *17*, 127–179. [CrossRef]
11. Lucas, R.M.; Byrne, S.N.; Correale, J.; Ilschner, S.; Hart, P.H. Ultraviolet radiation, vitamin D and multiple sclerosis. *Neurodegener. Dis. Manag.* **2015**, *5*, 413–424. [CrossRef] [PubMed]
12. Lindqvist, P.G.; Epstein, E.; Nielsen, K.; Landin-Olsson, M.; Ingvar, C.; Olsson, H. Avoidance of sun exposure as a risk factor for major causes of death: A competing risk analysis of the Melanoma in Southern Sweden cohort. *J. Intern. Med.* **2016**, *280*, 375–387. [CrossRef] [PubMed]

13. Lindqvist, P.G.; Landin-Olsson, M. The relationship between sun exposure and all-cause mortality. *Photochem. Photobiol. Sci.* **2016**, *16*, 354–361. [CrossRef] [PubMed]
14. World Health Organization; International Commission on Non-Ionizing Radiation Protection. *Global Solar UV Index: A Practical Guide*; World Health Organization: Geneva, Switzerland, 2002. Available online: https://apps.who.int/iris/handle/10665/42459 (accessed on 29 April 2021).
15. Ministério da Saúde. Instituto Nacional de Câncer José Alencar Gomes da Silva. Estimativa 2020: Incidência de Câncer no Brasil. 2019. Available online: https://www.inca.gov.br/sites/ufu.sti.inca.local/files/media/document/estimativa-2020-incidencia-de-cancer-no-brasil.pdf (accessed on 12 June 2021).
16. Fountoulakis, I.; Diémoz, H.; Siani, A.-M.; Laschewski, G.; Filippa, G.; Arola, A.; Bais, A.F.; De Backer, H.; Lakkala, K.; Webb, A.R.; et al. Solar UV Irradiance in a Changing Climate: Trends in Europe and the Significance of Spectral Monitoring in Italy. *Environments* **2019**, *7*, 1. [CrossRef]
17. EEAP. *Environmental Effects and Interactions of Stratospheric Ozone Depletion, UV Radiation, and Climate Change*; 2018 Assessment Report; Environmental Effects Assessment Panel, United Nations Environment Programme (UNEP): Nairobi, Kenya, 2018; pp. 5–18. Available online: https://ozone.unep.org/science/assessment/eeap (accessed on 23 April 2022).
18. Cadet, B.; Goldfarb, L.; Faduilhe, D.; Baldy, S.; Giraud, V.; Keckhut, P.; Réchou, A. A sub-tropical cirrus clouds climatology from Reunion Island (21°S, 55°E) lidar data set. *Geophys. Res. Lett.* **2003**, *30*, 1130. [CrossRef]
19. Cazorla, A.; Olmo, F.J.; Alados-Arboledas, L. Development of a sky imager for cloud cover assessment. *J. Opt. Soc. Am. A* **2007**, *25*, 29–39. [CrossRef]
20. Saiz-Lopez, A.; Lamarque, J.-F.; Kinnison, D.E.; Tilmes, S.; Ordóñez, C.; Orlando, J.J.; Conley, A.J.; Plane, J.M.C.; Mahajan, A.S.; Santos, G.S.; et al. Estimating the climate significance of halogen-driven ozone loss in the tropical marine troposphere. *Atmos. Chem. Phys.* **2012**, *12*, 3939–3949. [CrossRef]
21. Estupiñán, J.G.; Raman, S.; Crescenti, G.H.; Streicher, J.J.; Barnard, W.F. Effects of clouds and haze on UV-B radiation. *J. Geophys. Res. Earth Surf.* **1996**, *101*, 16807–16816. [CrossRef]
22. Moreira, D.S.; Longo, K.M.; Freitas, S.R.; Yamasoe, M.A.; Mercado, L.M.; Rosário, N.E.; Gloor, E.; Viana, R.S.M.; Miller, J.B.; Gatti, L.V.; et al. Modeling the radiative effects of biomass burning aerosols on carbon fluxes in the Amazon region. *Atmos. Chem. Phys.* **2017**, *17*, 14785–14810. [CrossRef]
23. Chand, D.; Guyon, P.; Artaxo, P.; Schmid, O.; Frank, G.P.; Rizzo, L.V.; Mayol-Bracero, O.L.; Gatti, L.V.; Andreae, M.O. Optical and physical properties of aerosols in the boundary layer and free troposphere over the Amazon Basin during the biomass burning season. *Atmos. Chem. Phys.* **2006**, *6*, 2911–2925. [CrossRef]
24. Bevan, S.L.; North, P.; Grey, W.M.F.; Los, S.O.; Plummer, S.E. Impact of atmospheric aerosol from biomass burning on Amazon dry-season drought. *J. Geophys. Res. Earth Surf.* **2009**, *114*, D09204. [CrossRef]
25. Artaxo, P.; Dias, M.A.F.D.S.; Nagy, L.; Luizão, F.J.; da Cunha, H.B.; Quesada, C.A.N.; Marengo, J.A.; Krusche, A. Perspectivas de pesquisas na relação entre clima e o funcionamento da floresta Amazônica. *Ciência e Cultura.* **2014**, *66*, 41–46. [CrossRef]
26. Teramoto, É.T.; Escobedo, J.F.; Martins, D. Modelos estatísticos para estimativa da irradiação solar UV horária em Botucatu/SP/Brasil. *Rev. Bras. De Energ. Sol.* **2014**, *5*, 44–51. Available online: https://rbens.emnuvens.com.br/rbens/article/view/107 (accessed on 15 April 2022).
27. Alvares, C.A.; Stape, J.L.; Sentelhas, P.C.; Moraes, G.J.L.; Sparovek, G. Köppen's climate classification map for Brazil. *Meteorol. Z.* **2013**, *22*, 711–728. [CrossRef]
28. Jacinto, A.I.; Simas, M.T.M.; Bianchi, R.; Oliveira, K.N.; Rech, C.M.C.B. Aspectos Físicoterritoriais e Atrações Turísticas do Município de Santarém, Pará. 2006. Available online: http://www2.ifes.com.br/webifes/revista/REVIST (accessed on 11 May 2022).
29. de Pádua Andrade, S.C.; de Jesus Corrêa, J.A.; Mestre em Meteorologia, U.A.D.; Grande, P.B.C. Estimativa do saldo de radiação instantâneo à superfície para a cidade de Santarém-PA, através de imagens do Landsat 5-TM. *Rev. Bras. Geogr. Física* **2014**, *7*, 653–661. [CrossRef]
30. Williams, E. Contrasting Convective Regimes over the Amazon: Implications for Cloud Electrification. *J. Geophys. Res.* **2002**, *107*, 8082. [CrossRef]
31. Apogee Instruments. Ultraviolet Sensor Model SU-100 Manual. Available online: https://www.apogeeinstruments.com/content/SU-100-spec-sheet.pdf (accessed on 11 March 2019).
32. Redemet (n.d.). API Redemet. Available online: https://www.redemet.aer.mil.br/?i=facilidades&p=api-redemet) (accessed on 29 April 2021).
33. Como Decodificar o METAR e o SPECI. Força Aérea Brasileira. Available online: https://ajuda.decea.mil.br/base-de-conhecimento/como-decodificar-o-metar-e-o-speci/ (accessed on 28 April 2021).
34. Silva, A.A.; Souza-Echer, M.P. Ground-based observations of clouds through both ver automatic imager and human observation. *Meteorol. Appl.* **2015**, *23*, 150–157. [CrossRef]
35. Cadet, J.-M.; Portafaix, T.; Bencherif, H.; Lamy, K.; Brogniez, C.; Auriol, F.; Metzger, J.-M.; Boudreault, L.-E.; Wright, C.Y. Inter-Comparison Campaign of Solar UVR Instruments under Clear Sky Conditions at Reunion Island (21° S, 55° E). *Int. J. Environ. Res. Public Health* **2020**, *17*, 2867. [CrossRef]
36. Neto, J.V.; dos Santos, C.B.; Torres, É.M.; Estrela, C. Boxplot: Um recurso gráfico para a análise e interpretação de dados quantitativos. *Odontológica Bras. Cent.* **2017**, *26*, 1–6. Available online: https://www.robrac.org.br/seer/index.php/ROBRAC/article/view/1132/897 (accessed on 8 January 2022).

37. Porfirio, A.C.S.; De Souza, J.L.; Lyra, G.B.; Lemes, M.A.M. An assessment of the global UV solar radiation under various sky conditions in Maceió-Northeastern Brazil. *Energy* **2012**, *44*, 584–592. [CrossRef]
38. Lamy, K.; Portafaix, T.; Brogniez, C.; Godin-Beekmann, S.; Bencherif, H.; Morel, B.; Pazmino, A.; Metzger, J.M.; Auriol, F.; Deroo, C.; et al. Ultraviolet radiation modelling from ground-based and satellite measurements on Reunion Island, southern tropics. *Atmos. Chem. Phys.* **2018**, *18*, 227–246. [CrossRef]
39. Sacchetti, F.Z.; Gisbert, R.F. La Radiacion Ultravioleta en Bolivia. 2003. Available online: https://iris.paho.org/handle/10665.2/31072 (accessed on 10 February 2022).
40. Corrêa, M.D.P.; Godin-Beekmann, S.; Haeffelin, M.; Brogniez, C.; Verschaeve, F.; Saiag, P.; Pazmiño, A.; Mahé, E. Comparison between UV index measurements performed by research-grade and consumer-products instruments. *Photochem. Photobiol. Sci.* **2010**, *9*, 459–463. [CrossRef] [PubMed]
41. Sentelhas, P.C.; Pereira, A.R.; Angelocci, L. Meteorologia agrícola. Departamento de Física e Meteorologia. ESALQ/USP. 2000. Available online: https://www.yumpu.com/pt/document/read/50581317/apostila-meteorologia-agra-cola-2007-leb-esalq-usp (accessed on 18 January 2022).
42. Longo, K.M.; Freitas, S.R.; Andreae, M.O.; Yokelson, R.; Artaxo, P.; Rizzo, L.V.; Paixão, M.; De Lucca, S.; Oliveira, P.H.; Lara, L.L.; et al. Biomass burning in Amazonia: Emissions, long-range transport of smoke and its regional and remote impacts. In *Amazonia and Global Change*; American Geophysical Union: Washington, DC, USA, 2009; Volume 186, pp. 207–232. [CrossRef]
43. de Sá, S.S.; Rizzo, L.V.; Palm, B.B.; Campuzano-Jost, P.; Day, D.A.; Yee, L.D.; Wernis, R.; Isaacman-VanWertz, G.; Brito, J.; Carbone, S.; et al. Contributions of biomass-burning, urban, and biogenic emissions to the concentrations and light-absorbing properties of particulate matter in central Amazonia during the dry season. *Atmos. Chem. Phys.* **2019**, *19*, 7973–8001. [CrossRef]
44. Cirino, G.G.; Souza, R.A.F.; Adams, D.K.; Artaxo, P. The effect of atmospheric aerosol particles and clouds on net ecosystem exchange in the Amazon. *Atmos. Chem. Phys.* **2014**, *14*, 6523–6543. [CrossRef]
45. Eck, T.F.; Holben, B.N.; Reid, J.S.; O'Neill, N.T.; Schafer, J.S.; Dubovik, O.; Smirnov, A.; Yamasoe, M.A.; Artaxo, P. High aerosol optical depth biomass burning events: A comparison of optical properties for different source regions. *Geophys. Res. Lett.* **2003**, *30*, 2003GL017861. [CrossRef]
46. Procopio, A.S.; Artaxo, P.; Kaufman, Y.J.; Remer, L.A.; Schafer, J.S.; Holben, B.N. Multiyear analysis of amazonian biomass burning smoke radiative forcing of climate. *Geophys. Res. Lett.* **2004**, *31*, L03108. [CrossRef]
47. Hatfield, J.L.; Sauer, T.; Prueger, J. Radiation Balance. In *Encyclopedia of Soils in the Environment*; Elsevier: Amsterdam, The Netherlands, 2005; pp. 355–359. [CrossRef]

3.4 Article II overview and thesis contribution

The UV index is a dimensionless indicator designed to report the intensity of UV incident on the Earth's surface. It has five exposure categories, ranging from low to extreme, with recommended sun protections at each level. The higher the value, the greater the health risk. With only few stations reporting long-term ground-based UV measurements in several countries, which significantly restricts its extrapolations to all populated areas, a way for continuous monitoring UV on a global scale is through satellites. In this work, the monthly and seasonal variability of the incident UVI in Santarém, Pará, was analyzed. For this, a 13-year time series of daily noontime UVI data from the OMI satellite instrument was used, as well as the 13-year noontime UVI time series from the GOME-2 satellite instrument.

This paper "UV Index Seasonal Variability in an Amazonian City of Brazil Based on Satellite Data" contributes to the first specific objective of this thesis by analyzing the temporal variability of the UV index (UVI) in Santarém. Using 13-year time series data from OMI and GOME-2 satellite instruments, the study highlights expected UVI patterns in Santarém due to its low latitude, with averaged UVI levels ranging from high to extreme around solar noon and minimal seasonal variation. Both OMI and GOME-2 showed two annual maxima at the equinoxes. A divergence was found: OMI recorded higher UVI averages during rainy months, while GOME-2 showed higher values in dry period months. The comparison of monthly UV index and solar zenith angles indicated that the lowest solar zenith angles months are in austral spring at Santarem's latitude, therefore the highest UV index levels are expected be in this period too, corroborating with the GOME-2 results. Nevertheless, without longer ground-based time series, it remains challenging to confirm the exact timing of peak UV levels in Santarém. This article is significant for using satellite data to assess the UV index levels in a region where, at the time of the research, there were no ground-based instruments measuring or reporting it.

3.5 Publication status

REIS, Gabriela Cacilda Godinho dos; PERES, Lucas Vaz; SILVA, Rodrigo da; et al. UV index seasonal variability in an Amazonian city of Brazil based on satellite data. **Ciência e Natura**, v. 45, n. esp. 2, p. e76670, 2023. Available in: https://doi.org/10.5902/2179460X76670.

3.6 Article II

UV index seasonal variability in an Amazonian city of Brazil based on satellite data

Gabriela Cacilda Godinho Dos Reis, Hassan Bencherif, Kevin Lamy, Lucas Vaz Peres, Marco Antonio Godinho Dos Reis, Damaris Kirsch Pinheiro, Rodrigo Da Silva, Thierry Portafaix

UFSM

CIÊNCIA e NATURA

ISSN 2179-460X
OPEN ACCESS

Ci.e Nat., Santa Maria, v. 45, spe. n. 2, e76670, p. 01–17, 2023 • https://doi.org/10.5902/2179460X76670
Submitted: 25/04/2023 • Approved: 09/05/2023 • Published: 22/11/2023

Special Edition

UV index seasonal variability in an Amazonian city of Brazil based on satellite data

Variabilidade sazonal do Índice UV em uma cidade Amazônica do Brasil com base em dados de satélite

Gabriela Cacilda Godinho dos Reis [II], Lucas Vaz Peres [II], Rodrigo da Silva [II], Marco Antonio Godinho dos Reis [I], Damaris Kirsch Pinheiro [I], Kevin Lamy [III], Hassan Bencherif [III], Thierry Portafaix [III]

[I] Universidade Federal de Santa Maria, Santa Maria, RS, Brazil
[II] Federal University of Western Pará, Santarém, PA, Brazil
[III] University of Reunion Island, Saint-Dennis, Réunion, France

ABSTRACT

The solar ultraviolet radiation - UV (280-400 nm) is a highly energetic component of the solar spectrum that needs to be monitored especially because of the effects on human health and on the ecosystems. The UV index (UVI) is a dimensionless indicator designed to report the intensity of UV incident on the Earth's surface. It has five exposure categories, ranging from low to extreme, with recommended sun protections at each level. The higher the value, the greater the health risk. With only few stations reporting long-term ground-based UV measurements in several countries, which significantly restricts its extrapolations to all populated areas, a way for continuous monitoring UV on a global scale is through satellites. In this work, the monthly and seasonal variability of the incident UVI in Santarém, Pará, was analyzed. For this, a 13-year time series of daily UVI data from the OMI satellite instrument was used, as well as the 13-year UVI time series from the GOME-2 satellite instrument. According to the results, the dry period (July to December) shows higher average UVI than the rainy period (January to June) for the GOME-2 time series. The rainy period, on the other hand, in both series presents greater amplitude in the variability of the UVI.

Keywords: Solar ultraviolet radiation; Temporal variability; Santarém-Brazil

RESUMO

A radiação solar ultravioleta - UV (280-400 nm) é um componente altamente energético do espectro solar que precisa ser monitorado especialmente devido aos efeitos sobre a saúde humana e sobre os ecossistemas. O índice UV (IUV) é um indicador sem dimensões projetado para relatar a intensidade

do incidente UV na superfície terrestre. Ele tem cinco categorias de exposição, variando de baixa a extrema, com as proteções solares recomendadas em cada nível. Quanto maior o valor, maior é o risco à saúde. Com apenas poucas estações relatando medições UV de longo prazo no solo em vários países, o que restringe significativamente suas extrapolações para todas as áreas povoadas, uma forma de monitoramento contínuo da radiação UV em escala global é através de satélites. Neste trabalho, a variabilidade mensal e sazonal do IUV em Santarém, Pará, foi analisada. Para isto, foi utilizada uma série temporal de 16 anos de dados diários de IUV derivados do instrumento de satélite OMI, bem como a série temporal de IUV de 13 anos do instrumento de satélite GOME-2. De acordo com os resultados, o período seco (julho a dezembro) mostra uma média de IUV maior do que o período chuvoso (janeiro a junho) para a série temporal do GOME-2. O período chuvoso, por outro lado, em ambas as séries apresenta uma maior amplitude na variabilidade do IUV.

Palavras-chave: Radiação solar ultravioleta; Variabilidade temporal; Santarém-Brasil

1 INTRODUCTION

Solar Ultraviolet Radiation (UV) is an important environmental parameter, affecting living organisms, materials, and atmospheric chemical processes (Medhaug et al., 2009). UVR corresponds to electromagnetic waves with wavelengths of 100-400 nm, constituting approximately 5% of the energy emitted by the sun (Cadet et al., 2020). Beside this small percentage, UVR affects the biosphere having both benefits and detrimental effects, whose relative importance depends strongly on time of exposure, latitude, season and on various meteorological parameters like total ozone, clouds, aerosols, and surface albedo (Porfírio et al., 2012; Brogniez et al., 2016).

Diseases related to the accumulation of UVR exposure, like skin cancer and cataract, are largely preventable with proper sun protection (Who, 2002). In view of the need for this type of information, the World Health Organization – WHO released the Ultraviolet Index - UVI, a dimensionless indicator that inform the amount of UVR that reaches the Earth's surface and has varying values on a scale from 0 to 11 or more (Who, 2002). Based on this scale, the Who defines five exposure categories, ranging from low to extreme, with recommended protections at each level.

UVR data measured by ground-based monitoring stations comprise an essential component of datasets of UVR, however, these measuring facilities are limited in

number at only certain locations due to the cost of these facilities and the need for skilled maintenance personnel (Parisi et al., 2021). With only few stations reporting long-term UVR measurements in several countries (like Brazil), which significantly restricts its extrapolations to all populated areas (Gonzáles-Rodríguez et al., 2022), the only way for continuous monitoring UVR on a global scale is through satellites, although ground-based monitoring of UVR is more accurate than satellite retrievals (Kosmopoulos et al, 2021).

In Brazil, there are still few cities monitoring surface UVR, and fewer are those monitoring it continuously for more than 10 years (Teramoto et al., 2014). In the Brazilian Amazon region, the lack of ground-based UVR data is even greater (Reis et al., 2022) with only two published papers using ground-based UVR measurements in the region. One for the city of Humaitá in the state of Amazonas (Alves et al., 2022). The other one, for the city of Santarém, state of Pará, both published in 2022 and using only data referring to the years 2019 and 2020 (Reis et al., 2022).

In addition, the Amazon region is under increasing threat from both climate change and human practices such as deforestation and biomass burning (Bevan et al., 2009). Thus, cities such as Santarém, the study area of this research, may become a common pattern, representing a new challenge to understanding the atmosphere-biosphere interactions. Furthermore, even with the importance of monitoring UVR, especially in a tropical region, at a low altitude, where there is a low photoperiod variation and higher UVR throughout the year (Reis et al., 2022), Santarém does not have a ground-based weather station monitoring UVR over a long period, and satellite data is needed for a better understanding of how UVR varies in this area.

Therefore, given the UVR importance and the lack of ground-based data the aim of this study is to characterize the monthly and seasonal variability at Santarém, Pará, using satellite data. This research represents an important scientific contribution regarding UV patterns in an Amazonian city. In addition, to serve as a basis for future research, for better understanding about UV variability and to be considered for the development of an excess UV exposure prevention strategy.

2 MATERIAL AND METHODS

Santarém (2°25'S, 54°44'W) is situated in the Western Pará, in North of Brazil at approximately 51 m above sea level (Figure 1).

Figure 1 – Map showing the location of Santarém in north Brazil

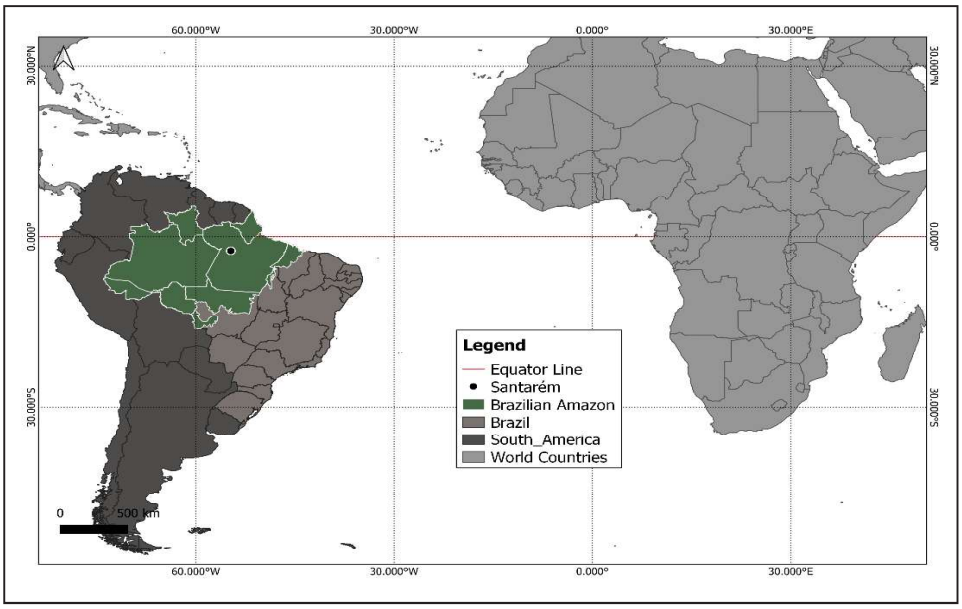

Source: Authors (2022)

The climate in Santarém is humid equatorial with a well-defined dry and wet seasons (Alvares et al., 2013). Precipitation in Santarém is dominated by convection with a summer rainy and a winter dry season (Bevan et al., 2009). The rainy season generally lasts from January to June. The dry season comprises the months between July and December (Jacinto et al., 2006). This area also presents small variability in relative humidity, air temperature, atmospheric pressure, wind speed and UVR, due its location at tropical latitude, close to the Equator (Andrade & Corrêa, 2014; Reis et al., 2022).

2.1 UV index derived from satellite-based instruments

The main objective of this study is to characterize the temporal variability of UVR in monthly and seasonal time scale. To this end, daily time series of UVI obtained from the OMI instrument (Ozone Monitoring Instrument) on board the AURA satellite and from GOME-2 instrument (Global Ozone Monitoring Experiment) on board the Metop-A/B/C satellites are used. All this data is available online and free for download through the websites listed on table 1.

Table 1 – Satellite sources of UV index data

Satellite	Instrument	Type of data	Time	Website
AURA	OMI	UVI	01/2008–12/2021	https://giovanni.gsfc.nasa.gov/giovanni/
Metop-A/B/C	Gome-2	UVI	01/2008–12/2021	https://safserver.fmi.fi/index.html

Source: Organized by the authors (2022)

The study period is from 2005 to 2021, varying according to each data source (Table 1 - Time). The UVI is a dimensionless indicator, usually divided into five risk categories: UVI < 2 (low); 2 ≤ UVI < 5 (medium); 5 ≤ UVI < 7 (high); 7 ≤ UVI < 11 (very high); and UVI ≥ 11 (extreme). This index is defined by the equation (1) (WHO, 2002).

$$UVI = K_{er} \int_{250nm}^{400nm} E_{\lambda} S_{er} d\lambda \quad (1)$$

where is a scaling factor originally equal to 40m2W-1,Eλ is the erythemal action spectrum, and is the spectral solar irradiance at the surface (Who, 2002; Parra et al., 2019).

2.2 OMI data

The OMI is a nadir viewing spectrometer that measures solar reflected and backscattered light in a selected range of ultraviolet and visible spectrum (Levelt et al., 2006, Ialongo et al., 2011). This instrument is onboard the NASA EOS Aura spacecraft,

flying in a sun-synchronous polar orbit since July 2004 (Ialongo et al., 2011). The Aura satellite crosses the equator at 1:45 pm local time, providing global daily coverage of ozone columns and profiles, aerosols, clouds, spectral irradiance data at solar noon in the UVA waveband at 324 nm and 380 nm, as well as in the UVB waveband at 305 nm and 310 nm, solar noon daily erythemal irradiance, erythemal daily exposure and the solar noon UVI (used in this study) (Ialongo et al., 2011, Parisi et al., 2020). The OMI-based evaluation is of the order of 7% to 30% higher than ground measured data, due to absorbing aerosols in the boundary layer not being taken into account (Parisi et al., 2020). Also, additional errors sources are changes in the cloud cover between the satellite overpass time and solar noon, variations over the size of a pixel, diurnal variations in the cloud cover for the calculation of daily exposures and variations in albedo and aerosols (Tanskanen et al., 2006).

2.3 GOME-2 data

The GOME-2 instrumentation is an optical spectrometer on board the three Metop sun-synchronous polar orbiting satellites of Metop-A, Metop-B and Metop-C (Kujanpää & Kalakoski, 2015). The first Metop satellite was launched in 2006, with the other two following at five-year intervals (Krebs, 2022). The GOME-2 instrument provides UV data products as well information on atmospheric trace gases. Daily maximum UVA (315-400 nm) irradiance at solar noon, total daily UVA exposure, total daily erythemal irradiance, unweighted UVB, solar noon UVI and other products are provided by this instrument. Comparison with ground-based data has shown that the GOME-2 daily erythema UV exposures are generally higher by 10%-20% (Parisi et al.,2021).

2.3 Statistical Analysis

To provide information about data variability using statistical measures, boxplots were prepared. From the daily measurements, the monthly distribution was also performed, as well the discussion of the seasonal distribution of the year (rainy period and dry period).

3 RESULTS

In this section, the UVI time variability is presented to demonstrate how UVI varies in monthly and seasonal time scale, according to the 2 satellite-instruments data.

3.1 UV index monthly and seasonal variability

Figure 2 – Monthly variability for OMI and GOME-2 time series at Santarém (month average in red line) over 2008-2021 periods

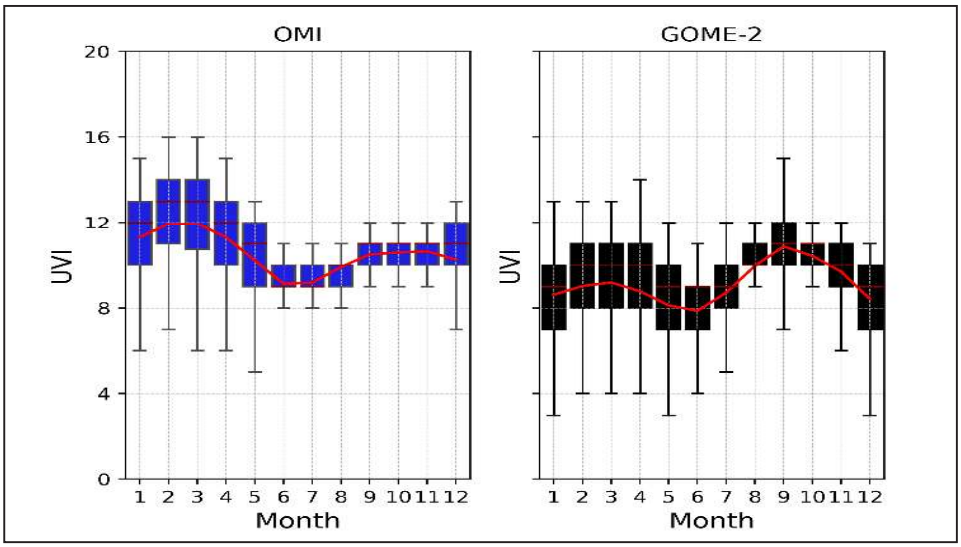

Source: Authors (2022)

The Figure 2 presents the UVI monthly variability at Santarém according to OMI and GOME-2 time series. The seasonal characteristic is evident, with the lowest averages recorded in the early austral winter months, with the average increasing with the arrival of spring and summer.

Generally, one of the main factors affecting the intensity of UVI is the season of the year: in summer the sun is higher than in winter, resulting in more intense UVI in summer than in winter (Sacchetti *et al*., 2022), even though, at Santarem's latitude

(equatorial), one does not distinguish four seasons, but only two seasons, summer and winter, which correspond to the rainy and dry seasons, respectively (Reis et al., 2022). It is also possible to observe that the OMI series presented higher UVI than the GOME-2 series, as for example, with the UV index levels achieving 16 in the raining period. These higher levels were expected, since the literature describes that UVR data from OMI are more over estimated when compared to ground-based data, than GOME-2 data (Ialongo et al., 2011, Brogniez et al., 2016, Parisl et al., 2021).

As can be seen in Figure 2, the minimum records in both time series occurred in the rainy period months. However, the averages and maximums were higher in this period for the OMI series, while for the GOME-2 series, the dry period presented higher averages and maximum. Porfírio et al., (2012) found similar results in his study at Maceió-Northeastern Brazil, with global and UV maximum irradiances also occurring in the Spring/Summer months (dry period). Surface UVR had similar variation throughout the year in 2019-2020 at the Santarém, according to Reis et al., (2022). Another point to be highlighted is the amplitude, which is higher in in the rainy period in both series. During the rainy period, clouds are expected to play an important role in the variability of UVR (Reis et al., 2022), therefore UVI, mostly by attenuation, what can explain the minimums over this period, but sometimes by increasing the intensity reaching the ground (Corrêa et al., 2010).

Taking into account that there is no ground-based derived UV index for Santarém, in order to make a comparison and clarify which of the two satellite time series better represent the reality of the UVI variability in this area, the variation of the solar zenith angle (SZA) over the year for Santarém was plotted (Figure 3), so that it was possible to understand which series presents variability more in accordance with the variability of the SZA. The SZA is the angle measured from the surface between the Sun and a point directly above the observer (Du Preez, 2019; Cadet et al., 2020). Smaller SZAs results in greater solar flux reaching the Earth's surface, this happens more frequently around noon and during summer months (Wald, 2018). At larger SZAs (at dawn and

dusk time), UVR is lower, as the path through the atmosphere is longer and results in more attenuation of UVR through the scattering and absorption by particles and gases in the atmosphere (Wald, 2018; Du Preez, 2019).

Figure 3 – Noontime UVI monthly average in all-sky conditions and the corresponding noontime solar zenith angles-monthly averaged (indicated with the red line and the right vertical axis) for Santarém

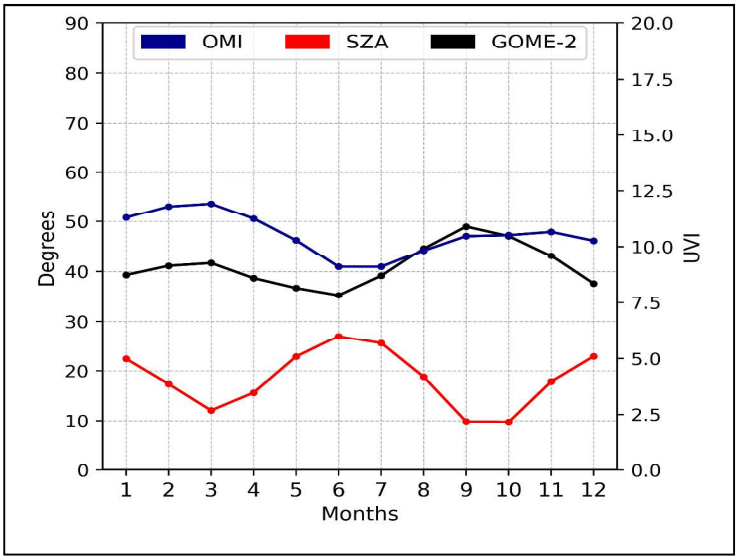

Source: Authors (2022)

At places within the Tropic of Capricorn the sun is at its peak twice a year and the stations register two annual maximums (Coariti, 2017). For Santarém, the noontime averaged UV index peaks occurred in the end of summer (around march), and in spring (around September) (Figure 3), in the GOME-2 series, in accordance with the SZA variability. The UVI OMI series varied in agreement to the SZA variation in the rainy period, but in the dry period it peaked in November, instead of around September and October. In comparison with research conducted in other places with a latitude close to the latitude of Santarém, two-year maximums were similarly reported by Kirchhoff

et al. (2000) and Coariti (2017) for the city of Natal (5.84°S, 35.21°W), also by Lamyet al. (2021) for Mahé (4.67°S, 55.53°E).

Figure 4 – Noontime frequency of the UV index levels under all-sky conditions as function of the instrument (OMI, GOME-2) and period of the year (Rainy, Dry) for Santarém

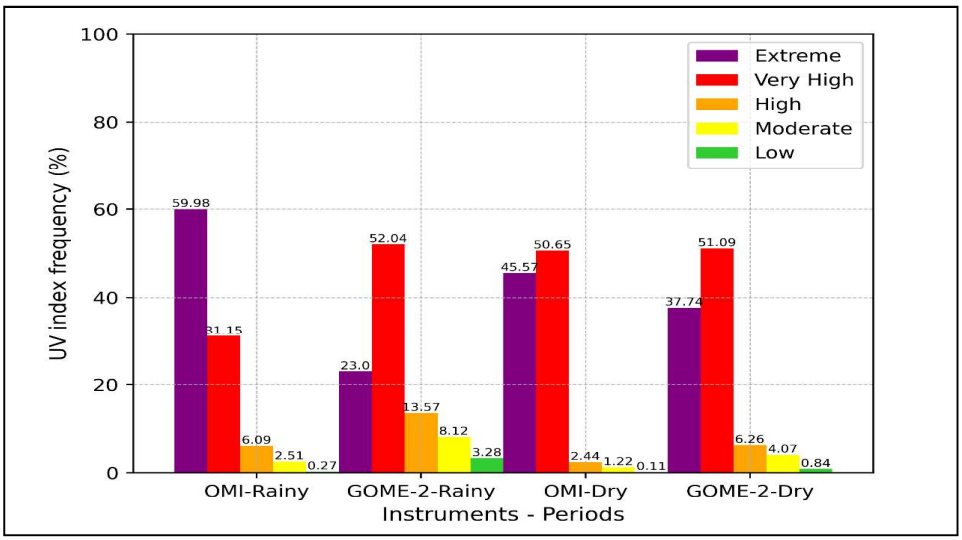

Source: Authors (2022)

Figure 4 shows the frequency of the UV index levels as a function of the instrument (Omi, Gome-2) and of the period of the year (rainy or dry seasons). According to the U.S. Environmental Protection Agency (Epa) a low danger from the sun's UV rays only occurs when the UV index ranges from 0 to 2. Even so, it is recommended to wear sunglasses on clear days, protect yourself with clothing, and use broad spectrum SPF30+ sunscreen (Epa, 2017). Only 0.27% of the noontime UV index levels under all sky conditions were low during the rainy period, and 0.11% during the dry period, according with the OMI series. The GOME-2 series presented a bit higher percentage of Low levels, 3.38% and 0.84, rainy and dry period respectively.

When the level is at most moderate the recommendations are as follows: Stay in shade; if outdoors, wear protective clothing, a wide brimmed hat and UV-blocking

sunglasses; generously apply broad spectrum SPF30+ sunscreen every 2 hours, even on cloudy days and after swimming or sweating; watch out for bright surfaces, like sand, water and snow, which reflect and increase UV (Epa, 2017). When UV index is high (6 to 7) or very high (8 to 10), the same recommendations as the ones cited before are necessary but is also recommended to reduce time in sun if there is a high or very high risk (Who, 2002).

Together, moderate, high, and very high UVI levels represent 39.75% of the UVI incident at noontime during the rainy period in Santarém and 54.31% during the dry period, for the OMI series. Even during the rainy period, when there are greater presence of cloud cover and precipitation (Reis *et al*., 2022), approximately 60% of the incident UV index at Santarém at noontime is extreme. For the GOME-2 series just 23% of the UVI levels were extreme during the rainy period and 37.74% in the dry period. If there is no use of sun protection, skin and eyes can have sunburn in minutes if the UV index is extreme (Who, 2002). It is recommended to avoid sun exposure when these levels are reached and take all the recommendations cited before (Who, 2002; Epa, 2017).

In summary, the dry period showed higher average UVI, according to the GOME-2 series, with 11 (extreme) being the average UVI in the dry period and 10 (very high) being the average UVI in the rainy period, at noontime. The average was also between very high and extreme in the OMI series, but with the rainy period being extreme. These characteristics of both time series reinforce that during the rainy as well the dry period the maximum protective measures need to be taken to avoid overexposure to UVR.

Santarém is in a tropical region, at a low latitude, close to the equator, therefore solar zenith angle (SZA) is lower throughout the year, which induces a higher UVR, smaller amplitude between the seasons, as well as a very low photoperiod variation (REIS et al., 2022). Predictably, the UVI is higher around solar noon when the SZA is minimum, therefore these higher UVI levels were expected. UVI in this range was expected for Santarém, given its location. The presence of seasonality but small amplitude of UVI between rainy and dry periods was also expected. As well as higher values of UVI in the OMI series than in the GOME-2 series.

The divergence between the higher means and medians found in the rainy months in the OMI series in contrast to those found in the dry months in the GOME-2 series is a characteristic to be further investigated, for example, with the insertion of a comparison of UVI data from the Tropomi instrument, from reanalysis, and in the future with ground-based data for a better understanding of the UVR variability in the Brazilian Amazon region.

4 CONCLUSIONS

Through this work it was possible to characterize the monthly variability of the UVI for the city of Santarém, as well as to analyze how UVI varies between the seasons of the year, using data from two different instruments on board satellites. The patterns found are in agreement with the literature, for example, with the highest average UVI recorded during the dry period, in the months corresponding to spring and summer, in the GOME-2 series. The results also reinforce that at solar noontime maximum protective measures need to be taken to avoid overexposure to UVR, both during rainy and dry periods. Comparison with ground-based data is needed for a more robust and complete work, as well as comparison with UVI obtained from other sources, such as from another satellite or reanalysis, to better understand the variability of UVR in this Amazonian city.

ACKNOWLEDGEMENTS

We acknowledge support and funding of this work by FAPESPA (Amazon Foundation for the Support of Studies and Research) for the PhD scholarship in the Post Graduate Program in Society Nature and Development, at Federal University of Western Pará. To CAPES (Coordination for the Improvement of Higher Education Personnel) and COFECUB (French Evaluation Committee of the University and Scientific Cooperation with Brazil) for the sandwich PhD scholarship awarded to the MESO project (Modeling and Prediction of the Secondary Effects of the Antarctic Ozone hole).

REFERENCES

Alvares, C. A.; Stape, J. L.; Sentelhas, P. C.; Moraes, G. J. L.; Sparovek, G. Köppen's climate classification map for Brazil. *Meteorol.Z.* 2013, *22*, 711–728. https://doi.org/10.1127/0941-2948/2013/0507.

Alves, P., Querino, A., C., Vaz, A., M., Sacardi Biudes, M., Moura, A. L., Santos, L. O., Lopes, P. J. (2022). Sazonalidade anual e a variabilidade horária mensal do índice ultravioleta para a cidade de Humaitá, Amazonas, Brasil. *Revista Brasileira de Climatologia*, 30(18), 504–523. https://doi.org/10.55761/abclima.v30i18.14622

Andrade, S. C., Corrêa, J.A., Grande, P. B. C. Estimativa do saldo de radiação instantâneo à superfície para a cidade de Santarém-PA, através de imagens do Landsat 5-TM. *Rev. Bras. Geogr. Física.* 2014, *7*, 653–661.

Bevan, S. L., et al. Impact of Atmospheric Aerosol from Biomass Burning on Amazon Dry-Season Drought. *Journal of Geophysical Research*, vol. 114, no D9, may 2009, p. D09204. *DOI.org (Crossref)*, https://doi.org/10.1029/2008JD011112.

Brogniez, C., et al. Validation of Satellite-Based Noontime UVI with NDACC Ground-Based Instruments: Influence of Topography, Environment and Satellite Overpass Time. *Atmospheric Chemistry and Physics*, vol. 16, no 23, dezembro de 2016, p. 15049–74. *acp.copernicus.org*, https://doi.org/10.5194/acp-16-15049-2016

Cadet, J.-M.; Portafaix, T.; Bencherif, H.; Lamy, K.; Brogniez, C.; Auriol, F.; Metzger, J.-M.; Boudreault, L.-E.; Wright, C. Y. Inter-Comparison Campaign of Solar UVR Instruments under Clear Sky Conditions at Reunion Island (21°S, 55°E). *Int. J. Environ. Res. Public Health 2020, 17,* 2867. https://doi.org/10.3390/ijerph17082867

Coariti, Jaime Rodriguez. "Características da Radiação Ultravioleta Solar e seus efeitos na saúde humana nas cidades de La Paz–Bolívia e Natal–Brasil." (2017). https://repositorio.ufrn.br/bitstream/123456789/24952/1/Caracter%C3%ADsticasRadiacaoUltravioleta_Coariti_2017.pdf

Corrêa, M. D. P.; Godin-Beekmann, S.; Haeffelin, M.; Brogniez, C.; Verschaeve, F.; Saiag, P.; Pazmiño, A.; Mahé, E. Comparison between UV index measurements performed by research-grade and consumer-products instruments. *Photochem. Photobiol. Sci.* 2010, *9*, 459–463. https://doi.org/10.1039/b9pp00179d.

du Preez, D. J., Ajtić, J. V., Bencherif, H., Bègue, N., Cadet, J.-M., and Wright, C. Y.: Spring and summer time ozone and solar ultraviolet radiation variations over Cape Point, South Africa, *Ann. Geophys*., 37, 129–141, https://doi.org/10.5194/angeo-37-129-2019, 2019.

EPA. United States Envrironmental Protection Agency. IV Index Scale. 2017. Available online: https://19january2017snapshot.epa.gov/sunsafety/uv-index-scale-1_.html.

González-Rodríguez, Lisdelys, et al. Spatio-Temporal Estimations of Ultraviolet Erythemal Radiation in Central Chile. *Air Quality, Atmosphere & Health*, abril de 2022. *DOI.org (Crossref)*, https://doi.org/10.1007/s11869-022-01195-y.

Ialongo, I., et al.Use of Satellite Erythemal UV Products in Analysing the Global UV Changes. *Atmospheric Chemistry and Physics,* vol. 11, no 18, setembro de 2011, p. 9649–58. *acp. copernicus.org*, https://doi.org/10.5194/acp-11-9649-2011.

Jacinto, A.I.; Simas, M.T.M.; Bianchi, R.; Oliveira, K.N.; Rech, C.M.C.B. Aspectos Físicoterritoriais e Atrações Turísticas do Município de Santarém, Pará. 2006. Available online: http://www2.ifes.com.br/webifes/revista/REVIST. Accessed on 11 May 2022.

Kirchhoff, V. W. J. H., et al. "A Variação Sazonal Da Radiação Ultravioleta Solar Biologicamente Ativa". Revista Brasileira de Geofísica, vol. 18, no 1, março de 2000, p. 63–74. DOI.org (Crossref), https://doi.org/10.1590/S0102-261X2000000100006.

Kosmopoulos, P. G., et al. Real-Time UV Index Retrieval in Europe Using Earth Observation-Based Techniques: System Description and Quality Assessment. *Atmospheric Measurement Techniques,* vol. 14, no 8, agosto de 2021, p. 5657–99. *DOI.org (Crossref)*, https://doi.org/10.5194/amt-14-5657-202.

Krebs, Gunter D. "METOP A, B, C". Gunter's Space Page. Retrieved September 27, 2022, from https://space.skyrocket.de/doc_sdat/metop.htm.

Kujanpää, J. and Kalakoski. N. Operational Surface UV Radiation Product from GOME-2 and AVHRR/3 Data. *Atmospheric Measurement Techniques*, vol. 8, no 10, outubro de 2015, p. 4399–414. *DOI.org (Crossref)*, https://doi.org/10.5194/amt-8-4399-2015.

Lamy, Kevin, et al. "UV-Indien Network: Ground-Based Measurements Dedicated to the Monitoring of UV Radiation over the Western Indian Ocean". Earth System Science Data, vol. 13, no 9, setembro de 2021, p. 4275–301. DOI.org (Crossref), https://doi.org/10.5194/essd-13-4275-2021.

Levelt, P. F., et al. The ozone monitoring instrument. *IEEE Transactions on Geoscience and Remote Sensing*, vol. 44, no 5, maio de 2006, p. 1093–101. *IEEE Xplore*, https://doi.org/10.1109/TGRS.2006.872333.

Medhaug, I., et al. UV Radiation and Skin Cancer in Norway. *Journal of Photochemistry and Photobiology.* B, Biology, vol. 96, no 3, setembro de 2009, p. 232–41. PubMed, https://doi.org/10.1016/j.jphotobiol.2009.06.011.

Parisi, A. V., et al. Satellite Monitoring of Environmental Solar Ultraviolet A (UVA) Exposure and Irradiance: A Review of OMI and GOME-2. *Remote Sensing,* vol. 13, no 4, janeiro de 2021, p. 752. *www.mdpi.com*, https://doi.org/10.3390/rs13040752.

Parra, René, et al. Maximum UV Index Records (2010–2014) in Quito (Ecuador) and Its Trend Inferred from Remote Sensing Data (1979–2018). *Atmosphere,* vol. 10, no 12, dezembro de 2019, p. 787. www.mdpi.com, https://doi.org/10.3390/atmos10120787.

Porfirio, A. C. S., et al. An Assessment of the Global UV Solar Radiation under Various Sky Conditions in Maceió-Northeastern Brazil. *Energy,* vol. 44, no 1, agosto de 2012, p. 584–92. ScienceDirect, https://doi.org/10.1016/j.energy.2012.05.042.

Reis, G., et al. Solar Ultraviolet Radiation Temporal Variability Analysis from 2-Year of Continuous Observation in an Amazonian City of Brazil. *Atmosphere,* vol. 13, no 7, julho de 2022, p. 1054. *DOI.org (Crossref)*, https://doi.org/10.3390/atmos13071054.

Sacchetti, F.Z. and Gisbert, R.F. Radiacion ultravioleta en Bolivia. *La Atmosfera*.2003. La Paz, Bolivia. Available online: https://iris.paho.org/handle/10665.2/31072. Accessed on 10 February 2022.

Tanskanen, A., et al. Surface ultraviolet irradiance from OMI. *IEEE Transactions on Geoscience and Remote Sensing*, vol. 44, no 5, maio de 2006, p. 1267–71. *IEEE Xplore*, https://doi.org/10.1109/TGRS.2005.862203.

Teramoto, É. T.; Escobedo, J. F.; Martins, D. Modelos estatísticos para estimativa da irradiação solar UV horária em Botucatu/SP/Brasil. *Rev. Bras. de Energ. Sol.* 2014, *5, 44-51*. Available online: https://rbens.emnuvens.com.br/rbens/article/view/107. Accessed on 15 April 2022.

Wald, Lucien. Basics in solar radiation at Earth surface. 2018. https://hal-mines paristech. archivesouvertes.fr/hal-01676634v1/preview/2018_basics_solaire_wald_v1.pdf.

World Health Organization. International Commission on Non-Ionizing Radiation Protection. *Global Solar UV Index: A Practical Guide*; World Health Organization: Geneva, Switzerland, 2002. Available online: https://apps.who.int/iris/handle/10665/42459. Accessed on 29 April 2022.

Authorship contributions

1 – Gabriela Cacilda Godinho dos Reis

Federal University of Western Pará – UFOPA, Master's in environment Science from the Postgraduate in Natural Resources of the Amazon – PPGRNA
https://orcid.org/0000-0001-9243-214X • gabriela.godinho-dos-reis@univ-reunion.fr
Contribution: Writing – original draft

2 – Lucas Vaz Peres

Federal University of Western Pará – UFOPA, PhD in Meteorology from the Universidade Federal de Santa Maria
https://orcid.org/0000-0002-5612-5991 • lucas.peres@ufopa.edu.br
Contribution: Writing – original draft

3 – Rodrigo da Silva

University of Western Pará – UFOPA, PhD in Physics from Universidade Federal de Santa Maria
https://orcid.org/0000-0001-9222-5861 • rodrigo.silva@ufopa.edu.br
Contribution: Writing – original draft

4 – Marco Antonio Godinho dos Reis

Universidade Federal de Santa Maria – UFSM, Master's student in Meteorology in the Graduate Program in Meteorology – PPGMET, researcher from Atmospheric Sciences in the Amazon - CNPq
https://orcid.org/0000-0001-6364-1049 • reis.marco@acad.ufsm.br
Contribution: Writing – original draft

5 – Damaris Kirsch Pinheiro

Universidade Federal de Santa Maria – UFSM, PhD in Space Geophysics from the National Institute for Space Research
https://orcid.org/0000-0001-6939-7091 • damaris@ufsm.br
Contribution: Writing – original draft

6 – Kevin Lamy

University of Reunion Island, Researcher at the University of La Réunion
https://orcid.org/0000-0002-9115-1319 • kevin.lamy@univ-reunion.fr
Contribution: Writing – original draft

7 – Hassan Bencherif

University of Reunion Island, Professor at University of La Réunion
https://orcid.org/0000-0003-1815-0667 • hassan.bencherif@univ-reunion.fr
Contribution: Writing – original draft

8 – Thierry Portafaix

University of Reunion Island, Professor in atmospheric Physics
https://orcid.org/0000-0003-0630-0752 • thierry.portafaix@univ-reunion.fr
Contribution: Writing – original draft

How to quote this article

Reis, G. C. G. dos, Peres, L. V., Silva, R. da, Reis, M. A. G. dos, Pinheiro, D. K., Lamy, K., Bencherif, H., & Portafaix, T.(2023) UV index seasonal variability in an Amazonian city of Brazil based on satellite data. *Ciência e Natura*, *45*(spe 2), e76670. DOI: https://doi.org/10.5902/2179460X76670. Retrieved from https://periodicos.ufsm.br/cienciaenatura/article/view/76670. Accessed in: day month abbr. year.

4 RESULTS: Comparative analysis of ground-based and satellite-derived UV index levels in Natal, Brazil

4.1 Article III overview and thesis contribution

This paper aimed to compare the levels of UV index measured on the ground and by satellite (OMI and GOME-2) over Natal, Brazil (05.78°S; 35.21°W) from 2005 to 2022. The comparison was made under clear-sky conditions selected using METAR cloud cover and LER data as cloud cover proxies. Characterization of the diurnal and seasonal variability of the ground-based UV index levels under all and clear-sky conditions is also reported.

This paper contributes to the first, second, and third specific objectives of this thesis by characterizing the diurnal and seasonal variability of UV index in a low-latitude South American site (Natal), assessing its variability under all and clear skies, and by comparing ground-based and satellite-derived UV index levels in Natal, Brazil, under clear-sky conditions.

The study found a semi-annual cycle with two maxima during austral summer and spring, and smaller levels during austral winter. The UV index average around noon remained very high even during winter. A daily maximum of 16 UVI was recorded in different years in the ground-based and OMI noontime series, while GOME-2 and OMI overpass reached less than 15, indicating, in any case, extreme UV levels. The presence of cloud cover around noontime was consistent throughout the years, with clear-sky conditions prevailing during night hours and more hours of clear sky between August and November, the dry period in the region.

It was found that around noon, UVI is more intense (6.8% higher) under all-sky conditions, likely due to the prevalence of broken clouds during this time. This suggests the influence of cloud cover in enhancing UV levels at certain moments, aligning with literature that reports broken clouds can increase UV radiation.

The comparison showed that OMI data are less biased than GOME-2, with OMI often overestimating and GOME-2 underestimating ground UVI levels. Metrics such as MAE, MAPE, and RMSE indicated good agreement between satellite and ground-based measurements, with low overall differences. Even more, the differences in clear-sky identification methods were notable, with LER identifying significantly more clear-sky days than METAR. These discrepancies emphasize the importance of accurate sky condition determination to reduce uncertainties related to cloud coverage analysis and, therefore, improve the reliability of UV radiation assessments.

This study differs from previous studies and contributes to the scientific understanding of UV radiation levels using unpublished UV index data from a ground-based station in a city located near the equator, in South America's tropical region, where until now, there has been relatively limited research focusing on this field of study. "With the reliability of these satellite and ground-based data assessed for Natal, future studies can explore trends in the UV index at this tropical Brazilian site. These findings contribute to a better understanding of UV patterns in tropical low-latitude South America regions, providing solid base for future research and public health strategies.

4.2 Publication status

DOS REIS, Gabriela Cacilda Godinho; BENCHERIF, Hassan; SILVA, Rodrigo; *et al*. Comparative Analysis of Ground-Based and Satellite-Derived UV Index Levels in Natal, Brazil. **Remote Sensing**, v. 16, n. 24, p. 4687, 2024. Available in: <https://www.mdpi.com/2072-4292/16/24/4687>.

4.3 Article III

remote sensing

MDPI

Article

Comparative Analysis of Ground-Based and Satellite-Derived UV Index Levels in Natal, Brazil

Gabriela Cacilda Godinho dos Reis [1,2,*], Hassan Bencherif [1], Rodrigo Silva [3], Lucas Vaz Peres [3], Marco Antonio Godinho dos Reis [4], Damaris Kirsch Pinheiro [5], Francisco Raimundo da Silva [6], Kevin Lamy [1] and Thierry Portafaix [1,7]

[1] Laboratoire de l'Atmosphère et des Cyclones, LACy, UMR 8105 CNRS, Physics Department, Faculty of Sciences and Technologies, Université de La Réunion, Météo-France, 97400 Saint-Denis de La Réunion, France; hassan.bencherif@univ-reunion.fr (H.B.); kevin.lamy@univ-reunion.fr (K.L.); thierry.portafaix@univ-reunion.fr (T.P.)
[2] Programa de Pós-Graduação em Sociedade, Natureza e Desenvolvimento, Universidade Federal do Oeste do Pará, Santarém 68035110, Brazil
[3] Instituto de Engenharia e Geociências, Universidade Federal do Oeste do Pará, Santarém 68035110, Brazil; rodrigo.silva@ufopa.edu.br (R.S.); lucas.peres@ufopa.edu.br (L.V.P.)
[4] Programa de Pós-Graduação em Meteorologia, Universidade Federal de Santa Maria, Santa Maria 97105900, Brazil; reis.marco@acad.ufsm.edu.br
[5] Centro de Tecnologia, Departamento de Engenharia Química, Universidade Federal de Santa Maria, Santa Maria 97105900, Brazil; damaris@ufsm.br
[6] Instituto Nacional de Pesquisas Espaciais, Natal 66077830, Brazil; francisco.raimundo@inpe.br
[7] Institut de Recherche pour le Développement, IRD, DRIE, Antananarivo 101, Madagascar
* Correspondence: gabriela.godinho-dos-reis@univ-reunion.fr or gabriela.reis@discente.ufopa.edu.br; Tel.: +33-262-693-51-73-18

Abstract: The ultraviolet radiation index (UV index–UVI) is a dimensionless indicator that informs the intensity of ultraviolet radiation on the Earth's surface. It makes it easier for people to assess UV levels and understand how to protect themselves from excessive Sun exposure. In Brazil, however, the information regarding UV is scarce, with low spatial and temporal coverage. Thus, continuous monitoring is conducted through satellites, although ground-based monitoring of UV is more accurate than satellite retrievals, and comparisons are necessary for validation. This paper aims to compare the levels of UV index measured on the ground and by satellite (OMI and GOME-2) over Natal, Brazil (05.78°S; 35.21°W) from 2005 to 2022. The comparison was made under clear-sky conditions using METAR cloud cover and LER data. Characterization of the diurnal and seasonal variability of the ground-based UV index levels under all and clear-sky conditions is also reported. The analysis indicates that in Natal, noontime all-sky UV index were 6.8% higher during periods of prevalent broken clouds. The two satellite sources (OMI noontime and overpass) and GOME-2 noontime are reliable sources for UV index, which show good agreement with ground-based measurements, with UVI estimated from OMI both at the overpass and noontime being less biased than GOME-2-estimated UVI. Such a process of data verification is important should these data be used for long-term trend analysis or the monitoring of UV exposure risk and possible impacts on human health.

Keywords: solar ultraviolet radiation; UV index; ground-based measurements; satellite-derived data; OMI; GOME-2; cloud cover; Brazil

Citation: dos Reis, G.C.G.; Bencherif, H.; Silva, R.; Vaz Peres, L.; dos Reis, M.A.G.; Pinheiro, D.K.; da Silva, F.R.; Lamy, K.; Portafaix, T. Comparative Analysis of Ground-Based and Satellite-Derived UV Index Levels in Natal, Brazil. *Remote Sens.* **2024**, *16*, 4687. https://doi.org/10.3390/rs16244687

Academic Editor: Chang-Keun Song

Received: 4 December 2023
Revised: 2 January 2024
Accepted: 3 January 2024
Published: 16 December 2024

1. Introduction

Solar ultraviolet radiation (UV) corresponds to electromagnetic waves with wavelengths of 100–400 nm, constituting approximately 5% of the energy emitted by the Sun [1]. The risks and benefits of exposure to UV for life on Earth have been known for many years [2–4] and include impacts on human health [5–9], materials [10,11], terrestrial and aquatic ecosystems [12–14], and biogeochemical cycles [15,16]. The benefits and detrimental

effects of UV depend on the time of exposure and several other factors, the relative importance of which depends strongly on the highly spatiotemporal UV variability, which is influenced by Sun elevation, total ozone, cloud cover, aerosols, albedo, and altitude [17–19]. Less important factors controlling UV include the ozone profile, trace gases, seasonal changes in the Earth–Sun distance, changes in solar activity, and volcanic eruptions [4,20].

UV is divided into three regions, closely associated with the biological effect of the different wavelengths: UV–A (315–400 nm), UV–B (280–315 nm), and UV–C (100–280 nm) [21–23]. As sunlight passes through the atmosphere, all UV–C and approximately 90% of UV–B are absorbed by ozone, water vapor, oxygen, and carbon dioxide, while UV–A is less affected by the atmosphere [21–24]. Therefore, the UV radiation reaching the Earth's surface is largely composed of UV–A (94%) with a small UV–B component (6%) [25,26].

Diseases related to the accumulation of exposure to UV, like skin cancer and cataracts, are largely preventable with proper Sun protection [25]. Given the need for this type of information, the World Health Organization (WHO) released the ultraviolet index—UVI (UV index)—a dimensionless indicator that provides the amount of UV that reaches the Earth's surface and has varying values on a scale from 0 to 11 or more [25]. Based on this scale, the WHO defines five exposure categories, ranging from low to extreme, with recommended protections at each level. The UV index is an important resource that increases public awareness of the risks of overexposure to the Sun [27].

Brazil is a country of continental dimensions with a large heterogeneity of climates and massive mixing of the population with almost the entire national territory located between the equator and the Tropic of Capricorn, where the Earth's axial tilt to the south makes it one of the countries of the world with the greatest extent of land in proximity to the Sun [28]. Due to geographic characteristics and cultural trends, Brazilians are among the people with the highest annual exposure to the Sun [28]. For the 2020–2022 triennium, in Brazil, about 177,000 new cases of non-melanoma skin cancer were estimated by the Brazilian National Cancer Institute [29]. Non-melanoma skin cancer is the most common type of cancer in men in the south, central west, and southeast regions [29]. In the northeast and north, it ranks second [29]. For women, non-melanoma skin cancer is the most common in all Brazilian regions [29]. Cataracts are the leading cause of blindness and low vision in Brazil [30]. An annual GDP (Gross Domestic Product) loss of more than USD 9 million has been estimated for Latin America and the Caribbean due to blindness and vision impairment, in contrast to just over USD 3 million if education and prevention programs to address risk factors (such as about prolonged and unprotected exposure to UV) were put into practice [30].

In middle-income countries like Brazil, networks and instruments for monitoring UV are often sparse and poorly supported in terms of capacity and funding, and thus, obtaining reliable UV data is difficult. The northern and central–western regions of Brazil have no stations reporting long-term UV series. Of the few studies published on UV variability in Brazilian cities, most were conducted in the southeast and, second, the northeast. An important UV monitoring site in northeastern Brazil is Natal, which is along the Brazilian coastline. Measurements of the UV index in Natal from 2001 to 2007 made using a GUV-511 C surface radiometer were used to produce the curves of hourly mean values for all days between 2001 and 2007 and monthly mean values for the same period by [31]. Their results showed that in Natal, high UV index levels happened before 9:30 a.m. (local time) during all the studied years [31]. Other studies on UV in Natal are available [27,32,33].

Even though Natal is one of the only cities in Brazil where UV has been monitored for more than 10 years, they still do not report data on cloud cover from ground-based imagers. Clouds are important regulators of the radiance balance of the Earth's atmosphere system [34]. The influence of clouds is difficult to accurately account for because they attenuate and enhance UV [35,36]. During cloudy days, they can notably reduce UV at the surface [37]. On days with the partial presence of clouds, UV can be greater than in clear-sky conditions (e.g., UV enhancement under broken clouds) [35–37]. Traditionally, cloud cover is observed from the ground by human observers [38,39] (e.g., METAR, the regular aerodrome weather report). With the advent of new technologies, cloud observations

have been improved using automatic ground-based and orbital imagers [39]. Satellites provide the opportunity for systematic and continuous observation of cloud cover over large spatial scales [40] and provide other ways for cloud characterization, such as using LER (Lambertian equivalent reflectivity). LER can be used for cloud characterization to select clear-sky days for the comparison of ground-based and satellite-derived UV index levels at South African sites [41].

With only a few stations reporting long-term UV measurements in several countries, which significantly restricts its extrapolations to all populated areas [42], a way for continuous UV monitoring on a global scale is through satellites, although ground-based monitoring of UV is more accurate than satellite retrievals [32,43]. Satellite measurements, similar to ground-based observations, are not only affected by instrument errors but are also subject to uncertainties in the algorithms used to derive surface UV radiation [44,45]. Therefore, evaluation of satellite-based estimates of surface UV against available ground measurements at many locations around the world is needed to characterize the errors and further refine the surface UV estimates [45], especially in the southern hemisphere, where there has been relatively limited work to compare ground-based and satellite-derived UV [46].

Given these complexities, the main objective of this study is to conduct a comparative analysis of the ground-based and satellite-derived solar UV indices for Natal, Brazil. Two objectives were identified: (1) to characterize the time variability of the ground-based derived UV index levels in Natal from 2006 to 2022 under all and clear-sky conditions; (2) to compare ground-based and satellite-derived UV index levels in Natal using 2 different techniques to select clear-sky conditions.

Until now, the entire dataset measured by the ground-based Davis 6490 UV sensor used in this research has not been analyzed or compared to satellite-estimated UV index data for the same site. A process of data verification is important to ensure that these data can be used for long-term trend analysis or for monitoring UV exposure risks and potential impacts on human health. In addition, since cloudy conditions pose difficulties with comparisons between ground-based and satellite-derived UV [47], clear-sky conditions offer a more consistent and controlled scenario, eliminating the variable attenuation effects of clouds on UV, which ensures that any differences observed between the two sets of measurements can be attributed more directly to the sensors themselves rather than to other atmospheric conditions. Even more, comparing satellite-derived data with ground-based measurements helps in validating the accuracy of satellite data, which can help identify any discrepancies and improve the satellite data retrieval algorithms, leading to more accurate satellite-derived UV products.

Using these different instruments and techniques, this research promotes a greater understanding of both the variability of UV in Natal, based on different data sources, and the limitations of the instruments and techniques themselves. Also, it is important to highlight that this study contributes to the scientific understanding of UV radiation levels in South America's tropical region, where until now, there has been relatively limited research focusing on this field of study.

2. Materials and Methods

The main aim of this paper is to conduct a comparative analysis of ground-based and satellite-derived UV index levels from OMI and GOME-2 in Natal, Brazil (05.78°S; 35.20°W, 30 m above sea levels (a.s.l)), under clear-sky conditions. To this end, hourly ground-based UV index and daily time series of UV index at noontime and overpass time obtained from the OMI (Ozone Monitoring Instrument) on board the AURA satellite and UV index at noontime derived from GOME-2 instrument (Global Ozone Monitoring Experiment) on board the Metop-A/B/C satellites were used. All the satellite data are available online and free for download through the websites listed in Table 1.

Table 1. Satellite-derived data sources.

Satellite	Instrument	Type of Data	Period	Website
AURA	OMI	UV index (Noontime) UV index (Overpass time) LER	January 2005–December 2022	https://giovanni.gsfc.nasa.gov/giovanni/ (accessed on 13 July 2022) https://search.earthdata.nasa.gov/search (accessed on 13 July 2022) https://search.earthdata.nasa.gov/search (accessed on 13 July 2022)
Metop-A/B/C	GOME-2	UV index (Noontime)	January 2008–December 2022	https://safserver.fmi.fi/index.html (accessed on 13 July 2022)

2.1. Site Description

Natal is a tourist city with beautiful beaches and approximately 896,708 inhabitants [48,49] located on the east coast of northeast Brazil (Figure 1). Its proximity to the equator determines great luminosity and high levels of solar radiation [27]. The city is called "Sun City" by its inhabitants due to the high intensity of solar radiation throughout the year [27,50]. In this city, the UV index is classified as "extreme" from October to April and "very high" from May to August [33]. The average annual UV index observed for the 2001–2012 period was 11 (±1.0) [27]. In the daily cycle, the maximum UV index occurs around 11:20 a.m. It is classified as "high" from 9:00 a.m. to 10:00 a.m. (UTC-3), after which the intensity is considered "very high" [27,51]. In Natal, the average annual temperature and relative humidity are, respectively, 26 °C and 77.3% [33]. The annual accumulated precipitation is 1465.4 mm [52]. The rainy season occurs between April and July, with predominance in April (265 mm) [52,53]. The dry season occurs between August and November [53]. The strongest winds are observed in September, and the weakest occur in April [33].

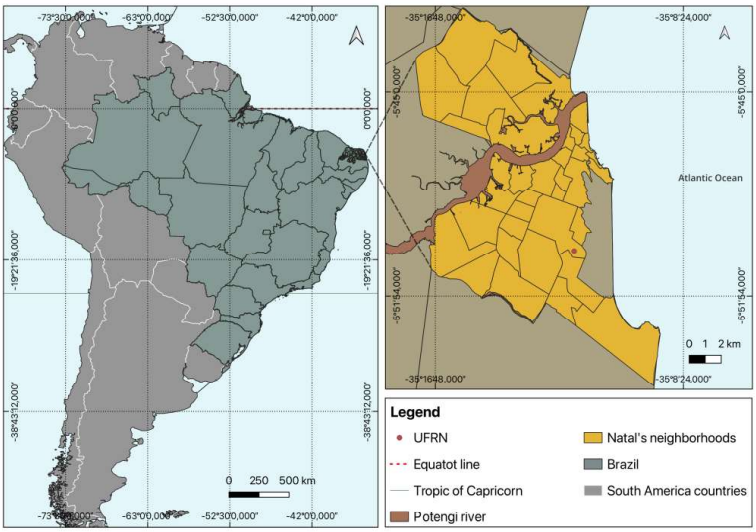

Figure 1. Geographical location of ground−based solar UV sensor in Natal, Rio Grande do Norte, Brazil.

2.2. UV Index

The lower the wavelength in the UV range, the greater the biological response, such that small increases in UV–B irradiance may have substantial biological effects [2,26]. The erythemal action spectrum informs the effectiveness of the wavelengths to produce the

erythema (sunburn) [2]. When UV is weighted by the erythemal action spectrum, it is then named ultraviolet erythemal radiation (UVER) [54,55]. UVER is used to estimate other variables, such as the UV index, standard erythemal doses (SEDs), minimum erythemal doses (MEDs), and Sun exposure time [56]. The UV index (UVI) is a dimensionless indicator, usually divided into five risk categories: UVI $\leq$ 2 (low); 3 $\leq$ UVI $\leq$ 5 (moderate); 6 $\leq$ UVI $\leq$ 7 (high); 8 $\leq$ UVI $\leq$ 10 (very high); and UVI $\geq$ 11 (extreme). This index is defined by Equation (1) [25]:

$$\mathrm{UVI} = K_{er} \int_{250nm}^{400nm} E_{\lambda} S_{er} d\lambda \quad (1)$$

where K_{er} is a scaling factor originally equal to 40 m^2W^{-1}, E_{λ} is the erythemal action spectrum, and S_{er} is the spectral solar irradiance at the surface Wm^2nm^{-1} [25,37].

2.3. Ground-Based Measurements

Monitoring of the UV index in the city of Natal was carried out using the Davis 6490 UV sensor instrument, installed at the Rio Grande do Norte Federal University (UFRN) at an altitude of 30 m a.s.l. This sensor measures the sum of the components of UV transmitted directly and those scattered in the atmosphere [57]. The sensor is a semiconductor photodiode calibrated against a Yankee Environmental Systems' Ultraviolet Pyranometer, model UVB-1, in natural summer daylight [57]. The spectral response is 280 to 360 nm [57], with UV index being one of the sensor outputs with a range from 0 to 16 Index and an accuracy of $\pm$5% [57].

Due to the sensitivity of UV sensors, Davis Instruments recommends recalibration after a period. Since an approximately 2% drift per year on the readings from these sensors is reported [57], the Natal sensor was calibrated every 2 years against a GUV 511 radiometer until 2008. After this period, the GUV 511 used for calibration was sent to another city, and the calibrations in Natal were carried out with a spectrophotometer Brewer 073 until 2017. In 2018, the Davis Sensor was substituted for a brand-new Davis 6490, which is currently in use.

The UV monitored with this sensor covered the years 2006 to 2022, with a sampling frequency of 10 min, which was averaged to the hourly frequency to be used in this study.

2.4. Satellite-Based Instruments

Radiative transfer codes are used for satellites to retrieve UV using ozone, aerosol contents, cloudiness, and surface albedo as input [18]. Some of these inputs, such as ozone and cloudiness, are products of the satellite instrument itself, while aerosol content and albedo come from climatologies [18]. The characteristics of the two satellite instruments that were used in this work (OMI and GOME-2) are detailed below.

2.4.1. Ozone Monitoring Instrument (OMI)

The OMI, onboard NASA's Aura satellite, launched in July 2004 into a Sun-synchronous quasi-polar orbit, is a nadir-viewing UV/visible spectrometer whose mission is the monitoring of atmospheric ozone, trace gases, aerosol, cloudiness, and surface UV [45]. OMI has a spectral resolution of about 0.45 nm in the UV, a wide viewing swath of 2600 km, and a spatial resolution at a nadir of 13 km (along the track) $\times$ 24 km (across-track) [45,58]. The Aura spacecraft circulates in a 98.2° inclination, Sun-synchronous polar orbit at 705 km altitude, with a local afternoon equator crossing time at 13:45 $\pm$ 15 min, providing 14 orbits a day [58,59].

OMI UVI presents a positive bias when compared to ground-based UVI due to, in large part, absorbing aerosols [60–62]. According to [18] and [63], the OMI algorithm version v1.3 applied a correction factor to the algorithm v1.2 that accounts for absorbing aerosols via aerosol climatology, improving the UV estimations. Another uncertainty is added when the satellite overpass happens at a time significantly different from local noon [18] since the OMI UVI given at noontime is estimated using the correction factor estimated at the time

of the overpass [18,61]. The resulting uncertainty of OMI UVI is about 5–10% in clear-sky conditions and about 7–14% in cloudy conditions [18].

2.4.2. Global Ozone Monitoring Experiment (GOME-2)

The GOME-2 is a nadir-viewing scanning UV/VIS spectrometer measuring backscattered and reflected radiation from the Earth's atmosphere in a spectral range between 240 and 790 nm [64,65]. The first GOME-2 was launched in October 2006 onboard the EUMETSAT Metop-A satellite, and a second GOME-2 was launched in September 2012 onboard Metop-B. The long-term dataset was further extended by the third GOME-2 on the Metop-C platform launched in November 2018 [66]. The Metop satellites are flying in Sun-synchronous orbits with equator crossing times of approximately 09:30 LT (local time) and a repeat cycle of 29 days (412 orbits). The summary of the GOME-2 instrument characteristics is in Table 2.

The UV processing algorithm involves the gridding of GOME-2 total ozone data, the inversion of cloud optical depth from reflectance data, and finally, the calculation of surface UV quantities from the radiative transfer model [65]. The GOME-2 UV products include the daily dose and maximum dose rates of integrated UV–B, and UV–A radiation, together with values obtained by different biological weighting functions and solar noon UV index [67].

Table 2. Summary of the GOME-2 instrument characteristics. Retrieved and adapted from [68].

Sensor	GOME-2A	GOME-2B	GOME-2C
Operational Period	January 2007–November 2021	December 2012–Present	January 2019–Present
Spectral Range	240–790 nm	240–790 nm	240–790 nm
Ground Pixel Resolution	80 km × 40 km/40 km × 40 km	80 km × 40 km	80 km × 40 km
Swath Width	1920 km/960 km	1920 km	1920 km
Equator Crossing Time	9:30 (local time)	9:30 (local time)	9:30 (local time)
Global Coverage	1.5 days	1.5 days	1.5 days

The GOME-2 irradiance modeling depends on ozone, surface albedo, cloud, and aerosols; therefore, the uncertainty of GOME-2-derived UVI comes from these factors, with the resulting uncertainty of about 8–16% in clear-sky conditions and about (20–40%) in cloudy conditions [18].

2.5. Techniques to Select Clear-Sky Condition

In this work, the "all-sky UV index" from OMI at noon and overpass time was used. The UV index at overpass time refers to the file attribute named OPUV index from OMUVBG product level 2G. This Surface UV Irradiance Product from OMI contains gridded surface UV irradiance, dose quantities, UV index, cloud optical thickness, and LER [69]. From GOME-2, the noontime "all-sky UV index" was also used.

To only keep clear-sky days for the comparison (ground-based vs. satellite-derived UV index), two different techniques were applied to identify clear-sky conditions: the OMI Lambertian equivalent reflectivity (LER) and cloud-cover data extracted from METAR. The LER applied in this work is derived from the OMI-measured radiance (I_{360}) near 360 nm, which can be expressed as a sum of the atmospheric backscatter above a specified Lambertian surface [70]. LER is used for cloud characterization and can be obtained in the same dataset as the UV index at overpass time from OMI [62]. Only days with an LER smaller than 10% were used [41,62].

Cloud-cover data were obtained from METAR data from Natal's international airport. This METAR is available in 1 h intervals and is free to download through the REDEMET (Air Force Command Meteorology Network) Brazilian application. METAR is a regular aerodrome weather report that contains data on temperature, wind, lightning, and others,

such as cloud cover [71]. The World Meteorological Organization defines rules for the register of cloud cover that have been traditionally carried out by human observers [72,73]. Observers divide the sky into 8 regions (octas) and evaluate the regions covered by clouds to estimate the cloud cover [72]. Here, a clear sky is considered 0 octas, denoted by the acronym CAVOK ("Ceiling in Visibility OK"), and 1 to 2 octas, denoted by the acronym FEW, corresponding to less than 30% of sky coverage [73].

2.6. Statistical Analysis

All the datasets were prepared separately and scrutinized for obvious errors. The datasets were also in UTC (Coordinated Universal Time) and had the timing adjusted to the corresponding time of Natal, which is used here (UTC-2). As the cloud cover, METAR data were in hourly frequency, and the ground-based UV index series were grouped according to the hourly average for the selection of the hours corresponding to the clear-sky condition. Then, ground-based data were analyzed for diurnal and seasonal variability under all-sky and clear-sky conditions. For ground-based measurements, a percentage difference in the hourly average UV index under clear and all-sky conditions was also calculated. This aids in better understanding how the UV index fluctuates throughout the day under these differing sky conditions. The percentage difference (PDI) was calculated as in Equation (2).

$$PDI = \left(\frac{avg_{ck} - avg_{ak}}{avg_{ak}} \right) \times 100\% \quad (2)$$

where avg_{ck} is the averaged UV index value under clear-sky conditions for the specified hour and the avg_{ak} is the averaged UV index value under all-sky conditions for the specified hour. This formula determines how much the UVI under clear-sky conditions differs from that under all-sky conditions, expressed as a percentage of the UV index under all-sky conditions.

The datasets were compared at local noontime and at the overpass time (around 1:45 p.m. local time for OMI). METAR cloud-cover data was used to select clear-sky hours in the noontime datasets. To the overpass dataset, both METAR and LER were applied since LER from OMI corresponds to the overpass time (Table 3).

Table 3. Summary of the technique used to select clear sky for each dataset of comparison.

Comparison	Technique to Select Clear Sky
Ground-based noontime vs. OMI noontime	Octas 0, 1 and 2 (METAR)
Ground-based noontime vs. GOME-2 noontime	Octas 0, 1 and 2 (METAR)
Ground-based overpass vs. OMI overpass	Octas 0, 1 and 2 (METAR) LER < 10%

To compare the ground-based with satellite data, the following metrics were calculated and analyzed: the Pearson correlation coefficient (r), the coefficient of determination (the square of the Pearson correlation coefficient r^2), Mean Bias Error (MBE), Mean Absolute Error (MAE), Mean Absolute Percentage Error (MAPE), the Root Mean Square Error (RMSE), and the p-value to determine the statistical significance of the relationship between the variables.

The Pearson's coefficient (r), Equation (3), commonly used in linear regression, is a popular correlation coefficient used to measure how strong a relationship is between two variables [74]. The correlation between the two variables is quantified with a number that varies between -1 and $+1$ [75]. Zero means there is no correlation, whereas 1 means a complete or perfect correlation [76]. A negative r means that the variables are inversely related [76]. The r^2 (coefficient of determination) represents the proportion of variance in the dependent variable that can be explained by the independent variable [77]. The MBE is an average of algebraic errors, while the MAE is an average of the absolute errors

(Equations (4) and (5), respectively) [78]. In this work, the MBE can indicate whether the satellite-derived UV index overestimates or underestimates the ground-based measurements. The MAPE measures the average absolute error of a model as a percentage of the actual value [79]. It represents a measure of accuracy in statistics [80], expressed as Equation (6). The RMSE is a measure of the differences between calculated values (in this study, OMI and GOME-2 data) and observed values (ground-based observations). The smaller the RMSE values, the lower the residual variance [41]. This metric is calculated as in Equation (7).

$$r = \frac{\sum_{i=1}^{n}\left(S_{GND,i} - \overline{S}_{GND}\right)\left(S_{SAT,i} - \overline{S}_{SAT}\right)}{\sqrt{\left(\sum_{i=1}^{n}\left(S_{GND,i} - \overline{S}_{GND}\right)^2\right)\left(\sum_{i=1}^{n}\left(S_{SAT,i} - \overline{S}_{SAT}\right)^2\right)}} \quad (3)$$

$$MBE = \frac{1}{n}\sum_{i=1}^{n}\left(S_{SAT,i} - S_{GND,i}\right) \quad (4)$$

$$MAE = \frac{1}{n}\sum_{i=1}^{n}\left|S_{SAT,i} - S_{GND,i}\right| \quad (5)$$

$$MAPE = \frac{1}{n}\sum_{i=1}^{n}\left(100 * \frac{\left|S_{SAT,i} - S_{GND,i}\right|}{S_{GND,i}}\right) \quad (6)$$

$$RMSE = \sqrt{\frac{1}{n-1}\sum_{i=1}^{n}\left(S_{SAT,i} - S_{GND,i}\right)^2} \quad (7)$$

where S is the UV index, $\overline{S}$ is the averaged UV index, SAT is the satellite observation, GND is the ground-based observation, and n is the number of observations.

These metrics together provide a comprehensive view of the accuracy and reliability of satellite data as compared to ground-based data. It helps in identifying potential biases, understanding the strength of the relationship, and quantifying the magnitude and relative importance of the errors.

3. Results

3.1. Ground-Based Derived UV Index Time Variability

Hourly data from the ground-based UV measurements in Natal were analyzed for the period 2006–2022. Raw data are provided in Figure 2. Data gaps are evident, with the longest being between 2017 and the end of 2018. A total of 53,286 h of UV index data was collected, with the maximum reaching 16 (extreme UV index) and an average of 6.22 (high UV index level). Throughout the years, high levels of UV start at 9 a.m. going until 3 p.m., reaching extreme between 10 a.m. and 2 p.m., as expected from a typical diurnal solar UV pattern, characterized by the increase of UV index levels during the day, to a peak reached at solar noon, and the decrease during the afternoon as solar zenith angle increases again [41].

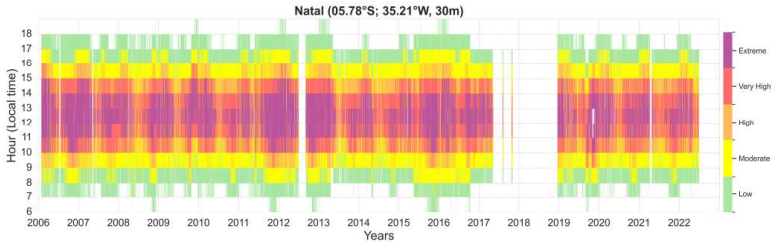

Figure 2. UV index observations as a function of day and hour per day for Natal, Brazil, from 2006 to 2022.

In this study, the comparison of ground-based and satellite-derived UV indices is made only using data from clear-sky conditions. Figure 3 shows the monthly climatological average cloud cover (in octas) for Natal for all available years between 2006 and 2022, shown as a function of time of day and month of the year, to illustrate how the cloud cover varies in Natal according to METAR cloud cover data.

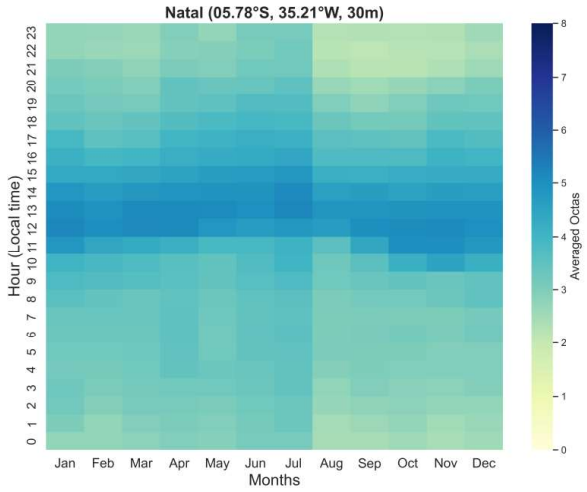

Figure 3. The monthly climatological average cloud cover (in octas) for Natal for all available years between 2006 and 2022 shown as a function of time of day and month of the year.

Around noon, there is a greater presence of cloud cover throughout the year. Clear-sky conditions prevail during night hours, as can be seen with the clear colors during these times and more hours of clear sky from August to November. These months correspond to the dry season in this region, from August to November [81]. Ref. [27] reported a similar pattern in cloud-cover variability throughout the year in their study of UV extreme events in northeast Brazil.

Figure 4a shows the percentage distribution of cloud cover for Natal for the period between 2006 and 2022, considering all day and night hours and only day hours. The clear-sky condition represents 24.18% of the day and night hours. It represents an even smaller percentage when taking into consideration only daylight hours (6 a.m. to 6 p.m.), exactly 15.21%, corresponding to 2925 h of clear-sky conditions during the days.

As indicated in Figure 4b, from 6 a.m. to 11 a.m., the averaged cloud clover indicates the predominance of scattered clouds (SCT = 3, 4 octas), while between 12 and 1 p.m., broken clouds prevail (BKN = 5, 6, 7 octas). In the afternoon, the scattered clouds prevail, but with a higher average, indicating a lower prevalence than in the morning hours. The short-term variability of the UV radiation reaching the Earth's surface is mainly controlled by changes in cloud cover [21,43,44], which mainly has an attenuating effect on the UV (20% to 70% for overcast skies) [44] but also enhancement effects manifested by increased UV irradiance at the surface compared with the equivalent clear-sky situation [21,44]. According to [45], enhancements were found to be most pronounced for large cloud cover of 5 to 7 octas (broken clouds) when the solar disk is unoccluded. This result of cloud-cover variability indicates that in Natal, around noontime, there is a greater presence of cloud cover (broken clouds), which can explain the higher UV index values registered under all-sky than under clear-sky conditions at noontime (5 and 6).

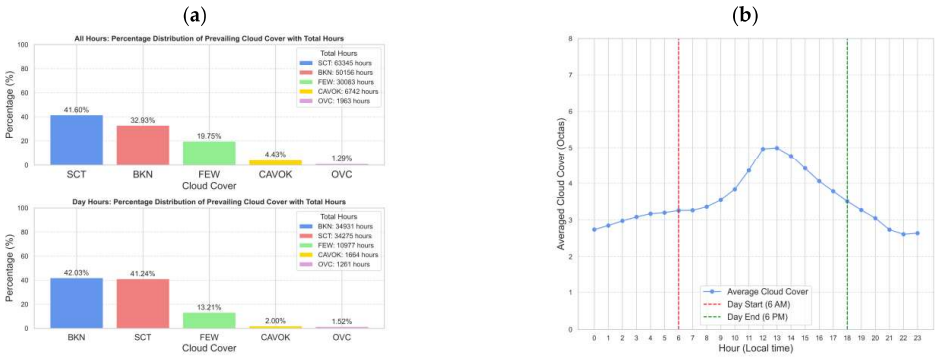

Figure 4. (**a**) Percentage distribution of cloud cover for Natal for the period between 2006 and 2022 considering all day and night hours (upper plot) and only day hours (bottom plot). (**b**) Daily climatological average cloud cover (in octas) for Natal for the period of 2006 to 2022.

In Figure 5, the monthly average ground-based UV index levels for Natal for all available years between 2006 and 2022 as a function of time of the day and month of the year under all and clear-sky conditions are presented. The UV index shows a semi-annual cycle with two maxima and a minimum in a year (Figure 5). At stations within the Tropic of Capricorn, the case of Natal, the Sun is at its peak twice a year, around the equinoxes when the Sun is directly overhead at the equator, and the stations register two annual maxima [82]. For Natal, the two peaks occurred in the summer and spring months. Similar results were reported by [48,82], and two-year maxima were also reported by [83] for Mahé. The effects of latitude on solar UV index levels are apparent, where even during austral winter months, high, very high, and extreme UV index levels were registered. Natal is located at latitude 05.78°S, where the solar zenith angle is lower throughout the year, which induces higher-intensity UV throughout the year.

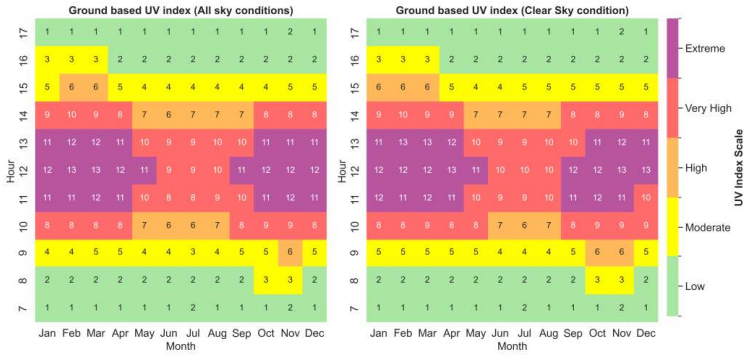

Figure 5. The monthly average ground-based UV index levels in Natal for the years between 2006 and 2022 as a function of time of day and month of the year under all and clear-sky conditions.

The UV index values were generally higher under clear-sky conditions; however, during noontime, the months of January, February, and March showed higher UV index levels under all-sky conditions than under clear-sky conditions. A similar characteristic occurred at 11 a.m. in December. The percentage difference in hourly average UV index levels between clear sky and all-sky conditions for Natal, shown in Figure 6, reinforces this result.

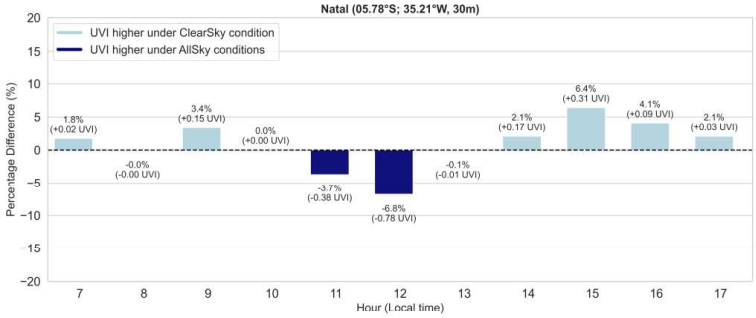

Figure 6. Percentage difference in hourly average UV index levels between clear sky and all-sky conditions for Natal for all available years between 2006 and 2022.

The UV index is higher under clear-sky conditions during the early morning and late afternoon hours. It is important to note that the difference is small, with the UV index under clear-sky conditions being at most 0.31 units higher than under all-sky conditions, peaking at 3 p.m. At noon, when the cloud average is in the broken cloud's interval (Figure 4b), the UV index under all-sky conditions is 6.8% higher than under clear-sky conditions, which means a 0.78 UV index unit higher. Ref. [82] reported an increase of 18% in the UV levels under a partially cloudy sky due to multiple reflections for the city of Maceió (9.28°S, 35.49° W, 127 m), northeast Brazil.

According to [84], surface UV can be enhanced under scattered or broken cloud conditions, occurring when the Sun is not obscured by clouds and there are clouds present elsewhere in the sky. The rainy season in Natal is concentrated between May and July [81]; however, the monthly rainfall starts to increase from December onwards [85]. Ref. [73] reported higher UV averages under all-sky conditions than under clear-sky conditions during some months (April, May, and December) of the rainy season for the city of Santarém, Northern Brazil. According to the authors, during the rainy season, factors such as the presence of cumulus or deep cirrus clouds can produce multiple scatterings, which can locally increase the UV reaching the surface [73,74].

Regarding the hourly UV index variability, the Environmental Protection Agency (EPA) informs that for the average person, low danger from the Sun's UV rays only occurs when the UV index ranges from 0 to 2. Even so, it is recommended to wear sunglasses on clear days, protect yourself with clothing, and use broad-spectrum SPF30+ sunscreen [86]. In Natal, this low-danger period only occurs until 8 in the morning and 4 in the afternoon (Figure 7). It is important to note that even during those hours, moderate levels were recorded (Figure 7).

At 9 a.m., the predominance is moderate, achieving high intensity. At 3 p.m., most of the UV is moderate, and very high levels are achieved. When the level is at most moderate, the recommendations are as follows: Stay in the shade; if outdoors, wear protective clothing, a wide-brimmed hat, and UV-blocking sunglasses; generously apply broad-spectrum SPF30+ sunscreen every 2 h, even on cloudy days and after swimming or sweating; avoid long stay over bright surfaces, like sand, water, and snow, which reflect and increase UV [86].

Between 10 a.m. and 2 p.m., extreme levels were recorded, with noon having medium and average UV index under all-sky conditions in the extreme range (UVI $\geq$ 11). Unprotected skin and eyes can have a sunburn in minutes if the UV index is 11 or more and there is no Sun protection [86]. It is recommended to avoid Sun exposure when these levels are reached and take all the recommendations recommended by [21,49]. During 5 h of the day, between 10 a.m. and 2 p.m. (UTC-2), the population in Natal can be exposed to extreme UV levels. The World Health Organization recommends Sun protection mainly between 10 a.m.

and 4 p.m. when radiation is most intense [21]. According to these results, protection is needed from 8 a.m. for those who frequent the city of Natal. Considering the hours with extreme levels, maximum protective measures need to be taken from 10 a.m. (UTC-2).

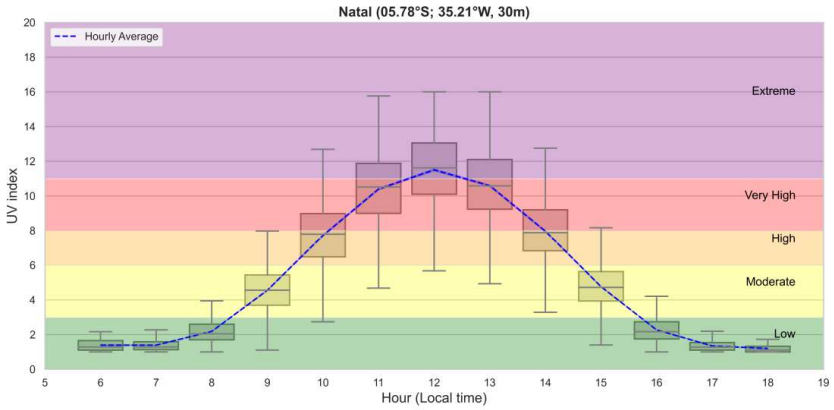

Figure 7. Hourly averaged UV index levels for Natal from 2006 to 2022.

The daily cycle of the UV index reported by [33] for the year 2008 also achieved moderate levels at 8 a.m., high at 9 a.m., and very high and extreme from 10 a.m. Similar results were reported by [31] regarding the monthly hourly UV index averages for the period of 2001–2007.

3.2. Comparison of Ground-Based vs. Satellite-Derived UV Index

Figure 8 shows the time series of the noontime and overpass time (respective to OMI) UV index from ground-based (GB) measurements in Natal under all-sky conditions. It also shows the UV index derived from OMI at noon and overpass time and from GOME-2 at noontime. The satellite, as well as the GB time series, shows a semi-annual cycle with two maxima in a year. In Natal, a daily maximum of 16 UV index has been recorded in different years. Ground-based and OMI noontime UV index presented a UV index maximum of 16, while the GOME-2 and OMI overpass reached a maximum of 14.72 and 14.80, respectively. Nevertheless, in all cases, these values represent an extreme UV index, as expected for noon and overpass time, which is around noon (approximately 1.45 p.m.).

The average UV index level from the GB at noontime was 11.50. From OMI at noontime, it was 11.41. From GOME-2 at noontime, 10.31, and according to OMI at overpass time, the average over the whole period was 8.73. In comparison with other cities around the same latitude, measurements made from 2017 to November 2020 in the city of Mahé (4.67°S, 55.53°E, 15 m a.s.l.) in Seychelles indicated UVI averages around 14 at noontime, while cities further south (Antananarivo, Anse Quitor and Saint-Denis) showed UVI averages at noontime of around 10 [83]. According to the authors, this difference is due to the difference in latitude [81]. Mahé is located at latitude 4.6.S (closer to Natal's latitude (5.78°S), and the other cities are at latitude near 20°S. Therefore, the solar zenith angle in Mahé, as in Natal, is lower throughout the year, which induces a higher-intensity UV.

Figure 9 shows the time series comparing ground-based versus satellite-derived solar UV index data from 2006 to 2022 at satellite noon and overpass time. The comparisons were performed only for clear-sky days selected with METAR, LER, and the days considered clear sky using both LER and METAR. Table 4 brings the descriptive statistics for each dataset for each comparison.

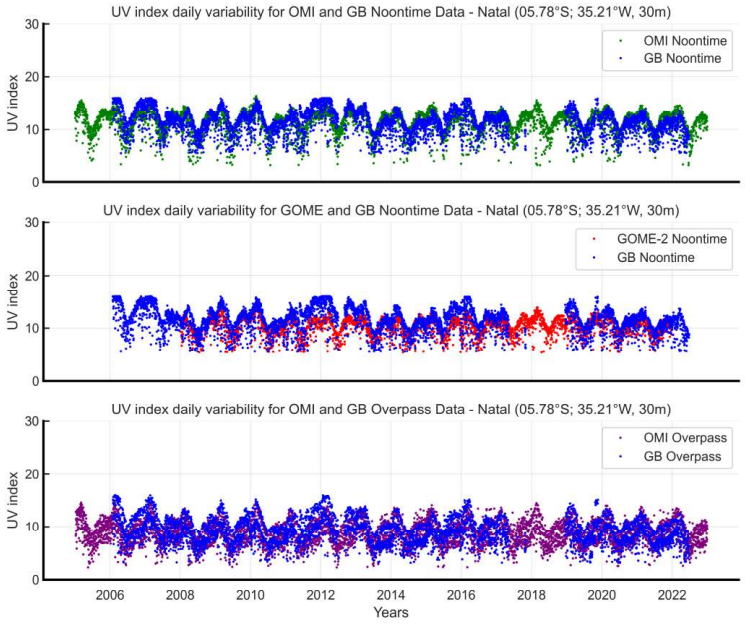

Figure 8. Daily variability of the UV index in Natal for all years of study. GB noontime refers to the ground-based data at noontime. GB overpass refers to the ground-based data at OMI overpass time.

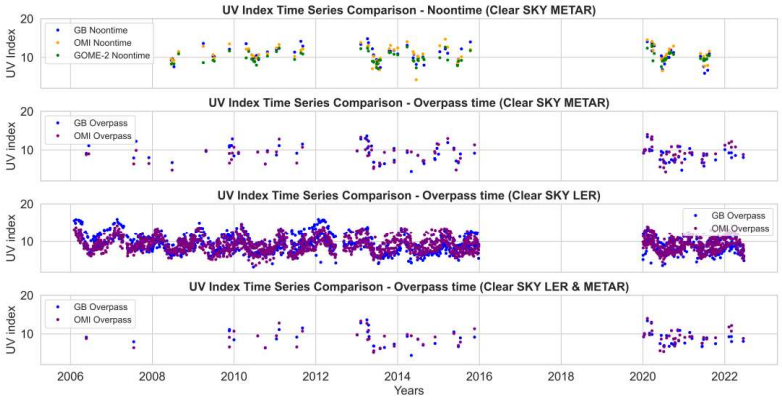

Figure 9. Time series comparing ground-based versus satellite-derived solar UV index data from 2006 to 2022 at satellite noon and overpass time. The comparisons were performed only for clear-sky days selected with METAR and LER, and the days considered clear sky using both LER and METAR.

For certain periods, a visual comparison shows large differences between the UV index levels taken from different instruments. For example, from 2008 to 2009, the differences between the noontime UVI from GB measurements and GOME-2 increased. Correlation analysis confirmed the smallest correlation between these two datasets (GB noontime vs. GOME-2 noontime) (Figure 10), where R and R^2 values ranged from a moderate positive

correlation for GB noontime vs. GOME-2 noontime to a strong positive correlation for GB noontime vs. OMI noontime.

Table 4. Summary of descriptive statistics for each time series comparison where GB Noon (ground-based UV index at local noontime) and GB OVP (ground-based UV index at local OMI overpass time); CKT (clear-sky technique) refers to the technique used to select clear-sky days.

Metrics	N	Mean	Std	Min	25%/75%	50%	Max	CKT
GB Noon	109	10.75	1.89	5.86	9.65/12.08	10.46	14.81	METAR
OMI Noon	109	10.81	1.92	4.18	9.54/12.20	10.65	14.71	METAR
GOME-2 Noon	109	9.96	1.42	7.06	9.0/11.13	9.57	13.24	METAR
GB OVP	138	9.08	2.08	4.15	7.48/10.41	9.05	15.12	METAR
OMI OVP	138	8.96	2.09	4.31	7.24/10.64	9.05	14.01	METAR
GB OVP	1928	9.14	2.18	3.16	7.46/10.53	8.95	15.96	LER
OMI OVP	1928	9.24	1.93	3.80	7.79/10.55	9.10	14.70	LER
GB OVP	95	8.98	1.98	4.15	7.44/10.26	8.96	15.12	Both
OMI OVP	95	9.06	1.98	5.20	7.55/10.69	9.06	14.01	Both

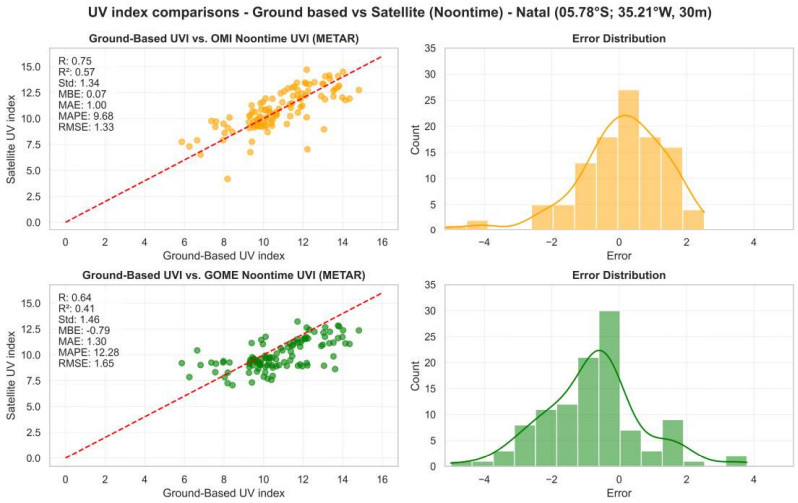

Figure 10. Correlation between ground-based UV index and satellite-derived UV index data (OMI, GOME-2) from 2008 to 2022 for Natal at local noontime and under clear-sky conditions selected with METAR. The Red dashed line represents the line of perfect agreement (y = x). *p*values : 2.68×10^{-21}, 4.48×10^{-06}. The first p − value refers to GB vs. OMI (noontime) and the second to GB vs. GOME-2 (noontime).

GB overpass vs. OMI overpass, in all scenarios (clear-sky LER, clear-sky METAR, and clear-sky both), also presented moderate to strong positive correlation (0.62, 0.69, and 0.70, respectively). Ref. [41] reported a positive moderate correlation between ground−based versus OMI−derived UV index for the city of Pretoria (25.73°S, 28.18°E, 1330 m from 1994 to May 2003 and 25.81°S, 28.49°E, 1228 m from May 2003 to 2015) in South Africa.

The positive MBE (Figure 10) suggests that, on average, UVI derived from OMI at noontime overestimates the GB UVI by 0.07 units in Natal. From the comparison of GB noontime vs. GOME-2 noontime, the negative MBE suggests that, on average, the UVI derived from GOME-2 at noontime underestimates the GB UVI by −0.79 units. For the overpass time (Figure 11), the negative MBE suggests that on average, UVI derived from

OMI overpass (METAR) also underestimates the GB UVI by −0.12 units, while when using LER to select clear-sky days, the MBE suggests that on average UVI derived from OMI at overpass time overestimates the GB UVI by 0.10 units. When using both techniques, it has the smallest absolute MBE of the three, indicating it is the least biased.

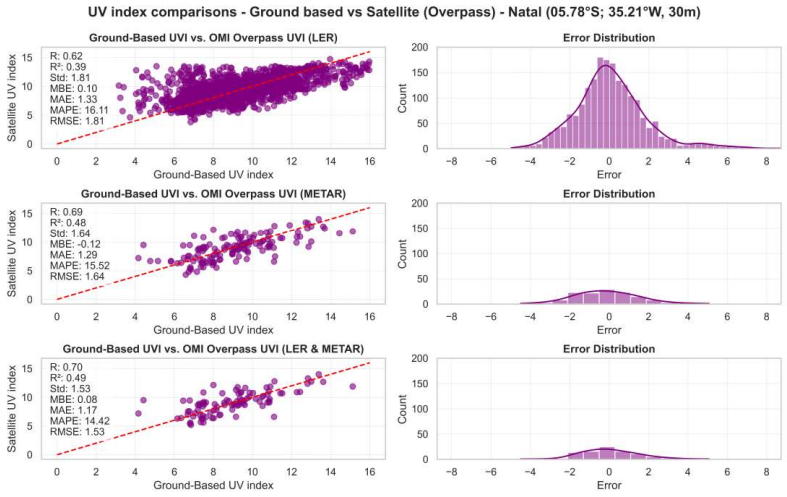

Figure 11. Correlation between ground-based UV index and satellite-derived UV index data (OMI) from 2006 to 2022 for Natal at overpass time and under clear-sky conditions selected with LER, METAR, and hour considered clear sky using both techniques (LER, METAR). p values : 1.80×10^{-206}, 3.93×10^{-21}, 2.51×10^{-15}. The first $p-$value refers to GB vs. OMI (overpass−LER), the second to GB vs. OMI (overpass−METAR), and the third to GB vs. OMI (overpass−LER and METAR).

According to [87], the validation of UV index retrieved from OMI at noontime against ground-based measurements at different climates in Egypt performed in all-sky conditions in the period 2012–2017 at three sites: Aswan (23.97°N, 32.78°E, 192.5 m, Pyranometer), Cairo (30.08°N, 31.28°E, 34.4 m, Pyranometer) and Matruh 31.33°N, 27.22°E, 25 m, Brewer MK II) showed that OMI overestimates ground-based observations in all seasons at all stations with annual mean bias of 0.52, 0.68 and 1.02 to Aswan, Cairo and Matruh, respectively.

Ref. [88] examined the OMI UV performance in different cloudiness conditions using ground-based observations in Jokioinen (60.8°N, 23.5°E) and Sodankylä (67.3°N, 26.6°E) for the years 2005 to 2011 at the time of satellite overpass. They reported that for both Jokioinen and Sodankylä, OMI UV overestimates the surface UV index with a mean bias of 0.50 for Jokioinen and 0.26 for Sodankylä under clear-sky conditions. Ref. [3] found that at Irene (25.91°S, 28.21°E, 1523 m), De Aar (30.67°S, 23.99°E, 1284 m) and Upington (28.48°S, 21.12°E, 848 m), the GOME-2 data underestimated surface UVA measurements with MBE of −5.5, −11.2 and −12.8 at Irene, De Aar and Upington, respectively, under clear-sky conditions.

The MAE of 1 means that, on average, the absolute difference between the UVI derived from OMI and the GB at noontime is 1, and for GOME-2 is 1.30. The MAE at overpass time, using the three techniques, is higher than the MAE from OMI noontime, indicating that the OMI overpass UVI has the largest average deviation from the GB UVI, even though the difference is quite small between all the datasets. The MAPE of 9.68 implies that the UVI derived from OMI deviates by about 9.68% on average from the GB UVI at noontime. The largest deviation occurred between the OMI and GB overpass time when using the LER technique, with a deviation of 16.11%.

Ref. [41] reported that the MAPE between OMI and ground-based index at overpass time using LER were 27% for Pretoria (25.73°S, 28.18°E, 1330 m, 1994 to May 2003), 28% for Durban (29.97°S, 31.00°E, 9 m, 1994 to May 2010) and 46% for De Aar (30.67°S, 23.99°E 1286 m 2002 to 2015). Comparisons between ground-based and OMI-derived UV index at noontime showed annual MAPE of 10.6% for Aswan (23.97°N, 32.78°E, 192.5 m, Pyranometer), 17.3% for Cairo (30.08°N, 31.28°E, 34.4 m, Pyranometer) and 26.0% for Maltruh (31.33°N, 27.22°E, 25 m, Brewer MK II) for the period between 2012 and 2017, under all-sky conditions [87]. This means that even if the MAPE at overpass time in this work is higher than at noontime, still the agreement is better than the agreement between OMI overpass and the ground-based measurements made in Cairo and Maltruh cities in Egypt by [87] and in Pretoria, Durban, and De Aar in South Africa [41].

The comparison between GB and OMI at noontime has the lowest RMSE (1.33) of all comparisons. This suggests that the OMI noontime estimations are in closer agreement with the GB non-noontime measurements compared to the GOME-2 noontime and OMI overpass estimations. Nevertheless, the difference between the metrics results is quite small between the datasets, showing that satellite UV index measurements have a good agreement with the ground-based measurements, as indicated by the moderate to high correlation coefficients and the clustering of points near the red line in the scatter plots. Another indicator of this good agreement is the error distribution plots. These plots reveal that most errors cluster around zero. Notably, the GOME-2 noontime and OMI overpass (METAR) data are slightly skewed to the left, aligning with the negative Mean Bias Error (MBE) and reinforcing the slight underestimation observed.

4. Discussion

The Davis 6490 UV sensor used to monitor UV levels in Natal has an accuracy of ±5%, with a drift of up to ±2% per year [57]. The most notable error sources for this instrument include troubleshooting due to cable connections, plugs not firmly seated, and lack of calibration in the frequency recommended in the user manual [57]. For the first time, the entire dataset from 2006 to 2022 of UV index levels in Natal monitored with the Davis Sensor 6490 has been analyzed for diurnal and seasonal variability under all and clear-sky conditions. Furthermore, the main objective of this study was to conduct a comparative analysis of ground-based and satellite-derived UV index levels from OMI and GOME-2 in Natal, Brazil, under clear-sky conditions, to assess the reliability of different satellite-derived UV index data for this site, should these data be used for long-term trend analysis, or the monitoring of solar UV exposure risk and possible impacts to the environment.

Regarding the UV time variability in Natal, the UV index showed a semi-annual cycle with two maxima in a year, during austral summer and spring, with smaller UV index levels during austral winter. The less-intense levels during austral winter, around noon, continue to be very high levels on the UV index scale. These characteristics agree with what is expected for a city at the location of Natal, at latitude 05.78°S, where the solar zenith angle is lower throughout the year, inducing higher-intensity UV throughout the year. Also, since Natal is within the Tropic of Capricorn, the Sun is at its peak twice a year, around the equinoxes when the Sun is directly overhead at the equator, with the stations recording two annual maxima [40].

Another important characteristic is that in Natal, around noon, there is a greater presence of cloud cover throughout the year (average in the broken clouds interval). Clear-sky conditions prevail during night hours, and there are more hours of clear sky between August and November, the dry period in the region. The clear-sky condition represents only 15.21% of daylight hours. This pattern of cloud-cover variability can explain the higher UV index values registered under all-sky than under clear-sky conditions at 11 a.m. and 12 p.m. since it is already indicated in the literature that partially cloudy skies, under scattered or broken clouds, can produce multiple scatterings that can increase locally UV levels at the surface, reaching levels higher than under clear skies [17,46,74].

These results indicate that in Natal, even during clear or all-sky conditions, the UV index is generally high. Between 10 a.m. and 2 p.m., the population in Natal can be exposed to extreme UV levels. Therefore, protection is needed from 8 a.m. for those who frequent the city of Natal. Considering the hours with extreme levels, maximum protective measures need to be taken from 10 a.m. It is important to note that this study uses UTC-2, according to the latitude at which Natal is located, but the inhabitants of Natal follow the UTC of the capital of Brazil, Brasilia (UTC-3). This means that from 7 a.m., anyone visiting or living in Natal must protect themselves adequately from the UV radiation, with maximum protective measures needed from 9 a.m. onwards if following UTC-3.

Regarding the comparisons between ground-based and satellite-derived UV index, OMI UVI at the overpass and noontime presents less bias than GOME-2 UVI. While OMI mainly overestimates the UV index levels in comparison with ground-based measurements, GOME-2 underestimates it. UV products derived from OMI are known to overestimate ground-based measurements [60–62,87,88]. Part of the positive bias between OMI UVI and ground-based UVI is due to absorbing aerosols [18,62]. It is important to emphasize that this is not a statement particular about the Natal, although the inaccurate description of the absorbing aerosols is a possible explanation for the observed discrepancies. Other factors of uncertainty are clear-sky irradiance modeling (depending on ozone surface albedo), the cloud–aerosol correction factor, and satellite overpass occurring at a time significantly different from local noon [18]. In Natal, the satellite overpass of OMI is about 13:45 $\pm$ 15 min LT), not too different from the noontime, 12 p.m. While the overpass time of the GOME-2 (09:30 a.m. LT) is more distant from noontime. Another factor of uncertainty on GOME-2 UV products is also the climatology of aerosols and surface albedo used in the algorithm, which was not determined from observations [3].

Through this study, it was possible to identify that the technique used to select a clear sky also affects the statistical comparison metrics. For example, regarding the difference between the techniques used to identify clear-sky conditions, the LER method identified a significantly larger number of clear-sky days (1928 days) compared to the METAR method (138 days) at overpass time. This significant difference suggests that the LER method could have more flexible criteria for defining "clear-sky" conditions, potentially including days with more cloud cover compared to what METAR considers as clear-sky. The difference in the number of clear-sky days identified confirms that these two methods have vastly different criteria for identifying clear-sky days. METAR seems to be more conservative than LER. The difference between the METAR alone and the combined METAR and LER (43 days) indicates that there are days that METAR identifies as clear-sky days but are not considered clear-sky days when using the combined approach. This could potentially be days with minor cloud cover that METAR considers, but LER does not. These differences highlight the importance of understanding the specific criteria each method uses to identify clear-sky days and suggest that a careful selection or combination of methods might be necessary to obtain the most accurate representation of clear-sky days for each specific study or application.

Another point is that the negative MBE values associated with the METAR technique indicate that the satellite-derived UV index levels are, on average, lower than the ground-based UV index measurements. This discrepancy could potentially be due to the METAR data indicating clear skies, while the satellite data identifies these days as not entirely clear, estimating lower UVI values. The METAR data are usually based on observations at airports and represent local clear-sky conditions more accurately than satellite data, which captures a larger area. For satellite observations, the variation introduced by clouds is spatially averaged over the area of the pixel [89]; therefore, the satellite data might be noticing atmospheric or cloud-cover variations over a broader region that are not captured in the localized METAR. Implementing sky cameras installed near the UV sensor could reduce uncertainties associated with the technique used to determine clear-sky conditions. These cameras would provide clear images of the sky, helping to determine the

actual sky conditions more accurately, thus potentially reducing uncertainty related to the sky condition.

Overall, metrics such as MAE, MAPE, and RMSE indicate that differences between the satellite and ground-based measurements are generally low. Together with the moderate and strong correlation coefficients, the clustering of points near the red line in the scatter plots, and the error distribution plots clustered around zero, the analysis indicates that the two satellite sources (OMI noontime and overpass) and GOME-2 noontime are a reliable source for UV index data, showing good agreement with ground-based measurements.

5. Conclusions

The main aim of this paper was to conduct a comparative analysis between the ground-based measured UV index levels in Natal, Brazil, and the satellite-derived UV index from OMI and GOME-2. The comparison reported here was carried out using UV index levels under clear-sky conditions. The hours of clear sky were selected using cloud-cover data from METAR, using LER, and applying both techniques together. Furthermore, in this paper, an analysis of the diurnal and seasonal variability of the UV index under all clear-sky conditions in Natal was also reported.

For all the time series, the UV index showed an annual cycle with two maxima in a year, during austral summer and spring, with smaller UV index levels during austral winter. The less-intense levels during austral winter, around noon, continue to be very high levels on the UV index scale. In Natal, a daily maximum of 16 UV indexes were recorded in different years in the ground-based and OMI noontime time series. The UV index was derived from GOME-2, and the OMI overpass reached less than 15. Nevertheless, in all cases, these values represent an extreme UV index.

There has been a greater presence of cloud cover around noontime in Natal all over the years. Clear-sky conditions prevail during night hours, with hours of clear sky representing only 15.21% of daylight. There are more hours of clear sky between August and November, the dry period in the region. The UV index under all-sky is higher than under clear-sky conditions from 11 a.m. to noon, hours when the averaged cloud cover indicates a greater presence of broken clouds, suggesting the influence of cloud cover in enhancing the ground-based UV index levels under partially cloudy skies.

In Natal, the low-danger period of exposure to UV rays only occurs until 8 a.m. and from 4 p.m. onwards. However, even during those hours, moderate levels were recorded. Therefore, protection is needed from 8 a.m. for those who frequent the city of Natal. Between 10 a.m. and 2 p.m., the population in Natal is exposed to extreme UV levels. Considering the hours with extreme levels, maximum protective measures need to be taken from 10 a.m., considering UTC-2. When following UTC-3, these recommendations should be followed 1 h in advance.

The differences between the techniques used to identify clear-sky conditions highlight the importance of understanding the specific criteria each method uses to identify clear-sky days and suggest that a careful selection or combination of methods might be necessary to obtain the most accurate representation of clear-sky days for each specific study.

The errors between the satellite and ground-based measurements are generally low, with the analysis indicating that the two satellite sources (OMI noontime and overpass) and GOME-2 noontime are reliable sources for UV index data, showing good agreement with ground-based measurements. OMI UVI at noon and overpass time are less biased than GOME-2 noontime UVI.

This study differs from previous studies and contributes to the scientific understanding of UV radiation levels using unpublished UV index data from a ground-based station in a city located near the equator, in South America's tropical region, where until now, there has been relatively limited research focusing on this field of study. With the reliability of these satellite data accessed for Natal, we will study the trends of the UV index in this tropical Brazilian site in future works.

Author Contributions: Conceptualization, G.C.G.d.R. and H.B.; methodology, G.C.G.d.R.; software, G.C.G.d.R.; validation, G.C.G.d.R., H.B., K.L. and F.R.d.S.; formal analysis, G.C.G.d.R. and M.A.G.d.R.; investigation, G.C.G.d.R.; resources, R.S., L.V.P., T.P., D.K.P. and F.R.d.S.; data curation, G.C.G.d.R. and M.A.G.d.R.; writing—original draft preparation, G.C.G.d.R.; writing—review and editing, G.C.G.d.R.; visualization, G.C.G.d.R., H.B., M.A.G.d.R. and L.V.P.; supervision, R.S., L.V.P., H.B. and T.P.; project administration, G.C.G.d.R.; funding acquisition, G.C.G.d.R., D.K.P., L.V.P., R.S. and T.P. All authors have read and agreed to the published version of the manuscript.

Funding: This research was funded by FAPESPA (Amazon Foundation for the Support of Studies and Research), by CAPES (Coordination for the Improvement of Higher Education Personnel), a foundation linked to the Brazilian Ministry of Education, CAPES project number 88887.130199/2017—01, COFECUB (French Evaluation Committee of the University and Scientific Cooperation with Brazil) and by the French Government under the 2023 Campus France project of cotutelle cost-sharing doctoral scholarships. The APC was funded by Universidade Federal do Oeste do Pará.

Data Availability Statement: Data are available on request from G.C.G.d.R.

Acknowledgments: We acknowledge the support and funding of this work by the FAPESPA for the PhD scholarship in the Post Graduate Program in Society Nature and Development. To CAPES (Coordination for the Improvement of Higher Education Personnel) and COFECUB (French Evaluation Committee of the University and Scientific Cooperation with Brazil) for the sandwich PhD scholarship awarded to the MESO project (Modeling and Prediction of the Secondary Effects of the Antarctic Ozone hole). To the French Government, Campus France, LACy (UMR 8105 CNRS, Météo-France), and the University of Réunion.

Conflicts of Interest: The authors declare no conflicts of interest.

References

1. Cadet, J.-M.; Bencherif, H.; Cadet, N.; Lamy, K.; Portafaix, T.; Belus, M.; Brogniez, C.; Auriol, F.; Metzger, J.-M.; Wright, C.Y. Solar UV Radiation in the Tropics: Human Exposure at Reunion Island (21° S, 55° E) during Summer Outdoor Activities. *Int. J. Environ. Res. Public Health* **2020**, *17*, 8105. [CrossRef]
2. Diffey, B.L. Solar Ultraviolet Radiation Effects on Biological Systems. *Phys. Med. Biol.* **1991**, *36*, 299–328. [CrossRef] [PubMed]
3. Du Preez, D.J.; Parisi, A.V.; Millar, D.A.; Benchérif, H.; Wright, C.Y. Comparison of GOME-2 UVA Satellite Data to Ground-Based UVA Measurements in South Africa. *Photochem. Photobiol.* **2020**, *96*, 1342–1349. [CrossRef]
4. United Nations Environment Programme. *Environmental Effects of Stratospheric Ozone Depletion, UV Radiation, and Interactions with Climate Change: 2022 Assessment Report*; UNEP Ozone Secretariat: Nairobi, Kenya, 2023. Available online: https://ozone.unep.org/system/files/documents/EEAP-2022-Assessment-Report-May2023.pdf (accessed on 27 October 2023).
5. Lucas, R.M.; Yazar, S.; Young, A.R.; Norval, M.; de Gruijl, F.R.; Takizawa, Y.; Rhodes, L.E.; Sinclair, C.A.; Neale, R.E. Human Health in Relation to Exposure to Solar Ultraviolet Radiation under Changing Stratospheric Ozone and Climate. *Photochem. Photobiol. Sci.* **2019**, *18*, 641–680. [CrossRef]
6. Lucas, R.M.; Byrne, S.N.; Correale, J.; Ilschner, S.; Hart, P.H. Ultraviolet Radiation, Vitamin D and Multiple Sclerosis. *Neurodegener. Dis. Manag.* **2015**, *5*, 413–424. [CrossRef]
7. Lindqvist, P.G.; Epstein, E.; Nielsen, K.; Landin-Olsson, M.; Ingvar, C.; Olsson, H. Avoidance of Sun Exposure as a Risk Factor for Major Causes of Death: A Competing Risk Analysis of the Melanoma in Southern Sweden Cohort. *J. Intern. Med.* **2016**, *280*, 375–387. [CrossRef]
8. Lindqvist, P.G.; Landin-Olsson, M. The Relationship between Sun Exposure and All-Cause Mortality. *Photochem. Photobiol. Sci.* **2017**, *16*, 354–361. [CrossRef]
9. Olsen, C.M.; Wilson, L.F.; Green, A.C.; Bain, C.J.; Fritschi, L.; Neale, R.E.; Whiteman, D.C. Cancers in Australia Attributable to Exposure to Solar Ultraviolet Radiation and Prevented by Regular Sunscreen Use. *Aust. N.Z. J. Public Health* **2015**, *39*, 471–476. [CrossRef]
10. Yousif, E.; Haddad, R. Photodegradation and Photostabilization of Polymers, Especially Polystyrene: Review. *SpringerPlus* **2013**, *2*, 398. [CrossRef]
11. Andrady, A.L.; Heikkilä, A.M.; Pandey, K.K.; Bruckman, L.S.; White, C.C.; Zhu, M.; Zhu, L. Effects of UV Radiation on Natural and Synthetic Materials. *Photochem. Photobiol. Sci.* **2023**, *22*, 1177–1202. [CrossRef]
12. Bornman, J.F.; Barnes, P.W.; Robinson, S.A.; Ballaré, C.L.; Flint, S.D.; Caldwell, M.M. Solar Ultraviolet Radiation and Ozone Depletion-Driven Climate Change: Effects on Terrestrial Ecosystems. *Photochem. Photobiol. Sci.* **2015**, *14*, 88–107. [CrossRef] [PubMed]
13. Ballaré, C.L.; Caldwell, M.M.; Flint, S.D.; Robinson, S.A.; Bornman, J.F. Effects of Solar Ultraviolet Radiation on Terrestrial Ecosystems. Patterns, Mechanisms, and Interactions with Climate Change. *Photochem. Photobiol. Sci.* **2011**, *10*, 226. [CrossRef]
14. Bancroft, B.A.; Baker, N.J.; Blaustein, A.R. Effects of UVB Radiation on Marine and Freshwater Organisms: A Synthesis through Meta-Analysis. *Ecol. Lett.* **2007**, *10*, 332–345. [CrossRef]

15. Sulzberger, B.; Austin, A.T.; Cory, R.M.; Zepp, R.G.; Paul, N.D. Solar UV Radiation in a Changing World: Roles of Cryosphere—Land—Water—Atmosphere Interfaces in Global Biogeochemical Cycles. *Photochem. Photobiol. Sci.* **2019**, *18*, 747–774. [CrossRef] [PubMed]
16. Erickson III, D.J.; Sulzberger, B.; Zepp, R.G.; Austin, A.T. Effects of Stratospheric Ozone Depletion, Solar UV Radiation, and Climate Change on Biogeochemical Cycling: Interactions and Feedbacks. *Photochem. Photobiol. Sci. S* **2015**, *14*, 127–148. [CrossRef]
17. Porfirio, A.C.S.; De Souza, J.L.; Lyra, G.B.; Maringolo Lemes, M.A. An Assessment of the Global UV Solar Radiation under Various Sky Conditions in Maceió-Northeastern Brazil. *Energy* **2012**, *44*, 584–592. [CrossRef]
18. Brogniez, C.; Auriol, F.; Deroo, C.; Arola, A.; Kujanpää, J.; Sauvage, B.; Kalakoski, N.; Pitkänen, M.R.A.; Catalfamo, M.; Metzger, J.-M.; et al. Validation of Satellite-Based Noontime UVI with NDACC Ground-Based Instruments: Influence of Topography, Environment and Satellite Overpass Time. *Atmos. Chem. Phys.* **2016**, *16*, 15049–15074. [CrossRef]
19. Vitt, R.; Laschewski, G.; Bais, A.; Diémoz, H.; Fountoulakis, I.; Siani, A.-M.; Matzarakis, A. UV-Index Climatology for Europe Based on Satellite Data. *Atmosphere* **2020**, *11*, 727. [CrossRef]
20. Bernhard, G.H.; Bais, A.F.; Aucamp, P.J.; Klekociuk, A.R.; Liley, B.; McKenzie, R. Stratospheric Ozone, UV Radiation, and Climate Interactions. *Photochem. Photobiol. Sci.* **2023**, *22*, 937–989. [CrossRef]
21. World Health Organization. Solar Ultraviolet Radiation: Global Burden of Disease from Solar Ultraviolet Radiation. Available online: https://www.who.int/publications/i/item/9241594403 (accessed on 13 October 2023).
22. de Paula Corrêa, M. Solar Ultraviolet Radiation: Properties, Characteristics and Amounts Observed in Brazil and South America. *An. Bras. Dermatol.* **2015**, *90*, 297–313. [CrossRef]
23. Suarez Salas, L.F.; Flores Rojas, J.L.; Pereira Filho, A.J.; Karam, H.A. Ultraviolet Solar Radiation in the Tropical Central Andes (12.0° S). *Photochem. Photobiol. Sci.* **2017**, *16*, 954–971. [CrossRef]
24. Estupiñán, J.G.; Raman, S.; Crescenti, G.H.; Streicher, J.J.; Barnard, W.F. Effects of Clouds and Haze on UV-B Radiation. *J. Geophys. Res. Atmos.* **1996**, *101*, 16807–16816. [CrossRef]
25. World Health Organization; World Meteorological Organization; United Nations Environment Programme & International Commission on Non-Ionizing Radiation Protection. Global Solar UV Index: A Practical Guide. Available online: https://apps.who.int/iris/handle/10665/42459 (accessed on 13 October 2023).
26. Bilbao, J.; de Migue, A. Erythemal Solar Irradiance, UVER, and UV Index from Ground-Based Data in Central Spain. *Appl. Sci.* **2020**, *10*, 6589. [CrossRef]
27. Lopo, A.B.; Helena, M.; Sérgio Lúcio, P.; Pinheiro, M. UV Extreme Events in Northeast Brazil. *Ciência E Nat.* **2014**, *36*, 482–490. [CrossRef]
28. Schalka, S.; Steiner, D.; Ravelli, F.N.; Steiner, T.; Terena, A.C.; Marçon, C.R.; Ayres, E.L.; Addor, F.A.S.; Miot, H.A.; Ponzio, H.; et al. Brazilian Consensus on Photoprotection. *An. Bras. Dermatol.* **2014**, *89*, 1–74. [CrossRef]
29. Herman, J.R.; DeLand, M.T.; Huang, L.; Labow, G.J.; Larko, D.; Lloyd, S.A.; Mao, J.; Qin, W.; Weaver, C.J. A Net Decrease in the Earth's Cloud, Aerosol, and Surface 340 Nm Reflectivity during the Past 33 Yr (1979–2011). *Atmos. Chem. Phys.* **2013**, *13*, 8505–8524. [CrossRef]
30. Augusto, J.; Ottaiano, A.; Pereira De Ávila, M.; Caixeta, C.; Alexandre, U.; Taleb, C. As Condições de Saúde Ocular No Brasil 2019. 2008. Available online: https://www.cbo.com.br/novo/publicacoes/condicoes_saude_ocular_brasil2019.pdf (accessed on 5 September 2023).
31. da Silva, F.R.; de Oliveira, H.S.M.; Marinho, G.S. Variação Do Índice de Radiação Solar Ultravioleta Em Natal—RN Entre 2001 E 2007. In Proceedings of the Congresso Brasileiro de Energia Solar-CBENS, Florianópoli, Brazil, 18–21 November 2008. Available online: https://anaiscbens.emnuvens.com.br/cbens/article/view/1336/1329 (accessed on 2 September 2023).
32. Marinho, G.S.; da Silva, F.R. Aspectos Da Radiação Ultravioleta Solar Em Natal—RN–BRASIL. *Soc. E Territ.* **2013**, *25*, 29–41. Available online: https://periodicos.ufrn.br/sociedadeeterritorio/article/view/3522 (accessed on 3 September 2023).
33. Lopo, A.B.; Spyrides, M.H.C.; Lucio, P.S.; Sigró, J. Radiação Ultravioleta, Ozônо E Total Aerossóis Na Cidade de Natal—RN. *HOLOS* **2013**, *6*, 3–21. [CrossRef]
34. Cadet, B.; Goldfarb, L.; Faduilhe, D.; Giraud, S.; Keckhut, P.; Réchou, A. A Sub-Tropical Cirrus Clouds Climatology from Reunion Island (21°S, 55°E) Lidar Data Set. *Geophys. Res. Lett.* **2003**, *30*. [CrossRef]
35. Fountoulakis, I.; Diémoz, H.; Siani, A.-M.; Laschewski, G.; Filippa, G.; Arola, A.; Bais, A.F.; De Backer, H.; Lakkala, K.; Webb, A.R.; et al. Solar UV Irradiance in a Changing Climate: Trends in Europe and the Significance of Spectral Monitoring in Italy. *Environments* **2020**, *7*, 1. [CrossRef]
36. United Nations Environment Programme (UNEP). Environmental Effects and Interactions of Stratospheric Ozone Depletion, UV Radiation, and Climate Change; 2018 Assessment Report; Nairobi, Kenya. Available online: https://ozone.unep.org/science/assessment/eeap (accessed on 23 September 2023).
37. Parra, R.; Cadena, E.; Flores, C. Maximum UV Index Records (2010–2014) in Quito (Ecuador) and Its Trend Inferred from Remote Sensing Data (1979–2018). *Atmosphere* **2019**, *10*, 787. [CrossRef]
38. Fontana, F.; Lugrin, D.; Seiz, G.; Meier, M.; Foppa, N. Intercomparison of Satellite- and Ground-Based Cloud Fraction over Switzerland (2000–2012). *Atmos. Res.* **2013**, *128*, 1–12. [CrossRef]
39. Silva, A.A.; Pereira, M. Ground-Based Measurements of Local Cloud Cover. *Meteorol. Atmos. Phys.* **2013**, *120*, 201–212. [CrossRef]
40. Damiani, A.; Cordero, R.R.; Cabrera, S.; Laurenza, M.; Rafanelli, C. Cloud Cover and UV Index Estimates in Chile from Satellite-Derived and Ground-Based Data. *Atmos. Res.* **2014**, *138*, 139–151. [CrossRef]

41. Cadet, J.-M.; Bencherif, H.; Portafaix, T.; Lamy, K.; Ncongwane, K.; Coetzee, G.J.R.; Wright, C.Y. Comparison of Ground-Based and Satellite-Derived Solar UV Index Levels at Six South African Sites. *Int. J. Environ. Res. Public Health* **2017**, *14*, 1384. [CrossRef] [PubMed]
42. González-Rodríguez, L.; Rodríguez-López, L.; Jiménez, J.; Luis, J.; García, W.; Duran-Llacer, I.; Pereira, A.; Barja, B. Spatio-Temporal Estimations of Ultraviolet Erythemal Radiation in Central Chile. *Air Qual. Atmos. Health* **2022**, *15*, 837–852. [CrossRef]
43. Kosmopoulos, P.G.; Kazadzis, S.; Schmalwieser, A.W.; Raptis, P.I.; Papachristopoulou, K.; Fountoulakis, I.; Masoom, A.; Bais, A.F.; Bilbao, J.; Blumthaler, M.; et al. Real-Time UV Index Retrieval in Europe Using Earth Observation-Based Techniques: System Description and Quality Assessment. *Atmos. Meas. Tech.* **2021**, *14*, 5657–5699. [CrossRef]
44. Bernhard, G.; Seckmeyer, G. Uncertainty of Measurements of Spectral Solar UV Irradiance. *J. Geophys. Res. Atmos.* **1999**, *104*, 14321–14345. [CrossRef]
45. Zhang, H.; Wang, J.; Castro García, L.; Zeng, J.; Dennhardt, C.; Liu, Y.; Krotkov, N.A. Surface Erythemal UV Irradiance in the Continental United States Derived from Ground-Based and OMI Observations: Quality Assessment, Trend Analysis and Sampling Issues. *Atmos. Chem. Phys.* **2019**, *19*, 2165–2181. [CrossRef]
46. du Preez, D.J.; Bencherif, H.; Portafaix, T.; Lamy, K.; Wright, C.Y. Solar Ultraviolet Radiation in Pretoria and Its Relations to Aerosols and Tropospheric Ozone during the Biomass Burning Season. *Atmos.* **2021**, *12*, 132. [CrossRef]
47. Kerr, J.B.; Fioletov, V.E. Surface Ultraviolet Radiation. *Atmos.-Ocean* **2008**, *46*, 159–184. [CrossRef]
48. Kirchhoff, V.W.J.H.; Echer, E.; Leme, N.P.; Silva, A.A. A Variação Sazonal Da Radiação Ultravioleta Solar Biologicamente Ativa. *Rev. Bras. Geofísica* **2000**, *18*, 63–74. [CrossRef]
49. Instituto Brasileiro de Geografia Estatística (IBGE). Estimativas Da População Residente Para Os Municípios E Para as Unidades Da Federação | IBGE. Available online: https://www.ibge.gov.br/estatisticas/sociais/populacao/9103-estimativas-de-populacao.html (accessed on 15 September 2023).
50. Furtado, E.M. A Onda Do Turismo Na Cidade Do Sol: A Reconfiguração Urbana de Natal. Available online: https://repositorio.ufrn.br/handle/123456789/13723 (accessed on 27 September 2023).
51. da Silva, F.R. Estudo Da Radiação Ultravioleta Na Cidade de Natal-RN. Ph.D. Thesis, Universidade Federal do Rio Grande do Norte, Natal, Brazil. Available online: https://oasisbr.ibict.br/vufind/Record/UFRN_54fe33d9c54657ddf7cceedfad43aa48 (accessed on 27 November 2023).
52. Instituto Nacional de Meteorologia (INMET). Normais Climatológicas Do Brasil 1961–1990. Available online: https://portal.inmet.gov.br/normais (accessed on 2 October 2023).
53. Neves, J.A. *Um Índice de Sustentabilidade Ao Fenômeno Da Seca Para O Semi-Árido Nordestino*; Repositorio UC: Santiago, Chile, 2010.
54. Bilbao, J.; Román, R.; Yousif, C.; Pérez-Burgos, A.; Mateos, D.; de Miguel, A. Global, Diffuse, Beam and Ultraviolet Solar Irradiance Recorded in Malta and Atmospheric Component Influences under Cloudless Skies. *Sol. Energy* **2015**, *121*, 131–138. [CrossRef]
55. Mckinlay, A.; DIffey, B. A Reference Action Spectrum for Ultraviolet Induced Erythema in Human Skin. Available online: https://hero.epa.gov/hero/index.cfm/reference/details/reference_id/57760 (accessed on 27 October 2023).
56. González-Rodríguez, L.; de Oliveira, A.P.; Rodríguez-López, L.; Rosas, J.; Contreras, D.; Baeza, A.C. A Study of UVER in Santiago, Chile Based on Long-Term in Situ Measurements (Five Years) and Empirical Modelling. *Energy* **2021**, *14*, 368. [CrossRef]
57. Davis Instruments. UV Sensor 6490 Vantage pro Espec Sheet. Available online: https://support.davisinstruments.com/article/qxi17f3woz-spec-sheet-solar-power-kit-heavy-duty-solar-power-kit-specifications-6612-6614 (accessed on 27 August 2023).
58. Levelt, P.F.; van den Oord, G.H.J.; Dobber, M.R.; Malkki, A.; Visser, H.; de Vries, J.; Stammes, P.; Lundell, J.O.V.; Saari, H. The Ozone Monitoring Instrument. *IEEE Trans. Geosci. Remote Sens.* **2006**, *44*, 1093–1101. [CrossRef]
59. Taipe, C.W.; Mendoza, E.G.; Flores, H.H. Validation of Ultraviolet Index Data from the Ozone Monitoring Instrument (OMI) Based on Measurements from Meteorological Stations in the City of Puno. *J. Phys. Conf. Ser.* **2021**, *1841*, 012005. [CrossRef]
60. Tanskanen, A.; Lindfors, A.; Määttä, A.; Krotkov, N.; Herman, J.; Kaurola, J.; Koskela, T.; Lakkala, K.; Fioletov, V.; Bernhard, G.; et al. Validation of Daily Erythemal Doses from Ozone Monitoring Instrument with Ground-Based UV Measurement Data. *J. Geophys. Res.* **2007**, *112*, 2. [CrossRef]
61. Jégou, F.; Godin-Beekmann, S.; Correa, M.P.; Brogniez, C.; Auriol, F.; Peuch, V.-H.; Haeffelin, M.; Pazmiño, A.; Saïag, P.; Goutail, F.; et al. Validity of Satellite Measurements Used for the Monitoring of UV Radiation Risk on Health. *Atmos. Chem. Phys.* **2011**, *11*, 13377–13394. [CrossRef]
62. Antón, M.; Cachorro, V.E.; Vilaplana, J.M.; Toledano, C.; Krotkov, N.A.; Arola, A.; Serrano, A.; de la Morena, B. Comparison of UV Irradiances from Aura/Ozone Monitoring Instrument (OMI) with Brewer Measurements at El Arenosillo (Spain)—Part 1: Analysis of Parameter Influence. *Atmos. Chem. Phys.* **2010**, *10*, 5979–5989. [CrossRef]
63. Kinne, S.; O'Donnel, D.; Stier, P.; Kloster, S.; Zhang, K.; Schmidt, H.; Rast, S.; Giorgetta, M.; Eck, T.F.; Stevens, B. MAC-V1: A New Global Aerosol Climatology for Climate Studies. *J. Adv. Model. Earth Syst.* **2013**, *5*, 704–740. [CrossRef]
64. Munro, R.; Lang, R.; Klaes, D.; Poli, G.; Retscher, C.; Lindstrot, R.; Huckle, R.; Lacan, A.; Grzegorski, M.; Holdak, A.; et al. The GOME-2 Instrument on the Metop Series of Satellites: Instrument Design, Calibration, and Level 1 Data Processing—An Overview. *Atmos. Meas. Tech.* **2016**, *9*, 1279–1301. [CrossRef]
65. Kujanpää, J.; Kalakoski, N. Operational Surface UV Radiation Product from GOME-2 and AVHRR/3 Data. *Atmos. Meas. Tech.* **2015**, *8*, 4399–4414. [CrossRef]
66. Liu, S.; Valks, P.; Beirle, S.; Loyola, D.G. Nitrogen Dioxide Decline and Rebound Observed by GOME-2 and TROPOMI during COVID-19 Pandemic. *Air Qual. Atmos. Health* **2021**, *14*, 1737–1755. [CrossRef]

67. Ialongo, I.; Arola, A.; Kujanpää, J.; Tamminen, J. Use of Satellite Erythemal UV Products in Analysing the Global UV Changes. *Atmos. Chem. Phys.* **2011**, *11*, 9649–9658. [CrossRef]
68. Chan, K.L.; Valks, P.; Heue, K.-P.; Lutz, R.; Hedelt, P.; Loyola, D.; Pinardi, G.; Van Roozendael, M.; Hendrick, F.; Wagner, T.; et al. Global Ozone Monitoring Experiment-2 (GOME-2) Daily and Monthly Level-3 Products of Atmospheric Trace Gas Columns. *Earth Syst. Sci. Data* **2023**, *15*, 1831–1870. [CrossRef]
69. Kalakoski, N. OMI UVB Level 2G HDF-EOS5 Format Specification Document. Available online: https://omi.fmi.fi/docs/OMUVB_L2_Format_Specification_Document_v2_6.pdf (accessed on 2 September 2023).
70. Sammes, P.; Noordhoek, R. OMI Algorithm Theoretical Basis Document Volume III. In *Clouds, Aerosols, and Surface UV Irradiance*; 2002. Available online: https://eospso.nasa.gov/sites/default/files/atbd/ATBD-OMI-03.pdf (accessed on 5 September 2023).
71. Força Aéra Brasileira (FAB). Como Decodificar O METAR E O SPECI?—Central de Ajuda DECEA. Available online: https://ajuda.decea.mil.br/base-de-conhecimento/como-decodificar-o-metar-e-o-speci/ (accessed on 27 October 2023).
72. Silva, A.A.; Souza-Echer, M.P. Ground-Based Observations of Clouds through Both an Automatic Imager and Human Observation. *Meteorol. Appl.* **2015**, *23*, 150–157. [CrossRef]
73. Reis, G.; Alves, S.; Bezerra, H.; Branches, R.; Silva, R.; Vaz Peres, L.; Pinheiro, D.K.; Lamy, K.; Benchérif, H.; Portafaix, T. Solar Ultraviolet Radiation Temporal Variability Analysis from 2-Year of Continuous Observation in an Amazonian City of Brazil. *Atmosphere* **2022**, *13*, 1054. [CrossRef]
74. de Paula, M.; Godin-Beekmann, S.; Haeffelin, M.; Brogniez, C.; Verschaeve, F.; Saiag, P.; Pazmino, A.; Mahé, E. Comparison between UV Index Measurements Performed by Research-Grade and Consumer-Products Instruments. *Photochem. Photobiol. Sci.* **2010**, *9*, 459–463. [CrossRef]
75. Glen, S. Correlation Coefficient: Simple Definition, Formula, Easy Calculation Steps. Available online: https://www.statisticshowto.com/probability-and-statistics/correlation-coefficient-formula (accessed on 25 August 2023).
76. Akoglu, H. User's Guide to Correlation Coefficients. *Turk. J. Emerg. Med.* **2018**, *18*, 91–93. [CrossRef] [PubMed]
77. Chicco, D.; Warrens, M.J.; Jurman, G. The Coefficient of Determination R-Squared Is More Informative than SMAPE, MAE, MAPE, MSE and RMSE in Regression Analysis Evaluation. *PeerJ Comput. Sci.* **2021**, *7*, e623. [CrossRef] [PubMed]
78. Barbieri, F.; Rajakaruna, S.; Ghosh, A. Very Short-Term Photovoltaic Power Forecasting with Cloud Modeling: A Review. *Renew. Sustain. Energy Rev.* **2017**, *75*, 242–263. [CrossRef]
79. Sathishkumar, V.E.; Ramu, A.G.; Cho, J. Machine Learning Algorithms to Predict the Catalytic Reduction Performance of Eco-Toxic Nitrophenols and Azo Dyes Contaminants (Invited Article). *Alex. Eng. J.* **2023**, *72*, 673–693. [CrossRef]
80. Lillo-Bravo, I.; Vera-Medina, J.; Fernández-Peruchena, C.M.; Pérez-Aparicio, E.; López-Álvarez, J.A.; Delgado-Sanchez, J.M. Random Forest Model to Predict Solar Water Heating System Performance. *Renew. Energy* **2023**, *216*, 119086. [CrossRef]
81. Coariti, J.R. Características Da Radiação Ultravioleta Solar E Seus Efeitos Na Saúde Humana Nas Cidades de La Paz–Bolívia E Natal–Brasil. Ph.D. Thesis, Universidade Federal do Rio Grande do Norte, Natal, Brazil, 2017.
82. Lamy, K.; Portafaix, T.; Brogniez, C.; Lakkala, K.; Pitkänen, M.R.A.; Arola, A.; Forestier, J.-B.; Amélie, V.; Abdoulwahab Toihir, M.; Rakotoniaina, S. UV-Indien Network: Ground-Based Measurements Dedicated to the Monitoring of UV Radiation over the Western Indian Ocean. *Earth Syst. Sci. Data* **2021**, *13*, 4275–4301. [CrossRef]
83. Alvares, C.A.; Stape, J.L.; Sentelhas, P.C.; de Moraes Gonçalves, J.L.; Sparovek, G. Köppen's Climate Classification Map for Brazil. *Meteorol. Z.* **2013**, *22*, 711–728. [CrossRef]
84. Cede, A.; Blumthaler, M.; Luccini, E.; Piacentini, R.D.; Nuñez, L. Effects of Clouds on Erythemal and Total Irradiance as Derived from Data of the Argentine Network. *Geophys. Res. Lett.* **2002**, *29*, 76-1–76-4. [CrossRef]
85. de Oliveira, P.T.; Silva CM, S.E.; Lima, K.C. Linear Trend of Occurrence and Intensity of Heavy Rainfall Events on Northeast Brazil. *Atmos. Sci. Lett.* **2013**, *15*, 172–177. [CrossRef]
86. EPA (Unites States Environmental Protection Agency). UV Index Scale. Available online: https://19january2017snapshot.epa.gov/sunsafety/uv-index-scale-1_.html (accessed on 23 August 2023).
87. Mohamed, M.S.; Abdel, M.; El-Metwally, M.; El-Nobi, E.F. Validation of UV-Index Retrieved from Three Satellites against Ground-Based Measurements at Different Climates in Egypt. *Egypt. J. Remote Sens. Space Sci.* **2023**, *26*, 361–367. [CrossRef]
88. Pitkänen MR, A.; Arola, A.; Lakkala, K.; Koskela, T.; Lindfors, A.V. Comparing OMI UV Index to Ground-Based Measurements at Two Finnish Sites with Focus on Cloud-Free and Overcast Conditions. *Egypt. J. Remote Sens. Space Sci.* **2015**, *8*, 487–516. [CrossRef]
89. Bernhard, G.; Arola, A.; Dahlback, A.; Fioletov, V.; Heikkilä, A.; Johnsen, B.; Koskela, T.; Lakkala, K.; Svendby, T.M.; Tamminen, J. Comparison of OMI UV Observations with Ground-Based Measurements at High Northern Latitudes. *BIBSYS Brage* **2015**, *15*, 7391–7412. [CrossRef]

5 RESULTS: Comparative analysis of ground-based and satellite-derived UV index: variability and reliability from three south American low and mid-latitudes sites

5.1 Article IV overview and thesis contribution

This study compares ground-based and satellite-derived UV Index levels from OMI at overpass time during clear sky conditions, which are determined using LER (Lambertian Equivalent Reflectivity). A characterization of the diurnal and seasonal variability of the ground-based UV index levels is also reported. The study period ranges from 2005 to 2022, varying according to each data source, and comprises data from two Brazilian cities – Itajubá (22.41ºS, 45.44ºW, 885 m, Davis 6490 UV sensor), Santa Maria (29.4°S, 53.8°W, 476 m, Brewer Spectrophotometer MKIII #167), and from Buenos Aires in Argentina (34.58º S, 58.48°W, 25 m, Solar Light UV Biometer – Radiometer model 501).

This study contributes to the first and third specific objectives of this thesis by characterizing the diurnal and seasonal variability of ground-based UV index levels and comparing these with satellite-derived UV Index levels in Itajubá, Santa Maria, and Buenos Aires under clear sky conditions.

With this study it was found that the typical diurnal solar UV pattern is evident with UV index levels increasing during the day, reaching a peak at solar noon, and decreasing during the afternoon as solar zenith angles increase again for Itajubá, Santa Maria and Buenos Aires. Annual variability, modulated by the seasonal cycle, is also evident, with summer UV index values regularly achieving very high and extreme UV index levels at all the three sites and smaller UV index levels during austral winter.

The UV index levels at Itajubá were lower than expected for its latitude and altitude, which typically, would increase UV levels. Nevertheless, Itajubá showed lower UV indices than Santa Maria and Buenos Aires, suggesting potential calibration or data accuracy issues with local UV measurement methods. These unexpected values were reflected in the comparison results, that showed that Itajubá's data had the largest differences between ground-based and satellite derived UV index levels, with a moderate correlation and the highest MBE, MAPE, MAE, and RMSE values, indicating significant measurement deviations. Both Santa Maria and Buenos Aires showed a stronger correlation between ground based and satellite measurements, with Buenos Aires presenting the strongest relationship. The MBE, MAPE, MAE and RMSE were lower for these cities as well, indicating smaller relative errors.

The consistent results in Santa Maria and Buenos Aires emphasize the crucial hours for sun protection and validate the accuracy of the OMI (Ozone Monitoring Instrument) and ground-based instruments (Brewer Spectrophotometer MKIII #167 in Santa Maria, and Solar Light UV Biometer - model 501 in Buenos Aires) in capturing UV patterns. The verification of these data is vital for their use in future long-term trend analysis, monitoring UV exposure risks, and assessing potential impacts on human health.

In future work, it is necessary to examine Itajubá's UV index discrepancies by reviewing sensor calibration records, maintenance logs, and site-specific environmental factors that may influence readings. Additionally, conducting a trend analysis to understand the long-term changes in UV radiation levels will help better understand the dynamics of the spatial-temporal variability of surface UV in South America.

5.2 Publication status

REIS, G.; BENCHERIF, H.; REIS, M. et al. Comparative Analysis of Ground-Based and Satellite-Derived UV Index: Variability and Reliability from Three South American Mid-Latitudes Sites. In: **EGU General Assembly 2024**, Vienna, Austria, 14–19 Apr 2024. Available in: https://doi.org/10.5194/egusphere-egu24-2543.

5.3 Materials and Methods

In the articles I, II and III the materials and methods applied to the northern low-latitude cities of this study (Santarém and Natal) were presented. In this fourth phase, the focus shifts to the three southernmost locations in this study: Itajubá (22.41ºS, 45.44ºW, 885 m, Davis 6490 UV sensor) and Santa Maria (29.4°S, 53.8°W, 476 m, Brewer Spectrophotometer MKIII #167) still at low latitudes, and Buenos Aires (34.58ºS, 58.48ºW, 25 m, Solar Light UV Biometer – Radiometer model 501) at mid-latitude (Figure 18) and (Table 2).

Table 2 – Ground-based UV index data Sources. The time zone of the three sites is UTC-3.

Station	Instrument	Type of data	Geographical Position	Coordinates	Altitude (a.s.l)	Period
Itajubá	Davis 6490 – UV Sensor	UV index	Federal University of Itajubá	22.41°S; 45.44°W	885m	01/2016 to 12/2021
Santa Maria	Brewer Spectrophotometer MKIII #167	UV Index	Suthern Space Observatory	29.4°S; 53.8°W	476m	01/2005 to 12/2017

Buenos Aires	UV Biometer Radiometer model 501	UV index	GAW Regional Staion – WMO Region III	34.58°S; 58.48°W	25m	01/2013 to 10/2017

Source: Author (2019).

These three sites are included together in an analysis with the objectives to compare ground-based and satellite-derived UV Index levels from the OMI at overpass time during clear-sky conditions, determined using LER, and to provide a characterization of the diurnal and seasonal variability of the ground-based UV index levels. This approach was chosen due to the lack of free METAR data for Itajubá and Buenos Aires and to maintain consistency in the analysis across all locations. Additionally, GOME-2 and OMI noontime data were not used because the LER used here, is derived from OMI overpass time.

Figure 18 – Locations of UV index monitoring stations.

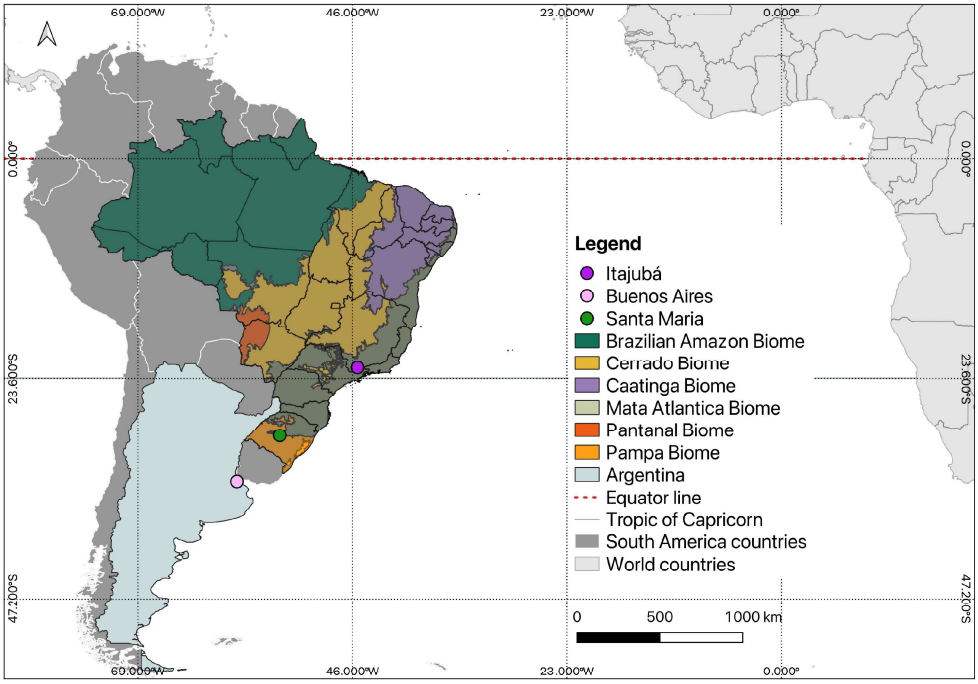

Source: Author (2024).

The OMI overpass UV index and LER data can be downloaded for free from the link provided in Table 3. This methodology enabled the characterization of ground-based UV variability over low and mid-latitudes in South America and facilitated a reliable comparison of UV index levels. The study period ranges from 2005 to 2022, varying according to each data source (Table 2).

Table 3 – Satellite-derived data sources.

Satellite	Instrument	Type of Data	Period	Website
AURA	OMI	UV index (overpass time) LER	01/2005 – 12/2022	https://search.earthdata.nasa.gov/search

Source: Author (2023).

5.3.1 Sites Description

Itajubá is located on the mountainsides of the Serra da Mantiqueira, in the south of the state of Minas Gerais and has approximately 97.782 inhabitants (IBGE, 2021). According to the Köppen climate classification the climate of Itajubá is Cwa, that is, humid temperate climate with dry winter and hot summer (REBOITA et al., 2015, SANTOS et al., 2019). The highest average temperature is 23.3º C in February and the lowest is 15.1º C in July. The total average annual rainfall is 1458 mm, with about 80% of this value occurring between the months of October to March (rainy season) (REBOITA et al., 2017, ALVES et al., 2021). The daily cycle of UVI for the period from 2006 to 2009 for the city of Itajubá revealed a maximum of 15.6, with 28% of the measurements classified as “extreme”, with the maximums occurring around 1:00 to 2:00 pm local time (UTC-3) (COARITI, 2011).

Santa Maria is in the central region of the state of Rio Grande do Sul. The city has approximately 285.159 inhabitants (IBGE 2021). Santa Maria, according to the Köppen classification, presents a rainy temperate climate whose average temperature of the warmest month is 24.80°C, in January, and the average temperature of the coldest month, in July, is 14.10°C (KUINCHTNER, 2001; LONGHI et al., 2000). The average annual precipitation is 1769 mm/year (LONGHI et al., 2000). According to Lopes (2022), measures of UV Index for the period of 2005 to 2017, made at Santa Maria, shows a maximum of 12 “extreme”, mainly between December and end of January. During fall and spring, it varies between very high and high. During winter monthly mean presents moderate UV index (LOPES, 2022).

Buenos Aires city, is the federal capital of Argentina, situated 240 km from the Atlantic Ocean. It’s one of South America’s most populous cities (DAEMEI, EGHBALI & KHOTBEHSARA, 2019). The climate in this city is sub-humid to humid and would be categorized as type Cfa, mesothermal with no dry season, according to the modified Köppen classification system (PEREYRA & RIMOLDI, 2003). The mean annual rainfall is 1200 mm, the mean annual temperature 15°C and the mean annual relative humidity is 71% (PEREYRA & RIMOLDI, 2003; DAEMEI, EGHBALI & KHOTBEHSARA, 2019). A UV index of about 11.5 “extreme” was

registered in 1997 in Buenos Aires also UV levels achieving high values for typical days of each season of the year during this same year (MICHELETTI et al., 2003).

5.3.2 Ground-Based Measurements

Monitoring of the UV index in the city of Itajubá was done using the Davis 6490 UV sensor instrument (Figure 19). The same type of instrument that was used to monitor UV levels at Natal. This sensor measures the sum of the components of UV transmitted directly and those scattered in the atmosphere (DAVIS Instruments, 2024). The sensor is a semiconductor photodiode calibrated against a Yankee Environmental Systems' Ultraviolet Pyranometer, model UVB-1, in natural summer daylight (DAVIS Instruments, 2024). The spectral response is 280 to 360 nm (DAVIS Instruments, 2024), with UV index being one of the sensor outputs with a range from 0 to 16 Index and an accuracy of ±5% (DAVIS Instruments, 2024).

Figure 19 – Davis 6490 UV Sensor.

Source: Retrieved from COLE-PARMER an Antylia scientific company – Davis Instruments 6490 UV Sensor (https://www.coleparmer.com/i/davis-instruments-6490-uv-sensor-for-vanatage-pro2-wireless/3224547).

Given the sensitivity of UV sensors, Davis Instruments advises periodic recalibration. Their reports indicate an annual drift of approximately 2% in sensor readings (DAVIS Instruments, 2024). To address this, the UV sensor used in Itajubá was returned to the manufacturer for recalibration every two years.

For the city of Santa Maria, UV data was obtained using the brewer spectrophotometer (Brewer Model Mark - MKIII no. 167 (Figure 20) operated at the Southern Space Observatory (SSO). The Brewer MKIII no. 167 is a fully automated instrument designed for terrestrial measurements of spectral irradiations in the UV-B range of the solar spectrum at five wavelengths, 306.3, 310.1, 313.5, 316.8, and 320.1 nm (Kerr, 2002).

The Brewer instrument operated at SSO/INPE is part of Brewer's Brazilian network and every 15 days, the spectral responsivity of the Brewer spectrophotometer was verified by irradiating the

entrance optics with a 1.000 W quartz-halogen tungsten reference lamp with certified spectral irradiance. This calibration procedure ensured the instrument's accuracy by regularly assessing its spectral response, as described in the Brewer Operator Manual (SCI-TEC Instruments, 1999).

Figure 20 – Southern Space Observatory Building and Brewer Spectrophotometer MKIII #167.

Source: Retrieved and adapted from Peres (2016).

For the city of Buenos Aires, UV data were measured using a UV Biometer – Radiometer Model 501 (Solar Light) (Figure 21 - right side), installed at the Buenos Aires Observatory (Figure 21 – left side), which makes part of the GAW Regional station in WMO Region III – South America (GERARDO, 2016). This instrument is the continuation of the line of Robertson-Berger Weatherproof meters, that have been employed in the worldwide network for UV-B monitoring (VERTMARKETS, 2023). Model 501 UV biometers are permanent outdoor UV measurement system, measuring UV from artificial and natural sources with wavelengths above 280 nm to 400 nm (SOLAR LIGHT, 2023). It presents an expected daily uncertainty of ±5%. In South America, the Argentine National Weather Service (SMN in Spanish) of Argentina, acting as the WMO South-American Regional Calibration Centre, ensures the accuracy and reliability of these measurements by employing rigorous calibration protocols. The SMN performs periodic calibrations of solar UV radiometers, including the Solar Light Model 501 UV Biometer, maintaining high standards for UV monitoring.

Figure 21 – Buenos Aires Observatory and the UV Biometer - Radiometer Model 501.

Source: Retrieved from Gerardo (2016) and retrieved and adapted from (Solar Light, 2023).

The ground-based UVI data for Itajubá and Santa Maria was provided by collaborating researchers who also worked with analysis of UV in South America. UVI data for Buenos Aires was obtained for free from the World Ozone and Ultraviolet Radiation Data Centre (WOUDC) through the website (https://woudc.org/data/explore.php?lang=en). WOUDC is one of six World Data Centers that are part of the Global Atmosphere Watch (GAW) program of the World Meteorological Organization (WMO). The WOUDC contains ozone and UV data measured by instruments located on ground-based, shipborne, or airborne platforms.

5.3.3 Statistical Analysis

All the datasets were analyzed, and obvious errors were removed. Timing was also adjusted to the corresponding time UTC-3 (Coordinated Universal Time) for all three. The original time series of Itajubá had a sampling frequency of 10 minutes, while data from Santa Maria were sampled every 30 minutes and from Buenos Aires at an hourly frequency. To standardize the frequency across all locations, the ground-based UV Index data were aggregated into hourly averages. This allowed for consistent selection of the hours corresponding to the overpass clear-sky condition (±1:45 PM).

The satellite derived UV index used in this work was “all-sky UV index” from OMI at overpass time, which refers to the file attribute named OPUVindex from OMUVBG product level 2G. The Surface UV Irradiance Product from OMI has dose quantities, UV index, cloud optical thickness, LER among others (KALAKOSKI, 2012).

The comparisons were done with UV index under clear-sky conditions, selected using the OMI LER as cloud cover proxy. The LER applied in this work is derived from the OMI-measured radiance (I_{360}) near 360 nm, which can be expressed as a sum of the atmospheric backscatter above a specified Lambertian surface (STAMMES & NOORDHOEK, 2022). The LER values represent the equivalent scene reflectivity, which is the combined reflectivity of clouds, aerosols, and the

surface as observed from space, excluding the contribution of Rayleigh scattering (LABOW et al., 2011). Such datasets have been used to assess surface reflectivity climatology (Kleipool et al., 2008) and cloud variability (Damiani et al., 2014). In unpolluted regions and in the absence of snow, significant changes in LER are primarily attributed to clouds (Herman et al., 2009; Damiani et al., 2013; Damiani et al., 2014). LER values range from 0 to 1, but they are often expressed as a percentage from 0% to 100%. A day is considered cloud-free during the OMI overpass if the LER is lower than 10% (ANTÓN et al., 2010; Cadet et al., 2017). Therefore, only days with an LER value smaller than 10% were used in this study.

To compare ground-based data with satellite-derived data, different statistical metrics were employed. The Pearson correlation coefficient (r) (2), commonly applied in linear regression, quantifies the strength of the relationship between two variables (CORRÊA et al., 2010). This coefficient ranges from −1 to +1, where zero indicates no correlation, +1 represents a perfect positive correlation, and negative values indicate an inverse relationship between the variables (GLEN, 2023; AKOGLU, 2018). Additionally, the coefficient of determination (r^2), calculated as the square of the Pearson correlation coefficient, reflects the proportion of variance in the dependent variable that is explained by the independent variable (CHICCO et al., 2021).

Error metrics were also calculated to evaluate performance. The Mean Bias Error (MBE) (3) represents the average algebraic error, while the Mean Absolute Error (MAE) (4) measures the average magnitude of errors in absolute terms (BARBIERI et al., 2017). The Mean Absolute Percentage Error (MAPE) (5) expresses the average absolute error as a percentage of the observed values, providing a statistical measure of accuracy (SATHISHKUMAR et al., 2023; LILLO-BRAVO et al., 2023). The Root Mean Square Error (RMSE) (6) calculates the differences between predicted (OMI-derived) and observed (ground-based) values, with smaller RMSE values indicating lower residual variance (CADET et al., 2017). To assess the statistical significance of the relationships between the datasets p-values were determined.

$$r = \frac{\sum_{i=1}^{n}(S_{GND,i} - \overline{S}_{GND})(S_{SAT,i} - \overline{S}_{SAT})}{\sqrt{(\sum_{i=1}^{n}(S_{GND,i} - \overline{S}_{GND})^2)(\sum_{i=1}^{n}(S_{SAT,i} - \overline{S}_{SAT})^2)}} \quad (2)$$

$$MBE = \frac{1}{n}\sum_{i=1}^{n}(S_{SAT,i} - S_{GND,i}) \quad (3)$$

$$\mathrm{MAE} = \frac{1}{n}\sum_{i=1}^{n}\left|S_{SAT,i} - S_{GND,i}\right| \quad (4)$$

$$\mathrm{MAPE} = \frac{1}{n}\sum_{i=1}^{n}\left(100 * \frac{\left|S_{SAT,i} - S_{GND,i}\right|}{S_{GND,i}}\right) \quad (5)$$

$$\mathrm{RMSE} = \sqrt{\frac{1}{n-1}\sum_{i=1}^{n}\left(S_{SAT,i} - S_{GND,i}\right)^2} \quad (6)$$

where S is the UV index, $\overline{S}$ is the averaged UV index, SAT is the satellite observation, GND is the ground-based observation, and n is the number of observations.

These metrics together help in identifying potential biases, understanding the strength of the relationship, and quantifying the magnitude and relative importance of the errors. Therefore, provide a comprehensive view of the accuracy and reliability of satellite data as compared to ground-based data. Furthermore, characterizing the diurnal and seasonal variability of UV radiation in these low and mid-latitude South American sites is important for accurate public health advisories and environmental assessments. Such evaluations are essential for improving UV radiation monitoring and for enhancing the accuracy of UV assessments.

5.4 Article IV results

5.4.1 Ground-based UV index temporal variability

Hourly data from the three ground-based UV measurements sites were analyzed for the period 2005–2021. Hourly data are provided in Figure 22. The station of Santa Maria initiated observations in 2005, while the station of Buenos Aires initiated in 2013 and Itajubá even later, in 2016.

Figure 22 – UV index observations as function of day and hour per day for Itajubá, Santa Maria and Buenos Aires from 2005 to 2021.

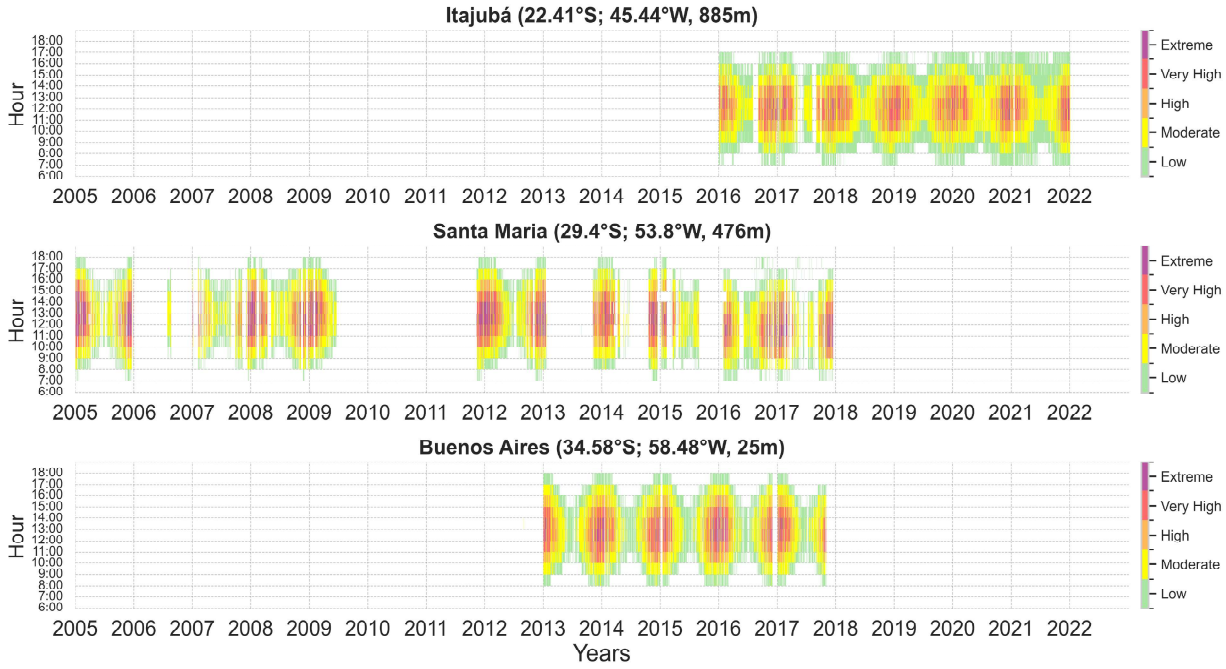

Source: Author (2024).

Data gaps are evident, with the longest being at Santa Maria between 2009 and 2011. The typical diurnal solar UV pattern is evident with UV index levels increasing during the day, reaching a peak at solar noon, and decreasing during the afternoon as solar zenith angles increase again. Annual variability, modulated by the seasonal cycle, is also evident in Figure 22, with summer UV index values regularly achieving high, very high and sometimes extreme UV index levels at all the three sites.

Regarding the city of Itajubá, the maximum UV index there was 12.78 (extreme), registered during noontime in February, a month of austral summer season (Figure 22, 24 and Table 4). The average and the 50% were moderate (Table 4). For cities located in a latitude range close to Itajubá's latitude, Lamy et al. (2021) reported that in Saint-Denis, Reunion Island (20.90°S, 55.48°E, 82 m a.s.l.), UV index levels of ±15 were registered for the period between 2016 and 2020. This maximum also happened at noontime, as the maximum at Itajubá. When it is about the averages, a maximum hourly average UV index of a high level (6–7) at noontime was registered for Itajubá (Figure 24), while very high (8-10) for Saint-Denis (LAMY et al., 2021).

The peak of the UV index in Itajubá occurs in summer (Figures 22 and 23). Because of its southern location and its position between the Tropic of Capricorn and the Equator, Itajubá presents

a peak spread with very high averaged UV index levels from November to February (Figure 23). The Earth's axial tilt and orbit around the Sun cause the Sun's apparent movement across the sky. This results in the Sun passing directly over Itajubá's latitude as the Earth moves towards the Tropic of Capricorn and again as it shifts back towards the equator. This apparent movement is what leads to changes in the intensity of solar radiation received at different times of the year, like during these summer months. This happens in a shorter time, closer months (Figure 23), than for example the case of Natal, where there are clearly two peaks in different seasons. For Antananarivo (18.916°S, 47.565°E, 1370 m a.s.l.) and Anse Quitor (19.758°S, 63.368°E, 32m), Lamy et al. (2021) also reported higher UV index levels during summer, but reaching max monthly UV index average of more than 15 in both cities for the period of 2016 to 2020.

Table 4 – Descriptive Statistics of ground-based derived UV Index for Itajubá, Santa Maria, and Buenos Aires.

Local	N	Mean	Std	50%	Max
Itajubá	16994	3.86	2.53	3.07	12.78
Santa Maria	16807	4.66	3.19	3.66	15.86
Buenos Aires	11180	4.23	2.83	3.33	13.51

Source: Author (2024).

At Santa Maria's latitude, the months of greatest intensity of UV are the austral summer months (Figures 22 and 23), with January presenting the highest levels. The maximum UV index reached was 15.86 at noontime in January (Table 4, Figure 22 and 24). The average and 50% over the hole period of study were moderate (Table 4). Santa Maria is located between the Tropic of Capricorn and the Antarctic Circle, therefore, only one peak of solar radiation is expected during the year, in austral summer, especially on days around the summer solstice (late December) in the southern hemisphere. Lopes (2022) reported a similar pattern, with the highest UV index levels happening during summer. For the city of Durban (29.61°S, 31.11°, 103 m a.s.l.), which is situated in a latitude close to Santa Maria's latitude (29.41°S), Cadet et al. (2017) reported the highest UV index levels happening also during summer, in January with maximum UV index level of almost 15, at local noontime.

Figure 23 – The monthly climatological average ground-based UV index levels for Itajubá, Santa Maria and Buenos Aires for all available years and shown as a function of time of day and month of the year. For seasons to be shown more easily, the plot shows the first month on the X-axis as July through to December, followed by January through to June. Therefore, summer months are in the middle of the plot.

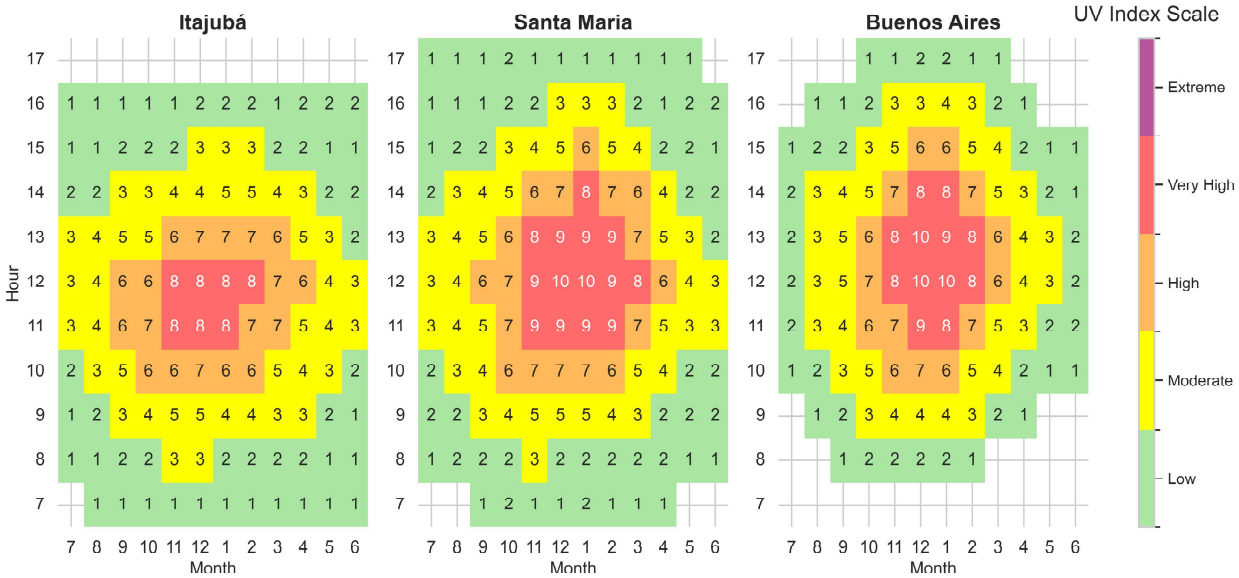

Source: Author (2024).

Regarding the variability of the UV index in Buenos Aires, the maximum value recorded during the entire study period was 13.5 (extreme) (Table 4). The average and median UV index over the period were in the moderate range, similar to the findings for Itajubá and Santa Maria. In 1997, Buenos Aires experienced an extreme UV index of around 11.5, with high values typical for each season, as reported by (MICHELETTI et al., 2003). During the winter of the same year, the UV index reached a maximum of 3. According to (LUCCINI et al., 2006), monthly mean UV index values in low-elevation regions of Argentina range from approximately 12 in the north to 6 in the south during summer, and from 4 to less than 1 in winter. Palancar & Toselli (2004) noted that solar zenith angle variations predict UV–B maxima around December 22nd in Córdoba (31.44°S, 64.19°W), which is close to the latitude of Buenos Aires (34.59°S). Buenos Aires, located at a mid-latitude, experiences its highest UV intensity during the austral summer months, especially in December, when the summer solstice occurs.

Figure 24 – Hourly averaged UV index and variability for Itajubá, Santa Maria and Buenos Aires, across the period from 2005 to 2021. Note: Data availability varies by location (Table 2).

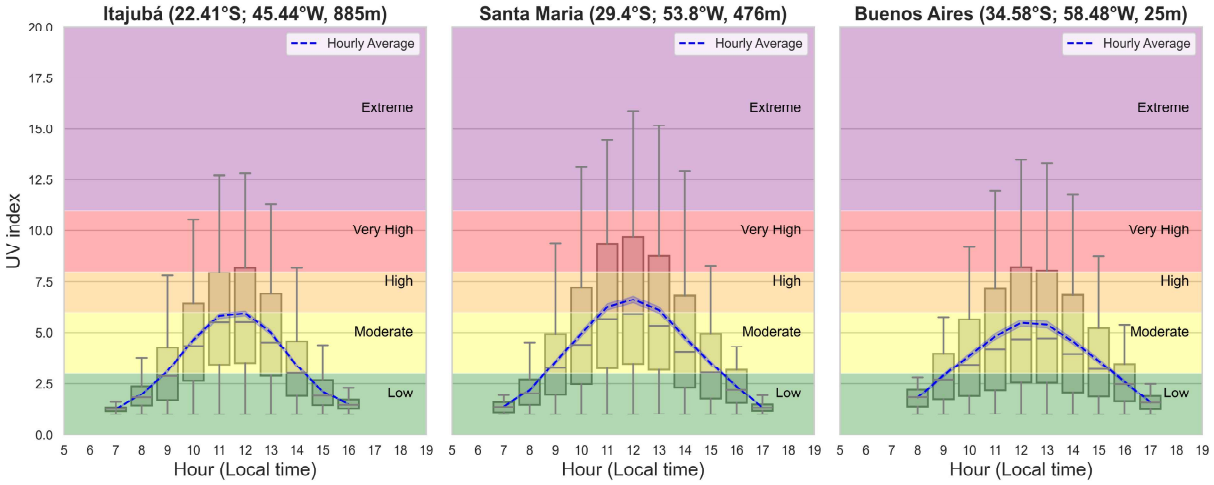

Source: Author (2024).

Regarding the hourly variability over the entire period for each location, Itajubá exhibits low to moderate UV Index levels until 8 AM (Figure 24). From 9 AM onward, high levels begin to be reached, peaking between 11 AM and 1 PM, and then gradually decreasing after 2 PM. Coariti (2011) reported high values from 11 AM, with very high and extreme indices occurring between noon and 2 PM in Itajubá, for the period of 2006 to 2009. At Saint-denis (20.902°S, 55.485°E 82 m a.s.l.), measurements made from 2016 to November 2020 shows extreme UV Index levels from 10 AM to 2 PM (LAMY et al., 2021), while in Itajubá, extreme levels were observed only between 11 AM and 1 PM.

From sunrise to 8 AM, the maximum UV Index in Santa Maria was of moderate level (Figure 24). By 9 AM, UVI levels range mainly from low to moderate, with occasional readings reaching very high levels. The highest UV intensities were recorded between 10 AM and 2 PM, with the maximum UVI occurring at local noon. During these peak hours, UV index levels were extreme, even exceeding 15 at 12 AM and 1 PM. By 4 PM, UV Index readings were maximum moderate, eventually declining to low levels as sunset approached. These findings align with those reported by (LOPES 2022), who also observed maximum UV Index values of 15 and extreme levels between 11 AM and 2 PM, peaking at noon. Similarly, Cadet et al. (2017) documented a comparable pattern in Durban (29.61°S, 31.11°, 103 m a.s.l.), South Africa, a city situated at nearly the same latitude as Santa Maria.

Regarding the hourly variability in Buenos Aires (Figure 24), the UV Index is predominantly low to moderate from sunrise until 10 AM, with UV index levels starting to reach very high at this

hour. Between 11 AM and 2 PM, extreme levels were recorded. After 3 PM, the UV Index decreases to moderate levels, with occasional peaks reaching very high, and by 5 PM, it predominantly falls to low.

According to the U.S. Environmental Protection Agency (EPA), low danger from the sun's UV rays occurs when the UV Index ranges from 0 to 2. Even under these conditions, it is recommended to wear sunglasses on clear days, protect yourself with clothing, and use broad-spectrum SPF30+ sunscreen (EPA, 2016). The EPA also warns that unprotected skin and eyes can burn in minutes when the UV Index reaches 11 or higher, emphasizing the need to avoid sun exposure during these times and to follow protective measures (EPA, 2016). Itajubá experienced three hours of extreme UV levels between 11 AM and 1 PM, Buenos Aires had four hours between 11 AM and 2 PM, and Santa Maria recorded extreme levels for five hours between 10 AM and 2 PM. These results highlight the importance of taking protective measures against overexposure to ultraviolet radiation, as moderate, high, and very high levels are reached from the early morning hours in these locations and during several hours extreme UV levels occur.

In summary, Santa Maria exhibited the highest UV index levels, followed by Buenos Aires. Despite its lower latitude and higher altitude, which typically would result in increased UV levels, Itajubá showed lower UV indices compared to Santa Maria and Buenos Aires. Further investigation is needed in Itajubá to determine whether these lower levels are due to differences in cloud characteristics between the cities or if there are discrepancies in the UV index readings caused by sensor calibration, maintenance practices, or other site-specific environmental factors.

5.4.2 Comparison of Ground-Based and Satellite-Derived UV index

Figure 25 shows the time series of the OMI overpass time UV index for the three sites of study, as well the respective ground-based (GB) measurements under clear-sky conditions. The satellite, as well as the GB time series, shows an annual cycle with one maximum in a year, during austral summer.

Figure 25 – Time series comparing ground-based versus satellite-derived solar UV index data for 2005 to 2021 at satellite overpass time (the comparison was performed at the satellite overpass time and only clear sky days are selected with LER).

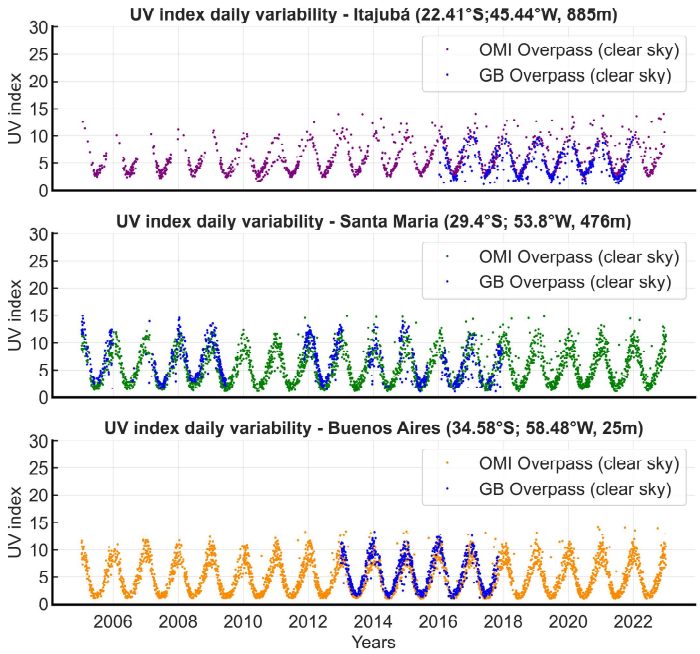

Source: Author (2024).

In Itajubá, maximum UV index of approximately 14 has been recorded in different years in the OMI series (Figure 25), while the ground-based at overpass time reached a maximum of 11.30 (Figure 24). Nevertheless, these values represent extreme UV index, as expected for overpass time, which is around noon (approximately 1.45 pm). For Santa Maria, satellite and ground-based metrics were more similar, with both presenting a maximum around 14 (extreme), as well as similar average of high UV index (Table 5). In the case of Buenos Aires, the metrics were also similar, with satellite and ground-based mean and max being both high and extreme.

Table 5 – Summary of descriptive statistics for each time series comparison where GB OVP (ground-based UV index at local OMI overpass time under clear-sky conditions).

Metrics	N	Mean	Std	Min	50%	Max	Local
GB OVP	431	4.68	2.21	1.20	4.28	10.48	Itajubá
OMI OVP	431	6.03	2.76	2.09	5.20	14.03	Itajubá
GB OVP	607	6.90	3.41	1.01	6.61	14.86	Santa Maria
OMI OVP	607	6.42	3.34	1.50	6.28	14.67	Santa Maria
GB OVP	337	6.49	3.29	1.56	6.40	13.31	Buenos Aires
OMI OVP	337	5.67	3.16	1.22	5.31	11.84	Buenos Aires

Source: Author (2024).

Correlation analysis revealed the weakest correlation between the two datasets (GB OVP vs. OMI OVP) for Itajubá, with R and R^2 values indicating a moderate positive correlation for Itajubá,

a strong positive correlation for Santa Maria, and a very strong correlation for Buenos Aires (Figure 26).

These results suggest that while the satellite UV index generally increases as the ground-based UV index increases, the relationship is notably weaker for Itajubá. Specifically, only 38% of the variability in the satellite UV index for Itajubá is explained by the ground-based UV index, as indicated by its low R^2 value. This low R^2 suggests that the two datasets do not align well, meaning the satellite data does not replicate the ground-based data with high accuracy. Additionally, the possibility that ground-based measurements may be problematic contributes to this discrepancy and supports the need for a review of the ground-based data, particularly given the unexpectedly low values for Itajubá's latitude and altitude, as discussed in the previous results section.

Figure 26 – Comparative analysis of Ground-Based and Satellite-Derived UV Index with Error Distributions for Itajubá, Santa Maria, and Buenos Aires. For all three sites: $p < 0.001$

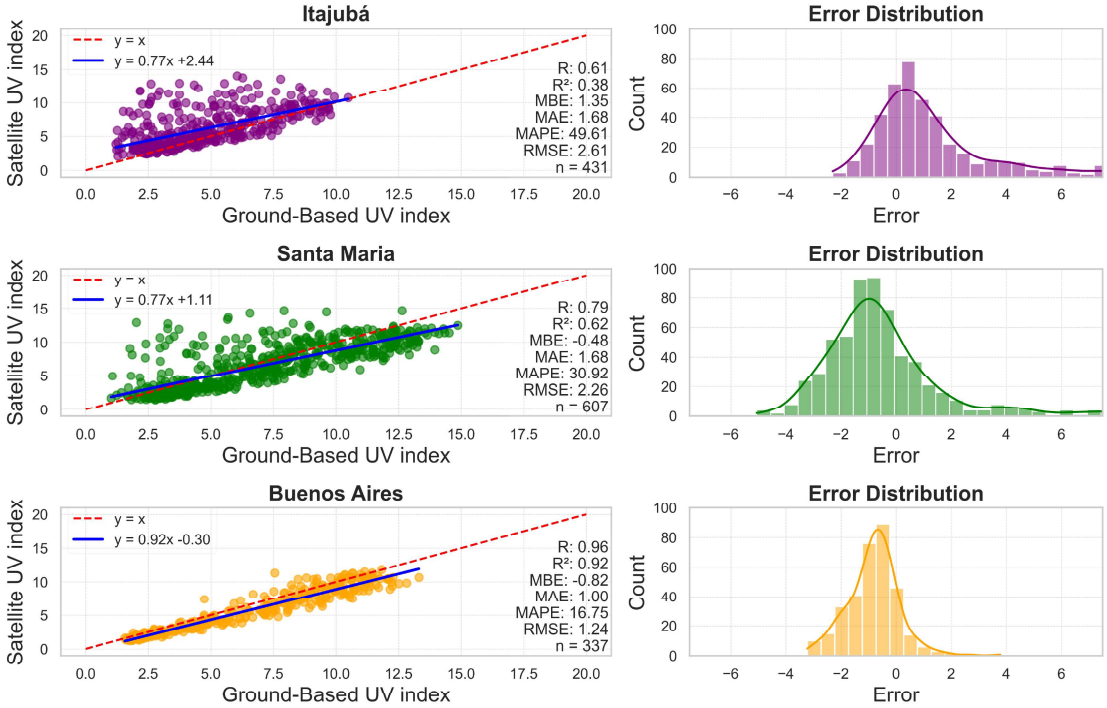

Source: Author (2024).

Cadet et al. (2017) reported a positive moderate correlation between ground−based versus OMI−derived UV index for the city of Pretoria (25.73°S, 28.18°E, 1330 m from 1994 to May 2003 and 25.81°S, 28.49°E, 1228 m from May 2003 to 2015) in South Africa. They also reported strong correlation coefficient of 0.88 for Durban (29.97°S, 31.00°E, 9 m, 1994 to May 2010). The comparison was done using clear-sky OMI overpass UVI, selected using LER and the ground-

based instrument was a broadband UV-biometer model 501 manufactured by Solar Light, similar as the one used in Buenos Aires.

The positive MBE value for Itajubá (Figure 26) indicates that the satellite UV index data generally overestimates the ground-based UV index by an average of 1.35 units. Santa Maria and Buenos Aires presented negative MBE, which means that the satellite UV index data tends to underestimate the ground-based UV index by an average of 0.48 units and 0.82 for Santa Maria and Buenos Aires respectively.

Pitkänen et al. (2015) reported that in some special cases OMI underestimated UV index, for example, when broken sky may be falsely interpreted as clear sky or overcast. This is possible to happen when clouds are present within OMI footprint, but the clouds do not obscure the sun (PITKÄNEN ET AL., 2015). Zempila et al. (2016) also reported OMI underestimations. In their study, Zempila et al., (2016) compared NILU-UV multichannel radiometer measurements with OMI UV irradiance estimates for Thessaloniki, Greece. For the 324 nm and 380 nm wavelengths, the local noontime satellite estimations under clear skies comparisons showed a satellite under-estimation of -3.75% and -4.15%, respectively, and the overpass time comparisons showed underestimations ranging between -1.55% and -1.90% for the same wavelengths (ZEMPILA et al., 2016). According with (ANTÓN et al., 2010; BROGNIEZ et al., 2016) uncertainty in OMI-derived UVI is due to uncertainties in the clear sky irradiance modelling (depending on ozone, surface albedo) and in the cloud–aerosol correction factor.

Other studies reported OMI overestimations, as example: Mohamed et al. (2023) assessed the performance of the noontime OMI-derived UV index against ground-based measurements under all-sky conditions for the period of 2012–2017 at three Egyptian sites. For Aswan (23.97°N, 32.78°E, 192.5 m, Pyranometer), Cairo (30.08°N, 31.28°E, 34.4 m, Pyranometer), and Matruh (31.33°N, 27.22°E, 25 m, Brewer MK II) the results showed annual mean bias of 0.52, 0.68 and 1.02 to Aswan, Cairo and Matruh, respectively, revealing that OMI consistently overestimated UV measurements across all seasons and sites. Pitkänen et al. (2015) also reported OMI overestimations. They evaluated the accuracy of OMI UV data under varying cloud conditions by comparing it to ground-based observations from Jokioinen (60.8°N, 23.5°E) and Sodankylä (67.3°N, 26.6°E) during the satellite overpass times between 2005 and 2011. They found that OMI UV overestimated the surface UV index, with mean biases of 0.50 for Jokioinen and 0.26 for Sodankylä in clear-sky conditions.

The MAE values indicate that, on average, the satellite UV index is off by 1.68 units for both Itajubá and Santa Maria, while it is more accurate in Buenos Aires, with an average error of 1.00, suggesting that the satellite data is generally more aligned with ground measurements in Buenos Aires compared to the other two cities. The MAPE, that expresses the accuracy as a percentage, showing the magnitude of errors relative to the actual values, was higher at Itajubá, 49.61%. Santa Maria had a moderate MAPE of 30.92%, and Buenos Aires has the lowest MAPE at 16.75%, again, reflecting the highest accuracy among the three cities. These discrepancies can be influenced by potential issues with the ground-based or the satellite-derived data, suggesting that both sources of data may require further examination to determine the root causes of the differences.

Mohamed et al. (2023) compared OMI-derived and ground-based UV index measurements at noontime under all-sky conditions for the period 2012–2017. They reported annual MAPE values of 10.6% for Aswan (23.97°N, 32.78°E, 192.5 m, Pyranometer), 17.3% for Cairo (30.08°N, 31.28°E, 34.4 m, Pyranometer), and 26.0% for Matruh (31.33°N, 27.22°E, 25 m, Brewer MK II). Cadet et al. (2017) analyzed MAPE at satellite overpass time using LER as clear sky cloud proxy and found values of 27% for Pretoria (25.73°S, 28.18°E, 1330 m, 1994–2003), 28% for Durban (29.97°S, 31.00°E, 9 m, 1994–2010), and 46% for De Aar (30.67°S, 23.99°E, 1286 m, 2002–2015). This means that the MAPE at overpass time in this work still within the range of the MAPE found from the comparisons made at the previous cited sites.

The RMSE values suggest that there are deviations between the satellite and ground-based UV index data in Itajubá (2.61) and Santa Maria (2.26), whereas Buenos Aires has the smallest RMSE (1.24), indicating fewer large discrepancies. This means that the alignment between the satellite and ground-based data is closer in Buenos Aires, resulting in fewer and less severe errors. An RMSE of 2.57 was reported for De Aar (30.67°S, 23.99°E 1286 m 2002 to 2015) by (CADET et al., 2017) when comparing ground-based UV index at overpass time under clear sky, also selected using LER. For the other cities of their study, the RMSE values ranged between 1.46 to 1.93. This indicates that the RMSE values obtained in this study (ranging from 1.24 to 2.61) are consistent with the range reported by Cadet et al. (2017), suggesting similar levels of agreement between satellite-derived and ground-based UV index data under comparable conditions.

In Buenos Aires, the scatter plots and error distribution plots reinforce the better agreement between satellite and ground-based UV index measurements, with most data points clustering near the red line and errors clustered around zero, indicating the strength of the correlations. However,

in Itajubá and Santa Maria, the error distributions show a slight skew, consistent with positive and negative MBEs, indicating minor overestimation and underestimation, respectively.

The metrics collectively indicate that satellite data is most accurate for Buenos Aires, with the smallest errors both in absolute and relative terms. In contrast, Santa Maria and Itajubá exhibit more significant discrepancies, especially in Itajubá, where the errors are larger and more variable. Localized adjustments may be necessary to address specific environmental factors or calibration issues, particularly in Itajubá, where the discrepancies are more pronounced.

These differences highlight the varying reliability of satellite and ground-based UV index estimations across different locations, suggesting that site-specific factors might be influencing the accuracy of these measurements. This variability underscores the need for further investigation into the sources of these errors, whether they arise from satellite data, ground-based measurements, or environmental factors affecting both.

5.4.3 Conclusions

This study identified the typical diurnal solar UV pattern at the three studied sites. UV index levels increased throughout the morning, peaked at solar noon, and declined in the afternoon as solar zenith angles increased. The maximum UV index levels observed were 15.86 at Santa Maria, 12.78 at Itajubá, and 13.51 at Buenos Aires. Annual variability, driven by the seasonal cycle, was also evident. During the austral summer, UV index levels frequently reached very high to extreme levels across all three locations, while the austral winter exhibited lower UV levels.

The comparison between satellite-derived and ground-based UV index measurements revealed significant differences. Itajubá exhibited the largest discrepancies, with moderate correlation and the highest MBE, MAPE, MAE, and RMSE values, indicating substantial measurement deviations. Santa Maria and Buenos Aires showed stronger correlations between satellite and ground-based measurements, with Buenos Aires demonstrating the most accurate relationship. The relative errors for these two cities were also smaller.

Itajubá's lower UV index levels and higher error metrics underscore the need for a thorough review of measurement methodologies, including calibration, maintenance of instruments, and an investigation into environmental factors that could be influencing these readings. Meanwhile, the consistency observed at Santa Maria and Buenos Aires highlights the reliability of the OMI (Ozone Monitoring Instrument) and ground-based instruments such as the Brewer Spectrophotometer MKIII #167 in Santa Maria and the Solar Light UV Biometer - model 501 in Buenos Aires. Future

research should address the discrepancies at Itajubá and conduct long-term trend analyses to enhance understanding of surface UV radiation's temporal variability across South America.

6 SUMMARY, LIMITATIONS AND FUTURE WORK

The main objective of this thesis was to analyze and characterize the temporal variability of solar ultraviolet radiation at low and mid-latitude South American sites, focusing on Santarém, Natal, Itajubá, and Santa Maria in Brazil, and Buenos Aires in Argentina. This research aimed to contribute to a better understanding of UV radiation patterns in these regions. Throughout the previous six chapters, a theoretical and bibliographic review was presented, explaining the basic concepts of UV radiation and summarizing important research in this field. The study areas were described in detail, along with the specific ground-based and satellite instruments and techniques used to characterize and analyze UV radiation and cloud cover conditions at these South American sites. Below is a summary of the main results obtained during the development of this thesis:

Impact of latitude on UV levels at low and mid-latitude South American sites:

The effects of latitude on the variability of solar UV radiation were confirmed in this study. The two low-latitude cities in this research (Santarém and Natal) displayed a semi-annual cycle with two maxima per year, as well as smaller seasonal amplitude and higher UV levels throughout the year. This is consistent with locations that experience lower solar zenith angles year-round. Natal, located within the Tropic of Capricorn, recorded two annual maxima, occurring around the equinoxes when the Sun is directly overhead its location.

Due to the short-term time series and gap of data available for Santarém, it was not possible to conclusively confirm the semi-annual cycle based on ground-based data. Even though, satellite-derived UV index from OMI and GOME-2 indicated a semi-annual cycle but with discrepancies. OMI showed higher UV index levels during the rainy austral summer months, while GOME-2 indicated spring, during dry season, as the period with the highest UV index levels. Differences in OMI and GOME-2 were already reported in the literature, for example, Ialongo et al. (2021) reported that different cloud cover assumptions in the OMI and GOME-2 algorithms can contribute to the differences between their datasets. According to Parisi et al. (2021), the main factors influencing UV irradiance variations between OMI, GOME-2 and ground based for a given solar zenith angle are clouds and aerosols.

The comparison of monthly UV index and solar zenith angles indicated that the lowest solar zenith angles months are in austral spring at Santarem's latitude, therefore the highest UV index levels are expected be in this period too, corroborating with the GOME-2 results. Nevertheless, without a longer ground-based time series, it remains challenging to confirm the exact timing of peak UV levels in Santarém

The latitude effect was also evident in the southern low- and mid-latitude cities, which exhibited an annual cycle with a single peak during the austral summer and lower UV levels during the austral winter months. Itajubá, situated between the Tropic of Capricorn and the Equator, experienced a broader period of high average UV index levels from November to February. This pattern arised from the Earth's axial tilt and orbital movement, causing the Sun to pass directly over Itajubá's latitude twice a year, in shorter period, closer months. Unlike Natal and Santarém, which have two distinct UV peaks in different seasons. Santa Maria, located between the Tropic of Capricorn and the Antarctic Circle, follows the expected pattern for its latitude, with a single annual peak of solar radiation during the austral summer. This peak occurs around the summer solstice in the southern hemisphere. Buenos Aires, a mid-latitude city, similarly experiences its highest UV intensity during the austral summer months, particularly in December, coinciding with the summer solstice.

Itajubá's special Case:

Itajubá, which is located at the highest altitude among the study sites and at a lower latitude than Santa Maria and Buenos Aires, presented unexpected results. Despite its favorable characteristics for higher UV levels (lower latitude and higher altitude), the ground-based UV index levels in Itajubá were lower than those observed in Santa Maria and Buenos Aires. This discrepancy was also reflected in the comparison between ground-based and satellite-derived UV index data. Itajubá showed the largest differences, with moderate correlation coefficients and the highest values for MBE, MAPE, MAE, and RMSE. These findings indicate significant measurement deviations and suggest the need for further investigation into potential local factors influencing UV radiation levels at this site.

The influence of cloud cover:

The results of this thesis also highlight the influence of cloud cover on UV variability, showing its dual role in both attenuating and enhancing UV levels.

In Santarém, UV variability was analyzed under all-sky and clear-sky conditions, as well as during the rainy and dry seasons. Under all-sky conditions, certain months (such as April, May, and December) exhibited higher average UV levels than under clear-sky conditions. These months correspond to the rainy season and the transition from the dry to rainy season. This suggests that cloud cover, which is higher during the rainy period, may be enhancing UV levels. This characteristic aligns with the literature, which explains that certain cloud types, such as cumulus or thin cirrus, can enhance UV levels by producing multiple scattering, thereby increasing the UV levels that reaches the surface.

Both ground-based and satellite-derived UV data indicate a higher amplitude in UV levels for Santarém during the rainy period. This suggests a significant role of clouds in controlling UV variability, primarily through attenuation, which explains the lower noontime UV index values observed during this period, but sometimes by increasing it, as shown in the ground-based analysis.

In Natal, there is a greater presence of cloud cover around noon throughout the year, with clear skies prevailing during nighttime and in the dry season (August to November). Between 12 and 1 PM, broken clouds are predominant. Although UV index values are generally higher under clear-sky conditions, at noontime during January, February, and March, UV index levels are higher under all-sky conditions. A similar pattern is observed at 11 AM in December.

At noon, the UV index under all-sky conditions is 6.8% higher than under clear-sky conditions, corresponding to an increase of 0.78 UV index units. The rainy season in Natal is concentrated between May and July, however, monthly rainfall starts increasing from December onwards. This characteristic of enhanced surface UV levels during some rainy months was also observed in the study for Santarém. It was already reported that surface UV levels can be enhanced under scattered or broken cloud conditions, particularly when the Sun is not obscured by clouds, but clouds are present elsewhere in the sky (CEDE at al., 2002). Such enhancements are most pronounced under large cloud cover of 5 to 7 octas (broken clouds) when the solar disk remains unoccluded (ZHANG et al., 2019). This variability in cloud cover helps explain the higher UV index values observed under all-sky conditions compared to clear-sky conditions at noontime in Natal. Around noon, broken clouds are prevalent in Natal, contributing to these enhancements in UV levels.

These findings add to the scientific understanding of cloud-induced UV enhancements, highlighting their effects in both Santarém and Natal. In this study, cloud cover for both cities were assessed using METAR data due to the unavailability of other ground-based cloud cover

measurements. However, future research incorporating more robust methods, such as from sky cameras, would be essential to better understand and characterize the impact of clouds on UV variability.

For the southern cities included in this study, Itajubá and Buenos Aires, no free METAR data was available. Additionally, an analysis of UV variability under clear-sky conditions for Santa Maria was previously reported by Lopes et al. (2022). Therefore, here, the analysis of UV variability for these three low- and mid-latitude sites did not include a detailed exploration of UV under clear and all-sky conditions. This limitation restricted the understanding of diurnal and seasonal variability in UV at these sites to observations under all-sky conditions only.

Effect of Clear-Sky Selection Methods:

To assess clear-sky conditions, two different techniques were employed: one using ground-based data (METAR) and the other using satellite-derived data (LER). The LER method identified a significantly larger number of clear-sky days (1,928 days) compared to the METAR method (138 days) at OMI overpass time. This discrepancy suggests that the LER method applies more flexible criteria for defining clear-sky conditions, potentially giving a lower percentage for sky conditions that would not meet METAR's criteria for clear-sky.

Even with the divergence in number of clear sky hours, the difference between the metrics were small when comparing ground-based against OMI overpass time UV index using different cloud cover proxies. For example, with RMSE of 1.81, 1.64 and 1.53 when using LER, METAR and the combined dataset LER & METAR respectively. In fact, at overpass time, the best metrics resulted from the combined dataset.

METAR data, which is based on observations from airports, tend to represent local clear-sky conditions more accurately than satellite data, as METAR observations are localized. In contrast, satellite-derived data, such as LER, capture a larger area, and the variation introduced by clouds is spatially averaged over the area of a pixel. As a result, satellite data may detect atmospheric or cloud-cover variations over a broader region that are not captured in the localized METAR observations. These discrepancies underscore the importance of understanding the specific criteria each method uses and suggest that a thoughtful selection or combination of methods is crucial for obtaining the most accurate representation of clear-sky conditions for specific studies or applications.

Implementing sky cameras installed near the UV sensor could reduce uncertainties associated with the technique used to determine clear-sky conditions. These cameras would provide images of the sky, helping to determine the actual sky conditions more accurately, thus potentially reducing uncertainty related to the sky condition. Nevertheless, both techniques are useful for assessing cloud cover conditions in locations where this type of data is unavailable. By employing these two distinct methods, this study demonstrates that METAR data can be effectively used in scientific research, particularly in areas without dedicated cloud observation instruments but with METAR reports from airports. Additionally, the LER method broadens this capability to include locations where METAR data is also unavailable, further enhancing the potential for studying cloud cover and UV variability.

Accuracy and reliability of ground-based and satellite derived UV index:

In this thesis, ground-based and satellite-derived UV Index levels were compared for low- and mid-latitude South American sites using data from different instruments, with each location analyzed for its respective time period. To reduce errors related to cloud cover, comparisons were conducted under clear-sky conditions, identified using the LER method and, for Natal, the METAR method as well. For Santarém, no comparison could be performed due to the lack of ground-based UV Index data.

For the first time, the complete dataset (2006–2022) of UV Index levels in Natal, monitored using the Davis Sensor 6490, has been analyzed. Comparisons reveal that OMI UV Index data at overpass and noontime show less bias than GOME-2 noontime data. While OMI generally overestimates UV Index levels compared to ground-based measurements, GOME-2 tends to underestimate them. Overall, metrics such as MAE, MAPE, and RMSE indicate that the differences between satellite-derived and ground-based measurements are generally low. Coupled with moderate to strong correlation coefficients, the clustering of points near the red line in scatter plots, and the error distribution centered around zero, these results suggest that the two satellite sources (OMI noontime and overpass) and GOME-2 noontime provide reliable UV Index data. Their good agreement with ground-based measurements reinforces their value for monitoring UV radiation.

Even though it's the same model of sensor used at Natal and Itajubá (Davis Sensor 6490), the comparisons revealed that Itajubá's data had the largest differences between ground-based and satellite derived UV index levels of all site's studied, with a moderate correlation and the highest MBE, MAPE, MAE, and RMSE values, indicating significant measurement deviations. Both

Santa Maria and Buenos Aires showed a stronger correlation between ground based and satellite measurements, with Buenos Aires presenting the strongest relationship. The MBE, MAPE, MAE and RMSE were lower for these cities as well, indicating smaller relative errors.

Itajubá's weaker metrics results, such as higher MBE, RMSE, and other discrepancies, suggest the need for a thorough review of measurement methods to identify potential sources of error. In contrast, the consistent results observed in Natal, Santa Maria, and Buenos Aires validate the accuracy of key instruments, including the OMI noontime and overpass data, GOME-2 noontime data, and the Davis 6490 UV sensor installed in Natal. Additionally, the OMI overpass and ground-based instruments (Brewer Spectrophotometer MKIII #167 in Santa Maria and Solar Light UV Biometer Model 501 in Buenos Aires) demonstrated reliability in capturing UV patterns.

With the reliability of these satellite and ground-based instruments assessed for these locations, we now have the capability to conduct trend analyses and other studies, such as evaluating the long-term effects of UV radiation on public health. These findings provide a critical foundation for future studies aiming to understand UV variability, its interactions and effects in low- and mid-latitude South America, particularly in the tropical region, where data has historically been scarce.

UV Index and public awareness:

Since the UV index is an indicator of UV levels and serves as an important tool for raising public awareness about adequate sun exposure and protection, this thesis used UVI data to assess UV variability and the levels to which populations are exposed at the studied sites. Unfortunately, for Santarém, it was not possible to conduct a detailed analysis of ground-based UVI levels due to data limitations. However, an analysis of satellite-derived noontime UVI was performed.

In Santarém, moderate, high, and very high UVI levels represent 39.75% of the noontime UVI during the rainy period and 54.31% during the dry period, based on the OMI dataset. These levels already warrant protective measures. During the rainy period, when cloud cover and precipitation are more prevalent, approximately 60% of the noontime UVI is classified as extreme, according to OMI. In contrast, the GOME-2 dataset indicates that only 23% of the UVI levels are extreme during the rainy period, with 37.74% during the dry period. According to WHO (2002), extreme UVI levels can cause sunburn to skin and eyes within minutes if sun protection is not used. It is strongly recommended to avoid sun exposure at these levels and to follow all protective measures outlined by WHO (2002) and EPA (2017).

These findings from both datasets emphasize the importance of maximum protective measures during both the rainy and dry periods to avoid overexposure to UV radiation. Santarém's tropical location, characterized by a low solar zenith angle throughout the year and minimal photoperiod variation, predictably results in higher UVI levels, especially at noontime when the solar zenith angle is at its minimum. Understanding the diurnal pattern of UVI at this location is essential; however, the scarcity of ground-based data imposes limitations, restricting this study to noontime UVI analysis. Nevertheless, the results reinforce the critical need for maximum protective measures during solar noontime to minimize the risk of UV overexposure, regardless of the season.

In Natal, the UV index is generally high, under clear and all-sky conditions. The low-danger period of exposure to UV rays only occurs until 8 AM and from 4 PM onwards. However, even during those hours, moderate levels were recorded. Therefore, protection is needed from 8 AM for those who frequent the city of Natal. Between 10 AM and 2 PM, the population in Natal is exposed to extreme UV levels. Considering the hours with extreme levels, maximum protective measures need to be taken from 10 am, considering UTC-2. When following UTC-3, these recommendations should be followed 1h in advance.

Itajubá, exhibits low-danger period of exposure to UV rays only until 8 am and from 3 pm onwards, also with occasional moderate levels at these hours. Starting from 9 AM, very high levels are reached, peaking between 11 AM and 1 PM, and gradually decreasing after 2 PM. It is important to note that, compared to cities at similar latitudes and even those further south, Itajubá's UV Index levels are unexpectedly lower. Extreme UV levels in Itajubá were observed only between 11 AM and 1 PM, with fewer and shorter durations of extreme levels than expected. The specific reasons for these unexpected results remain a subject for future research.

In Santa Maria, the UV Index levels remain at maximum moderate from sunrise until 8 AM. By 9 AM, the UV Index typically ranges from low to moderate, with occasional very high levels. Extreme UV levels are observed between 10 AM and 2 PM, peaking at local noon when the UV Index exceeds 15. After 2 PM, the intensity gradually decreases. By 3 PM, most readings are at moderate levels, eventually declining to low levels as sunset approaches. This pattern emphasizes the need for maximum protective measures during the hours of highest UV intensity, particularly between 10 AM and 2 PM. Early morning and late afternoon provide safer periods, with lower UV levels, but moderate protection may still be advisable during those times.

Excluding Santarém due to a lack of data and Itajubá due to inconsistent results, Natal exhibited the highest UV Index levels, followed by Santa Maria and Buenos Aires. Aditionaly, although Santa Maria is located at a much higher latitude compared to Natal, the average UV levels were found to be just as high as those reported for Natal. The key difference lies in the seasonal distribution of extreme UV levels. In Natal, extreme monthly average UV Index levels are observed in all seasons except austral winter, when the levels decrease but remain very high. In contrast, Santa Maria experiences monthly average very high UV levels only during the summer months.

The UV Index in Buenos Aires is predominantly low to moderate from sunrise until 10 AM, with levels reaching very high starting at 10 AM. Between 11 AM and 2 PM, extreme levels were recorded. After 3 PM, the UV Index decreases to moderate levels, with occasional peaks reaching very high, and by 5 PM, it predominantly falls to low levels.

While Itajubá experienced three hours of extreme UV levels between 11 AM and 1 PM, Buenos Aires had four hours of extreme levels between 11 AM and 2 PM. Santa Maria and Natal recorded five hours of extreme levels between 10 AM and 2 PM. These findings highlight the critical importance of taking protective measures against overexposure to ultraviolet radiation, as moderate, high, and very high UV levels are reached starting in the early morning hours, with several hours of extreme UV exposure posing significant risks to the population.

7 CONCLUSIONS

The main objective of this doctoral research was to analyze and characterize the temporal variability of solar ultraviolet radiation at low- and mid-latitude South American sites, focusing on Santarém, Natal, Itajubá, and Santa Maria in Brazil, and Buenos Aires in Argentina, to contribute to a better understanding of UV radiation patterns in these regions. Even with the limitations related to lack and quality of UV and cloud cover data, all the specifics objectives were achieved.

The study confirmed the effects of latitude on solar UV radiation variability. Low-latitude cities, Santarém and Natal, displayed a semi-annual cycle with two annual maximums, smaller seasonal amplitude, and consistently higher UV levels due to lower solar zenith angles year-round. However, limited ground-based data and discrepancies between OMI and GOME-2 satellite estimates for Santarém made it challenging to confirm the exact timing of peak UV levels. Southern low- and mid-latitude cities showed an annual cycle with a single peak during austral summer and lower UV levels in winter. Itajubá experienced a broader peak of high UV levels from November

to February due to its position between the Tropic of Capricorn and the Equator. Santa Maria and Buenos Aires followed expected patterns, with the highest UV levels occurring in austral summer, around the December solstice. Natal exhibited the highest UV Index levels, followed by Santa Maria and Buenos Aires.

This thesis also highlighted the dual role of cloud cover in UV variability, both attenuating and enhancing UV levels. In Santarém, certain months during the rainy season, when cloud coverage is greater, showed higher average UV levels under all-sky conditions compared to clear-sky conditions. In Natal, UV levels at noontime, a period when broken clouds were found to prevail, were 6.8% higher under all-sky conditions than under clear-sky conditions, corroborating with previously cloud-enhancement effects reported in the literature.

Another important contribution was the comparison of ground-based and satellite-derived UV Index levels for low- and mid-latitude South American sites, using data from different instruments and time periods. For the first time, the complete dataset (2006–2022) of UV Index levels in Natal, recorded by the Davis Sensor 6490, was analyzed. The results showed that OMI data both at overpass and noontime had less bias than GOME-2, with OMI tending to overestimate UV Index levels and GOME-2 to underestimate them. Despite these differences, metrics such as MAE, MAPE, and RMSE indicated generally low errors, confirming the reliability of OMI and GOME-2 data for this low latitude tropical site.

In contrast, at Itajubá, where the same model of instrument as used in Natal was employed to monitor UV, the largest discrepancies between ground-based and satellite-derived data were found. It exhibited a moderate correlation and the highest MBE, MAPE, MAE, and RMSE values, indicating significant measurement deviations and highlighting the need for further investigation into potential local factors affecting measurements. Meanwhile, both Santa Maria and Buenos Aires showed stronger correlations between ground-based and satellite data, with Buenos Aires presenting the better agreement. The MBE, MAPE, MAE, and RMSE were also lower for these cities, indicating smaller relative errors. These findings validate the reliability of key instruments, including the OMI and GOME-2 satellite datasets, as well as the ground-based instruments used in Natal, Santa Maria, and Buenos Aires. This reliability provides a basis for conducting trend analyses and further studies on UV variability, exposure risks, and public health impacts.

Another key finding of this thesis was diurnal pattern of UV levels to which the population is exposed at the studies sites. In Santarém, satellite-derived results revealed that extreme UV index

levels occur up to 60% of the time at noontime during the rainy season. Understanding the diurnal pattern of UVI at this location is essential; however, the scarcity of ground-based data imposed limitations, restricting the study to noontime UVI analysis. Nevertheless, the results reinforce the critical need for maximum protective measures during solar noontime to minimize the risk of UV overexposure, regardless of the season.

During five hours of the day, from 10 AM to 2 PM, the population in Natal and Santa Maria is exposed to extreme UV levels. In both locations, low-danger periods are confined to the early morning and late afternoon (before 8 AM and after 4 PM), although occasional moderate levels during these times may still require sun protection. In Buenos Aires, UV levels remain low to moderate from sunrise until 10 AM, with very high levels beginning from this hour onward. These findings underscore the critical importance of implementing protective measures against UV overexposure, as moderate, high, and very high levels are reached starting in the early morning, with extended periods of extreme UV exposure posing significant health risks to the population.

In conclusion, this thesis makes an important contribution to understanding the variability of UV radiation in South America, a region where UV-related studies are still limited. The methodologies applied here also hold potential for expanding UV and cloud cover research to other underrepresented areas. The findings are scientifically valuable and relevant for public health, offering information to guide awareness campaigns and strategies for UV protection. In a time of increasing environmental challenges, this work confirms the reliability of instruments and datasets, providing a foundation for environmental and health studies in the complex field of UV radiation, its interactions, and its effects, addressing a critical knowledge gap in atmospheric and environmental sciences.

REFERENCES

ADAM, M. El-Nouby. Atmospheric modulations of the ratio of UVB to broadband solar radiation: effect of ozone, water vapour, and aerosols at Qena, Egypt. **International journal of climatology**, vol. 34, no. 7, p. 2477–2488, 2014. Available at: http://dx.doi.org/10.1002/joc.3854.

ADAM, M.; AHMED, Emad A. Comparative analysis of cloud effects on ultraviolet-B and broadband solar radiation: Dependence on cloud amount and solar zenith angle. **Atmospheric research**, vol. 168, p. 149–157, 2016. Available at: https://linkinghub.elsevier.com/retrieve/pii/S0169809515002872.

AKOGLU, Haldun. User's guide to correlation coefficients. **Turkish journal of emergency medicine**, vol. 18, no. 3, p. 91–93, 2018. Available at: http://dx.doi.org/10.1016/j.tjem.2018.08.001.

ALVES, Guilherme Prado *et al.* Periferização, qualidade ambiental urbana e percepção dos moradores em cidades médias: estudo de caso no município de Itajubá/MG. **Research, Society and Development**, vol. 10, no. 1, p. e3710111332, 2021. Available at: http://dx.doi.org/10.33448/rsd-v10i1.11332.

ALVES, Pericles *et al.* Sazonalidade anual e a variabilidade horária mensal do índice ultravioleta para a cidade de Humaitá, Amazonas, Brasil. **Revista Brasileira de Climatologia**, vol. 30, p. 504–523, 2022. Available at: http://dx.doi.org/10.55761/abclima.v30i18.14622.

AMBACH, W.; BLUMTHALER, M.; WENDLER, G. A comparison of ultraviolet radiation measured at an arctic and an alpine site. **Solar energy**, vol. 47, no. 2, p. 121–126, 1991. Available at: http://dx.doi.org/10.1016/0038-092x(91)90043-v.

ANDRADY, A. L. *et al.* Effects of UV radiation on natural and synthetic materials. **Photochemical & photobiological sciences**, vol. 22, no. 5, p. 1177–1202, 2023. Available at: http://dx.doi.org/10.1007/s43630-023-00377-6.

ANTÓN, M. *et al.* Comparison of UV irradiances from Aura/Ozone Monitoring Instrument (OMI) with Brewer measurements at El Arenosillo (Spain) – Part 1: Analysis of parameter influence. **Atmospheric chemistry and physics**, vol. 10, no. 13, p. 5979–5989, 2010. Available at: http://dx.doi.org/10.5194/acp-10-5979-2010.

ANTÓN, M. *et al.* Extreme ultraviolet index due to broken clouds at a midlatitude site, Granada (southeastern Spain). **Atmospheric research**, vol. 118, p. 10–14, 2012. Available at: https://linkinghub.elsevier.com/retrieve/pii/S0169809512001822.

ARSENOVIC, Pavle *et al.* Implications of potential future grand solar minimum for ozone layer and climate. **Atmospheric chemistry and physics**, vol. 18, no. 5, p. 3469–3483, 2018. Available at: http://dx.doi.org/10.5194/acp-18-3469-2018.

ARTAXO, P. *et al.* **Aerosol Particles in Amazonia: Their Composition, Role in the Radiation Balance, Cloud Formation, and Nutrient Cycles**. *In*: Geophysical Monograph Series. Washington, D. C.: American Geophysical Union, 2009. p. 207–232.

ARTAXO, Paulo *et al.* Physical and chemical properties of aerosols in the wet and dry seasons in Rondônia, Amazonia. **Journal of geophysical research**, vol. 107, no. D20, 2002. Available at: http://dx.doi.org/10.1029/2001jd000666.

AUN, Margit *et al.* **UV radiation measurements in Marambio, Antarctica during years 2017–2019 in a wider temporal and spatial context**. 2019. Available at: http://dx.doi.org/10.5194/acp-2019-896.

BAIS, A. F. *et al.* Environmental effects of ozone depletion, UV radiation and interactions with climate change: UNEP Environmental Effects Assessment Panel, update 2017. **Photochemical & photobiological sciences,** vol. 17, no. 2, p. 127–179, 2018. Available at: http://dx.doi.org/10.1039/c7pp90043k.

BAIS, Alkiviadis F. *et al.* Spectral measurements of solar UVB radiation and its relations to total ozone, SO_2, and clouds. **Journal of geophysical research**, vol. 98, no. D3, p. 5199–5204, 1993. Available at: http://dx.doi.org/10.1029/92jd02904.

BARBIERI, Florian; RAJAKARUNA, Sumedha; GHOSH, Arindam. Very short-term photovoltaic power forecasting with cloud modeling: A review. **Renewable and Sustainable Energy Reviews**, vol. 75, p. 242–263, 2017. Available at: http://dx.doi.org/10.1016/j.rser.2016.10.068.

BASSET, H.; KORANY, M. The global and UV-B radiation over Egypt. **Atmosfera**, vol. 20, no. 4, p. 341–358, 2007. Available at:

https://www.revistascca.unam.mx/atm/index.php/atm/article/view/8586. Accessed at: 3 Dec. 2024.

BEKKI, S.; LEFEVRE, F. Stratospheric ozone: History and concepts and interactions with climate. **EPJ web of conferences**, vol. 1, p. 113–136, 2009. Available at: http://dx.doi.org/10.1140/epjconf/e2009-00914-y.

BERNHARD, Germar *et al.* Comparison of ultraviolet spectroradiometers in Antarctica. **Journal of geophysical research**, vol. 113, no. D14, 2008. Available at: http://dx.doi.org/10.1029/2007jd009489.

BERNHARD, G. H. *et al.* Stratospheric ozone, UV radiation, and climate interactions. **Photochemical & photobiological sciences**, vol. 22, no. 5, p. 937–989, 2023. Available at: http://dx.doi.org/10.1007/s43630-023-00371-y.

BERNHARD, G.; SECKMEYER, G. Uncertainty of measurements of spectral solar UV irradiance. **Journal of geophysical research**, vol. 104, no. D12, p. 14321–14345, 1999. Available at: http://dx.doi.org/10.1029/1999jd900180.

BERNHARD, Germar; STIERLE, Scott. Trends of UV radiation in Antarctica. **Atmosphere**, vol. 11, no. 8, p. 795, 2020. Available at: http://dx.doi.org/10.3390/atmos11080795.

BEVAN, Suzanne L. *et al.* Impact of atmospheric aerosol from biomass burning on Amazon dry-season drought. **Journal of geophysical research**, vol. 114, no. D9, 2009. Available at: http://dx.doi.org/10.1029/2008jd011112.

BHATTACHARYA, R. Annual variability and distribution of ultraviolet index over India using temis data. **Int J Eng Sci Technol** , vol. 4, p. 4577, 2012. Available at: https://www.idc-online.com/technical_references/pdfs/chemical_engineering/ANNUAL%20VARIABILITY.pdf. Accessed at: 15 Nov. 2024.

BILBAO, Julia *et al.* Global, diffuse, beam and ultraviolet solar irradiance recorded in Malta and atmospheric component influences under cloudless skies. **Solar Energy**, vol. 121, p. 131–138, 2015. Available at: http://dx.doi.org/10.1016/j.solener.2015.04.048.

BILBAO, Julia; DE MIGUE, Argimiro. Erythemal solar irradiance, UVER, and UV index from ground-based data in Central Spain. **Applied sciences**, vol. 10, no. 18, p. 6589, 2020. Available at: http://dx.doi.org/10.3390/app10186589.

BILBAO, Julia; DE MIGUEL, Argimiro. Estimation of UV-B irradiation from total global solar meteorological data in central Spain. **Journal of geophysical research**, vol. 115, no. D1, 2010. Available at: http://dx.doi.org/10.1029/2009jd012505.

BILBAO, J.; MIGUEL, A. Contribution to the study of UV-B solar radiation in Central Spain. **Renewable energy**, vol. 53, p. 79–85, 2013. Available at: https://linkinghub.elsevier.com/retrieve/pii/S0960148112007069.

BITTENCOURT, Gabriela Dornelles *et al.* Investigation of the behavior of the atmospheric dynamics during occurrences of the ozone hole's secondary effect in southern Brazil. **Annales geophysicae**, vol. 37, no. 6, p. 1049–1061, 2019. Available at: http://dx.doi.org/10.5194/angeo-37-1049-2019.

BORNMAN, J. F. *et al.* Solar ultraviolet radiation and ozone depletion-driven climate change: effects on terrestrial ecosystems. **Photochemical & photobiological sciences**, vol. 14, no. 1, p. 88–107, 2014. Available at: http://dx.doi.org/10.1039/c4pp90034k.

BRESCIANI, Caroline *et al.* Report of a large depletion in the ozone layer over southern Brazil and Uruguay by using multi-instrumental data. **Annales Geophysicae**, vol. 36, no. 2, p. 405–413, 2018. Available at: https://angeo.copernicus.org/articles/36/405/2018/. Accessed at: 17 Nov. 2024.

BROGNIEZ, Colette *et al.* Validation of satellite-based noontime UVI with NDACC ground-based instruments: influence of topography, environment and satellite overpass time. **Atmospheric chemistry and physics**, vol. 16, no. 23, p. 15049–15074, 2016. Available at: http://dx.doi.org/10.5194/acp-16-15049-2016.

BUNTOUNG, S. *et al.* An investigation of total solar ultraviolet radiation at Nakhon Pathom, Thailand. **Procedia engineering**, vol. 32, p. 427–432, 2012. Available at: http://dx.doi.org/10.1016/j.proeng.2012.01.1289.

BURNS, Angus C. *et al.* Day and night light exposure are associated with psychiatric disorders: an objective light study in >85,000 people. **Nature mental health**, vol. 1, no. 11, p. 853–862, 2023. Available at: https://www.nature.com/articles/s44220-023-00135-8. Accessed at: 17 Nov. 2024.

BURROWS, John P. *et al.* The global ozone monitoring experiment (GOME): Mission concept and first scientific results. **Journal of the atmospheric sciences**, vol. 56, no. 2, p. 151–175, 1999. Available at: http://dx.doi.org/10.1175/1520-0469(1999)056<0151:tgomeg>2.0.co;2.

BUTCHART, Neal. The brewer-Dobson circulation. **Reviews of geophysics**, vol. 52, no. 2, p. 157–184, 2014. Available at: http://dx.doi.org/10.1002/2013rg000448.

CABRERA, Sergio *et al.* UV index values and trends in Santiago, Chile (33.5°S) based on ground and satellite data. **Journal of photochemistry and photobiology,** vol. 115, p. 73–84, 2012. Available at: http://dx.doi.org/10.1016/j.jphotobiol.2012.06.013.

CADET, Jean-Maurice *et al.* Comparison of ground-based and satellite-derived solar UV index levels at six south African sites. **International journal of environmental research and public health**, vol. 14, no. 11, p. 1384, 2017. Available at: http://dx.doi.org/10.3390/ijerph14111384.

CADET, Jean-Maurice *et al.* Solar UV radiation in the tropics: Human exposure at Reunion Island (21° S, 55° E) during summer outdoor activities. **International journal of environmental research and public health**, vol. 17, no. 21, p. 8105, 2020. Available at: http://dx.doi.org/10.3390/ijerph17218105.

CAÑADA, J. *et al.* Influences of the clearness index for the whole spectrum and of the relative optical air mass on UV solar irradiance for two locations in the Mediterranean area, Valencia and Cordoba. **Journal of geophysical research**, vol. 105, no. D4, p. 4759–4766, 2000. Available at: http://dx.doi.org/10.1029/1999jd901106.

CAÑADA, J. Relationships between UV (0.290–0.385 μm) and broad band solar radiation hourly values in Valencia and Córdoba, Spain. **Energy (Oxford, England)**, vol. 28, no. 3, p. 199–217, 2003. Available at: http://dx.doi.org/10.1016/s0360-5442(02)00111-1.

CARSLAW, K. S. *et al.* A review of natural aerosol interactions and feedbacks within the Earth system. **Atmospheric chemistry and physics**, vol. 10, no. 4, p. 1701–1737, 2010. Available at: http://dx.doi.org/10.5194/acp-10-1701-2010.

CAZORLA, A.; OLMO, F. J.; ALADOS-ARBOLEDAS, L. Development of a sky imager for cloud cover assessment. **Journal of the Optical Society of America. A, Optics, image science, and vision**, vol. 25, no. 1, p. 29, 2008. Available at: https://opg.optica.org/abstract.cfm?URI=josaa-25-1-29. Accessed at: 17 Nov. 2024.

CBO, Conselho Brasileiro de Oftalmologia. **As Condições de Saúde Ocular no Brasil 2019**. 2019. Available at: https://www.cbo.com.br/novo/publicacoes/condicoes_saude_ocular_brasil2019.pdf. Accessed at: 17 Nov. 2024.

CCOHS, Canadian Center for Occupational Health and Safety. **Ultraviolet Radiation**. 2022. Available at: https://www.ccohs.ca/oshanswers/phys_agents/ultravioletradiation.html. Accessed at: 17 Nov. 2024.

CEDE, Alexander *et al.* Effects of clouds on erythemal and total irradiance as derived from data of the Argentine Network. **Geophysical research letters**, vol. 29, no. 24, 2002. Available at: http://dx.doi.org/10.1029/2002gl015708.

CHAN, Ka Lok *et al.* **Global ozone monitoring experiment-2 (GOME-2) daily and monthly level 3 products of atmospheric trace gas columns**. 2022. Available at: http://dx.doi.org/10.5194/essd-2022-315.

CHAND, D. *et al.* Optical and physical properties of aerosols in the boundary layer and free troposphere over the Amazon Basin during the biomass burning season. **Atmospheric chemistry and physics**, vol. 6, no. 10, p. 2911–2925, 2006. Available at: http://dx.doi.org/10.5194/acp-6-2911-2006.

CHICCO, Davide; WARRENS, Matthijs J.; JURMAN, Giuseppe. The coefficient of determination R-squared is more informative than SMAPE, MAE, MAPE, MSE and RMSE in regression analysis evaluation. **PeerJ. Computer science**, vol. 7, no. e623, p. e623, 2021. Available at: http://dx.doi.org/10.7717/peerj-cs.623.

CHOOSRI, P. *et al.* Development of a method for mapping monthly average hourly diffuse erythemal ultraviolet radiation. **Journal of atmospheric and solar-terrestrial physics**, vol. 161, p. 19–27, 2017. Available at: https://linkinghub.elsevier.com/retrieve/pii/S1364682617300998.

COARITI, J. R. **Análise dos efeitos da radiação solar ultravioleta (r-uv) em populações habitantes a diferentes altitudes**. 2011. UNIFEI, Itajubá, 2011. Available at: https://repositorio.unifei.edu.br/jspui/handle/123456789/1345. Accessed at: 18 Nov. 2024.

COARITI, J. R. **Características da Radiação Ultravioleta Solar e seus efeitos na saúde humana nas cidades de La Paz – Bolívia e Natal - Brasil**. 2017. - UFRN, Natal, 2017. Available at:https://repositorio.ufrn.br/bitstream/123456789/24952/1/Caracter%C3%ADsticasRadiacaoUltravioleta_Coariti_2017.pdf. Accessed at: 17 Nov. 2024.

CORDERO, Raúl R. *et al.* Persistent extreme ultraviolet irradiance in Antarctica despite the ozone recovery onset. **Scientific reports**, vol. 12, no. 1, 2022. Available at: http://dx.doi.org/10.1038/s41598-022-05449-8.

CORDERO, R. R. *et al.* Aerosol effects on the UV irradiance in Santiago de Chile. **Atmospheric research**, vol. 149, p. 282–291, 2014. Available at: https://linkinghub.elsevier.com/retrieve/pii/S0169809514002646.

CORRÊA, Marcelo de Paula. Solar ultraviolet radiation: properties, characteristics and amounts observed in Brazil and South America. **Anais brasileiros de dermatologia**, vol. 90, no. 3, p. 297–313, 2015. Available at: http://dx.doi.org/10.1590/abd1806-4841.20154089.

CORRÊA, Marcelo de Paula *et al.* Exposome extrinsic factors in the tropics: The need for skin protection beyond solar UV radiation. **The Science of the total environment**, vol. 782, no. 146921, p. 146921, 2021. Available at: http://dx.doi.org/10.1016/j.scitotenv.2021.146921.

CORRÊA, Marcelo de Paula; C. M. PIRES, Luciana. Doses of erythemal ultraviolet radiation observed in Brazil. **International journal of dermatology**, vol. 52, no. 8, p. 966–973, 2013. Available at: http://dx.doi.org/10.1111/j.1365-4632.2012.05834.x.

CORRÊA, Marcelo de Paula; PLANA-FATTORI, Artemio. Uma análise das variações do índice ultravioleta em relação às observações de conteúdo de ozônio e da espessura óptica dos aerossóis sobre a cidade de São Paulo. **Brazilian Journal of Meteorology**, vol. 21, no. 1, p. 24–32, 2006. Available at: https://www.scirp.org/reference/referencespapers?referenceid=1161687. Accessed at: 17 Nov. 2024.

CORTESI, Ugo *et al.* Advanced Ultraviolet Radiation and Ozone Retrieval for applications (AURORA): A project overview. **Atmosphere**, vol. 9, no. 11, p. 454, 2018. Available at: http://dx.doi.org/10.3390/atmos9110454.

COSTA, Rodrigo Santos; MARTINS, Fernando Ramos; PEREIRA, Enio Bueno. Atmospheric aerosol influence on the Brazilian solar energy assessment: Experiments with different horizontal visibility bases in radiative transfer model. **Renewable energy**, vol. 90, p. 120–135, 2016. Available at: http://dx.doi.org/10.1016/j.renene.2015.12.053.

DAEMEI, Abdollah Baghaei; EGHBALI, Seyed Rahman; KHOTBEHSARA, Elham Mehrinejad. Bioclimatic design strategies: A guideline to enhance human thermal comfort in Cfa climate zones. **Journal of building engineering**, vol. 25, no. 100758, p. 100758, 2019. Available at: http://dx.doi.org/10.1016/j.jobe.2019.100758.

DAMIANI, A. *et al.* Cloud cover and UV index estimates in Chile from satellite-derived and ground-based data. **Atmospheric research**, vol. 138, p. 139–151, 2014. Available at: http://dx.doi.org/10.1016/j.atmosres.2013.11.006.

DAMIANI, A. *et al.* Satellite-derived UV irradiance for a region with complex morphology and meteorology: comparison against ground measurements in Santiago de Chile. **International journal of remote sensing**, vol. 34, no. 16, p. 5812–5833, 2013. Available at: http://dx.doi.org/10.1080/01431161.2013.796101.

DAVIS, Instruments. **UV sensor 6490 Vantage Pro Spec Sheet**. Available at: https://www.meteosystem.com/davis/6490_spec.pdf. Accessed at: 15 Nov. 2024.

DAY, T. A. *et al.* Growth and reproduction of Antarctic vascular plants in response to warming and UV radiation reductions in the field. **Oecologia**, vol. 119, no. 1, p. 24–35, 1999. Available at: http://dx.doi.org/10.1007/s004420050757.

DE BOCK, V. *et al.* Relations between erythemal UV dose, global solar radiation, total ozone column and aerosol optical depth at Uccle, Belgium. **Atmospheric chemistry and physics**, vol. 14, no. 22, p. 12251–12270, 2014. Available at: http://dx.doi.org/10.5194/acp-14-12251-2014.

DIAS NUNES, Mateus; MARIANO, Glauber Lopes; ALONSO, Marcelo Félix. Variabilidade espaço-temporal da coluna total de ozônio e sua relação com a radiação ultravioleta na América do Sul. **Revista Brasileira de Geografia Física**, vol. 13, no. 5, p. 2053–2073, 2020. Available at: http://dx.doi.org/10.26848/rbgf.v13.5.p2053-2073.

DIÉMOZ, Henri *et al.* Solar ultraviolet irradiance measurements in Aosta (Italy): An analysis of short- and middle-term spectral variability. *In*: , 2013. **AIP Conference Proceedings**: AIP, 2013. p. 856–859.

DIFFEY, B. L. Solar ultraviolet radiation effects on biological systems. **Physics in medicine and biology**, vol. 36, no. 3, p. 299–328, 1991. Available at: http://dx.doi.org/10.1088/0031-9155/36/3/001.

DIFFEY, Brian L. Sources and measurement of ultraviolet radiation. **Methods,** vol. 28, no. 1, p. 4–13, 2002. Available at: http://dx.doi.org/10.1016/s1046-2023(02)00204-9.

D'ORAZIO, John *et al.* UV radiation and the skin. **International journal of molecular sciences**, vol. 14, no. 6, p. 12222–12248, 2013. Available at: http://dx.doi.org/10.3390/ijms140612222.

SANTOS, Weslley Veira *et al.* Percepção Ambiental e Climática de Alunos de Escolas Públicas de Itajubá – MG. **Geography Department University of Sao Paulo**, vol. 37, p. 70–79, 2019. Available at: http://dx.doi.org/10.11606/rdg.v37i0.149132.

DOUGLASS, Anne R.; NEWMAN, Paul A.; SOLOMON, Susan. The Antarctic ozone hole: An update. **Physics today**, vol. 67, no. 7, p. 42–48, 2014. Available at: http://dx.doi.org/10.1063/pt.3.2449.

DRAGANOVA-FILIPOVA, Milena; BOJILOVA, Vanina; ZAGORCHEV, Plamen. Alzheimer's disease: the hypotheses, known and unknown connections between UV-radiation, mtDNA haplotypes and life span – a review. **Folia Medica**, vol. 64, no. 6, p. 878–883, 2022. Available at: https://foliamedica.bg/article/68268/. Accessed at: 17 Nov. 2024.

DRING, M. J. *et al.* Seasonal and diurnal variations in ultraviolet-B and ultraviolet-A irradiances at and below the sea surface at Helgoland (North Sea) over a 6-year period. **Helgoland marine research**, vol. 55, no. 1, p. 3–11, 2001. Available at: http://dx.doi.org/10.1007/s101520000063.

DU PREEZ, D. Jean *et al.* Comparison of GOME-2 UVA satellite data to ground-based UVA measurements in South Africa. **Photochemistry and photobiology**, vol. 96, no. 6, p. 1342–1349, 2020. Available at: http://dx.doi.org/10.1111/php.13308.

DU PREEZ, D. Jean *et al.* Solar ultraviolet radiation in Pretoria and its relations to aerosols and tropospheric ozone during the biomass burning season. **Atmosphere**, vol. 12, no. 2, p. 132, 2021. Available at: http://dx.doi.org/10.3390/atmos12020132.

ECHER, E. *et al.* **A Rede De Detectores De Radiação Ultravioleta Solar Do INPE**. Brazilian Society of Geophisics 1999. Available at:https://sbgf.org.br/mysbgf/eventos/expanded_abstracts/6th_CISBGf/The_Atmosphere_and_Lightning/sbgf008.pdf. Accessed at: 22 Nov. 2024.

NASA, Nasa Earth Observatory. **Earth matters**. 2016. Available at: https://earthobservatory.nasa.gov/blogs/earthmatters/2016/04/. Accessed at: 17 Nov. 2024.

ESCOBEDO, João F. *et al.* Modeling hourly and daily fractions of UV, PAR and NIR to global solar radiation under various sky conditions at Botucatu, Brazil. **Applied energy**, vol. 86, no. 3, p. 299–309, 2009. Available at: http://dx.doi.org/10.1016/j.apenergy.2008.04.013.

ESCOBEDO, J. F. *et al.* Radiações solares UV, PAR e IV: I-estimativa em função da global. **Avances en Energías Renovables y Médio Ambiente**, vol. 10, p. 11-79-11–86, 2006. Available at: https://repositorio.usp.br/item/001619514.

RAMAN, S. *et al.* Effects of clouds and haze on UV-B radiation. **Journal of geophysical research**, vol. 101, no. D11, p. 16807–16816, 1996. Available at: http://dx.doi.org/10.1029/96jd01170.

EUMESAT. **Metop series**. 2020. Available at: https://www.eumetsat.int/our-satellites/metop-series. Accessed at: 15 Nov. 2024.

FAB. **Como decodificar o METAR e o SPECI? – Central de Ajuda DECEA. Força Aérea Brasileira**. 2020. Available at: https://ajuda.decea.mil.br/base-de-conhecimento/como-decodificar-o-metar-e-o-speci/. Accessed at: 15 Nov. 2024.

FARMAN, J. C.; GARDINER, B. G.; SHANKLIN, J. D. Large losses of total ozone in Antarctica reveal seasonal ClOx/NOx interaction. **Nature**, vol. 315, no. 6016, p. 207–210, 1985. Available at: http://dx.doi.org/10.1038/315207a0.

FIOLETOV, Vitali; KERR, James B.; FERGUSSON, Angus. The UV index: Definition, distribution and factors affecting it. **Canadian journal of public health. Revue canadienne de sante publique**, vol. 101, no. 4, p. I5–I9, 2010. Available at: http://dx.doi.org/10.1007/bf03405303.

FONTANA, Fabio *et al.* Intercomparison of satellite- and ground-based cloud fraction over Switzerland (2000–2012). **Atmospheric research**, vol. 128, p. 1–12, 2013. Available at: http://dx.doi.org/10.1016/j.atmosres.2013.01.013.

FOUNTOULAKIS, Ilias *et al.* Solar UV irradiance in a changing climate: Trends in Europe and the significance of spectral monitoring in Italy. **Environments**, vol. 7, no. 1, p. 1, 2019. Available at: http://dx.doi.org/10.3390/environments7010001.

FREDERICK, J. E. *et al.* Solar ultraviolet irradiance observed from southern Argentina: September 1990 to March 1991. **Journal of geophysical research**, vol. 98, no. D5, p. 8891–8897, 1993. Available at: http://dx.doi.org/10.1029/93jd00030.

GERARDO, Carbajal Beniez. **Buenos Aires Observatorio (Argentina). Global atmosphere watch station information system (GAWSIS)**. Available at: https://gawsis.meteoswiss.ch/GAWSIS/index.html#/search/station/stationReportDetails/0-20008-0-BSO. Accessed at: 15 Nov. 2024.

GHOLAMI, M.; YOUSEFI, L. **Solar ultraviolet-B radiation monitoring in Khorram Abad city in Iran**. 2009. Available at: https://ijrr.com/article-1-570-fa.html. Accessed at: 15 Nov. 2024.

GHOLAMNIA, Reza *et al.* Spatiotemporal analysis of solar ultraviolet radiation based on Ozone Monitoring Instrument dataset in Iran, 2005–2019. **Environmental pollution,** vol. 287, no. 117643, p. 117643, 2021. Available at: http://dx.doi.org/10.1016/j.envpol.2021.117643.

GHONEIM, Adel A.; KADAD, Ibrahim M.; ALTOUQ, Majida S. Statistical analysis of solar UVB and global radiation in Kuwait. **Energy**, vol. 60, p. 23–34, 2013. Available at: http://dx.doi.org/10.1016/j.energy.2013.07.027.

GONG, Wei *et al.* Measurement and estimation of ultraviolet radiation in Pearl River Delta, China. **Journal of atmospheric and solar-terrestrial physics**, vol. 123, p. 63–70, 2015. Available at: https://linkinghub.elsevier.com/retrieve/pii/S1364682614002922.

Glen, S. **Correlation Coefficient: Simple Definition, Formula, Easy Calculation Steps**. Available online: https://www.statisticshowto.com/probability-and-statistics/correlation-coefficient-formula Acessed 25 August 2023.

GONZÁLEZ-RODRÍGUEZ, Lisdelys *et al.* A study of UVER in Santiago, Chile based on long-term in situ measurements (five years) and empirical modelling. **Energies**, vol. 14, no. 2, p. 368, 2021. Available at: http://dx.doi.org/10.3390/en14020368.

GONZÁLEZ-RODRÍGUEZ, Lisdelys *et al.* Spatio-temporal estimations of ultraviolet erythemal radiation in Central Chile. **Air quality, atmosphere, & health**, vol. 15, no. 5, p. 837–852, 2022. Available at: http://dx.doi.org/10.1007/s11869-022-01195-y.

GREINERT, Rüdiger *et al.* European Code against Cancer 4th Edition: Ultraviolet radiation and cancer. **Cancer epidemiology**, vol. 39, p. S75–S83, 2015. Available at: https://linkinghub.elsevier.com/retrieve/pii/S1877782115000028.

GRIMM, A. M. **Meteorologia Básica**, 2006. Available at: http://fisica.ufpr.br/grimm/aposmeteo. Accessed at: 17 Nov. 2024.

GRÖBNER, J. *et al.* Variability of spectral solar ultraviolet irradiance in an Alpine environment. **Journal of geophysical research**, vol. 105, no. D22, p. 26991–27003, 2000. Available at: http://dx.doi.org/10.1029/2000jd900395.

GUPTA, Vishal; SHARMA, Vinod Kumar. Skin typing: Fitzpatrick grading and others. **Clinics in dermatology**, vol. 37, no. 5, p. 430–436, 2019. Available at: https://linkinghub.elsevier.com/retrieve/pii/S0738081X1930121X.

HERMAN, J. R. *et al.* Changes in cloud and aerosol cover (1980–2006) from reflectivity time series using SeaWiFS, N7-TOMS, EP-TOMS, SBUV-2, and OMI radiance data. **Journal of geophysical research**, vol. 114, no. D1, 2009. Available at: http://dx.doi.org/10.1029/2007jd009508.

HU, Li-Wen *et al.* Diurnal variations in solar ultraviolet radiation at typical anatomical sites. **Biomedical and environmental sciences,** vol. 23, no. 3, p. 234–243, 2010. Available at: http://dx.doi.org/10.1016/s0895-3988(10)60058-x.

HU, Bo; WANG, Yuesi; LIU, Guangren. Variation characteristics of ultraviolet radiation derived from measurement and reconstruction in Beijing, China. **Chemical and physical meteorology**, vol. 62, no. 2, p. 100, 2010. Available at: http://dx.doi.org/10.1111/j.1600-0889.2010.00452.x.

HU, Lw *et al.* Diurnal variations in solar ultraviolet radiation on horizontal and vertical plane. **Iranian journal of public health**, vol. 39, no. 3, p. 70–81, 2010. Available at: https://pubmed.ncbi.nlm.nih.gov/23113025/.

HUACA P, José M.; SALUM, Graciela M. Solar erythemal irradiance in Ibarra, Ecuador (high altitude equatorial city). Ground and satellite measurements and model calculations. **Bionatura**, vol. 3, no. 1, 2018. Available at: http://dx.doi.org/10.21931/rb/2018.03.01.3.

HUOVINEN, Pirjo; GÓMEZ, Iván; LOVENGREEN, Charlotte. A five-year study of solar ultraviolet radiation in southern Chile (39° S): Potential impact on physiology of coastal marine algae?. **Photochemistry and photobiology**, vol. 82, no. 2, p. 515–522, 2006. Available at: http://dx.doi.org/10.1562/2005-07-05-ra-601.

IALONGO, I. *et al.* Use of satellite erythemal UV products in analysing the global UV changes. **Atmospheric chemistry and physics**, vol. 11, no. 18, p. 9649–9658, 2011. Available at: http://dx.doi.org/10.5194/acp-11-9649-2011.

IALONGO, I.; CASALE, G. R.; SIANI, A. M. Comparison of total ozone and erythemal UV data from OMI with ground-based measurements at Rome station. **Atmospheric chemistry and physics**, vol. 8, no. 12, p. 3283–3289, 2008. Available at: http://dx.doi.org/10.5194/acp-8-3283-2008.

IBGE, Instituto Brasileiro de Geografia e. Estatística. **Estimativa Populacional 2021**. Available at: http://www.ibge.gov.br/. Accessed at: 17 Nov. 2024.

INCA, Instituto Nacional de Câncer José Alencar Gomes da Silva. Ministério da Saúde. **Estimativa 2020: Incidência de Câncer no Brasil**. 2019. Available at: https://www.inca.gov.br/sites/ufu.sti.inca.local/files/media/document/estimativa-2020-incidencia-de-cancer-no-brasil.pdf. Accessed at: 17 Nov. 2024.

INCA, Instituto Nacional de Câncer. Ministério da saúde. **Estimativa 2023: incidência de câncer no Brasil**. 2023. Available at: https://www.inca.gov.br/publicacoes/livros/estimativa-2023-incidencia-de-cancer-no-brasil. Accessed at: 17 Nov. 2024.

INMET, Instituto Nacional de Meteorologia. Normais Climatológicas do Brasil 1961–1990. Available at: https://portal.inmet.gov.br/normais. Accessed on 2 October 2023.

IPIÑA, Adriana *et al.* Ultraviolet radiation environment of a tropical megacity in transition: Mexico city 2000–2019. **Environmental science & technology**, vol. 55, no. 16, p. 10946–10956, 2021. Available at: http://dx.doi.org/10.1021/acs.est.0c08515.

JACOVIDES, C. *et al.* Solar global UV (280–380nm) radiation and its relationship with solar global radiation measured on the island of Cyprus. **Energy (Oxford, England)**, vol. 31, no. 14, p. 2728–2738, 2006. Available at: http://dx.doi.org/10.1016/j.energy.2005.11.021.

JANJAI, Serm *et al.* An investigation of solar erythemal ultraviolet radiation in the tropics: a case study at four stations in Thailand. **International journal of climatology: a journal of the Royal Meteorological Society**, vol. 30, no. 12, p. 1893–1903, 2010. Available at: http://dx.doi.org/10.1002/joc.2006.

JÉGOU, F. *et al.* Validity of satellite measurements used for the monitoring of UV radiation risk on health. **Atmospheric chemistry and physics**, vol. 11, no. 24, p. 13377–13394, 2011. Available at: http://dx.doi.org/10.5194/acp-11-13377-2011.

JOUBERT, Chandré *et al.* Field-grown grapevine berries use carotenoids and the associated xanthophyll cycles to acclimate to UV exposure differentially in high and low light (shade) conditions. **Frontiers in plant science**, vol. 7, 2016. Available at: http://dx.doi.org/10.3389/fpls.2016.00786.

Kalakoski, N. **OMI UVB Level 2G HDF-EOS5 Format Specification Document.** Available online:https://omi.fmi.fi/docs/OMUVB_L2_Format_Specification_Document_v2_6.pdf. 2012. Accessed on 2 September 2023.

KALLISKOTA, Sari *et al.* Comparison of daily UV doses estimated from Nimbus 7/TOMS measurements and ground-based spectroradiometric data. **Journal of geophysical research**, vol. 105, no. D4, p. 5059–5067, 2000. Available at: http://dx.doi.org/10.1029/1999jd900926.

KANCLER, Erik *et al.* Spectral observations and modeling of the Arctic surface radiation environment. **Journal of geophysical research**, vol. 110, no. D23, 2005. Available at: http://dx.doi.org/10.1029/2005jd005813.

KAZANTZIDIS, A. *et al.* Sensitivity of solar UV radiation to ozone and temperature profiles at Thessaloniki (40.5°N, 23°E), Greece. **Journal of atmospheric and solar-terrestrial physics**, vol. 67, no. 14, p. 1321–1330, 2005. Available at: http://dx.doi.org/10.1016/j.jastp.2005.05.003.

KERR, J. B. New methodology for deriving total ozone and other atmospheric variables from Brewer spectrophotometer direct sun spectra. **Journal of geophysical research**, vol. 107, no. D23, p. 22–17, 2002. Available at: http://dx.doi.org/10.1029/2001jd001227.

KERR, J. B.; FIOLETOV, V. E. Surface ultraviolet radiation. **Atmosphere-Ocean**, vol. 46, no. 1, p. 159–184, 2008. Available at: http://dx.doi.org/10.3137/ao.460108.

KHALIL, Samy A.; SHAFFIE, A. M. Prediction of clear-sky biologically effective erythematic radiation (EER) From global solar radiation (250–2800 nm) at Cairo, Egypt. **Advances in space research,** vol. 51, no. 9, p. 1727–1733, 2013. Available at: https://linkinghub.elsevier.com/retrieve/pii/S0273117712007405.

KIM, Jhoon *et al.* Effects of ozone and aerosol on surface UV radiation variability. **Journal of photochemistry and photobiology.** vol. 119, p. 46–51, 2013. Available at: http://dx.doi.org/10.1016/j.jphotobiol.2012.11.007.

KIM, Jin Cheol *et al*. Skin-aging pigmentation: Who is the real enemy?. **Cells**, vol. 11, no. 16, p. 2541, 2022. Available at: https://www.mdpi.com/2073-4409/11/16/2541. Accessed at: 17 Nov. 2024.

KINNE, Stefan *et al.* MAC-v1: A new global aerosol climatology for climate studies. **Journal of advances in modeling earth systems**, vol. 5, no. 4, p. 704–740, 2013. Available at: http://dx.doi.org/10.1002/jame.20035.

KIRCHHOFF, V. W. J. H. *et al.* A variação sazonal da radiação ultravioleta solar biologicamente ativa. **Revista Brasileira de Geofísica**, vol. 18, no. 1, p. 63–74, 2000. Available at: http://dx.doi.org/10.1590/s0102-261x2000000100006.

KIRCHHOFF, V. W. J. H. et al. The Brazilian network of stratospheric ozone monitors: Observations of the 1992 ozone hole. **Brazilian Journal of Geophysics**, vol. 11, no. 2, p. 205–213, 1993. Available at: https://sbgf.org.br/revista/index.php/rbgf/article/view/1147/1436. Accessed at: 22 Nov. 2024.

KLEIPOOL, Q. L. *et al.* Earth surface reflectance climatology from 3 years of OMI data. **Journal of geophysical research**, vol. 113, no. D18, 2008. Available at: http://dx.doi.org/10.1029/2008jd010290.

KOSMOPOULOS, Panagiotis G. *et al.* Real-time UV index retrieval in Europe using Earth observation-based techniques: system description and quality assessment. **Atmospheric measurement techniques**, vol. 14, no. 8, p. 5657–5699, 2021. Available at: http://dx.doi.org/10.5194/amt-14-5657-2021.

KROTKOV, N. A. *et al.* Satellite estimation of spectral surface UV irradiance: 2. Effects of homogeneous clouds and snow. **Journal of geophysical research**, vol. 106, no. D11, p. 11743–11759, 2001. Available at: http://dx.doi.org/10.1029/2000jd900721.

KROTKOV, N. A. *et al.* Satellite estimation of spectral surface UV irradiance in the presence of tropospheric aerosols: 1. Cloud-free case. **Journal of geophysical research**, vol. 103, no. D8, p. 8779–8793, 1998. Available at: http://dx.doi.org/10.1029/98jd00233.

KRZYŚCIN, Janusz W. *et al.* Improvement of the 24 hr forecast of surface UV radiation using an ensemble approach. **Meteorological applications**, vol. 27, no. 1, 2020. Available at: http://dx.doi.org/10.1002/met.1865.

KRZYŚCIN, Janusz W.; JAROSŁAWSKI, Janusz; SOBOLEWSKI, Piotr S. Effects of clouds on the surface erythemal UV-B irradiance at northern midlatitudes: estimation from the observations taken at Belsk, Poland (1999–2001). **Journal of atmospheric and solar-terrestrial physics**, vol. 65, no. 4, p. 457–467, 2003. Available at: http://dx.doi.org/10.1016/s1364-6826(03)00004-x.

KUINCHTNER, Angélica; BURIOL, Galileo Adeli. Título da revista. **Disciplinarum Scientia | Naturais e Tecnológicas**, vol. 2, no. 1, p. 171–182, 2001. Available at: https://periodicos.ufn.edu.br/index.php/disciplinarumNT/article/view/1136. Accessed at: 15 Nov. 2024.

KUJANPÄÄ, J.; KALAKOSKI, N. Operational surface UV radiation product from GOME-2 and AVHRR/3 data. **Atmospheric measurement techniques**, vol. 8, no. 10, p. 4399–4414, 2015. Available at: http://dx.doi.org/10.5194/amt-8-4399-2015.

KYLLING, A. *et al.*The effect of clouds and surface albedo on UV irradiances at a high latitude site. **Geophysical research letters**, vol. 27, no. 9, p. 1411–1414, 2000. Available at: http://dx.doi.org/10.1029/1999gl011015.

LABOW, Gordon J. *et al.* Diurnal variation of 340 nm Lambertian equivalent reflectivity due to clouds and aerosols over land and oceans. **Journal of geophysical research**, vol. 116, no. D11, 2011. Available at: http://dx.doi.org/10.1029/2010jd014980.

LAKKALA, Kaisa *et al.* Validation of the TROPOspheric Monitoring Instrument (TROPOMI) surface UV radiation product. **Atmospheric measurement techniques**, vol. 13, no. 12, p. 6999–7024, 2020. Available at: http://dx.doi.org/10.5194/amt-13-6999-2020.

LAMY, Kévin. **Projection Climatique du Rayonnement Ultraviolet au cours du 21ème siècle : impact de différents scénarios climatiques**. 2018. UR, Saint Denis, 2018. Available at: https://theses.hal.science/tel-01979875v1/document. Accessed at: 17 Nov. 2024.

LAMY, Kevin *et al.* UV-Indien network: ground-based measurements dedicated to the monitoring of UV radiation over the western Indian Ocean. **Earth system science data**, vol. 13, no. 9, p. 4275–4301, 2021. Available at: http://dx.doi.org/10.5194/essd-13-4275-2021.

LANGEMATZ, Ulrike. Stratospheric ozone: down and up through the anthropocene. **ChemTexts**, vol. 5, no. 2, 2019. Available at: http://dx.doi.org/10.1007/s40828-019-0082-7.

LEAL, S. S.; TÍBA, C.; PIACENTINI, R. Daily UV radiation modeling with the usage of statistical correlations and artificial neural networks. **Renewable energy**, vol. 36, no. 12, p. 3337–3344, 2011. Available at: http://dx.doi.org/10.1016/j.renene.2011.05.007.

LEE, Hyun-Ji; KIM, Miri. Skin barrier function and the microbiome. **International journal of molecular sciences**, vol. 23, no. 21, p. 13071, 2022. Available at: https://www.mdpi.com/1422-0067/23/21/13071. Accessed at: 17 Nov. 2024.

LEITER, Ulrike et al. Epidemiology of skin cancer: Update 2019. **Advances in Experimental Medicine and Biology**. Cham: Springer International Publishing, 2020. p. 123–139. Available at: https://link.springer.com/chapter/10.1007/978-3-030-46227-7_6. Accessed at: 17 Nov. 2024.

LESZCZYNSKI, Kirsti. **Assessment and comparison of methods for solar ultraviolet radiation measurements**. 1995. Available at: https://inis.iaea.org/collection/NCLCollectionStore/_Public/28/028/28028576.pdf. Accessed at: 17 Nov. 2024.

LEVELT, P. F. *et al.* The ozone monitoring instrument. **IEEE transactions on geoscience and remote sensing,** vol. 44, no. 5, p. 1093–1101, 2006. Available at: http://dx.doi.org/10.1109/tgrs.2006.872333.

LEVELT, Pieternel F. *et al.* The Ozone Monitoring Instrument: overview of 14 years in space. **Atmospheric chemistry and physics**, vol. 18, no. 8, p. 5699–5745, 2018. Available at: http://dx.doi.org/10.5194/acp-18-5699-2018.

LILLO-BRAVO, I. *et al.* Random Forest model to predict solar water heating system performance. **Renewable energy**, vol. 216, no. 119086, p. 119086, 2023. Available at: http://dx.doi.org/10.1016/j.renene.2023.119086.

LINDFORS, Anders V. *et al.* The TROPOMI surface UV algorithm. **Atmospheric measurement techniques**, vol. 11, no. 2, p. 997–1008, 2018. Available at: http://dx.doi.org/10.5194/amt-11-997-2018.

LINDQVIST, P. G. et al. Low sun exposure habits is associated with a dose-dependent increased risk of hypertension: a report from the large MISS cohort. **Photochemical & photobiological sciences,** vol. 20, no. 2, p. 285–292, 2021. Available at: http://dx.doi.org/10.1007/s43630-021-00017-x.

LIOU, K. N. **An introduction to atmospheric radiation**. San Diego, CA: Academic Press, 2002. Available at: Accessed at: 17 Nov. 2024.

LIU, Song *et al.* Nitrogen dioxide decline and rebound observed by GOME-2 and TROPOMI during COVID-19 pandemic. **Air quality, atmosphere, & health**, vol. 14, no. 11, p. 1737–1755, 2021. Available at: http://dx.doi.org/10.1007/s11869-021-01046-2.

LIU, Chenbin *et al.* Particle pollution estimation based on image analysis. **PloS one**, vol. 11, no. 2, p. e0145955, 2016. Available at: http://dx.doi.org/10.1371/journal.pone.0145955.

LONGHI, Solon Jonas *et al.* Aspectos fitossociológicos de fragmento de Floresta Estacional Decidual, Santa Maria, RS. **Ciencia Florestal**, vol. 10, no. 2, p. 59–74, 2000. Available at: http://dx.doi.org/10.5902/19805098471.

LOPES, Bibiana Culau. **Analysis of the UVB radiation during the events of influence of the Antarctic Ozone Hole over South of Brazil**. UFSM, Santa Maria, 2022. Available at: https://hal-meteofrance.archives-ouvertes.fr/tel-03771818/. Accessed at: 15 Nov. 2024.

LOPEZ, A. *et al.* Estimating the climate significance of halogen-driven ozone loss in the tropical marine troposphere. **Atmospheric chemistry and physics**, vol. 12, no. 9, p. 3939–3949, 2012. Available at: http://dx.doi.org/10.5194/acp-12-3939-2012.

LOPO, Alexandre Boleira et al. Radiação ultravioleta, ozônio total e aerossóis na cidade de Natal- RN. **HOLOS**, vol. 6, p. 3–21, 2013. Available at: http://dx.doi.org/10.15628/holos.2013.1839.80. Accessed at: 17 Nov. 2024.

LOPO, Alexandre Boleira et al. UV Index Modeling by Autoregressive Distributed Lag (ADL Model). **HOLOS**, vol. 4, p. 323–333, 2014. Available at: http://dx.doi.org/10.4236/acs.2014.42033. Accessed at: 17 Nov. 2024.

LOVENGREEN, Charlotte; FUENZALIDA, Humberto; VILLANUEVA, Lilian. Ultraviolet solar radiation at Valdivia, Chile (39.8°S). **Atmospheric environment**, vol. 34, no. 24, p. 4051–4061, 2000. Available at: http://dx.doi.org/10.1016/s1352-2310(00)00227-2.

LUCAS, R. M. *et al.* Human health in relation to exposure to solar ultraviolet radiation under changing stratospheric ozone and climate. **Photochemical & photobiological sciences**, vol. 18, no. 3, p. 641–680, 2019. Available at: http://dx.doi.org/10.1039/c8pp90060d.

LUCAS, Robyn M. *et al.* Ultraviolet radiation, vitamin D and multiple sclerosis. **Neurodegenerative disease management**, vol. 5, no. 5, p. 413–424, 2015. Available at: http://dx.doi.org/10.2217/nmt.15.33.

LUCCINI, Eduardo *et al.* Ultraviolet climatology over Argentina. **Journal of geophysical research**, vol. 111, no. D17, 2006. Available at: http://dx.doi.org/10.1029/2005jd006580.

MARINHO, George Santos; DA SILVA, Francisco Raimundo. Aspectos da radiação ultravioleta solar em Natal/Brasil. **Society and Territory**, vol. 25, no. 2, p. 29–41, 2013. Available at: https://periodicos.ufrn.br/sociedadeeterritorio/article/download/3522/2898/0. Accessed at: 17 Nov. 2024.

MAZZI, Alberto. **Modeling and production of metal nanoparticles through laser ablation and applications to photocatalytic water oxidation**. 2017. 132 f. University of Trento, 2017. Available at: Accessed at: 17 Nov. 2024.

MCKINLAY, A. F.; DIFFEY, B. L. **The CIE (1987) reference action spectrum for erythema in human skin**. 1987. Available at:

https://ec.europa.eu/health/scientific_committees/opinions_layman/en/sunbeds/figtableboxes/figure-2.htm. Accessed at: 17 Nov. 2024.

MICHELETTI, M. I. *et al.* The incidence of erythemal and UV solar irradiance over Buenos Aires, Argentina. **Journal of Optics A Pure and Applied Optics**, vol. 5, no. 5, p. S262–S268, 2003. Available at: http://dx.doi.org/10.1088/1464-4258/5/5/376.

MIKHALEV, A. V. *et al.* Variations of the ground-level ultraviolet radiation in East Siberia. **Advances in space research** vol. 27, no. 6–7, p. 1109–1114, 2001. Available at: http://dx.doi.org/10.1016/s0273-1177(01)00181-8.

MOHAMED, Marwa S. *et al.* Validation of UV-Index retrieved from three satellites against Ground-Based measurements at different climates in Egypt. **Egyptian journal of remote sensing and space sciences**, vol. 26, no. 2, p. 361–367, 2023. Available at: http://dx.doi.org/10.1016/j.ejrs.2023.04.006.

MOREIRA, Demerval S. *et al.* Modeling the radiative effects of biomass burning aerosols on carbon fluxes in the Amazon region. **Atmospheric chemistry and physics**, vol. 17, no. 23, p. 14785–14810, 2017. Available at: http://dx.doi.org/10.5194/acp-17-14785-2017.

MORENO, I. *et al.* Ground based ultraviolet (290–385 nm) and broadband solar radiation measurements in south-eastern Spain. **International journal of climatology**, vol. 18, no. 12, p. 1389–1400, 1998. Available at: http://dx.doi.org/10.1002/(sici)1097-0088(1998100)18:12<1389::aid-joc318>3.0.co;2-n.

MUNRO, Rosemary *et al.* The GOME-2 instrument on the Metop series of satellites: instrument design, calibration, and level 1 data processing – an overview. **Atmospheric measurement techniques**, vol. 9, no. 3, p. 1279–1301, 2016. Available at: http://dx.doi.org/10.5194/amt-9-1279-2016.

NEALE, R. E. *et al.* Environmental effects of stratospheric ozone depletion, UV radiation, and interactions with climate change: UNEP Environmental Effects Assessment Panel, Update 2020. **Photochemical & photobiological sciences**, vol. 20, no. 1, p. 1–67, 2021. Available at: http://dx.doi.org/10.1007/s43630-020-00001-x.

NOZAWA, Hiromasa *et al.* Ground-based observation of solar UV radiation in Japan, Brazil and Chile. **Revista Brasileira de Geofísica**, vol. 25, 2007. Available at: http://dx.doi.org/10.1590/s0102-261x2007000600003.

OLIVEIRA, Marcos José de *et al.* Ciclos climáticos e causas naturais das mudanças do clima. **Terrae didatica**, vol. 13, no. 3, p. 149, 2018. Available at: http://dx.doi.org/10.20396/td.v13i3.8650958.

PALANCAR, Gustavo G.; TOSELLI, Beatriz M. Effects of meteorology on the annual and interannual cycle of the UV-B and total radiation in Córdoba City, Argentina. **Atmospheric environment,** vol. 38, no. 7, p. 1073–1082, 2004. Available at: http://dx.doi.org/10.1016/j.atmosenv.2003.10.057.

PARISI, Alfio *et al.* Satellite monitoring of environmental solar ultraviolet A (UVA) exposure and irradiance: A review of OMI and GOME-2. **Remote sensing**, vol. 13, no. 4, p. 752, 2021. Available at: http://dx.doi.org/10.3390/rs13040752.

PARRA, René; CADENA, Eliana; FLORES, Camila. Maximum UV index records (2010–2014) in Quito (Ecuador) and its trend inferred from remote sensing data (1979–2018). **Atmosphere**, vol. 10, no. 12, p. 787, 2019. Available at: http://dx.doi.org/10.3390/atmos10120787.

PERES, L. V. **Monitoramento da coluna total de ozônio e a ocorrência de eventos de influência do buraco de ozônio antártico sobre o sul do Brasil**. 2016. - UFSM, Santa Maria, 2016. Available at: https://repositorio.ufsm.br/handle/1/12621. Accessed at: 18 Nov. 2024.

PEREYRA, Fernando X.; RIMOLDI, Horacio. Geological and environmental aspects of the development of megacities: the case of Buenos Aires metropolitan area (AMBA), Argentina. **Bulletin of engineering geology and the environment**, vol. 62, no. 4, p. 341–351, 2003. Available at: http://dx.doi.org/10.1007/s10064-003-0199-0.

PFISTER, G. *et al.* Cloud coverage based on all-sky imaging and its impact on surface solar irradiance. **Journal of applied meteorology**, vol. 42, no. 10, p. 1421–1434, 2003. Available at: http://dx.doi.org/10.1175/1520-0450(2003)042<1421:ccboai>2.0.co;2.

PINEDO V., J. L. *et al.* Spectral signature of ultraviolet solar irradiance in Zacatecas. **Geofisica Internacional**, vol. 45, no. 4, p. 263–269, 2006. Available at: http://dx.doi.org/10.22201/igeof.00167169p.2006.45.4.163.

PITKÄNEN, M. R. A. *et al.* **Comparing OMI UV index to ground-based measurements at two Finnish sites with focus on cloud-free and overcast conditions**. 2015. Available at: http://dx.doi.org/10.5194/amtd-8-487-2015.

PODSTAWCZYŃSKA, Agnieszka. UV and global solar radiation in Łódź, Central Poland. **International journal of climatology: a journal of the Royal Meteorological Society**, vol. 30, no. 1, p. 1–10, 2010. Available at: http://dx.doi.org/10.1002/joc.1864.

PORFÍRIO, Anthony Carlos Silva *et al.* An assessment of the global UV solar radiation under various sky conditions in Maceió-Northeastern Brazil. **Energy (Oxford, England)**, vol. 44, no. 1, p. 584–592, 2012. Available at: http://dx.doi.org/10.1016/j.energy.2012.05.042.

RAIMONDI, S. et al. Melanoma epidemiology and sun exposure. **Acta dermato-venereologica**, vol. 100, no. 11, p. adv00136, 2020. Available at: http://dx.doi.org/10.2340/00015555-3491.

RAMANATHAN, V. *et al.* Aerosols, climate, and the hydrological cycle. **Science,** vol. 294, no. 5549, p. 2119–2124, 2001. Available at: http://dx.doi.org/10.1126/science.1064034.

REBOITA, Michelle Simões *et al.* Aspectos climáticos do estado de Minas Gerais. **Revista Brasileira de Climatologia**, vol. 17, 2015. Available at: http://dx.doi.org/10.5380/abclima.v17i0.41493.

REBOITA, Michelle Simões *et al.* Caracterização atmosférica quando da ocorrência de eventos extremos de chuva na região sul de Minas Gerais. **Revista Brasileira de Climatologia**, vol. 21, 2017. Available at: http://dx.doi.org/10.5380/abclima.v21i0.47577.

REICHRATH, Jörg et al. Challenge and perspective: the relevance of ultraviolet (UV) radiation and the vitamin D endocrine system (VDES) for psoriasis and other inflammatory skin diseases. **Photochemical & photobiological sciences**, vol. 16, no. 3, p. 433–444, 2017. Available at: http://dx.doi.org/10.1039/c6pp00280c.

REIS, Gabriela *et al.* Solar ultraviolet radiation temporal variability analysis from 2-year of continuous observation in an amazonian city of Brazil. **Atmosphere**, vol. 13, no. 7, p. 1054, 2022. Available at: https://www.mdpi.com/2073-4433/13/7/1054. Accessed at: 17 Nov. 2024.

REN, Pu Bu Ci; SIGERNES, Fred; GJESSING, Yngvar. Ground-based measurements of solar ultraviolet radiation in Tibet: Preliminary results. **Geophysical research letters**, vol. 24, no. 11, p. 1359–1362, 1997. Available at: http://dx.doi.org/10.1029/97gl01319.

RYDZ, Ela *et al.* Solar ultraviolet radiation exposure among outdoor workers in Alberta, Canada. **Environmental research**, vol. 189, no. 109902, p. 109902, 2020. Available at: https://linkinghub.elsevier.com/retrieve/pii/S0013935120307970.

RODRÍGUEZ-LÓPEZ, Lien *et al.* Influence of (extreme) radiation and optical characteristics in physical and biological features of a regulated lake. **E3S web of conferences**, vol. 127, p. 02012, 2019. Available at: http://dx.doi.org/10.1051/e3sconf/201912702012.

SANTOS, Julia Bilbao; VILLÁN, David Mateos; CASTRILLO, Argimiro de Miguel. Analysis and cloudiness influence on UV total irradiation. **International journal of climatology: a journal of the Royal Meteorological Society**, vol. 31, no. 3, p. 451–460, 2011. Available at: http://dx.doi.org/10.1002/joc.2072.

SATHISHKUMAR, V. E.; RAMU, A. G.; CHO, Jaehyuk. Machine learning algorithms to predict the catalytic reduction performance of eco-toxic nitrophenols and azo dyes contaminants (Invited Article). **Alexandria Engineering Journal**, vol. 72, p. 673–693, 2023. Available at: http://dx.doi.org/10.1016/j.aej.2023.04.007.

SCHALKA, Sérgio *et al.* Brazilian Consensus on Photoprotection. **Anais brasileiros de dermatologia**, vol. 89, no. 6 suppl 1, p. 1–74, 2014. Available at: http://www.scielo.br/scielo.php?script=sci_arttext&pid=S036505962014000700001&lng=en&tlng=en. Accessed at: 17 Nov. 2024.

SCHMALWIESER, A. W.; SCHAUBERGER, G. A monitoring network for erythemally-effective solar ultraviolet radiation in Austria: determination of the measuring sites and visualisation of the spatial distribution. **Theoretical and applied climatology**, vol. 69, no. 3–4, p. 221–229, 2001. Available at: http://dx.doi.org/10.1007/s007040170027.

SCHOEBERL, M. R. *et al.* Overview of the EOS aura mission. **IEEE transactions on geoscience and remote sensing: a publication of the IEEE Geoscience and Remote Sensing Society**, vol. 44, no. 5, p. 1066–1074, 2006. Available at: https://ieeexplore.ieee.org/document/1624588.

SCHUCH, André *et al.* Identification of influential events concerning the Antarctic ozone hole over southern Brazil and the biological effects induced by UVB and UVA radiation in an

endemic treefrog species. **Ecotoxicology and environmental safety**, vol. 118, p. 190–198, 2015. Available at: http://dx.doi.org/10.1016/j.ecoenv.2015.04.029.

SCI-TEC INSTRUMENTS. Brewer mkiv spectrophotometer operator's manual. 1999. Available at: https://gml.noaa.gov/grad/neubrew/docs/manuals/Brewer_Operator_wTOC.pdf.

SECKMEYER, G. *et al.* **Broadband Instruments Measuring Erythemally Weighted Solar Irradiance. World Meteorological Report**. 2005. Available at: https://www.researchgate.net/publication/227860367_Instruments_to_Measure_Solar_Ultraviolet_Irradiance_Part_2_Broadband_Instruments_Measuring_Erythemally_Weighted_Solar_Irradiance. Accessed at: 17 Nov. 2024.

SILVA, Abel A. Medidas de radiação solar ultravioleta em Belo Horizonte e saúde pública. **Revista Brasileira de Geofísica**, vol. 26, no. 4, p. 417–425, 2008. Available at: http://dx.doi.org/10.1590/s0102-261x2008000400003.

SILVA, Luiz Felipe *et al.* Exposição do trabalhador rural à radiação ultravioleta: estudo no sul de Minas Gerais. **Revista Brasileira de Climatologia**, vol. 18, 2016. Available at: http://dx.doi.org/10.5380/abclima.v18i0.43651.

SILVA, Francisco Raimundo; DE OLIVEIRA, Hugo Sérgio Medeiros; MARINHO., And George Santos. Variação do índice de radiação solar ultravioleta em Natal-RN entre 2001 e 2007. **Congresso Brasileiro de Energia Solar-CBENS**. 2008. Available at: https://anaiscbens.emnuvens.com.br/cbens/article/view/1336. Accessed at: 17 Nov. 2024.

SILVA, Abel Antônio; SOUZA ECHER, Mariza Pereira. Ground-based measurements of local cloud cover. **Meteorology and atmospheric physics**, vol. 120, no. 3–4, p. 201–212, 2013. Available at: http://dx.doi.org/10.1007/s00703-013-0245-9.

SILVA, Abel Antônio; SOUZA-ECHER, Mariza Pereira. Ground-based observations of clouds through both an automatic imager and human observation. **Meteorological applications**, vol. 23, no. 1, p. 150–157, 2016. Available at: http://dx.doi.org/10.1002/met.1542.

SMITH, R. C. *et al.* Ozone depletion: Ultraviolet radiation and phytoplankton biology in Antarctic waters. **Science,** vol. 255, no. 5047, p. 952–959, 1992. Available at: http://dx.doi.org/10.1126/science.1546292.

SOFIU, V. *et al.* **Solar and Terrestrial Radiation with Measuring Instruments Overview**. 2011. Available at: https://www.researchgate.net/profile/VeisSerifi/publication/338633530_SOLAR_AND_TERRESTRIAL_RADIATION_WITH_MEASURING_INSTRUMENTS_OVERVIEW/links/5e20ac72299bf1e1fab7f294/SOLAR-AND-TERRESTRIAL-RADIATION-WITH-MEASURING-INSTRUMENTS-OVERVIEW.pdf. Accessed at: 17 Nov. 2024.

SOLANO, Francisco. Photoprotection and skin pigmentation: Melanin-related molecules and some other new agents obtained from natural sources. **Molecules**, vol. 25, no. 7, p. 1537, 2020. Available at: https://www.mdpi.com/1420-3049/25/7/1537. Accessed at: 17 Nov. 2024.

SOLAR LIGHT. **UV-Biometer 501 User's Manual**. Available at: https://solarlight.com/wpcontent/uploads/Meters_Model-501-UVBiometer-1-1.pdf. Accessed at: 15 Nov. 2024.

SRIVASTAVA, Manoj K. *et al.* Direct solar ultraviolet irradiance over Nainital, India, in the central Himalayas for clear-sky day conditions during December 2004. **Journal of geophysical research**, vol. 111, no. D8, 2006. Available at: http://dx.doi.org/10.1029/2005jd006141.

SUÁREZ, Luis Salas F. *et al.* Ultraviolet solar radiation in the tropical central Andes (12.0°S). **Photochemical & photobiological sciences**, vol. 16, no. 6, p. 954–971, 2017. Available at: http://dx.doi.org/10.1039/c6pp00161k.

STAMMES, p.; NOORDHOEK, R. OMI Algorithm Theoretical Basis Document Volume III Clouds, Aerosols, and Surface UV Irradiance. Available at: https://eospso.gsfc.nasa.gov/sites/default/files/atbd/ATBD-OMI-03.pdf.

SULZBERGER, B. *et al.* Solar UV radiation in a changing world: roles of cryosphere—land—water—atmosphere interfaces in global biogeochemical cycles. **Photochemical & photobiological sciences**, vol. 18, no. 3, p. 747–774, 2019. Available at: http://dx.doi.org/10.1039/c8pp90063a.

TAIPE, C. W.; MENDOZA, E. G.; FLORES, H. H. Validation of ultraviolet index data from the Ozone Monitoring Instrument (OMI) based on measurements from meteorological stations in the city of Puno. **Journal of physics. Conference series**, vol. 1841, no. 1, p. 012005, 2021. Available at: http://dx.doi.org/10.1088/1742-6596/1841/1/012005.

TANG, Xiaoyou *et al.* Current insights and future perspectives of ultraviolet radiation (UV) exposure: Friends and foes to the skin and beyond the skin. **Environment international**, vol. 185, no. 108535, p. 108535, 2024. Available at: https://linkinghub.elsevier.com/retrieve/pii/S0160412024001211.

TANSKANEN, Aapo *et al.* Validation of daily erythemal doses from Ozone Monitoring Instrument with ground-based UV measurement data. **Journal of geophysical research**, vol. 112, no. D24, 2007. Available at: http://dx.doi.org/10.1029/2007jd008830.

TERAMOTO, É. T.; ESCOBEDO, J. F.; MARTINS, D. Modelos estatísticos para estimativa da irradiação solar UV horária em Botucatu/SP/Brasil. **Brazilian Journal of Solar Energy**, vol. 5, p. 44–51, 2014. Available at: https://rbens.emnuvens.com.br/rbens/article/view/107. Accessed at: 17 Nov. 2024.

TERTSEA, Igbawua. Average solar UV radiation dosimetry in central Nigeria. **International journal of environmental monitoring and analysis**, [*s. l.*], vol. 1, no. 6, p. 323, 2013. Available at: http://dx.doi.org/10.11648/j.ijema.20130106.18.

THOMAS, Nicholas C. The early history of spectroscopy. **Journal of chemical education**, vol. 68, no. 8, p. 631, 1991. Available at: http://dx.doi.org/10.1021/ed068p631.

TIBA, Chigueru; LEAL, Sérgio. Modelagem do IUV a partir da irradiação UV (A+ B) em Recife (PE). **Brazilian Journal of Solar Energy**, vol. 3, no. 1, 2012. Available at: https://rbens.emnuvens.com.br/rbens/article/view/72. Accessed at: 17 Nov. 2024.

TOMASI, C.; LUPI, A. **Primary and Secondary Sources of Atmospheric AerosolAtmospheric Aerosols: Life Cycles and Effects on Air Quality and Climate**. 2017. Available at: https://application.wiley-vch.de/books/sample/3527336451_c01.pdf. Accessed at: 17 Nov. 2024.

TURNBULL, David J.; PARISI, Alfio V.; SCHOUTEN, Peter W. Empirical evaluation of global vitamin D effective ultraviolet irradiances under cloudy conditions for a subtropical southern hemisphere site. **Radiation research**, vol. 173, no. 5, p. 703–708, 2010. Available at: http://dx.doi.org/10.1667/rr1936.1.

UCAR CENTER FOR SCIENCE EDUCATION. **Cloud types**. Available at: https://scied.ucar.edu/learning-zone/clouds/cloud-types. Accessed at: 17 Nov. 2024.

ULTRAVIOLET RADIATION. 2024. Available at: https://www.ccohs.ca/oshanswers/phys_agents/ultravioletradiation.html. Accessed at: 17 Nov. 2024.

UNEP, UNITED NATIONS ENVIRONMENT PROGRAMME. **Environmental Effects and Interactions of Stratospheric Ozone Depletion, UV Radiation, and Climate Change Assessment Report 2018**. UNEP Ozone Secretariat 2018. Available at: https://ozone.unep.org/science/assessment/br. Accessed at: 17 Nov. 2024.

UNEP, UNITED NATIONS ENVIRONMENT PROGRAMME. **Environmental Effects of Stratospheric Ozone Depletion, UV Radiation, and Interactions with Climate Change: 2022 Assessment Report**. UNEP Ozone Secretariat: Nairobi, Kenya, 2023. Available online: https://ozone.unep.org/system/files/documents/EEAP-2022-Assessment-Report-May2023.pdf. Accessed at 27 October 2023.

U.S. Environmental Protection Agency (EPA). **UV Index Scale.** 2016. https://19january2017snapshot.epa.gov/sunsafety/uv-index-scale-1_.html. Accessed at: 27 October 2023.

UTRILLAS, M. P. *et al.* Relationship between erythemal UV and broadband solar irradiation at high altitude in Northwestern Argentina. **Energy,** vol. 162, p. 136–147, 2018. Available at: http://dx.doi.org/10.1016/j.energy.2018.08.021.

VERTMARKETS. **Model 501-UV Bimeter**. Available at: https://www.wateronline.com/doc/501-uv-biometer-0001. Accessed at: 15 Nov. 2024.

VILLAFANE, V. E. Annual patterns of ultraviolet radiation effects on temperate marine phytoplankton off Patagonia, Argentina. **Journal of plankton research**, vol. 26, no. 2, p. 167–174, 2004. Available at: http://dx.doi.org/10.1093/plankt/fbh011.

WALD, L. **Basics in Solar Radiation at Earth Surface**. 2018. UR, Saint Denis, 2018. Available at: https://minesparis-psl.hal.science/hal-01676634. Accessed at: 17 Nov. 2024.

WANG, Shangshang *et al.* Detection of skin thickness and density in healthy Chinese people by using high-frequency ultrasound. **Skin research and technology**, vol. 29, no. 1, 2023. Available at: http://dx.doi.org/10.1111/srt.13219.

WEBB, Ann R. Spectral Measurements of Solar Ultraviolet-B Radiation in Southeast England. **Journal of Applied Meteorolgy**, vol. 31, p. 212–216, 1991. Available at: https://www.jstor.org/stable/26186436. Accessed at: 18 Nov. 2024.

WEBB, A.; STEVEN, M. D. Measurement of solar UVB radiation in the English Midlands. **Archives for Meteorology, Geophysics, and Bioclimatology Series B**, vol. 35, no. 3, p. 221–231, 1984. Available at: http://dx.doi.org/10.1007/bf02263347.

WHO, World Health Organization. **Global solar UV index - a practical guide**. 2002. Available at: https://www.who.int/publications/i/item/9241590076. Accessed at: 17 Nov. 2024.

WHO, World Health Organization. **Solar ultraviolet radiation: Global burden of disease from solar ultraviolet radiation**. 2006. Available at: https://www.who.int/publications/i/item/9241594403. Accessed at: 17 Nov. 2024.

XIA, X. *et al.* Analysis of relationships between ultraviolet radiation (295–385 nm) and aerosols as well as shortwave radiation in North China Plain. **Annales geophysicae**, vol. 26, no. 7, p. 2043–2052, 2008. Available at: http://dx.doi.org/10.5194/angeo-26-2043-2008.

YAMAMOTO, Ana Letícia Campos; CORRÊA, Marcelo de Paula; CCOYLLO, Odón Roman Sánchez. Avaliação e Análise da Série Temporal de Radiação UV Coletadas em Diferentes Cidades Peruanas. **Revista Brasileira de Meteorologia**, vol. 33, no. 2, p. 298–305, 2018. Available at: http://dx.doi.org/10.1590/0102-7786332011.

YAMASOE, M. A. **Apostila da Disciplina Meteorologia Física II – ACA 0326**. 2006. Available at: https://edisciplinas.usp.br/pluginfile.php/7536076/mod_resource/content/1/apostila.pdf. Accessed at: 17 Nov. 2024.

YAMASOE, M. A.; DE PAULA CORRÊA, M. **Radiative Processes in the Atmosphere**. 2016. Available at: http://ofitexto.arquivos.s3.amazonaws.com/Processos-radiativos-na-atmosfera_DEG.pdf. Accessed at: 17 Nov. 2024.

YOON, Yuhchae; ANGEL, Jeremy D.; HANSEN, Douglas C. Atmospheric corrosion of silver in outdoor environments and modified accelerated corrosion chambers. **Corrosion**, vol. 72, no. 11, p. 1424–1432, 2016. Available at: http://dx.doi.org/10.5006/2079.

ZARATTI, Francesco Sacchetti et al. **La radiación ultravioleta en Bolivia**. PAHO/WHO, 2003. Available at: Accessed at: 17 Nov. 2024.

ZEMPILA, Melina-Maria *et al.* OMI/Aura UV product validation using NILU-UV ground-based measurements in Thessaloniki, Greece. **Atmospheric environment**, vol. 140, p. 283–297, 2016. Available at: http://dx.doi.org/10.1016/j.atmosenv.2016.06.009.

ZHANG, Huanxin *et al.* Surface erythemal UV irradiance in the continental United States derived from ground-based and OMI observations: quality assessment, trend analysis and sampling issues. **Atmospheric chemistry and physics**, vol. 19, no. 4, p. 2165–2181, 2019. Available at: http://dx.doi.org/10.5194/acp-19-2165-2019.

APPENDIX

Appendix A — Information on locations and instruments used by some studies investigating UV around the world.

Country	City	Latitude	Longitude	Altitude asl	Period	UV type	Instruments	Authors
England	Sutton Bonington	52°50'N	1°15'W	50m	1983	UVB	Light SEE 240 detector	Webb & Steven, 1984
Switzerland Alaska	Jungfraujoch Fairbanks	46.55°N 64.82°N	7.98°E 147.87°W	3576m 133m	1980 1979-1982	295 – 285nm	UV radiometer	Ambach, Blumthaler & Wendler, 1991
England	Reading	51.5°N	90°08E	3648m	1989-1990	295 – 285nm	Optronics spectroradiometers	Webb, 1991
China	Lhasa	29°40N	90°08E	3648m	1996	305nm 320nm 340nm	Multi-channel filter instrument (NILUV)	Ren, Sigernes & Gjessing, 1997
Spain	Granada Amería	37.18°N	3.58°W	660m	1994-1995	290-385nm	Eppley TUVR radiometer	Moreno, Vida & Arboledas, 1998
Spain	Valencia Cordoba	39.29°N 37.51°N	0.23°W 4.48°W	20m 125m	1996-1997	295-385nm	Eppley TUVR radiometer	Cañada, López & Boscá, 2000
Germany	Helgoland	54.12°N	7.54°E		1994-1999	305nm 320nm 340nm 380nm	Biospherical UV radiometer	Dring et al., 2001
Germany	Garmisch- Parternkirchen Wiblingen Seefeld	47.48°N 47.42°N 47.52°N 48.07°N 47.33°N	11.07°E 10.98°E 11.11°E 11.17°E 11.18°E	730m 2964m 1750m 600m 1200m	1999	290-400nm	Spectroradiometer	Gröbner et al., 2000
Austria	Wien Bad Voslau Linz/Steyregg	48.25°N 47.96°N 48.29°N	16.43°E 16.20°E 14.35°E	153m 286m 335m	1970-1996	UVI 250-400nm	UV-Biometers (Model 501)	Schmalwieser & Schauberger, 2001

	Graz Dornbirn Klagenfurt Inssbruck Mariapfarr Sonnblick	47.09ºN 47.43ºN 46.65ºN 47.26ºN 47.15ºN 47.05ºN	15.41ºE 9.72ºE 14.32ºE 11.35ºE 13.74ºE 12.95ºE	348m 410m 448m 578m 1153m 3106m				
Russia	Irkutsk	52ºN	104ºE		1998-2000	295-345nm	Spectrophotometer	Mikhalev et al., 2001
Spain	Valencia Córdoba	39.29ºN 37.51ºN	0.23°W 4.48ºW	20m 125m	1996-1998	290-385nm	Eppley TUVR radiometer	Canãda, Pedros & Bosca, 2003
Poland	Belsk	51.83ºN	20.78ºE		1999-2001	MED/h	Solar Light UV-biometer 501A	Krzyścin, Jaroslawski & Sobolewski, 2003
Greece	Thessaloniki	40.5ºN	23ºE		1994-1997	290-400nm	Tropospheric Ultraviolet and Visible (TUV) Version 4.0 model	Kazantzidis et. al., 2005
India	Nainital	24.4ºN	79.5ºE	1958m	2004	305.5nm 312.5nm 320nm	Microtops II (Microprocessor-controlled total ozone portable spectrometer) Tropospheric Ultraviolet and Visible (TUV)	Srivastava et al., 2006
Cyprus	Athalassa	35.15ºN	33.40ºE	165m	2004	280-380nm	Skye High-Output Sensors (430, 420)	Jacovides et. al., 2006
Za	Zacateas	22ºN	102°O	2500m	2005	290-320nm 320-400nm	Benthan Spectroradiometer	Pinedo et. al., 2006
Egypt	Aswan South Valley Hurghada El-Arish Rafah	23.97ºN 26.16ºN 27.28ºN 31.08ºN 31.22ºN	32.78ºE 32.70ºE 33.75ºE 33.83ºE 34.20ºE	192m 77.3m 6.5m 32m 73m	1994-2001	280-315nm 315-400nm	Empirical equations for estimating UV from global radiation	Basset & Korany, 2007
China	Xianghe	39.75°N	116.96ºE	30m	2004-2006	295-385nm	Eppley TUVR radiometer	Xia et. al., 2008

Italy	Rome	41.9ºN	12.5ºE	75m	1992	290-325nm	Brewer Spectrophotometer Broad-band Radiometer (YES UVB-1) Ozone Monitoring Instrument (OMI)	Ialongo, Casale & Siani, 2008
Spain	Valladolid	41.40ºN	4.50ºW	840m	2001-2008	290-385nm	Eppley TUVR radiometer	Santos, Villan & Castrillo, 2011
Spain	Valladolid	41.40ºN	4.50ºW	840m	2002-2006	280-315nm	YES UVB-1 pyranometer	Bilbao & Migue, 2010
Iran	Khorram Abad	30.23ºN	48.21°E	1171m	2005-2006	UVI	UV-Biometer Model 501	Gholami & Yoosefi, 2009
Poland	Lódz	51.45ºN	19.26ºE	220m	1997-2001	290-400nm	Kipp and Zone CUV3 radiometer	Podstawczynka, 2010
China	Shenyang Sanya	41.51ºN 18.19ºN	123.27ºE 109.42ºE	50m 4m	2004-2007	280-390nm	Solar-UV sensor (SUB-T)	Hu et. al., 2010
Thailand	Chiang Mai Ubon Ratchathani Nakhon Pathon Songkhla	18.78ºN 15.25ºN 13.82ºN 7.20ºN	98.98°E 104.87°E 100.04°E 100.60°E		2001-2005	EUV	Satellite-based EUV radiation model UV-biometer model 501A	Janjai et. al., 2010
China	Beijing	39.56ºN	116.17ºE	75m	2005-2008	290-400nm	CUV3 radiometer	HU & Liu 2010
Thailand	Nakhon Pathon	13.82ºN	100.04ºE	30m	2001-1010	290-384nm	Eppley TUVR radiometer	Buntoung et al., 2012
Spain	Granada	37.17ºN	3.61°W	680m	2006-2009	UVER	Broad band UV radiometer (UVB-1)	Antón et. al., 2012
India	Srinagar New Delhi Bhopal Ahmedabad Kolkata Mumbai Pune	34.09ºN 29.01ºN 23.23ºN 23.03ºN 22.57ºN 18.96ºN 18.52ºN	74.79ºE 77.38ºE 77.42ºE 72.61ºE 88.34ºE 72.82ºE 73.84ºE	1730m 239m 501m 56m 6.4m 11m 559m	2002-2012	UVI	TEMIS data	Bhattacharya et al., 2012

	Hyderabad Chennai	17.36ºN 13.08ºN	78.46ºE 80.27ºE	542m 8m				
Egypt	Cairo	30.05ºN	31.15ºE		1995-2005	UVER UVI	UV sensor model UVB-1	Khalil & Shaffie, 2013
Egypt	Qena	26.2º|N	32.75ºE	96m	2001-2005	280-320nm	Ultraviolet Pyranometer model UVB-1	Adam, 2014
Nigeria	Gboko	07.19ºN	09.02º	238m	2012	UVA UVB	Digital UV broad band meter	Tertsea, Barnabas & Emmanuel, 2013
Spain	Valladolid	41.49ºN	4.56ºW	848m	2002-2011	280-315nm	UVB-1 YES piranometer	Bilbao & de Migue, 2013
South Corea	Seoul	37.57ºN	28.98ºE		2004-2008	290-363nm	Brewer Spectrophotometer MKIV	Kim et. al., 2013
Italy	Aosta	45.75°N	7.35ºE	570m	2007-2011	290-500nm	MKIV Brewer spectrophotometer	Diémoz et. al., 2013
Kwait	Shuwaikh	29.21ºN	47.55ºE	23m	2010-2013	280-320nm	UV Biometer model 501	Ghoneim, Kadad & Altouq, 2013
Belgium	Uccle	50.49ºN	4.21ºE	100m	1991-2013	290-325nm EUV	Brewer spectrophotometer instrument #016	De Bock et. al., 2014
Malta	Marsaxlokk	35.50ºN	14.33ºE	10	2012	280-315nm UVER	UVB-1 piranometer	Bilbao et. al., 2015
China	Heshan	22.41ºN	112.54ºE	564m	2005-2011	290-400nm	CUV3 radiometer	Gong et al., 2015
Egypt	Qena	26.2º|N	32.75ºE	96m	2000-2009	280-320nm	SVU-MRS UVB-1 piranometer	Adam & Ahmed, 2016
EUA	Pt. Judith Kirtland AFB East Coast Chip West Coast Chip				2009-2011	250-500nm 320-400nm	SU-100 UV Sensor UVA lamps	Yoon, Angel & Hansen, 2016
Thailand	Chiang Mai U. Ratchathani Nakhon Pathom Songkhla	18.78ºN 15.25ºN 13.82ºN 7.20ºN	98.98ºE 104.87ºE 100.04ºE 100.60ºE		2011-2014	EUV	UV-biometers (501A) UV spectroradiometer (Bentham, model DMc150)	Choosri et. al., 2017

South Corea	Seoul	37.57ºN	126.95ºE	87m	2006-2010	286.5-363.0	Brewer spectrophotometer #148 KM-IV	Park et. al., 2017
Poland	Warsaw Lodz	51.17ºN 51.84ºN	20.97ºE 20.79ºE		2017	UVI	Davis Vantage PRO instruments	Krzyścin et. al., 2018
Malaysia		1-7ºN	99-105ºE		2015	EUV	Ozone Monitoring Instrument (OMI)	Tan, Lim & Jafri, 2020
Spain	Valladolid	41.7ºN	4.7°W	702m	2013-2019	280-320nm UVI UVER	YES UVB-1 pyranometer Brewer MKIII spectroradiometer	Bilbao & Migue, 2020
Canada	Alberta				2019	UVI	UVR dosimeters Brewer Spectrophotometer	Rydz et. al., 2020
Argentina	Ushuaia	45º59S			1990-1991	300-340nm	Scanning Spectroradiometer	Frederick et. al., 1993
Argentina	La Quiaca Pilar Rosario Buenos Aires Comodoro Riv. San Julián Ushuaia Base Marambio	22.12ºS 31.66ºS 32.96ºS 34.61ºS 45.78ºS 49.32ºS 54.80ºS 64.23ºS	65.57ºW 63.88ºW 60.62ºW 58.41ºW 67.50ºW 67.75ºW 68.27ºW 56.71ºW	3459m 338m 25m 25m 46m 62m 14m 300m	1996-1999	UVER	UV Biometers UVB-1 model 501 UV radiometer	Cede et al., 2002
Argentina	Patagonia	43ºS	65ºW		2001-2002	280-325nm 315-400nm	Broad-band Eldonet radiometer	Villafane, Barbieri & Helbling, et. al, 2004
Argentina	Córdoba	31.44ºS	64.19ºW		1999	280-420nm	Broadband pyranometer YES model UV-B1 Radiative transfer mode TUV 4.1	Palancar & Toselli, 2004

Chile	Valdívia	39.48ºS	73.14ºW	30m	1998-2003	290-600nm 290-340nm	Scanning spectroradiometer (SUC-100)	Huovinen, Gómez & Lovengreen, 2006
Argentina	La Quiaca Pilar Rosario Buenos Aires Comodoro Rivadavia San Julián Ushuaia Station Mendoza	21.25ºS- 55.25ºS	53.25ºW- 73.75ºW		1996-2000	UVI UVER	UV Biometers UVB-1 model 501 UV radiometer Radiative tranfer model (DISORT Algorithm)	Luccini et al., 2006
Australia	Toowoomba	27.36ºS	151.55ºE	693m	2004	280-400nm	UV Spectrodaradiometer	Parisi, Turnbull & Turner et. al., 2007
Chile	Santiago	33.43ºS	70.67ºW	640m	1995-2011	305nm 320nm 340nm 380nm UVI	Multi channel filter radiometer (PUV-510) OMI	Cabrera et al., 2012
Chile	Chajnantor Plateaus Paranal Observatory	23.00°S 24.37ºS	67.45ºW 70.24ºW	5100m 2365m	2013 2004-2012	280-600nm UVI	Double Monochromator-based spectroradiometer (USACH) OMI	Cordero et al., 2014
South Africa	Stellenboch				2013-2015	250-400nm	Apogee SU-100 UV sensor	Joubert et. al., 2016
South Africa	Pretoria Durban De Aar Port Elizabeth Cape Town Cape Point	25.73ºS 25.81ºS 29.97ºS 29.61ºS 30.67ºS 33.97ºS 33.98ºS 34.35ºS	28.18ºE 28.49ºE 31.00ºE 31.11ºE 23.99ºE 25.61ºE 18.60ºE 18.48ºE	1330m 1228m 9m 103m 1286m 63m 42m 228m	1994-2003 2003-2015 1994-2010 2010-2015 2002-2015 2000-2015 1994-2015 1997-2015	280-340nm UVI	Model 501 UV-biometer OMI	Cadet et al., 2017

Bolívia	La Paz	16.32ºS	68.03ºW	3459m	1998-2012	UVI DOSE	Brewer spectrophotometer Model TUV	Coariti et al., 2017
Peru	Ica Tacna Moquegua Arequipa Cajamarca Marcapomacocha	14.7ºS ºS ºS ºS ºS ºS	75.73ºW ºW ºW ºW ºW ºW		2005-2014	UVER	Biometers Light UVB 501	Yamamoto, Correa & Ccoyllo, 2018
Argentina	Salta El Rosal Tolar Grande	24.78ºS 24.39ºS 24.59ºS	65.41ºW 65.76ºW 67.45ºW	1190m 3355m 3560m	2013-2015	UVER	Kipp & Zonen UVS-E-T radiometers YES UVB-1 radiometer	Utrillas et al., 2018
Ecuador	Ibarra	0.36ºN	78.1ºW	2225m	2017	UVI	UV Kipp & Zonen radiometer	Huaca, Salum & Piacentini, 2018
France	Saint-Denis (Reunion Island)	20.90ºS	55.50ºE	80m	2009-2016	280-450nm UVI	Bentham DTMc300 spectroradiometer TUV model	Lamy et al., 2018
United States France France New Zealand United States United States	Mauna Loa Saint-Denis Villeneuve d'Ascq Lauder Barrow Palmer	19.54ºN 20.09ºN 50.61ºN 45.04ºN 71.32ºN 64.77ºN	155.58ºW 55.5ºW 3.14ºW 169.68ºW 156.68ºW 64.05ºW	3397m 370m 8m	2005-2017	280-450 nm UVI	Tropospheric Ultraviolet Model (TUV) OMI	Lamy et al., 2019
Chile	Laja Lake	36.54ºS	71.05ºW	1360m	2018	280-400nm	Apogee SU 100 UV sensor	Rodriguez-López et al., 2019
Ecuador	Quito	0.2ºS	78.5ºW	2850m	2010-2014	UVI 305nm 323nm 320nm 340nm 389nm 395nm	Multichanel radiometer GUV-2511 TEMIS UV index dataset	Parra, Cadena & Flores, 2019

Chile	Santiago	33.27ºS	70.38ºW	512m	2015-2018	UVER 280-315nm	UV-B Sensor model PMA-1101	Gonzáles-Rodriguez et al., 2019
France South Africa	Saint-Denis Cape Town	20.9ºS 33.98ºS	55.5ºE 18.6ºE	85m 42m	2009-2018	Erythemal UVR UVI 280-400nm 280-340nm	Double-monochromator Bentham DTMc300 UV-biometer model 501(SN#10414)	Cadet et al., 2019
South Africa	Cape Point	34.35ºS	18.50ºE	230m	2007-2016	UVI 280-320nm	Solar Light Model Biometer 501 radiometer	Du Preez et al., 2020
Antarctica	Marambio Princess Elisabeth Station Troll Station Palmer Station McMurdo Station Amundsen Scott South Pole Station	64.23ºS 71.95ºS 70.00ºS 64.77ºS 77.83ºS 90.0ºS	56.62ºW 23.35ºE 2.53ºE 64.05ºW 166.67°W 0.0ºE	198m 1390m 1553m 21m a.s.l 183m 2835m	2007-2019 2000-2013	305nm 313nm 320nm 340nm 380nm 555nm UVI	GUV-2511 multi filter radiometer NILU-UV multchanel radiometer	Aun et al., 2019
France	St-Denis (La Reunion)	20.9ºS	55.5ºE	85m	2018 2019	280-450nm Erythemal UVR UVI 280-340nm 280-400nm 280-360nm	High grade double monochromator Bentham DTMc300 Kipp&Zonen UVS-E-T SL501 UV-Biometer UV-Cosine sensor Radiometer Davis TUV model	Cadet et al., 2020
Antarctica	Marambio	64ºS	56ºW	198m	2017-2019	305nm 313nm 320nm 340nm 380nm 290-400nm	GUV-2511 multi-filter radiometer	Lakkala et al., 2020

						UVI		
Chile	Arica	18.49ºS	70.19ºW	25m	2007-2013	305nm 313nm 320nm 340nm 380nm	Broadband YES UV-A biometer GUV-2511 instrument	Rivas et al., 2020
South America		20ºS-55ºS	30ºW-90ºW		2005-2014	IUV	OMI	Dias Nunes, Mariano & Alonso, 2020
Chile	Santiago	35.27ºS	70.51ºW	512m	2015-2019	280-315nm UVER UVI	PMA-2101 detector	González-Rodriguez et al., 2021
South Africa	Pretoria	25.81ºS	28.26ºE	1300m	2009-2018	280-315nm UVI	Solar light 501 UVB radiometer TUV model	Du Preez et al., 2021
France	Saint-Denis (Re)	20.902°S	55.485°E	82m	2009-2020	UVI	BENTHAM DTMc 300 Radiometer Kipp Zonen	Lamy et al., 2021
	Maido (Re)	21.079°S	55.383°E	2200m	2016-2020		UVS-E-T 15-0124 Radiometer Kipp	
	Juan de Nova	17.054°S	42.711°E	10m	2019-2020		Zonen SUV-E 18-0020	
Madagascar	Antananavario	18.916°S	47.565°E	1370m	2016-2020		Radiometer Kipp Zonen SUV-E 18-0029	
	Diego Suarez	12.279°S	49.287°E	35m	2017-2020		Radiometer Kipp Zonen UVS-E-T 16-0159	
	Fort Dauphin	25.028°S	46.995°E	10m	2020-2020		Radiometer Kipp Zonen	
Seycheles	Mahé	4.679 °S	55.531°E	15m	2017-2020		UVS-E-T 17-0207 Radiometer Kipp	
Comores	Moroni	11.708°S	43.247°E	12m	2019-2020		Zonen SUV-E 18-0030	

Rodrigues	Anse Quitor	19.758°S	63.368°E	32m	2017-2020 2018-2020 2014-2020 2016-2020 2004-2020		Radiometer Kipp Zonen UVS-E-T 17-0207 Radiometer Kipp Zonen SUV-E 18-0027 Radiometer Kipp Zonen UVS-E-T 16-0158 TROPOMI GOME Model CAMS Model TEMIS	
Antarctica	King George Island	62.12ºS	58.58ºW		2016-2021	290-315nm	Bentham DMC150	Cordero et al., 2022
	Palmer Station	64.46ºS	64°03ºW)		1990-2020 2005-2020	315-400nm	Biospherical SUV-100 OMI	
Chile		32.32ºS-37.03ºS			2015-2020	UVER	Radiometric Stations	Gonzáles-Rodriguez et al., 2022
Brazil	Natal	5.84ºS	35.21ºW		1994-1999	280-380nm UVI	Biometers	Kirchhoff et al., 2000
	Campo Grande	19.25ºS	54.34ºW					
	Ribeirão Preto	21.17ºS	47.7ºW					
	Cachoeira Paulista	22.7ºS	45.0ºW					
	Blumenau	26.92ºS	49.05ºW					
	Porto Alegre	30.47ºS	50.38ºW					
Chile	Punta Arenas	53.2ºS	70.9ºW					
Bolivia	La Paz	16.54ºS	68.06ºW					
Brazil	Botucatu	22.85ºS	48.45ºO	785m	2001-2004	290-400nm	Radiometer CUV-3 Kipp&Zonen	Escobedo et al., 2006
Brazil	São Paulo	23.31ºS	46.37ºO	800m	1996-2002	UVI	Model UVGAME	Corrêa & Plana-Fattori, 2006

Brazil	São Martinho da Serra	29.4ºS	53.8ºW	490m	2002-2004	300-400nm	Spectroradiometer MS-701	Nozawa et al., 2007
Japan	Tokyo	35.7ºN	139.7ºE	65m			Radiometers	
Chile	Punta Arenas	53.1ºS	71.0ºW	10m			MS-212A	
							MS210A	
							MS-212W	
							MS-210W	
Brazil	Belo Horizonte	19.92ºS	43.94ºW	858m	2005-2007	UVER	Biometer Solar Light Model 501A	Silva, 2008
Brazil	Natal	5.45ºS	35.12ºW		2001-2007	UVI	Radiometer GUV-511 C	Silva, Oliveira & Marinho, 2008
Brazil	Botucatu	22.53ºS	48.26ºW	786m	2001-2005	290-390nm	Kipp-Zonen pyranometer model CUV-3	Escobedo et al., 2008
France	Palaiseasau	48.7ºN	2.2ºE	170m	2008	280-450nm	Solar meter UVI 6.5	Corrêa et al., 2010
					2009	UVI	Solarmeter Personal UV monitor	
							Décathlon 500 W UV	
							Oregon Scientific UV	
							BBW 213 station	
							Bentham Spectrometer	
Brazil	Belo Horizonte	19.92ºS	43.94ºW	858m	2007	EDR	Biometer Solar Light 501A	Silva, 2010
Brazil	Pesqueira	8.24ºS	36.46ºW	639m	2008-2010		Eppley TURV pyranometer	Leal, Tiba & Piacentini, 2011
	Araripina	7.34ºS	40.29ºW	622m				
Brazil	Maceió	9.28ºS	35.49ºW	127m	2008	290-400nm	Kipp & Zonen CUV3 radiometer	Porfíirio et al., 2012
Brazil	Recife	8.03ºS	34.55ºW	7	2010-2011	280-320nm	Biometer model 501 UV-B	Tiba & leal, 2012
						295-385nm	Radiometer TUVR	
Brazil	Natal	5.45ºS	35.12ºW		2001-2007	305nm	Radiometer GUV model 511-C	Marinho & Silva, 2013
						320nm		
						340nm		
						380nm		
Brazil	São Paulo	23.32ºS	46.38ºW	850m	2005-2009	UVER	Biometer model 501 radiometer	Corrêa & Pires, 2013
	Itajubá	22.25ºS	45.27ºW	850m				

	Ilhéus	14.47ºS	39.02ºW	0m				
Brazil	Botucatu	22.85ºS	48.43ºW	742m	2001-2007	290-400nm	Kipp & Zonen CUV3 radiometer	Teramoto et al., 2014
Brazil	Natal	5.48ºS	35.12ºW	58m	2001-2009	305nm 320nm 340nm 380nm IUV	Multiespectral radiometer GUV model 511-C	Lopo et al., 2013
Brazil	Botucatu	22.54ºS	48.27ºW	786m	2001-2005	290-390nm	Kipp-Zonen pyranometer model CUV-3	Escobedo et al., 2012
Brazil	Botucatu	22.51ºS	48.26ºW	742m	2000-2007	290-400nm	Kipp-Zonen pyranometer model CUV-3	Teramoto, Escobedo & Martins, 2014
Brazil	Natal	5.45ºS	35.12ºW	58m	2001-2012	UVI	Radiometer GUV Sensor Model UV-6490	Lopo et al., 2014
Brazil	Santa Maria	29.43ºS- 16.84ºS	53.43ºW 35.8ºW		2013	UVA UVB	Portable radiometer EKO UV monitor MS-211-1	Schuch et al., 2015
Brazil	Botucatu	22.51ºS	48.26ºW	742m	2000-2007	290-400nm	Kipp-Zonen pyranometer model CUV-3	Teramoto et al., 2020
Brazil	Recife Rio de Janeiro São Paulo Porto Alegre	8.1ºS 22.9ºS 23.6ºS 30.0ºS	4.9ºW 43.2ºW 46.7ºW 51.2ºW	5m 12m 765m 30m	2016 2017	UVER UVI	Scienterra UV dosimeters	Corrêa et al., 2021
Brazil	Humaitá	7.0ºS	63.0ºW	186m	2019-2020	UVI 200-370nm	Sensor UVM-30A	Alves et al., 2022